



DESIGN AND SYNTHESIS OF NOVEL BIO-NANOHYBRID MATERIALS: CATALYTIC APPLICATIONS IN REACTIONS OF INTEREST TO THE FINE- CHEMICAL/PHARMACEUTICAL INDUSTRIES

Ronald Alexander Miranda Acevedo

Dipòsit Legal: T. 189-2013

ADVERTIMENT. L'accés als continguts d'aquesta tesi doctoral i la seva utilització ha de respectar els drets de la persona autora. Pot ser utilitzada per a consulta o estudi personal, així com en activitats o materials d'investigació i docència en els termes establerts a l'art. 32 del Text Refós de la Llei de Propietat Intel·lectual (RDL 1/1996). Per altres utilitzacions es requereix l'autorització prèvia i expressa de la persona autora. En qualsevol cas, en la utilització dels seus continguts caldrà indicar de forma clara el nom i cognoms de la persona autora i el títol de la tesi doctoral. No s'autoritza la seva reproducció o altres formes d'explotació efectuades amb finalitats de lucre ni la seva comunicació pública des d'un lloc aliè al servei TDX. Tampoc s'autoritza la presentació del seu contingut en una finestra o marc aliè a TDX (framing). Aquesta reserva de drets afecta tant als continguts de la tesi com als seus resums i índexs.

ADVERTENCIA. El acceso a los contenidos de esta tesis doctoral y su utilización debe respetar los derechos de la persona autora. Puede ser utilizada para consulta o estudio personal, así como en actividades o materiales de investigación y docencia en los términos establecidos en el art. 32 del Texto Refundido de la Ley de Propiedad Intelectual (RDL 1/1996). Para otros usos se requiere la autorización previa y expresa de la persona autora. En cualquier caso, en la utilización de sus contenidos se deberá indicar de forma clara el nombre y apellidos de la persona autora y el título de la tesis doctoral. No se autoriza su reproducción u otras formas de explotación efectuadas con fines lucrativos ni su comunicación pública desde un sitio ajeno al servicio TDR. Tampoco se autoriza la presentación de su contenido en una ventana o marco ajeno a TDR (framing). Esta reserva de derechos afecta tanto al contenido de la tesis como a sus resúmenes e índices.

WARNING. Access to the contents of this doctoral thesis and its use must respect the rights of the author. It can be used for reference or private study, as well as research and learning activities or materials in the terms established by the 32nd article of the Spanish Consolidated Copyright Act (RDL 1/1996). Express and previous authorization of the author is required for any other uses. In any case, when using its content, full name of the author and title of the thesis must be clearly indicated. Reproduction or other forms of for profit use or public communication from outside TDX service is not allowed. Presentation of its content in a window or frame external to TDX (framing) is not authorized either. These rights affect both the content of the thesis and its abstracts and indexes.

Ronald Alexander Miranda Acevedo

DESIGN AND SYNTHESIS OF NOVEL BIO-NANOHYBRID
MATERIALS: Catalytic applications in reactions of interest to the fine-
chemical/pharmaceutical industries

Doctoral Thesis



UNIVERSITAT ROVIRA I VIRGILI

Departament d'Enginyeria Química

UNIVERSITAT ROVIRA I VIRGILI

DESIGN AND SYNTHESIS OF NOVEL BIO-NANOHYBRID MATERIALS: CATALYTIC APPLICATIONS IN REACTIONS OF INTEREST
TO THE FINE-CHEMICAL/PHARMACEUTICAL INDUSTRIES

Ronald Alexander Miranda Acevedo

Dipòsit Legal: T. 189-2013

UNIVERSITAT ROVIRA I VIRGILI

DESIGN AND SYNTHESIS OF NOVEL BIO-NANOHYBRID MATERIALS: CATALYTIC APPLICATIONS IN REACTIONS OF INTEREST
TO THE FINE-CHEMICAL/PHARMACEUTICAL INDUSTRIES

Ronald Alexander Miranda Acevedo

Dipòsit Legal: T. 189-2013

UNIVERSITAT ROVIRA I VIRGILI

DESIGN AND SYNTHESIS OF NOVEL BIO-NANOHYBRID MATERIALS: CATALYTIC APPLICATIONS IN REACTIONS OF INTEREST
TO THE FINE-CHEMICAL/PHARMACEUTICAL INDUSTRIES

Ronald Alexander Miranda Acevedo

Dipòsit Legal: T. 189-2013

Ronald Alexander Miranda Acevedo

DESIGN AND SYNTHESIS OF NOVEL BIO-NANOHYBRID MATERIALS:
Catalytic applications in reactions of interest to the fine-chemical/pharmaceutical
industries

Doctoral Thesis

Supervised by

Dr. Anna María Segarra González

Prof. Dr. Jesús E. Sueiras Romero

Engineering Chemical Department



UNIVERSITAT ROVIRA I VIRGILI

Tarragona, Spain

2012

UNIVERSITAT ROVIRA I VIRGILI

DESIGN AND SYNTHESIS OF NOVEL BIO-NANOHYBRID MATERIALS: CATALYTIC APPLICATIONS IN REACTIONS OF INTEREST
TO THE FINE-CHEMICAL/PHARMACEUTICAL INDUSTRIES

Ronald Alexander Miranda Acevedo

Dipòsit Legal: T. 189-2013

Dr. Anna M. Segarra González and Dr. Jesús E. Sueiras Romero

CERTIFY THAT the study entitled "Design and synthesis of novel bio-nanohybrid materials: Catalytic applications in reactions of interest to the fine-chemical/pharmaceutical industries" presented by Ronald Alexander Miranda Acevedo for the award of the degree of Doctor from the Rovira i Virgili University, has been carried out under our supervision at the Chemical Engineering Department of this University, and that it fulfils all the requirements to obtain the Doctor European Mention.

December 15th, 2011. Tarragona

The supervisors of the doctoral thesis

Dr. Anna M. Segarra González

Dr. Jesús E. Sueiras Romero

UNIVERSITAT ROVIRA I VIRGILI

DESIGN AND SYNTHESIS OF NOVEL BIO-NANOHYBRID MATERIALS: CATALYTIC APPLICATIONS IN REACTIONS OF INTEREST
TO THE FINE-CHEMICAL/PHARMACEUTICAL INDUSTRIES

Ronald Alexander Miranda Acevedo

Dipòsit Legal: T. 189-2013

Dra. Anna M. Segarra González y Dr. Jesús E. Sueiras Romero

CERTIFIQUEN QUE el treball titulat "Design and synthesis of novel bio-nanohybrid materials: Catalytic applications in reactions of interest to the fine-chemical/pharmaceutical industries" que presenta Ronald Alexander Miranda Acevedo per a l'obtenció del títol de Doctor per la Universitat Rovira i Virgili, ha estat realitzat sota la nostra direcció al Departament d'Enginyeria Química d'aquesta universitat i que compleix amb els requeriments per a optar a la Menció Europea.

Tarragona, 15 de desembre de 2011

Els supervisors de la tesi doctoral



Dr. Anna M. Segarra González



Dr. Jesús E. Sueiras Romero

UNIVERSITAT ROVIRA I VIRGILI

DESIGN AND SYNTHESIS OF NOVEL BIO-NANOHYBRID MATERIALS: CATALYTIC APPLICATIONS IN REACTIONS OF INTEREST
TO THE FINE-CHEMICAL/PHARMACEUTICAL INDUSTRIES

Ronald Alexander Miranda Acevedo

Dipòsit Legal: T. 189-2013

UNIVERSITAT ROVIRA I VIRGILI
DESIGN AND SYNTHESIS OF NOVEL BIO-NANOHYBRID MATERIALS: CATALYTIC APPLICATIONS IN REACTIONS OF INTEREST
TO THE FINE-CHEMICAL/PHARMACEUTICAL INDUSTRIES
Ronald Alexander Miranda Acevedo
Dipòsit Legal: T. 189-2013

To my awesome family,

To my best friends forever,

To my sweetheart.

UNIVERSITAT ROVIRA I VIRGILI

DESIGN AND SYNTHESIS OF NOVEL BIO-NANOHYBRID MATERIALS: CATALYTIC APPLICATIONS IN REACTIONS OF INTEREST
TO THE FINE-CHEMICAL/PHARMACEUTICAL INDUSTRIES

Ronald Alexander Miranda Acevedo

Dipòsit Legal: T. 189-2013

ACKNOWLEDGEMENTS (AGRADECIMIENTOS)

First of all, I would like to thank to **Universitat Rovira i Virgili** and **Fundació URV** for the predoctoral scholarship and for all the facilities given to me during my PhD and also thanks to **Ministerio de Education de España** for the mobility scholarship to obtain the European Mention in my doctoral degree.

However, in everywhere the persons are the responsible for every good job and there are many of them that I would like to thank for their encouragement and support during these last four years. I had been a lucky guy because I found much fruitful and joyful collaboration from most of the persons that I have known during this great travel.

I would like to thank my supervisors, **Anna M. Segarra** and **Jesús E. Sueiras**. You have been my mentors during my PhD. Eventhough we did not agree in some things I deeply thank you for our nice talks about Latinamerica, your guidance and your willingness to resolve my questions. I am deeply grateful to you.

To my third mentor, not less important, **Francisco Medina**, I would like to thank you for all your support and willingness to discuss my scientific doubts and also for listening my understandable jokes, and sometimes laught about them. Thanks you so much for all your guidance, your ideas and help during these four years.

I would like to thank **Jordi Llorca** from Institut de Tècniques Energètiques of the Universitat Politècnica de Catalunya for all your timely and accurate with the HRTEM analyses and results interpretations.

Elisabetta Finocchio, I can't think in a better balanced supervisor for my research stage. *Grazie Mille* for all our results discussions, your time to solve all my doubts in Genoa and by email. I would like also to thank your pleasant talks, your words of encouragement and hospitality in your lab. You cannot imagine how much I learned from you in this short time. Thank you so much!!

Yolanda Cesteros, thank you for inviting me to form part of the URV. You are an excellent professor and person, and I am really happy to meet you. Thanks for everything we share during this time, especially at the beginning of my PhD.

CATHETER, my second home during my PhD. Thank you to all my lab co-workers specially to **Mohammad “Kaveh” Yalfani** for your open personality, for helping me with the correction of my papers and also for being my friend and, to **Sandra Ramos** who was always there to listen, help and advise me, and the best, always with a smile. Thank you very much!!

Thanks to **Laboratorio di Chimica delle Superfici e Catalisi Industriale** from Genoa University for hosting me during three months. Especially Prof. **Gianguido Ramis** thank you for your orientations and nice talks. But, I would like also thank to Prof. **Guido Busca** for his help with the FT-IR interpretations; to **Carlo Pronzati** for attending my emergency calls to solve my connection problems and also for opening the lab door several times and, of course, to my excellent co-worker and friend **Gabriella Garbarino** for all your help at the lab, for the discussions about who paid for the delicious *cappuccino* and for showing me how nice are Genoese people!!!!. Finally special thanks to Prof. **Rodolfo Botter** for his excellent talks about the TGA 's world and for his nice disposition to work with me.

Thanks to all **GREENCAT** 's members for your support during my PhD. It was really nice to work in your pleasant and always clean lab.

Thanks to all technicians from **Servei de Recursos Científics i Tècnics** to the URV, specially to **Maria Rosa Ras**, **Francesc Gispert** and **Ramón Guerrero** who always helped me with my urgent samples and often with the results discussion.

Department d'Enginyeria Química, I cannot think of a better department in which to do my PhD work at the URV. I appreciate very much everyone at the department but specially to **Núria Juanpere** and **Merche Maurín** for their help and always smiling faces.

Sin embargo, nada en este viaje hubiera sido tan especial sin mis excelentes amigos. Gracias chicos por todos los momentos que compartimos, por las discusiones, los viajes, las *cermezas* y los bailes. Aunque me gustaría dedicarles un párrafo a cada uno, todos ustedes saben lo importantes que son para mí.

Tatiana Sánchez y **Adriana Aristizabal**, mis hermanas en este viaje, gracias por escuchar todas mis historias, por sus consejos y por reírse de mis chistes. **Oscar Osegueda** y **Olivier Jacquet** no puedo imaginarme este viaje sin nuestras multiples conversaciones acerca de nada, las risas y los paseos. Gracias chicos por toda su ayuda en este tiempo, por su amistad. Gracias a ustedes cuatro pude comprender que es posible tener 4 mejores amigos!!.

Espero no olvidar a nadie, pero tambien quiero agradecer a **Gemma García**, **Helena Pérez**, **Luis Iglesias**, **Iuliana Cota**, **Martha Segura**, **María Alba**, **Carolina Blanco**, **Clara Tatiana**

González y Santiago Builes con quienes me reí como nunca y de quienes aprendí que los mejores regalos suelen ser los mas baratos. A **Robison Buitrago, Jesús Roldán, Freddy Avellaneda, Helena Ramirez, Gustavo Orozco, Alejandro Jimenez, Klara Rusevova, Wester Bolaños, Vanessa Manz, Susana Dominguez, Ana Montero, Isabel Castro y Dolores González** por todos los momentos agradables que compartimos durante todo este *paseo*. Todos ustedes hicieron que este doctorado valiera mucho mas que un título. Mi mayor logro fue encontrar gente tan especial como ustedes. Muchas gracias!!! Bueno, de última pero no menos importante un especial agradecimiento a *nuestra Leidy*, sin ti muchas de nuestras conversaciones no hubieran sido tan fluidas.

A mis amigos de toda la vida, quienes a pesar de la distancia siempre han estado allí para ayudarme, aconsejarme y no dejarme caer en los momentos difíciles, en especial quiero agradecer a **Alix Duarte, Carlos Dulcey, Laura Duarte, Fabian Martínez, Ana Lucía Zabala, Fabian Orozco y Tatiana Mora**. Gracias chicos, porque durante estos cuatro años hablar con ustedes me ha hecho sentir en casa.

Por supuesto quiero agradecer a mi espectacular familia, **Jefferson Miranda**, muchas gracias por todos tus consejos, por tu ayuda y por ser uno de los soportes más importantes de mi vida, *viejo* te debo tanto que no hay palabras suficientes para darte las gracias. **Hainner Miranda**, mi hermanito, definitivamente estoy muy orgulloso de ti, gracias por todo lo que me enseñas a diario y por las mil risas que siempre compartimos en cada llamada. Gracias *cabezón*. A mis papás, **María Elena Acevedo y Libardo Miranda**, este doctorado es solo una parte de todo el esfuerzo que han hecho durante toda sus vidas, infinitas gracias por la paciencia, los consejos, regaños y silencios que me han enseñado a ser lo que soy. Los quiero montones!!.

My **bunny sweetheart**, thanks for encouraging me in the worse moments and shared the joy with me when I have succeeded. You have always shown a sincere interest for my work, for the chemistry's world and for everything that is important for me. Thanks for teaching me a lot of things about the social sciences, the social interactions and about myself. Thanks for answering my questions and for listening me in every moment that I have needed. Thanks for all your love.

PREFACE

The aim of this thesis work is to design nanohybrid materials based on biomolecules and hydrotalcite-like materials with total control over the immobilisation through the understanding of organic/inorganic interaction nature. The overall goal is to provide new nanohybrid materials with application as catalysts in interesting reactions to pharmaceutical and fine chemical industry. Furthermore, the results presented in this thesis are of relevance for the use of amino acids, poly amino acids and more complex biomolecules immobilised in inorganic matrices as heterogenised catalysts or in other potential applications such as regenerative medicine or bio-engineering. This work therefore focuses on synthesis and characterisation of nanohybrid materials based on L-Leucine, L-Proline and synthesised Poly-L-Leucine in rehydrated hydrotalcite in order to understand the organic/inorganic interaction. Moreover, understanding of the immobilisation nature of the synthesized materials is evaluated through the chemical properties using them as catalysts. In this context, the catalytic activity is evaluated in asymmetric Juliá-Colonna epoxidation reaction, direct asymmetric aldol reaction, Claisen-Schmidt reaction and Claisen-Schmidt-Juliá-Colonna one-pot reaction whose products are interesting in pharmaceutical and fine chemical industries.

This thesis is divided into five chapters which contain a brief summary of the more relevant results from our research.

Chapter 1 contains a brief introduction to the physical and chemical properties of amino acids, poly amino acids and hydrotalcite-like materials, principal synthesis methodologies presented in the literature and the catalytic applications of these materials, as well as the scope of this thesis.

Chapter 2 shows the synthesis and characterisation of nanohybrid materials based on L-Leucine and L-Proline immobilised in hydrotalcite-like materials. In this Chapter is explained the nature of organic/inorganic interaction between the immobilised amino acids and the rehydrated hydrotalcite according to the methodology used for their synthesis.

Chapter 3 contains the catalytic behaviour of the nanohybrid materials synthesised in Chapter 2 divided in two parts: firstly, L-Leucine/hydrotalcite materials as catalyst in asymmetric Juliá-Colonna epoxidation reaction of the chalcone and secondly, L-Proline/hydrotalcite materials in direct asymmetric aldol reaction of 4-nitrobenzaldehyde and acetophenone.

Chapter 4 presents the synthesis of Poly-L-Leucine by ring opening polycondensation method using triethylamine, water and hydrotalcite as initiators, as well as it presents the immobilisation of synthesised Poly-L-Leucine in rehydrated hydrotalcite through an anionic exchange protocol. In this chapter the organic/inorganic interaction of the immobilisation was in-deep studied through the physical properties of the immobilised and non-immobilised Poly-L-Leucine.

Chapter 5 discusses the use of rehydrated Hydrotalcite, Poly-L-Leucine and their nanohybrid materials as catalyst in asymmetric Juliá-Colonna epoxidation reaction and Claisen-Schmidt reaction. A preliminary study in the use of immobilised Poly-L-Leucine as the catalyst in one-pot Claisen-Schmidt-Juliá-Colonna reaction is included in this chapter.

Chapter 6 presents a summary of this thesis.

This thesis presents the research I have conducted at the Heterogeneous Catalysis Research Group - CATHETER - from the Chemical Engineering Department at Universitat Rovira i Virgili during the period 2007-2011 under the supervision of Prof. Dr. Jesús E. Sueiras and Dr. Anna María Segarra. The research was performed in collaboration with the Institut de Tècniques Energètiques from Universitat Politècnica de Catalunya and the Dipartimento di Ingegneria Chimica e di Process "G.B Bonino" from Università degli studi di Genova, where some characterisation experiments were performed. We gratefully acknowledge the financial support of the Universitat Rovira i Virgili and Fundació URV (predoctoral scholarship), Ministerio de Educación de España (Mobility Scholarship. TME2009-00414), Ministerio de Ciencia e Innovación de España (CTQ2009-12520-C03-02; NYAM-MICINN) and Generalitat de Catalunya (PAI2009A).

Tarragona, Spain. 2012

LIST OF MATERIALS USED IN THIS DOCUMENT

Materials Abbreviations

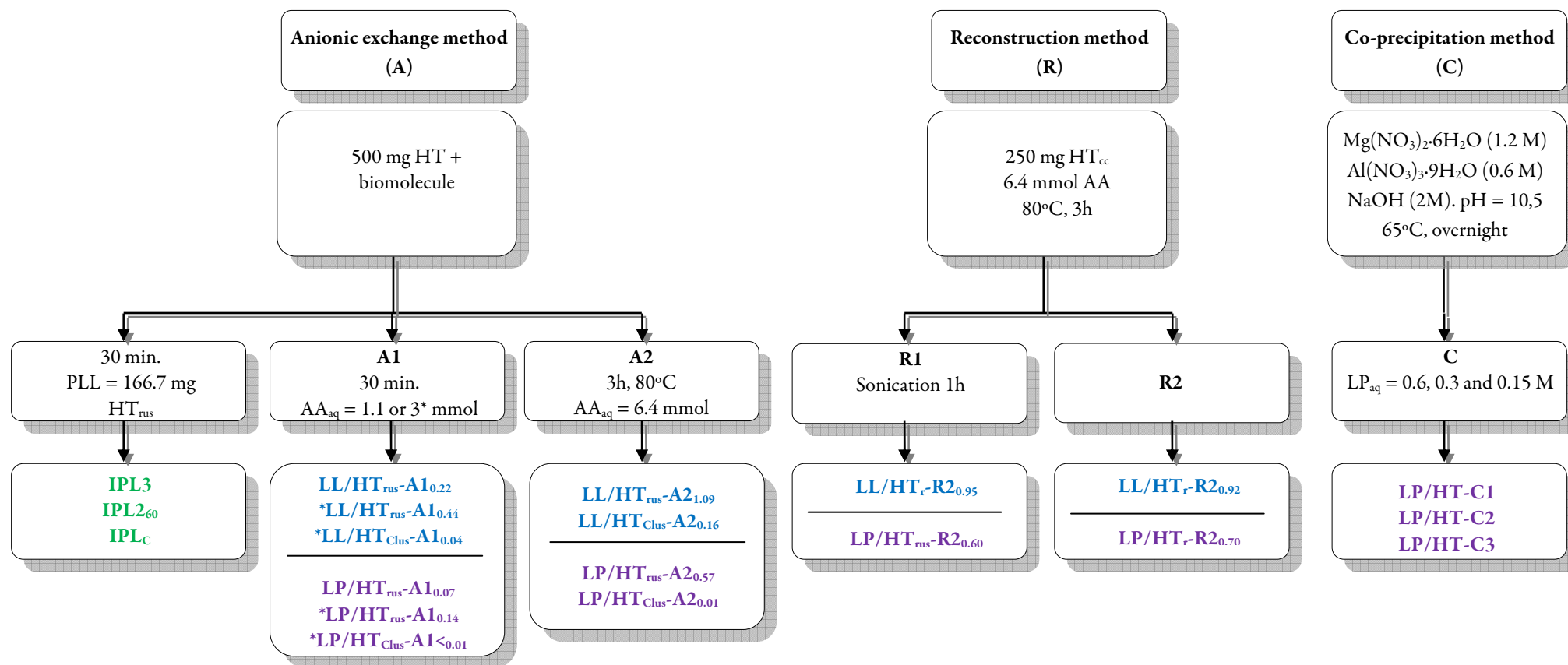
Abbreviation/ Symbol	Name
HT	Hydrotalcite-like material
L-Leu	L-Leucine
L-Pro	L-Proline
PLL	Poly-L-Leucine
LL/HT	L-Leucine immobilised in hydrotalcite
LP/HT	L-Proline immobilised in hydrotalcite
PLL/HT	Poly-L-Leucine immobilised in hydrotalcite

Materials Abbreviations (Methods of synthesis)

Material	Name	Method of synthesis	Location in the document	
			Chapter	Section
HT _{asym}	As-synthesised HT containing nitrate anions	Co-precipitation	2	2.1.1
HT _{cc}	Calcined HT	Calcination	2	2.1.1
HT _{rus}	Rehydrated HT under ultrasound treatment	Rehydration	2	2.1.1
HT _{Cl}	As-synthesised HT containing chloride anions	Co-precipitation	2	2.1.1
HT _{Clus}	As-synthesised HT containing chloride anions after ultrasound treatment	Sonication	2	2.1.1
LL/HT _{rus} -A1	L-Leu immobilised in HT _{rus}	Anion exchange 1	2	2.1.1
LL/HT _{Clus} -A1	L-Leu immobilised in HT _{Clus}	Anion exchange 1	2	2.1.2.1
LL/HT _{rus} -A1	L-Leu immobilised in HT _{rus}	Anion exchange 2	2	2.1.2.1
LL/HT _{Clus} -A2	L-Leu immobilised in HT _{Clus}	Anion exchange 2	2	2.1.2.1

LL/HT _{rus} -R1	L-Leu immobilised in HT using HT _{cc} as precursor	Reconstruction 1	2	2.1.2.2
LL/HT _r -R2	L-Leu immobilised in HT using HT _{cc} as precursor	Reconstruction 2	2	2.1.2.2
LP/HT _{rus} -A1	L-Pro immobilised in HT _{rus}	Anion exchange 1	2	3.1.2.1
LP/HT _{Clus} -A1	L-Pro immobilised in HT _{Clus}	Anion exchange 1	2	3.1.2.1
LP/HT _{rus} -A1	L-Pro immobilised in HT _{rus}	Anion exchange 2	2	3.1.2.1
LP/HT _{Clus} -A2	L-Pro immobilised in HT _{Clus}	Anion exchange 2	2	3.1.2.1
LP/HT _{rus} -R1	L-Pro immobilised in HT using HT _{cc} as precursor	Reconstruction 1	2	3.1.2.2
LP/HT _r -R2	L-Pro immobilised in HT using HT _{cc} as precursor	Reconstruction 2	2	3.1.2.2
LP/HT-C	L-Pro intercalated in HT _{asym}	Co-precipitation	2	3.1.2.3
LP/HT _{us} -C	L-Pro intercalated in HT _{asym} after ultrasound treatment	Co-precipitation + sonication	2	3.1.2.3
NCA	Monomer molecule in ROP	Dehydration	2	2.1.1
PLL#	Synthesised PLL at r.t. during 4 days (# = 1-3) using triethylamine as initiator	ROP	4	2.1.2
PLL# _{3d}	Synthesised PLL at r.t. during 3 days (# = 1-3) using triethylamine as initiator	ROP	4	2.1.2
PLL# ₆₀	Synthesised PLL at 60°C during 4 days (# = 1-2) using triethylamine as initiator	ROP	4	2.1.2
IPL3	PLL3 immobilised in HT _{rus}	Anionic exchange 1	4	3.1.2
IPL2 ₆₀	PLL2 ₆₀ immobilised in HT _{rus}	Anionic exchange 1	4	3.1.2
PLL4	Synthesised PLL at r.t. during 4 days using water as initiator	ROP	4	4.1.1
PLL5	Synthesised PLL at r.t. during 4 days using HT _{rus} as initiator in stoichiometric amount	ROP	4	4.1.1
PLL6	Synthesised PLL at r.t. during 4 days using HT _{rus} as initiator in excess	ROP	4	4.1.1
PLL _C	Commercial PLL	Commercial available	-	-
IPL _C	PLL _C immobilised in HT _{rus}	Anionic exchange 1	4	3.1.2

Diagram of methods



CONTENTS

ACKNOWLEDGEMENTS (Agradecimientos)	IX
PREFACE	XIII
LIST OF MATERIALS USED IN THIS DOCUMENT	XV
CONTENTS	XVIII

CHAPTER 1. Introduction and Scope

1. Bio-nano hybrid materials	2
1.1 Hydrotalcite-like materials	4
1.1.1 <i>Synthesis of HTs</i>	6
1.1.2 <i>Accesibility of the Brönsted-Base sites in rehydrated HT</i>	7
1.1.3 <i>Ion-exchange properties</i>	7
1.2 Amino acids and poly-amino acids	8
1.2.1 <i>Synthesis of poly-amino acids</i>	10
1.3 Bio-nano hybrid materials based on AAs, PAAs and HTs	14
1.3.1 <i>Synthesis of AAs immobilised in HTs (AA/HTs)</i>	14
1.3.2 <i>Synthesis of PAAs immobilised in HTs (PAA/HTs)</i>	20
2. Bio-nano hybrid materials as catalysts	22
2.1 Juliá-Colonna Asymmetric Epoxidation Reaction	23
2.2.1 <i>Three-phase system for Juliá-Colonna epoxidation using a phase-transfer co-catalyst (PTC)</i>	27
2.2.2 <i>Mechanistic considerations</i>	27
2.2 Direct asymmetric aldol reaction	29
2.2.1 <i>Intramolecular asymmetric aldol reaction</i>	30
2.2.2 <i>Aldol reaction catalysed by HTs</i>	36
2.2.3 <i>Aldol reaction catalysed by L-Pro immobilised in HTs</i>	37
2.3 One-pot reaction	38
2.3.1 <i>Claisen-Schmidt reaction</i>	38
2.3.2 <i>Claisen-Schmidt-Juliá-Colonna one-pot reaction</i>	39

3	Scope of this thesis	41
	References	43

CHAPTER 2. Synthesis and characterisation of nanohybrid materials based on L-Leucine and L-Proline immobilised on hydrotalcite-like materials

1.	Initial Considerations	52
2.	Nanohybrid materials based on L-Leucine immobilised on hydrotalcite-like materials	53
2.1	Experimental	53
2.1.1	<i>Synthesis of HTs</i>	53
2.1.2	<i>Synthesis of LL/HT materials</i>	54
2.2	Results and discussion	55
2.2.1	<i>X-ray diffraction and High Resolution TEM results</i>	56
2.2.2	<i>FT-IR and Raman spectroscopy results</i>	59
2.2.3	<i>MAS NMR spectroscopy results</i>	65
2.2.4	<i>Thermal evolution of HT and LL/HT materials</i>	67
2.2.5	<i>Nature of the organic/inorganic interaction</i>	74
3.	Nanohybrid materials based on L-Proline immobilised on hydrotalcite-like materials	77
3.1	Experimental	77
3.1.1	<i>Synthesis of HTs</i>	77
3.1.2	<i>Synthesis of LP/HT materials</i>	77
3.2	Results and discussion	80
3.2.1	<i>X-ray diffraction results</i>	80
3.2.2	<i>FT-IR and Raman spectroscopy results</i>	83
3.2.3	<i>MAS NMR spectroscopy results</i>	90
3.2.4	<i>Thermal evolution of LP/HT materials</i>	91
3.2.5	<i>Nature of the organic/inorganic interaction</i>	94
4	Conclusions	97
	References	99

CHAPTER 3. Nanohybrid materials based on AA and HTs as catalysts in fine chemistry reactions

1.	Initial considerations	104
2.	LL/HT nanohybrid materials as catalysts in asymmetric Juliá-Colonna epoxidation reaction	105
2.1	Experimental	105
2.1.1	<i>Synthesis of LL/HT materials</i>	105
2.1.2	<i>Asymmetric Juliá-Colonna epoxidation reaction</i>	106
2.2	Results and discussion	107
2.2.1	<i>Preliminary studies</i>	107
2.2.2	<i>Catalytic results</i>	108
3.	LP/HT Nanohybrid Materials as Catalysts in Direct Asymmetric Aldol Reaction	111
3.1	Experimental	112
3.1.1	<i>Synthesis of LP/HT materials</i>	112
3.1.2	<i>Direct asymmetric aldol reaction</i>	112
3.2	Results and discussion	114
3.2.1	<i>Preliminary studies</i>	114
3.2.2	<i>Catalytic evaluation</i>	115
4	Conclusions	120
	References	121

CHAPTER 4. Synthesis and characterisation of Poly-L-Leucine initialised and immobilised by rehydrated hydrotalcite

1.	Initial Considerations	124
2.	Synthesis of Poly-L-Leucine materials using triethylamine	125
2.1	Experimental	125
2.1.1	<i>Synthesis of α-Leucine-N-carboxy anhydride (NCA)</i>	125
2.1.2	<i>Synthesis of Poly-L-Leucine</i>	126
2.2	Results and discussion	126
2.2.1	<i>MALDI-TOF results</i>	127
2.2.2	<i>FT-IR and Raman spectroscopy results</i>	133

3.	Immobilisation of synthesised PLL in HT_{rus}	135
3.1	Experimental	135
3.1.1	<i>Synthesis of rehydrated hydrotalcite (HT_{rus})</i>	135
3.1.2	<i>Synthesis of Poly-L-Leu/HT materials</i>	135
3.2	Results and discussion	135
3.2.1	<i>X-ray diffraction and High Resolution TEM results</i>	136
3.2.2	<i>MALDI-TOF results</i>	137
3.2.3	<i>FT-IR and Raman spectroscopy results</i>	140
4.	Synthesis of Poly-L-Leucine using green initiators: water and HT_{rus}	142
4.1	Experimental	142
4.1.1	<i>Synthesis of PLL materials</i>	142
4.2	Results and discussion	142
4.2.1	<i>MALDI-TOF results</i>	143
4.2.2	<i>FT-IR and Raman spectroscopy results</i>	145
4.2.3	<i>3.2.1 X-ray diffraction and High Resolution TEM results</i>	148
5.	Thermal evolution of the synthesised materials	149
5.1	Thermal evolution of synthesised PLL	149
5.2	Thermal evolution of PLL/HT_{rus} nanohybrid materials	152
6.	Conclusions	156
	References	158

CHAPTER 5. Nanohybrid materials based on PLL and HTs as catalysts in fine chemistry reactions

1.	Initial Considerations	162
2.	PLL/HT nanohybrid materials as catalyst in asymmetric Juliá-Colonna epoxidation reaction	164
2.1	Experimental	164
2.1.1	<i>Synthesis of PLL and PLL/HT materials</i>	164
2.1.2	<i>Asymmetric Juliá-Colonna epoxidation reaction</i>	164

2.2	Results and discussion	164
2.2.1	<i>Asymmetric catalytic Juliá-Colonna epoxidation with non immobilised PLLs</i>	167
2.2.2	<i>Asymmetric catalytic Juliá-Colonna epoxidation with nanohybrid PLLs: reusability of nanohybrid materials</i>	170
3.	PLL/HT nanohybrid materials as catalyst in Claisen-Schmidt-Juliá-Colonna one-pot reaction	173
3.1	Experimental	173
3.1.1	<i>Synthesis of materials</i>	173
3.1.2	<i>Claisen-Schmidt reaction</i>	173
3.1.3	<i>Claisen-Schmidt-Juliá-Colonna one-pot reaction</i>	174
3.2	Results and discussion	175
3.2.1	<i>Claisen-Schmidt reaction</i>	175
3.2.2	<i>Claisen-Schmidt-Juliá-Colonna one-pot reaction</i>	177
4	Conclusions	181
	References	183
CHAPTER 6. Summary of this thesis		
		185
ANNEX 1. General information		
		189
ANNEX 2. Characterisation techniques		
		191
ANNEX 3. Characterisation results		
1.	Characterisation results from Chapter 2	193
2.	Characterisation results from Chapter 4	195
3.	Characterisation results from Chapter 5	197
ANNEX 4. Publications		
		201

SYNTHESIS AND CHARACTERISATION OF NANOHYBRID MATERIALS
BASED ON L-LEUCINE AND L-PROLINE IMMOBILISED ON HYDROTALCITE-
LIKE MATERIALS

Recently, considerable attention has been focused on the synthesis of new nanoscale materials which are chemically bound in an organised way. The nanomaterials often exhibit unique physical and chemical properties that are dramatically different and/or complementary from their component materials. In this way, the understanding of the interactions between all components provides a new paradigm in the efficient design and synthesis of functional nanostructure materials according with their future applications. This chapter attempts to rationalise the design, synthesis and characterisation of nanohybrid materials based on L-Leu and L-Pro using different preparation methods. Moreover, location and nature of the immobilised amino acid were further investigated to clarify the role of the immobilisation conditions in the stability of the L-Leu and L-Pro immobilised on HT-like materials.

-
- 1. Initial considerations**
 - 2. Nanohybrid materials based on L-Leucine immobilised on hydrotalcite-like materials**
 - 2.1 Experimental
 - 2.2 Results and discussion
 - 3. Nanohybrid materials based on L-Proline immobilised on hydrotalcite-like materials**
 - 3.1 Experimental
 - 3.2 Results and discussion
 - 4. Conclusions**
- References**
-

1. Initial Considerations

Nowadays, there is a considerable attention focused in the synthesis of nanohybrid materials which often exhibit extraordinary high synergistic and complementary behaviour between two components [1,2]. In this way, investigation and understanding of organic/inorganic interaction between bioactive molecules and the surface of inorganic materials have permitted their use as catalysts, carriers for drug delivery and geochemical supports [3-8]; however, organic/inorganic interactions remain incompletely understood. Many bioactive molecules (e.g. peptides, sugars, AAs, proteins, nucleic acids) are anions under natural and basic pH values so their interaction with positively charged solids should allow nanohybrid materials with strong interactions. One of this kind of materials are the HTs which are a family of naturally occurring layered clays which have low or null toxicity, good biocompatibility and high capacity of anion swelling. These properties have made the HTs interesting materials for applications in pharmaceutical, cosmetic, biochemistry, catalysis and even medical fields [7,9-11].

Due to the excellent anion exchange properties, HTs have been used as support in synthesis of nanohybrid materials. In this context, AAs which are anions in certain pH conditions, and have relative low molecular weight, have been immobilised in HTs. Particularly, understanding the interaction nature between AAs and HTs materials allows important information for the study of more complex organic matters such as peptides, proteins or hormones. In this context, many works have been reported using intercalation of AAs in HTs by three main methodologies: co-precipitation [7,12-18], ion-exchange [4,19] and reconstruction [3,20,21]. Using the co-precipitation method, immobilisation degrees between 0.35 mmol of glutamate/mol Al^{3+} and 1.09 mol Phe/ mol Al^{3+} have been reported. Choudary *et al.* reported the immobilisation of L-Pro in HT Mg/Al (3/1) using an anionic exchange protocol of 24 hours at 65°C obtaining an immobilisation ratio of 0.06 mol Proline/mol Al^{3+} [4]. Finally, by reconstruction method Narita *et al.* reported the highest immobilisation ratio (2.45 mol Phe/ mol Al^{3+}) in a synthesis which spent 14 days [21]. About the nature of the interaction, nowadays it is well known that immobilisation of AAs in HTs structures is pH dependent, nevertheless other factors such as the kind of HTs, conditions of synthesis, and

physical and chemical properties of the used AAs afford diverse materials which could be different among themselves. In this chapter we present the synthesis of nanohybrid materials based on L-Leu and L-Pro immobilised in HTs. Different synthetic procedures and their effects in the nature of the inorganic/organic interaction was studied to evaluate: i) the role of the immobilisation time and the relationship between the immobilisation speed and the strength and kind of basic centers in the HT; ii) the role of the HT precursor in the immobilisation process and iii) the nature of the AA structure in the immobilisation process.

2. Nanohybrid materials based on L-Leucine immobilised in hydrotalcite-like materials

In this section, nanohybrid materials were synthesised by anion-exchange and reconstruction method. The organic/inorganic interaction was investigated by EA, ICP, XRD, FT-IR, Raman, ^{13}C , ^{27}Al MAS NMR and thermal evolution using TG/DTA analyses and *in situ* FT-IR under outgassing conditions at increasing temperature'. In this section our interest was focused on clarifying the role of the protocol conditions in the synthesis of diverse kinds of L-Leu/HT materials with controllable location of the immobilised L-Leu.

2.1 Experimental

2.1.1 Synthesis of HTs

Mg-Al hydrotalcite with Mg/Al molar ratio = 2 containing nitrates [21] and chloride anions [22] were synthesised by co-precipitation method at constant pH = 10,5 and at room temperature. The obtained materials were named HT_{asym} and HT_{Cl} respectively. After drying process, HT_{Cl} was sonicated for 1 hour, while HT_{asym} was decomposed by calcination at 450°C overnight in air atmosphere. The calcined HT (HT_{cc}) was rehydrated under inert atmosphere using decarbonated water and ultrasound treatment for 1 hour. The obtained materials were named: HT_{Clus} and HT_{rus} respectively.

* A complete description of equipment and analytic methods is presented in Annex 2.

2.1.2 Synthesis of LL/HT materials

The nanohybrid materials were prepared by ion-exchange and reconstruction methods using deionised-decarbonated water under Ar atmosphere as follows:

2.1.2.1 Anionic-exchange method (Method A)

Two procedures were used to synthesise LL/HT_x-A_y_z materials. First, 500 mg of HT was added to a solution containing 320 or 160 mg (3.0 or 1.1 mmol, respectively) of L-Leu. The mixture was stirred during 30 min at room temperature (method A1). Second, 500 mg of HT were added to a solution containing 840.4 mg (6.4 mmol) of L-Leu. The mixture was stirred for 3 hours at 80°C (Method A2). In all cases, Ar atmosphere and deionised-decarbonated water were needed. Obtained materials were denoted as LL/HT_x-A_y_z, where *x* corresponds to the kind of HT (rus and Clus), *y* indicates the procedure followed (1 or 2) and *z* the amount of immobilised L-Leu determined by EA and ICP analyses. Materials synthesised by this method were named: LL/HT_{rus}-A1_{0.44}, LL/HT_{rus}-A1_{0.22}, LL/HT_{Clus}-A1_{0.04}, LL/HT_{rus}-A2_{1.09} and LL/HT_{Clus}-A2_{0.16}.

2.1.2.2 Reconstruction method (Method R)

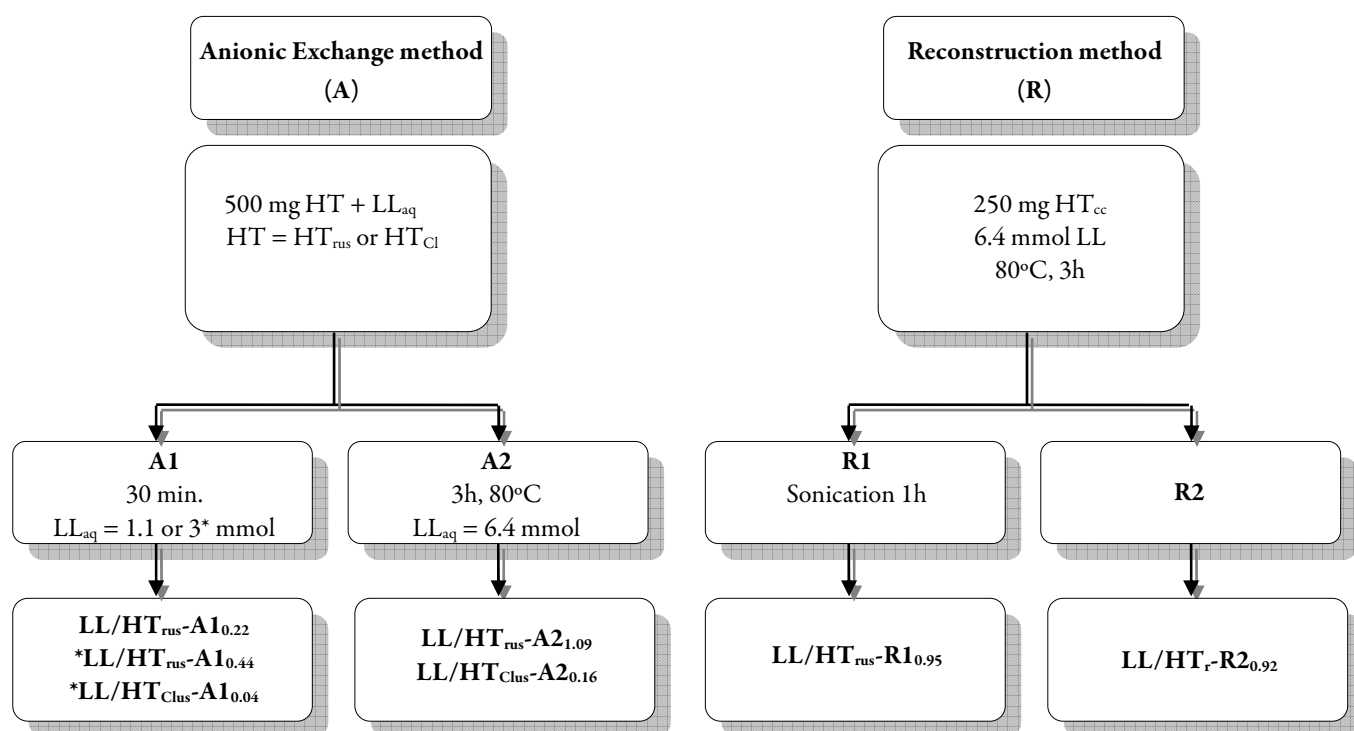
Two procedures were used to synthesise LL/HT_x-R_y_z materials using in both cases 250 mg of HT_{cc} added to a solution containing 736.9 mg (6.4 mmol) of L-Leu. First, L-Leu-HT_{cc} mixture was treated by sonication during 1 h and stirred during 30 min. After this process, the slurry was stirred during 3 h more at 80°C. The obtained material was named LL/HT_{rus}-R1_{0.95} (Method R1). Second, HT_{cc}-L-Leu mixture was stirred during 3 h at 80°C (Method R2). The obtained material was named LL/HT_r-R2_{0.92}.

Schematic representations of all synthetic methods are presented in Scheme 1.

* LL/HT_{Cl}-A1_{0.04} material was synthesized using 3 mmol of L-Leu.

2. Nanohybrid materials based on L-Leucine and HT-like materials

2.1 Experimental



Scheme 1 Summary of the synthesis methods

2.2 Results and discussion

Using the methodologies described below it was possible to study the organic/inorganic interaction in the synthesised LL/HT materials. Molecular formulae of all LL/HT materials are presented in Table 1.

Table 1 Characterisation data of HT and LL/HT materials

Entry	Material ^a	Molecular Formulae ^b
1	HT _{asym}	[Mg _{2.53} Al _{1.00} (OH) _{7.07}](CO ₃ ²⁻) _{0.85} (NO ₃ ⁻) _{3.15} •0.89H ₂ O
2	HT _{cc}	Mg _{2.53} Al _{1.00} (O) _x (CO ₃ ²⁻) _{0.32} (NO ₃ ⁻) _{0.10}
3	HT _{rus}	[Mg _{2.53} Al _{1.00} (OH) _{7.07}](CO ₃ ²⁻) _{1.18} (NO ₃ ⁻) _{0.10} •1.10H ₂ O
4	HT _{Cl}	[Mg _{2.31} Al _{1.00} (OH) _{6.62}](CO ₃ ²⁻) _{0.84} (Cl ⁻) _{0.52} •0.91H ₂ O
5	L-Leu	C ₆ H ₁₃ NO ₂
6	LL/HT _{rus} -A1 _{0.22}	[Mg _{2.63} Al _{1.00} (OH) _{7.25}](Leu) _{0.22} (CO ₃ ²⁻) _{2.36} (NO ₃ ⁻) _{0.10} •1.34H ₂ O
7	LL/HT _{rus} -A1 _{0.44}	[Mg _{2.63} Al _{1.00} (OH) _{7.25}](Leu) _{0.44} (CO ₃ ²⁻) _{2.30} (NO ₃ ⁻) _{0.10} •1.34H ₂ O
8	LL/HT _{Clus} -A1 _{0.04}	[Mg _{2.31} Al _{1.00} (OH) _{6.62}](Leu) _{0.04} (CO ₃ ²⁻) _{1.77} (Cl ⁻) _{0.52} •0.79H ₂ O
9	LL/HT _{rus} -A2 _{1.09}	[Mg _{2.39} Al _{1.00} (OH) _{6.79}](Leu) _{1.09} (CO ₃ ²⁻) _{1.19} (NO ₃ ⁻) _{0.10} •1.34H ₂ O
10	LL/HT _{Clus} -A2 _{0.16}	[Mg _{2.31} Al _{1.00} (OH) _{6.62}](Leu) _{0.16} (CO ₃ ²⁻) _{1.77} (Cl ⁻) _{0.52} •0.88H ₂ O
11	LL/HT _{rus} -R1 _{0.95}	[Mg _{2.63} Al _{1.00} (OH) _{7.25}](Leu) _{0.95} (CO ₃ ²⁻) _{3.34} (NO ₃ ⁻) _{0.10} •2.03H ₂ O
12	LL/HT _r -R2 _{0.92}	[Mg _{2.63} Al _{1.00} (OH) _{7.25}](Leu) _{0.92} (CO ₃ ²⁻) _{2.99} (NO ₃ ⁻) _{0.10} •1.80H ₂ O

^aSynthesis Conditions: Anionic exchange 1 (A1): HT and a solution of L-Leu were mixed and stirring during 0.5 h at r.t. Anionic exchange 2 (A2): HT and a solution of L-Leu were mixed and stirring for 3 h at 80°C. Reconstruction 1 (R1): HT_{cc} and a solution of L-Leu were mixed and sonicated for 1 h, following by stirring during 3 h at 80°C. Reconstruction 2 (R2): HT_{cc} and a solution of L-Leu were mixed and stirred for 3 h at 80°C. ^bCalculated by EA and ICP analysis. Water content was calculated by TG/DTA. ^cHT = hydrotalcite. HT_{asym} = As-synthesised HT. HT_{cc} = Calcined HT. HT_{rus} = rehydrated HT under ultrasound treatment. HT_{Cl} = As-synthesised HT containing chloride anions. HT_{Clus} = HT_{Cl} after ultrasound treatment.

2.2.1 X-ray diffraction and High Resolution TEM results

2.2.1.1 Nanohybrid synthesised by anionic exchange method

XRD patterns of nanohybrid materials synthesised by anionic exchange are presented in Figure 2. In all cases, the obtained materials exhibit the characteristic diffraction peaks of the meixnerite structure (JCPDS 35-0965). In agreement with Cavani *et al.*, HT_{rus} which mainly contains hydroxyl anions presented the main diffraction peak at 11.4 2 θ corresponding to a d_{003} =7.7 Å [23] (Figure 2a), whereas in the case of HT_{Clus}, this parameter was calculated as d_{003} =7.9 Å (Figure 2d).

XRD pattern of LL/HT_{Clus}-A1_{0.04} and LL/HT_{Clus}-A2_{0.16} (Figures 1f and 1g) confirmed that L-Leu molecules could not be highly exchanged by chloride anions (Table 1, entries 8 and 10); moreover, these results show that basic centers located on the HT surface are not strong enough to immobilise highly amount of L-Leu molecules.

XRD pattern of LL/HT_{rus}-A1 nanohybrid materials (Figure 1b) shows that d_{003} remained unchanged at 7.7 Å even after the anion exchange process. This observation indicates that L-Leu was immobilised on the edges of the HT_{rus} layers. The effect of the increasing amount of immobilised L-Leu is also observed in the XRD patterns through the loss of HT's crystallinity (Figure 2a-c).

* All HRTEM analyses presented in this thesis were performed at Institut de Tècniques Energètica from Universitat Politècnica de Catalunya (Spain) in collaboration with Prof. Dr. Jordi Llorca.

2.2 Results and discussion – XRD and HRTEM results

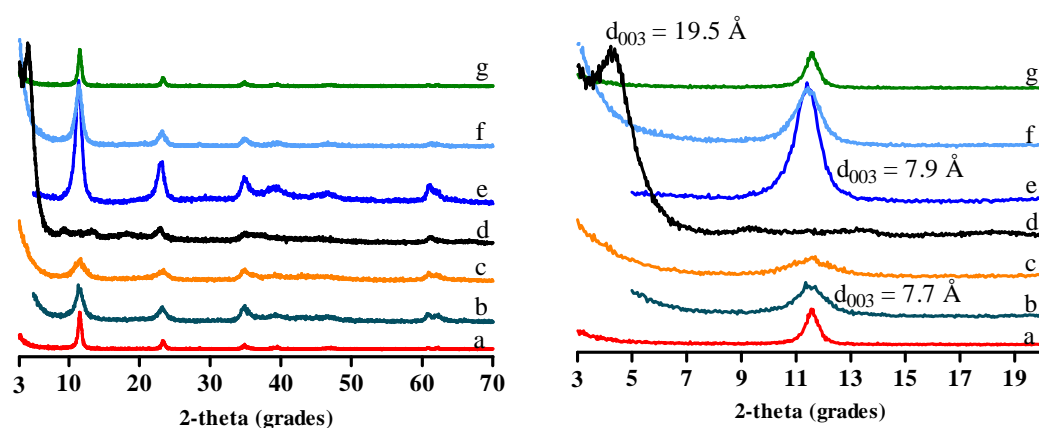


Figure 1 (left) XRD patterns of a) HT_{rus}, b) LL/HT_{rus}-A1_{0.22}, c) LL/HT_{rus}-A1_{0.44}, d) LL/HT_{rus}-A2_{1.09}, e) HT_{Clus}, f) LL/HT_{Clus}-A1_{0.04} and g) LL/HT_{Clus}-A2_{0.16}. (Right) XRD pattern in the 2θ range: 3-20°.

Increasing time and temperature of synthesis to obtain LL/HT_{rus}-A2_{1.09} also increased the amount of immobilised L-Leu to 1.09 mol L-Leu/mol Al³⁺. In this case the main diffraction peak shifted to 4.4 2 θ indicating increase of the interlayer space up to 19.9 Å. This finding shows that increase of the time and temperature of synthesis favour the swelling of the HT structure permitting the immobilisation of L-Leu molecules in its interlayer space. Loss of crystallinity in all nanohybrid materials was due to the decrease of the layers lengths by ultrasound effect.

HRTEM images of HT_{rus}, LL/HT_{rus}-A1_{0.22}, LL/HT_{rus}-A1_{0.44} and LL/HT_{rus}-A2_{1.09} are presented in Figure 2. HT_{rus} image (Figure 2a) shows aggregated layers up to about 100 nm in length with interlayer space around 7.6 Å as it was deduced by FT analysis.

HRTEM images of LL/HT_{rus}-A1_{0.22} and LL/HT_{rus}-A1_{0.44} (Figure 2a and 2b) show the layered morphology indistinguishable from that of the starting HT material. Moreover, any variation of the interlayer space indicates that the HT structure has not been altered by the presence of L-Leu, as well as L-Leu has not been incorporated into the HT layers. In contrast, HRTEM image of LL/HT_{rus}-A2_{1.09} (Figure 2d) exhibits a quite distinctive morphology. HT layers are no longer well-preserved and they show a low-order layer arrangement. Interlayer space was calculated by FT analysis in 19.2-19.8 Å recorded over all sample agreeing with the XRD analyses.

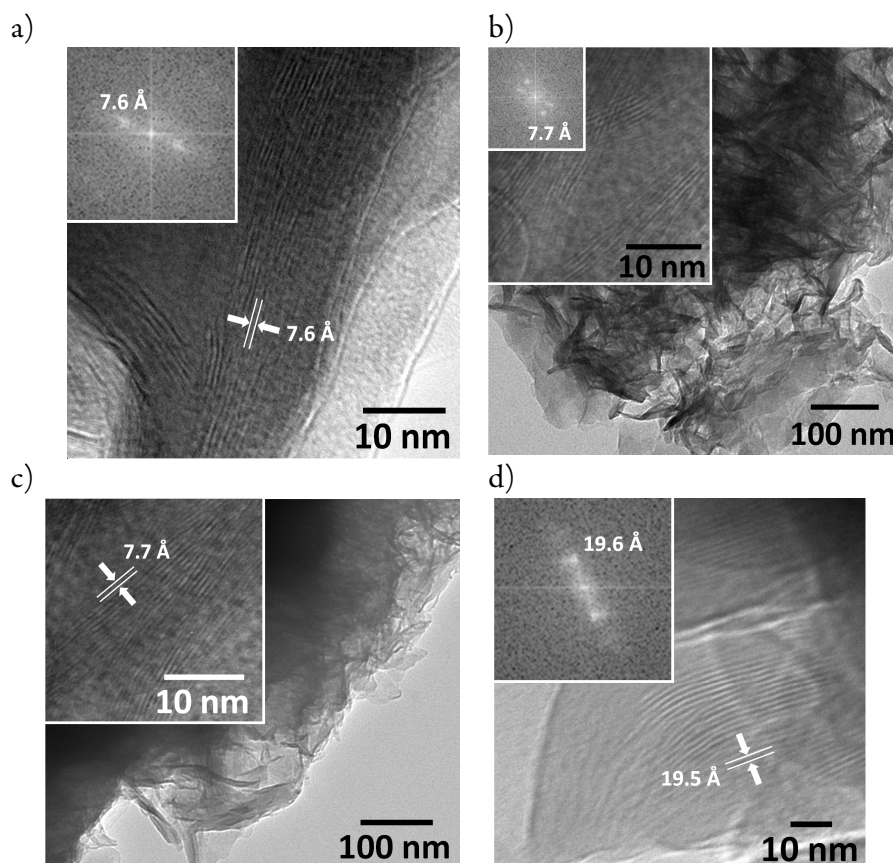


Figure 2 HRTEM images of the nanohybrids synthesised by anionic-exchange method: a) HT_{rus} , b) $LL/HT_{rus-A1_{0.22}}$, c) $LL/HT_{rus-A1_{0.44}}$ and d) $LL/HT_{rus-A2_{1.09}}$.

2.2.1.2 Nanohybrid synthesised by reconstruction method

XRD patterns of nanohybrid materials synthesised by reconstruction method are presented in Figure 3.

$LL/HT_{rus-R1_{0.95}}$ (Figure 4b) and $LL/HT_r-R2_{0.92}$ (Figure 3c) materials also exhibit an increased interlayer space up to around 20 Å. HRTEM images of the nanohybrid materials synthesised by this protocol (Figure 4) do not conserve the layer morphology of their HT precursor. Moreover, a detailed HRTEM analysis reveals interlayer spacing at 22.5-22.6 Å indicating that the immobilisation of L-Leu molecules occurs in the interlayer space from the HT. In addition to basal planes at 22.5-22.6 Å, both $LL/HT_{rus-R1_{0.95}}$ and $LL/HT_r-R2_{0.92}$ materials depicts lattice fringes at 14.8-14.9 Å.

2.2 Nanohybrid materials based on L-Leucine and HT-like materials

2.2 Results and discussion – XRD and HRTEM results

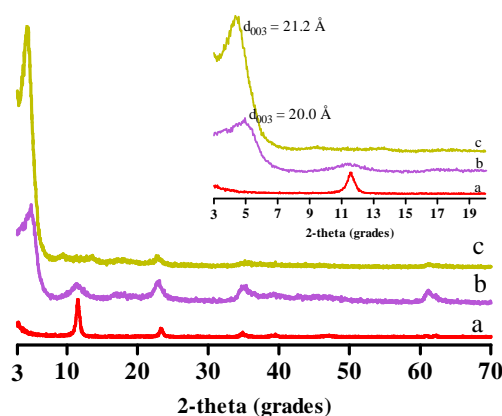


Figure 3 XRD patterns of (a) HT_{rus}, b) LL/HT_{rus}-R1_{0.95} and c) LL/HT_r-R2_{0.92}. Inset: XRD pattern in the 2θ range: 3-20°.

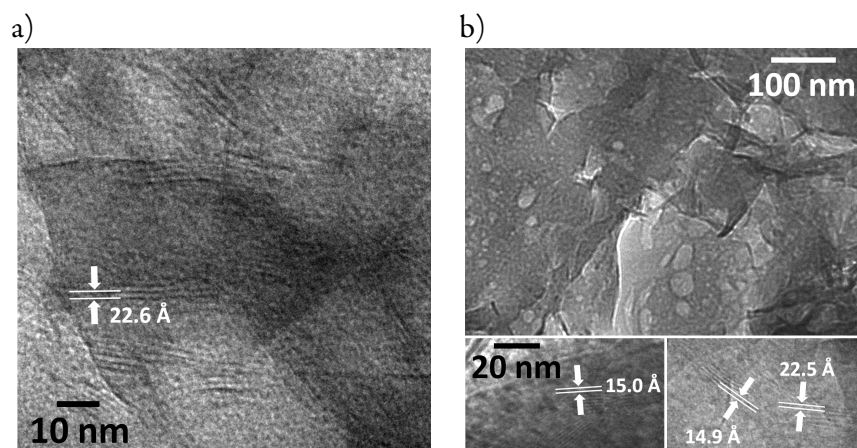


Figure 4 HRTEM images of the nanohybrids synthesised by reconstruction method: a) LL/HT_{rus}-R1_{0.95} and b) LL/HT_r-R2_{0.92}.

2.2.2 FT-IR and Raman spectroscopy results*

Skeletal FT-IR and Raman spectra of L-Leu, HT_{clus} and HT_{rus} are presented in Figure 5. FT-IR spectrum of commercial available L-Leu in KBr (Figure 5a, left) shows the zwitterionic nature of L-Leu. Bands due to $\nu(\text{NH}_3^+)$ and their deformations are detected at 3058, 2130, 1610 and 1516 cm^{-1} . Asymmetric, $\nu_a(\text{COO}^-)$, and symmetric, $\nu_s(\text{COO}^-)$, stretching bands of COO^- group are detected at 1581 and 1407 cm^{-1} . The broad band at 3378 cm^{-1} has been assigned to O-H interaction between different molecules of L-Leu, while the bands at 2957 and 2871 cm^{-1} correspond to the CH_3 stretching vibrations. In the Raman spectrum (Figure 5a, right), bands around 2886, 1227 and 835 cm^{-1} are due to CH stretching modes. Bands due to COO^- group

* All FT-IR spectra presented in this thesis were performed in Dipartimento di Ingegneria Chimica e di Processo "G.B. Bonino" form Università di Genova (Italy) during Mr. Miranda research stay. This stay was supervised by Prof. Dr. Gianguido Ramis in collaboration with Prof. Dr. Elisabetta Finocchio.

are detected at 1454, 1297, 1129, 835, 776 and 553 cm^{-1} , while bands due to NH_3^+ group are detected at 2987, 1625, 1583 and 1187 cm^{-1} [24,25].

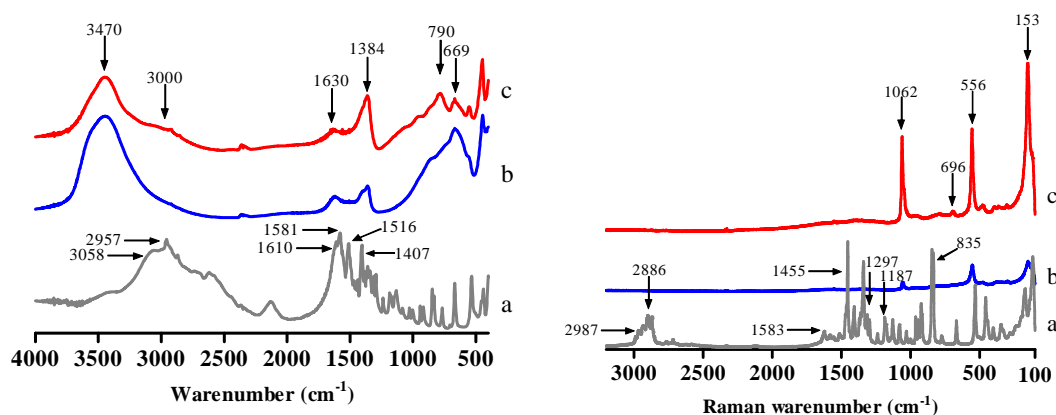


Figure 5 Skeletal FT-IR (left) and Raman (right) spectra of a) L-Leu, b) HT_{Clus} and c) HT_{rus} .

Skeletal FT-IR spectra of HT materials (Figure 5b and 5c, left) show a strong band between 3600 and 3000 cm^{-1} attributed to the twisting vibration of physisorbed water, CO_3^{2-} - H_2O bridging mode of the carbonate anions, vibration of the structural -OH groups and characteristic stretching modes of M-OH species [26]. In the low frequency, bands at 880 and 669 cm^{-1} are characteristic for the ν_4 (in-plane bending) and the ν_2 (out-plane deformation) of CO_3^{2-} ions. Bands at 790 and 554 cm^{-1} with their deformations at 925 and 1050 cm^{-1} are due to OH⁻ groups influenced by Al^{3+} . While bands at 635, 600 and 590 cm^{-1} are assigned to Al-OH groups influenced by Mg^{2+} ions. The broad band at 1630 cm^{-1} is due to the HOH bending vibration of physisorbed water. Higher intensity in bands at 3000 and 1384 cm^{-1} in HT_{rus} demonstrated higher reactivity of the basic centres which can interact easily with atmospheric CO_2 during its manipulation [10,27]. In the Raman spectra (Figure 5a and 5b, right), the interlayered carbonate ions are detected as a very strong and sharp band at 1061 cm^{-1} due to ν_1 mode and a very weak band at 694 cm^{-1} due to ν_4 mode of CO_3^{2-} ions. The band at 556 cm^{-1} is due to hydroxyl groups associated with mainly Al^{3+} metal, but also influenced by probably one Mg^{2+} in its coordination environment [26]. Finally, although the band at 153 cm^{-1} cannot be formerly assigned, this signal is likely related to framework vibrations [28].

2.2.2.1 Nanohybrid materials synthesised by anionic exchange method

Although basicity of the HTs is affected by the nature of the anions located in the interlayer space [22], we use HT_{Cl} because the anion exchange of Cl⁻ in the interlayer is difficult. So, as an approximation, surface of HT_{Cl} presents basic sites where the L-Leu can interact. Nevertheless, FT-IR (left) and Raman (right) spectra of LL/HT_{Clus}-A1_{0.04} do not present evidence of L-Leu immobilisation suggesting that from a general point of view, the immobilisation process does not occur on the surface of the HT material (Figure 6c). However, FT-IR spectrum of LL/HT_{Clus}-A2_{0.16} material, which was synthesised during 3 hours at 80°C, presents some differences respect to its HT precursor (Figure 6d, left). At high frequency, the bands at 2957 and 1581 cm⁻¹ are possibly due to some L-Leu molecules interacting with HT material. At low frequency, differences in the bands at 970, 790 and 553 cm⁻¹ respect to HT precursor suggest changes in the Al-OH species. These changes could be due to an increase in the water content, presence of higher amount of OH⁻ anions and some L-Leu molecules immobilised in the HT structure. However, Raman spectrum of LL/HT_{Clus}-A2_{0.16} does not present any evidence of immobilised L-Leu (Figure 6d, right).

FT-IR spectra of nanohybrid materials synthesised using HT_{rus} material besides the vibrational bands typical of the HT precursor, previously discussed, and the sharp components attributed to L-Leu which indicate its successful immobilisation. LL/HT_{rus}-A1_{0.22} FT-IR and Raman spectra (Figure 6f) exhibit bands due to immobilised L-Leu with small intensity which are according to the EA results (Table 1, entry 6), nevertheless, this effect makes the interpretation of the interaction nature difficult. Moreover, LL/HT_{rus}-A1_{0.44} and LL/HT_{rus}-A1_{1.09} spectra exhibit the bands due to C-H stretching mode at 2957 (ν_{CH}) and 2871 cm⁻¹ (ν_{CH₃}) confirming the higher immobilisation of the L-Leu.

FT-IR spectrum of LL/HT_{rus}-A1_{0.44} material (Figure 6g, left) exhibits the ν_{a(COO⁻)} and ν_{s(COO⁻)} stretching at 1560 and 1407 cm⁻¹ respectively, while bands due to NH₃⁺ group were not clearly detected. These findings show that immobilisation process occurred by anionic exchange between anionic L-Leu and the OH⁻ groups located on the HT edges. In a similar way, in the FT-IR spectrum of LL/HT_{rus}-A2_{1.09} material (Figure 6h, left) the ν_{a(COO⁻)} stretching at 1560 cm⁻¹ indicates the presence of the anionic L-Leu. An exhaustive study of this spectrum also shows small bands at 1581, 1610 and 1516 cm⁻¹ due to COO⁻ and NH₃⁺ groups of the zwitterionic L-

Leu. Decrease in the band due to CO_3^{2-} species at 1384 cm^{-1} in $\text{LL}/\text{HT}_{\text{rus}}\text{-A1}_{0.44}$ and $\text{LL}/\text{HT}_{\text{rus}}\text{-A2}_{1.09}$ materials suggests that the incorporation of the L-Leu in the materials causes the displacement of physisorbed water and the competition with the adsorption of CO_3^{2-} anions [18,29].

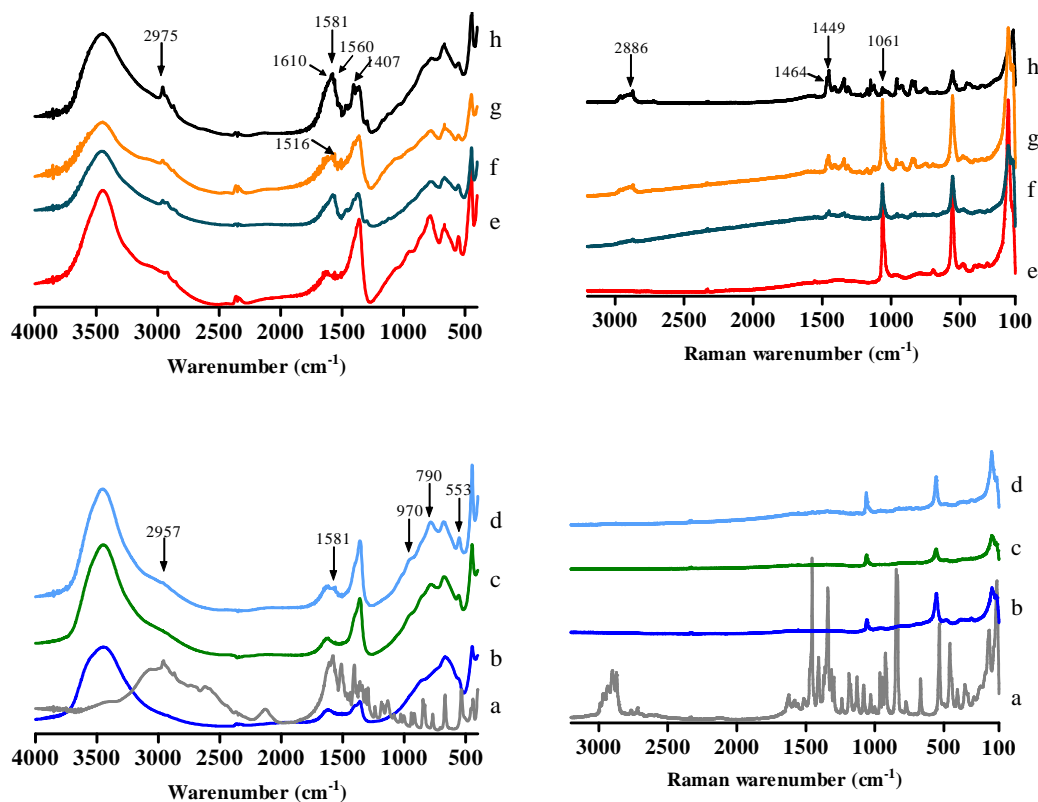


Figure 6 Skeletal FT-IR (left) and Raman (right) spectra of a) L-Leu, b) HT_{Cl} , c) $\text{LL}/\text{HT}_{\text{Clus}}\text{-A1}_{0.04}$, d) $\text{LL}/\text{HT}_{\text{Clus}}\text{-A2}_{0.16}$, e) HT_{rus} , f) $\text{LL}/\text{HT}_{\text{rus}}\text{-A1}_{0.22}$, g) $\text{LL}/\text{HT}_{\text{rus}}\text{-A1}_{0.44}$ and h) $\text{LL}/\text{HT}_{\text{rus}}\text{-A2}_{1.09}$.

Raman spectra of $\text{LL}/\text{HT}_{\text{rus}}\text{-A1}_{0.44}$ and $\text{LL}/\text{HT}_{\text{rus}}\text{-A2}_{1.09}$ materials (Figure 6g and 6h, right) present bands at 2886 , 1227 and 835 cm^{-1} due to CH stretching modes. In the case of $\text{LL}/\text{HT}_{\text{rus}}\text{-A1}_{0.44}$ material (Figure 6g, right) no strong conclusion could be drawn due to low intensity of the bands. In $\text{LL}/\text{HT}_{\text{rus}}\text{-A2}_{1.09}$ Raman spectrum (Figure 6h, right) bands at 1471 and 1455 cm^{-1} due to COO^- group in pure L-Leu shifted to 1464 and 1449 cm^{-1} , respectively. As well as the relative intensity between both bands changes after immobilisation. These shifts suggest the presence of two kinds of COO^- groups in L-Leu (anionic and zwitterionic). Changes in the relative intensity also indicate that both kinds of COO^- are interacting with the HT structure, anions located in the interlayer space and/or other L-Leu molecules. Moreover,

2.2 Results and discussion – FT-IR and Raman results

relative intensity of the band at 1061 cm^{-1} due to CO_3^{2-} species decreased after L-Leu immobilisation confirming the lower incorporation of atmospheric CO_2 in the HT structure.

2.2.2.2 Nanohybrid materials synthesised by reconstruction method

FT-IR (left) and Raman (right) spectra of nanohybrid materials synthesised by reconstruction method are presented in Figure 8. FT-IR spectrum of LL/HT_r-R2_{0.92} (Figure 8d, left) was completely consistent with the spectrum of pure L-Leu (Figure 7a). The broad bands at 3064 cm^{-1} and around 2700 cm^{-1} are assigned to stretching vibration and Fermi resonance modes of the NH_3^+ group, respectively. As well, the band at 2130 cm^{-1} resembles to the similar band in the spectra of amine hydrochlorides and is due to a combination band of asymmetric deformation and hindered rotation of NH_3^+ groups [30]. The relative intensity of the band at 2130 cm^{-1} and the peaks assigned to NH_3^+ group decreased following immobilisation. A possible explanation is the formation of H-bonds between the NH_3^+ group and the oxygen atoms of the HT layers. Additionally, bands due to $\nu_{\text{a}}(\text{COO}^-)$ and $\nu_{\text{s}}(\text{COO}^-)$ stretching were detected at 1581 and 1407 cm^{-1} similar to pure L-Leu. Although bands due to anionic L-Leu are not ruled out, it is clear that immobilised L-Leu using HT_{cc} without ultrasound treatment occurs mostly in its zwitterionic form.

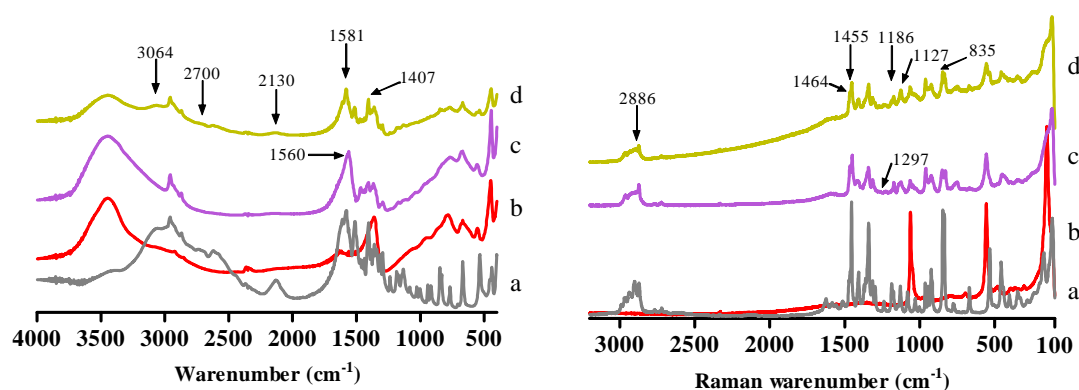


Figure 7 Skeletal FT-IR (left) and Raman (right) spectra of a) L-Leu, b) HT_{rus}, c) LL/HT_{rus}-R1_{0.95} and d) LL/HT_r-R2_{0.92}.

One possible explanation of this effect is because during the synthesis of LL/HT_r-R2_{0.92}, L-Leu molecules were interacting with the -OH groups of the forming HT layers, while the positive charge of the layer was compensated by OH⁻ anions. Raman spectrum of LL/HT_r-R2_{0.92} material (Figure 7d, right) presents bands at 2886, 1227 and 835 cm^{-1} due to CH

stretching modes. The band at 1455 cm^{-1} due to COO^- group remains unchanged after immobilisation process, while band at 1471 shifted to 1464 cm^{-1} after immobilisation. Moreover, detection of broad bands at 1186 cm^{-1} and shifted band at 1125 cm^{-1} due to NH_3^+ group demonstrated the immobilisation of both zwitterionic and anionic L-Leu molecules.

FT-IR and Raman spectra of LL/HT_{rus}-R1_{0.95} (Figure 7c) did not present significant differences respect to LL/HT_{rus}-A2_{1.09} one. The band due to $\nu_{\text{a}(\text{COO}^-)}$ stretching shifted to lower frequencies from 1581 down to 1560 cm^{-1} , while the bands corresponding to $\nu(\text{NH}_3^+)$ was not detected. In a similar way as LL/HT_{rus}-A2_{1.09}, this finding suggests that the immobilisation of the L-Leu occurs in its anionic form, in agreement with Aisawa *et al.* who studied the influence of the pH in the immobilisation of Phe in HT materials [15]. Only two differences in the Raman spectrum of LL/HT_{rus}-R1_{0.95} were detected in comparison with the LL/HT_{rus}-A2_{1.09} one. First, the band at 1297 cm^{-1} due to the inplane deformation mode of the $-\text{OH}$, and second, the band at 1187 cm^{-1} due to the NH_3^+ group were not detected confirming that the immobilization occurs mainly in the anionic form. In general, FT-IR and Raman spectra of nanohybrid materials synthesised by reconstruction method show that using ultrasound treatment during the synthesis of nanohybrid materials affords materials where the L-Leu molecules are immobilised in their anionic form.

Additionally, in accordance with Nakamoto [31], a difference between the asymmetric and symmetric stretching vibration frequencies [$\Delta\nu = \nu_{\text{a}(\text{COO}^-)} - \nu_{\text{s}(\text{COO}^-)}$] gives information about the symmetry of the interaction between the COO^- group and the hydroxylated layers, which is similar to salt-like compounds [32]. Table 2 summarises the findings to LL/HT materials according with the characterisation data.

2.2 Nanohybrid materials based on L-Leucine and HT-like materials
 2.2 Results and discussion – FT-IR and Raman results

Table 2 Summary of characterisation data for LL/HT materials

Material	Synthesis method ^a	Immobilisation Location in the HT ^b	$\nu_{a(\text{COO}^-)}$ ^c	$\nu_{s(\text{COO}^-)}$ ^c	$\Delta\nu$ ^d	L-Leu structure ^e	Kind of interaction with HT ^f
L-Leu	-	-	1582	1407	175	Z	-
LL/HT _{Clus} -A1 _{0.04}	A1	- ^g	-	-	-	-	-
LL/HT _{Clus} -A2 _{0.16}	A2	- ^g	-	-	-	-	-
LL/HT _{rus} -A1 _{0.22}	A1	Edges	DD ^h	DD	-	DD	DD
LL/HT _{rus} -A1 _{0.44}	A1	Edges	1560	1408	152	A	Brinding
LL/HT _{rus} -A2 _{1.09}	A2	Interlayer space	1560	1408	152	A	Brinding
			1581	1408	173	Z	H-bonding
LL/HT _{rus} -R1 _{0.95}	R1	Interlayer space	1560	1407	152	A	Brinding
LL/HT _r -R2 _{0.92}	R2	Interlayer space	1581	1407	175	Z	H-bonding

^aImmobilisation conditions: See table 1. A=Anionic exchange method and R=Reconstruction method. ^bDetermined by XRD analysis. ^cDetermined directly of the FT-IR spectra. ^d $\Delta\nu = \nu_{a(\text{COO}^-)} - \nu_{s(\text{COO}^-)}$. ^eBased on presence of NH_3^+ group by FT-IR. Z= zwitterionic and A= Anionic. ^f $\Delta\nu_{\text{L-Leu}} > \Delta\nu_{\text{nanohyb}}$. = bidentate interaction; $\Delta\nu_{\text{L-Leu}} < \Delta\nu_{\text{nanohyb}}$. = bridging interaction. According to Nakamoto [31]. ^gNot immobilisation. ^hDD= Difficult to determine.

2.1.3 MAS NMR spectroscopy results

As exposed below, higher amount of immobilised L-Leu were obtained using 80°C for 3 hours of magnetic stirring in both the methodologies used (anionic exchange and reconstruction). For this reason, the nature of the interaction using ²⁷Al and ¹³C MAS NMR was investigated for LL/HT_{rus}-A2_{1.09}, LL/HT_{rus}-R1_{0.95} and LL/HT_r-R2_{0.92} nanohybrid materials. Figure 8 shows the ²⁷Al MAS-NMR spectra of HT_{rus}, LL/HT_{rus}-A2_{1.09}, LL/HT_{rus}-R1_{0.95} and LL/HT_r-R2_{0.92} materials.

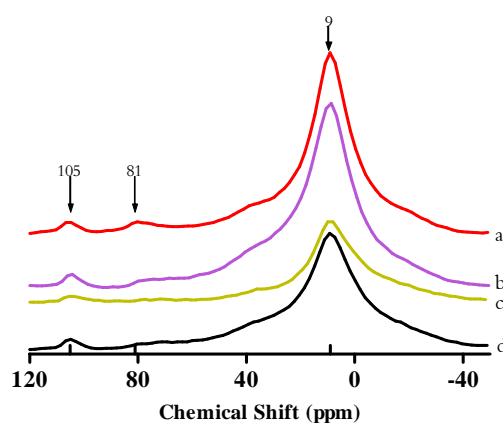


Figure 8 ²⁷Al-MAS NMR of a) HT_{rus}, b) LL/HT_{rus}-A2_{1.09}, c) LL/HT_{rus}-R1_{0.95} and d) LL/HT_r-R2_{0.92}.

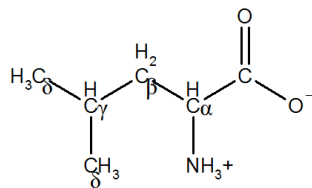
In agreement with several authors [33-35], ²⁷Al MAS-NMR spectrum of HT_{rus} (Figure 8a) exhibits a signal at 9 ppm due to the octahedral coordinated Al, while two small signals at

105 and 81 ppm are attributed to extra framework tetrahedral Al atoms still present after rehydration process. Additionally, any detectable variation in the coordination of Al atoms after immobilization of L-Leu suggests that the interaction between L-Leu and the HT layers does not occur directly with Al atoms.

¹³C MAS-NMR results of the nanohybrid are showed in Table 3. ¹³C MAS-NMR results of pure L-Leu (Table 3, entry 1) exhibits typical signals attributed to its zwitterionic state where signal at 177 ppm is due to the carboxylic acid group. C_α and C_β were detected at 55 and 44 ppm, respectively, while a broad band at 26 ppm is due to the C_γ and C_δ. The broad band effect is due to the different conformations of the pure L-Leu.

In LL/HT_{rus}-A2_{1.09} and LL/HT_{rus}-R1_{0.95} results (Table 3, entries 2 and 3) the signal due to the COO⁻ group shifted to 186 ppm. Shifting of this signal and small variations in the other carbon signals confirmed that L-Leu was immobilised in anionic form in the HT_{rus} precursor [20].

Table 3 ¹³C MAS NMR characterisation of LL/HT nanohybrid materials^a



Entry	Material	COO ⁻	C _α	C _β	C _γ	C _δ
1	L-Leu	176	55	44	26	26
2	LL/HT _{rus} -A2 _{1.09}	186 177 ^b	56	48	27	24
3	LL/HT _{rus} -R1 _{0.95}	186	58	49	27	25
4	LL/HT _r -R2 _{0.92}	177 186 ^b	56	48	27	25

^a See ¹³C MAS-NMR spectra in Annex 3, Fig. 1. ^bLess intense signal.

In agreement with FT-IR and Raman results, a small band at 177 ppm in LL/HT_{rus}-R1_{0.95} ¹³C MAS NMR spectrum suggests that a small amount of zwitterionic L-Leu is also immobilised in the material. On the other hand, LL/HT_r-R2_{0.92} material (Table 3, entry 4) shows two signals at 186 and 177 ppm. Relative intensities of these two signals show that zwitterionic L-Leu was mainly immobilised using this protocol

2.2.4 Thermal evolution of HT and LL/HT materials

Thermal behaviour of the HT_{asym}, HT_{rus} and LL/HT_{rus} nanohybrid materials was examined by simultaneous TG/DTA experiments. Figure 9 shows the TG (left) and DTA (right) curves of the HT_{asym} and HT_{rus} materials. According to Yang *et al.* decomposition of inorganic interlayer anions occurs from around 190°C up to 580°C divided in two main weight loss. The first occurs from 190 to 390 °C with a total decomposition of ~11.5% of physisorbed water and some CO₂ molecules and a second from 390 to 580°C with a total decomposition of ~88.5% of the total CO₂ contained in the HT structure [36]. In our case, HT_{asym} exhibits three main regions over the temperature range 30-230°C, 230-472°C and 472-900°C, which involves a total weight loss of 44.3%. In comparison with Yang *et al.* first weight loss from 30-230°C of 4.2% is due to the interlayer water in the HT structure, together with a relative smaller amount of NO₃⁻ and CO₃²⁻. The second distinct weight loss from 230-472°C of 31.3% is due to the evolution of H₂O, CO₂ and NO₂ species, resulting from desorption of the OH⁻ groups. In this range, two heat flows centered at 355 and 443°C were detected. A first small heat flow ranged in 230-380°C has a weight loss of 8.1% which agrees with the literature to the removal of H₂O associated to Al-(OH)-Mg OH⁻ groups [36]. A second heat flow presents the main weight loss of the material (23.2%). In this temperature range the dehydroxylation of Mg²⁺OH⁻ and Al³⁺OH⁻ species occurs. Finally, weight loss of 8.9% between 472-900°C is due to the removal of CO₃²⁻ and NO₃⁻ from the destroyed HT structure.

TG/DTA curves of HT_{rus} exhibit two main regions over the temperature range 30-245°C and 245-900°C, which involve a total weight loss of 42.9%. The first weight loss of 20.4% from 30-245°C exhibits three heat flows centered at 93, 195 and 234°C, respectively. The first heat flow ranging between 30-130°C with a weight loss of 5.3% is due to physisorbed H₂O on HT surface, while the other two heat flows ranging 130-245°C with a weight loss of 15.1% are due to interlayer NO₃⁻, CO₃²⁻ and H₂O. The second main weight loss of 22.5% from 245-900°C is due to the evolution of H₂O, CO₂ and NO₂ species, together with the dehydroxylation of the HT structure. Shifting of the second weight loss to lower temperature and any heat flow over 392°C confirmed that interlayer OH⁻ groups reduce the thermal resistance of the HT structure. Moreover, this shifting confirmed that the content of CO₃²⁻ in

the HT structure (Table 1) is due to contamination by manipulation and storage which is not mainly contained in the interlayer space from HTs.

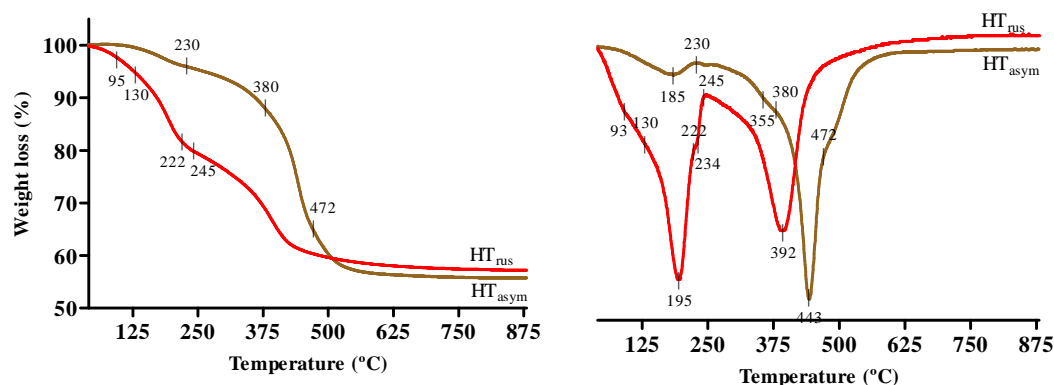


Figure 9 TG (left) and DTA (right) thermal analysis of HT_{asy} and HT_{rus}.

Figure 10 shows the FT-IR spectra in KBr of HT_{asy} outgassing at increasing temperature. Between room temperature to 220°C, the band at 1637 cm⁻¹ due to H₂O deformation disappears while a broad band at 3378 cm⁻¹ decrease slightly due to water loss of the HT structure agreeing with the TG/DTA results. One of the bands due to CO₃²⁻ ions initially detected at 1401 cm⁻¹ shifted up to 1519 cm⁻¹. No changes were observed above 1000 cm⁻¹ in this temperature range.

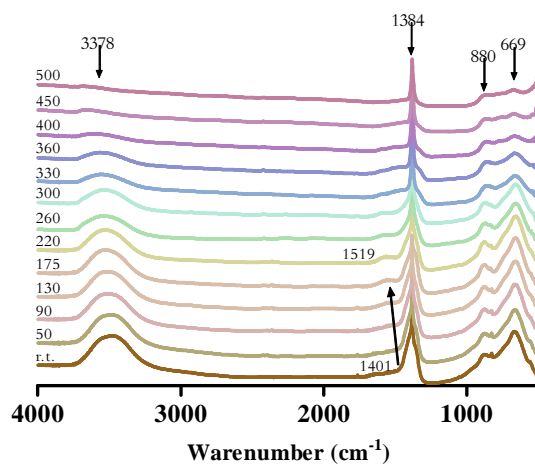


Figure 10 FT-IR spectra of HT_{asy} outgassing at increasing temperature in KBr.

In the range of 260-360°C the two characteristic bands of the interlayer CO₃²⁻ anions were stabilised at 1530 and 1320 cm⁻¹ agreeing with Yang *et al.* observations who explain that upper 300°C the interlayer water is loss and the CO₃²⁻ begins to interact more strongly with the backbone of the HT structure [36]. Decreasing of the bands at 880, 835 and 669 cm⁻¹

2.2 Results and discussion – Thermal evolution of HT and LL/HT materials

demonstrated both the elimination of CO_2^{3-} and changes in the $\text{Al}(\text{OH})$ and $\text{Mg}(\text{OH})$ species. Finally, in the temperature range of 360-500°C the HT structure is destroyed. Remained bands at 3660 cm^{-1} and below 1000 cm^{-1} are due to M-OH vibration of metal oxides. The band at 1384 cm^{-1} indicated that NO_3^- anions are thermally resisted to higher temperature, as it was confirmed by AE (Table 1, entry 2). Moreover, any change in the coordination of NO_3^- anions was detected by FT-IR.

Figure 11 shows the FT-IR spectra of HT_{rus} at increasing temperature. As explained in the experimental part, HT_{rus} was obtained using HT_{asym} as precursor and synthesized under Ar atmosphere after calcination at 450°C. Thermal behavior of HT_{rus} is similar to that of HT_{asym} . At lower frequencies, a band at 1384 cm^{-1} is assigned to the NO_3^- anions even present after calcination of the sample (Table 1, entry 3). Although the vibration modes of the CO_3^{2-} species shifted at higher frequencies as the temperature increases, nevertheless the position of the bands (1560 and 1420 cm^{-1}) are not the same as the precursor material. This finding agrees with the TG/DTA results which showed that CO_3^{2-} species are located mainly on the edges of the HT structure. Changes in the interlayer anions are also detected in the 1000 - 650 cm^{-1} region where the lower amount of OH, CO_3^{2-} and NO_3^- produces differences in the spectra around 669 and 880 cm^{-1} .

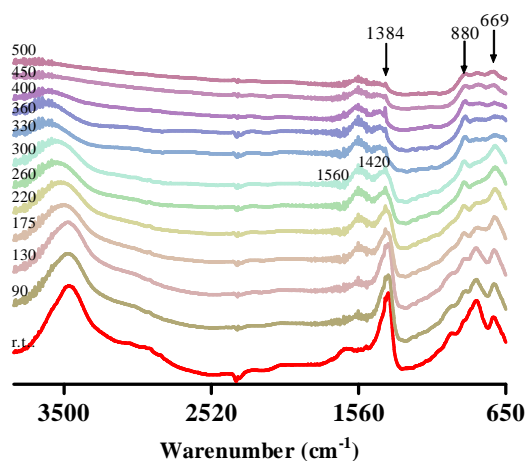


Figure 11 FT-IR spectra of HT_{rus} outgassing at increasing temperature in KBr.

TG/DTA curves and FT-IR spectra of L-Leu at increasing temperature are showed in Figures 12 and 13, respectively. Figure 13 shows that thermal evolution of L-Leu exhibits two main regions over the temperature range 30-319°C and 319-400°C, which involve total decomposition of the amino acid. First weight loss is divided in two ranges, between 30-206°C

and 206-319°C. In the range 30-206°C the weight loss was 0.27% and it is due to a small quantity of water retained in L-Leu structure. The absence of structural changes in the L-Leu in FT-IR spectra below 175°C confirmed this finding (Figure 13).

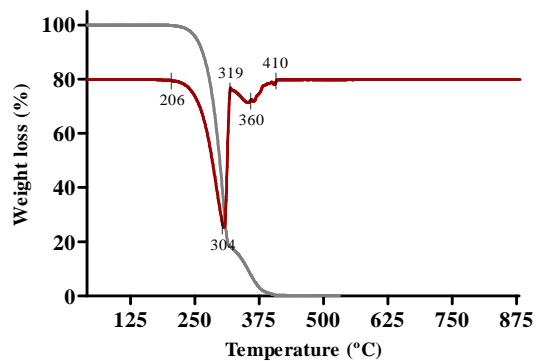


Figure 12 TG/ DTA thermal analysis of L-Leu.

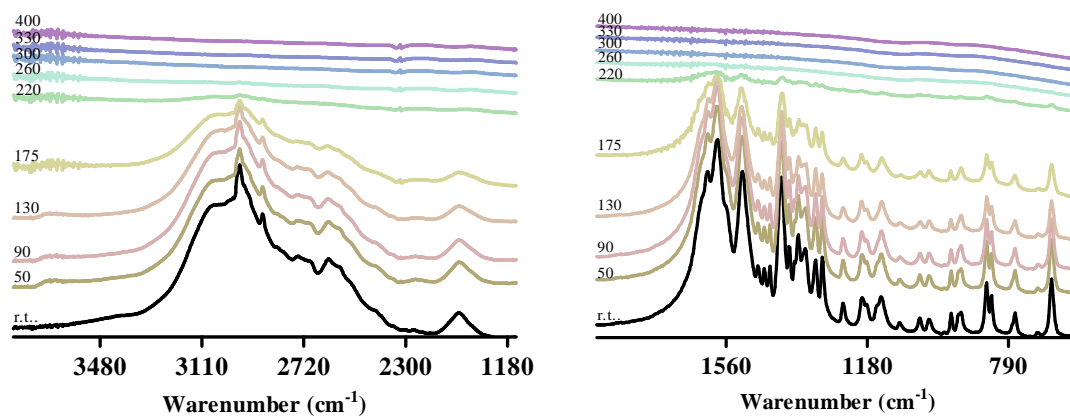


Figure 13 FT-IR spectra of L-Leu outgassing at increasing temperature in KBr in the frequency region of (left) 4000-1178 cm^{-1} and (right) 1178-600 cm^{-1} .

In the range of 206-319°C occurs the main weight loss (81.6%) centered at 304°C. FT-IR spectra in this range shows the decomposition of the L-Leu, where only the broad bands around 1600 and 1400-600 cm^{-1} due to carboxylate species arise from the decomposition. Above this temperature, Figure 13 shows a second weight loss of 18.1% centered at 360°C. Presence of this weight loss suggests the formation of secondary L-Leu structure due to the thermal exposition. At this point, Basiuk reported that the pyrolysis of L-Leu affords a group of polymer and cyclic compounds [37] while Choi *et al.* did not detected formation of these compounds to the pyrolysis of L-Leu [38]. In any case, under our experimental conditions band due to polymerisation was not observed. In fact, above 300°C no band was detected due to vacuum effects over the sample.

Thermal evolution of nanohybrid materials synthesised using HT_{rus} as precursor is presented in Figures 14-17. First of all, TG/DTA curves of LL/HT_{rus}-A2_{1.09} material exhibit three main regions over the temperature range 30-255°C, 255-384°C and 384-900°C (Figure 14), which involve a total weight loss of 59.0%. Increase of the weight loss respect to the HT_{rus} is due to immobilisation of the L-Leu in the material. In this case, three heat flows in the range 30-255°C centered at 87, 155 and 215 °C, respectively, were detected. First and second heat flows are due to H₂O physically adsorbed on HT surface with a weight loss of 12.0%. In the temperature range of 50-175°C, the FT-IR spectra (Figure 15) exhibit a band at 3058 cm⁻¹ which was not clearly detected in the air KBr experiment and is due to $\nu(\text{NH}_3^+)$. Since a general point of view, in this range LL/HT_{rus}-A2_{1.09} material is substantially stable. Shifting of the band at 3460 cm⁻¹ to 3547 cm⁻¹ is due to loss of water. From 203 to 255°C, TG/DTA curves exhibit a weight loss of 5.6% which suggests the condensation of zwitterionic L-Leu in the material, as well as, the elimination of NO₃⁻ and CO₃²⁻ anions content in the HT structure. Condensation of the zwitterionic L-Leu agrees with the FT-IR spectra at 220 and 260°C which present a small shoulder band at 1650 cm⁻¹ and it was not detected anymore above that temperature range. According to Whilton *et al.* this newly detected band is characteristic of the amide group forming likely through an *in situ* condensation of the zwitterionic AA [12].

In the range 255-384°C, the weight loss was 24.1%. FT-IR spectra recorded between 300-360°C do not present any evidence of immobilised L-Leu at lower frequency (Figure 15, right). Nevertheless a band remained around 2961 cm⁻¹ due to $\nu(\text{CH})$ vibrations and a new small band detected at 2168 cm⁻¹ indicated that decomposition products are still present at higher temperature. Finally, the third main weight loss of 15.84% occurs above 384°C. According with HT_{rus} results discussed below, elimination of CO₂ from CO₃²⁻ species occurs over that temperature. FT-IR spectra present the total decomposition of immobilised L-Leu above 400°C followed by the thermal destruction of the HT structure (Figure 15).

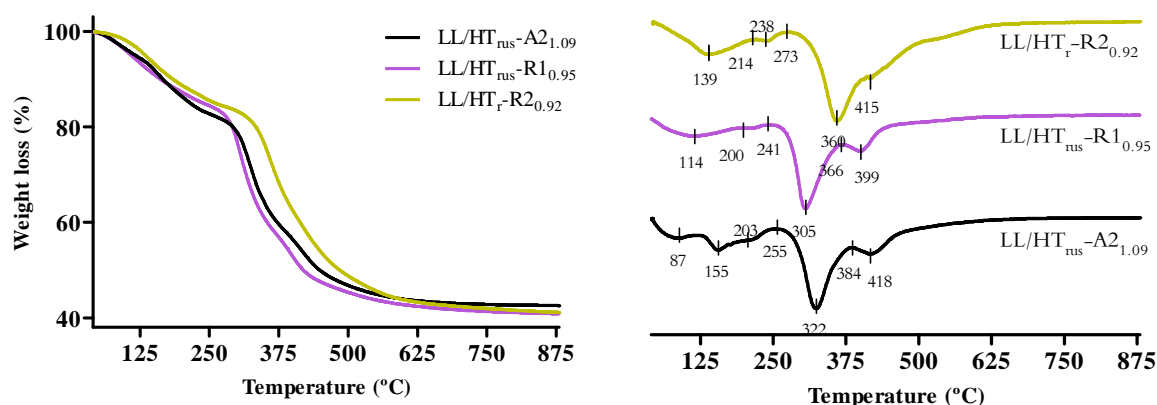


Figure 14 TG (left) and DTA (right) thermal analysis of LL/HT_{rus}-A2_{1.09}, LL/HT_{rus}-R1_{0.95} and LL/HT_r-R2_{0.92}.

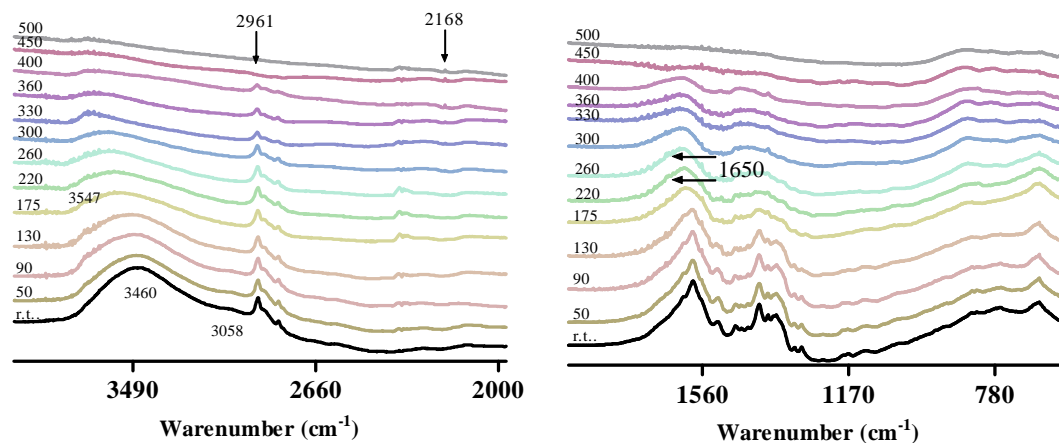


Figure 15 FT-IR spectra of LL/HT_{rus}-A2_{1.09} outgassing at increasing temperature in KBr in the frequency region of (left) 4000-1178 cm⁻¹ and (right) 1178-600 cm⁻¹.

TG/DTA curves of LL/HT_{rus}-R1_{0.95} exhibit a total weight loss of 59.3% divided into three main regions: 30-241°C, 241-366°C and 366-900°C (Figure 14). In a similar way as LL/HT_{rus}-A2_{1.09}, the first weight loss of 15.2% involves elimination of physisorbed water, NO₃⁻ and CO₃²⁻ anions content in the HT structure. The second weight loss of 26.8% is due to the dehydroxylation of the HT layers and the decomposition of L-Leu molecules and the third weight loss of 17.3% is due to the total decomposition of L-Leu and elimination of inorganic anions remaining in the HT structure. FT-IR spectrum of LL/HT_{rus}-R1_{0.95} (Figure 16) recorded at room temperature and under outgassing conditions showed that the band around 1570 cm⁻¹ due to COO⁻ group is divided into two broad bands at 1576 and 1560 cm⁻¹. Additionally any detected band due to NH₃⁺ group suggests that anionic L-Leu molecules could be interacting in two different forms with the HT structure, one inside the HT structure and two outside, on the edges of the HT layers. Characteristic signals of L-Leu were not detected any more above 220°C

2.2 Results and discussion – Thermal evolution of HT and LL/HT materials

at lower frequency (Figure 16b), while bands due to $\nu(\text{CH})$ remained up to 400°C. HT structure was totally destroyed above 400°C.

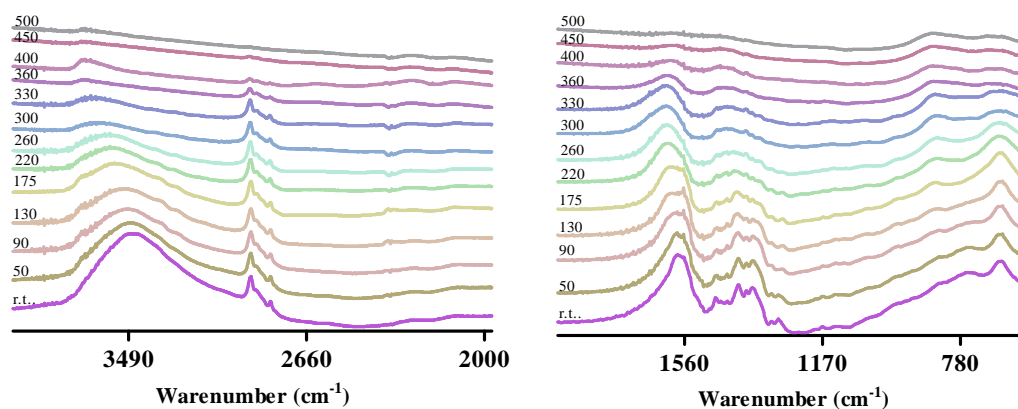


Figure 16 FT-IR spectra of LL/HT_{rus}-R1_{0.95} outgassing at increasing temperature in KBr in the frequency region of (left) 4000-1178 cm⁻¹ and (right) 1178-600 cm⁻¹.

Finally, TG/DTA curves and FT-IR spectra at increasing temperature of LL/HT_r-R2_{0.92} material show interesting findings in agreement with all experimental data reported here (Figures 14 and 17, respectively). The total weight loss of LL/HT_r-R2_{0.92} was 57.5% divided in three regions: 30-214°C, 214-273°C and 273-900°C. Weight loss of 3.3% between 214-273°C is compared with the FT-IR spectra at 220 and 260°C. In this case, presence of well formed band at 1650 cm⁻¹ and a small component at 1605 cm⁻¹ due to $\nu\text{C}=\text{O}$ and δNH of an amide group were detected. These bands as well the decrease of the broad band around 3064 cm⁻¹ (νNH_3^+) confirmed the poly-condensation of the L-Leu molecules.

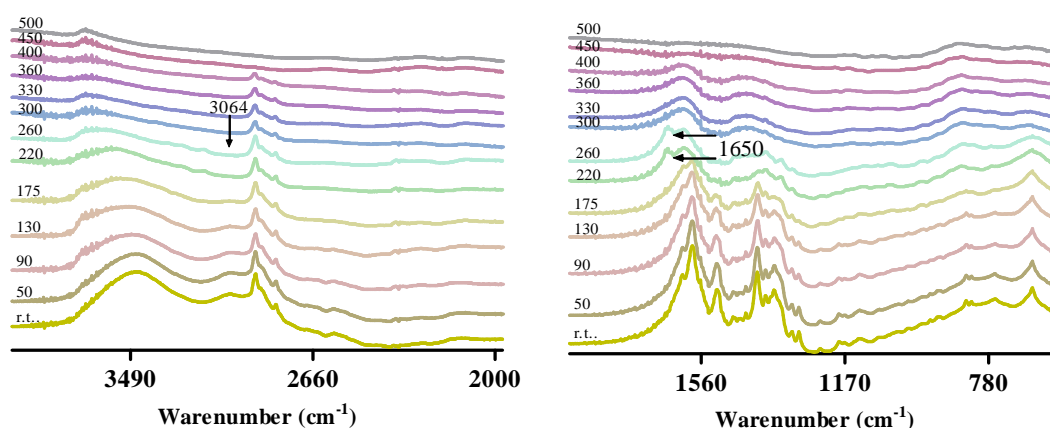


Figure 17 FT-IR spectra of LL/HT_r-R2_{0.92} outgassing at increasing temperature in KBr in the frequency region of (left) 4000-1178 cm⁻¹ and (right) 1178-600 cm⁻¹.

In accordance with ¹³C-MAS NMR, FT-IR and Raman spectra recorded in air, LL/HT_r-R2_{0.92} is formed mainly by zwitterionic L-Leu which favours the condensation of L-

Leu molecules. Main weight loss of 41.0% in the range 273-900°C presents two heat flows, the first centered at 360°C is due to dehydroxylation of HT layers, elimination of NO₂, CO₂ and total decomposition of the L-Leu; and the second weight loss centered at 415°C is due to elimination of inorganic anions remained in the HT structure.

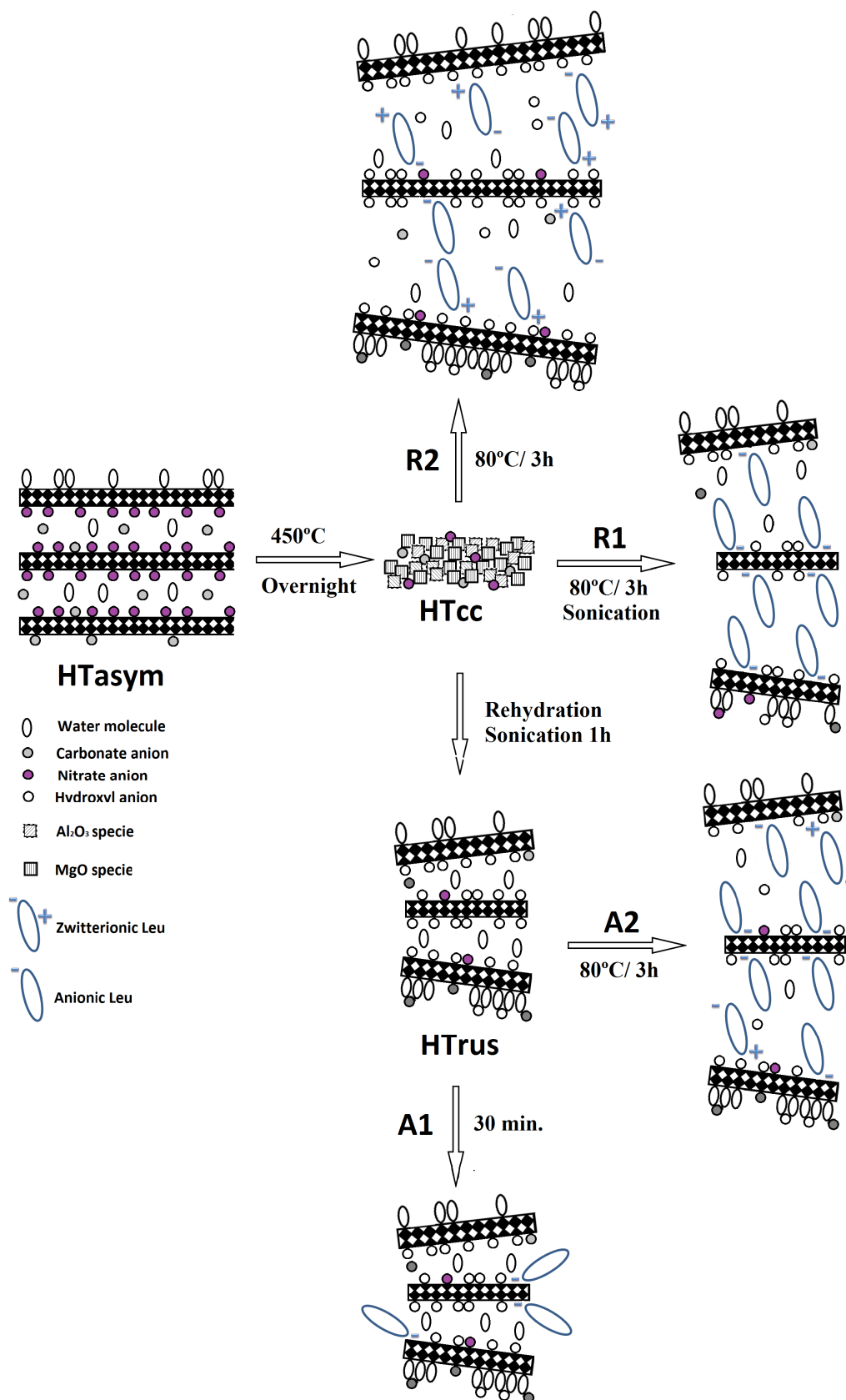
In LL/HT_{rus}-R1_{0.95} material which mainly contains anionic L-Leu the main weight loss was centered at 306°C, while for LL/HT_{rus}-A2_{1.09} and LL/HT_r-R2_{0.92}, the main weight losses were centered at 322 and 360°C respectively. These findings permitted to conclude that: first, anionic L-Leu replaces the OH⁻ interlayer anions making less thermally stable the HT structure and second, this effect stabilised the total charge of the HT layers preventing the co-intercalation of inorganic anions. In this case, high content of CO₃²⁻ detected by EA is due to contamination of the sample by atmospheric CO₂ in the remaining accessible basic centers. On the other hand, condensation of zwitterionic L-Leu in LL/HT_{rus}-A2_{1.09} and LL/HT_r-R2_{0.92} agree with Bujdák *et al.* who explained that polycondensation of AAs could occur by the formation of catalytic active centers on the alumina surface [39-41]. In that context, nowadays, it is well accepted that a cyclic anhydride dipeptide is formed from zwitterionic AAs supported on alumina. Here, we propose that thermal polycondensation of L-Leu starts between two closed immobilised zwitterionic L-Leu where HTs acts as the catalysts through stabilisation of the L-Leu. As it was discussed before, in this work only two materials have immobilised zwitterionic L-Leu (LL/HT_{rus}-A2_{1.09} and LL/HT_r-R2_{0.92}), and in both cases it could be detected the formation of a peptide bond around 220°C (Band at 1650 cm⁻¹). No band associated with cyclic-PLL was detected in FT-IR spectra at increasing temperature because at higher temperature the materials have higher movement of water molecules originating the ring-opening reaction. In the case of LL/HT_{rus}-R1_{0.95} material, thermal polymerisation could not be detected because the immobilisation of L-Leu occurs by anionic interactions without any immobilisation of zwitterionic L-Leu that impossibility the initiation of the poly-condensation reaction.

2.2.5 Nature of the organic/inorganic interaction

All characterisation data reported in this section show that variations in the immobilisation protocol permit to obtain materials with different characteristics which are represented in Scheme 2. As it is well know, HT materials exhibit *memory effect*, which permits

2.2 Results and discussion – Nature of the interaction

the reconstruction of the HT structure after its calcination. We synthesised two materials by reconstruction method (LL/HT_{rus}-R1_{0.95} and LL/HT_{rus}-R2_{2.99}). LL/HT_{rus}-R1_{0.95} was synthesised under ultrasound treatment while LL/HT_r-R2_{0.92} was synthesised without it. We propose that rehydration and immobilisation processes occur at the same time. While the HT layers are forming the positive charge is compensated with OH⁻ groups located in the interlayer space. Under conventional method without ultrasound treatment (R2), the immobilisation of L-Leu agrees with Nakayama *et al.* who explained that the immobilisation occurs by H-bonding between the NH₃⁺ group of the zwitterionic Leu with water and/or OH⁻ groups of the HT layers [20]. Nevertheless, when the immobilisation is performed under ultrasound treatment (R1), most of the L-Leu was immobilised in the anionic form. This behaviour is explained because during the synthesis of LL/HT_{rus}-R1_{0.95} more basic and accessible centres are formed in the material [10]. These “new” basic constantly-forming centres permit the compensation of the positive charge with anionic L-Leu molecules. As discussed below, in the case of LL/HT_r-R2_{0.92}, compensation of the positive charge was performed by OH⁻ and also NO₃⁻ and CO₃²⁻ anions, although immobilisation of some anionic L-Leu molecules is not ruled out. On the other hand, nanohybrid materials synthesised by anionic exchange method (LL/HT_{rus}-A1_{0.22}, LL/HT_{rus}-A1_{0.44} and LL/HT_{rus}-A2_{1.09}) have strong basic centers which were obtained before the immobilisation process. In this case, the immobilisation of the anionic L-Leu occurs up to all accessible centres are compensated, permitting also the immobilisation of some zwitterionic L-Leu molecules. In all cases, the immobilisation of the L-Leu in the interlayer space occurs because the increasing of the temperature favours the swelling of the HT material. Finally, in all materials reported here, the L-Leu could interact with the HT surface, but washes after synthesis removed most of these molecules, as it was verified using HT_{clus} as precursor (LL/HT_{clus}-A1_{0.04} and LL/HT_{clus}-A2_{0.16} materials).



Scheme 2 Schematic representation of the LL/HT materials obtained by the different protocols.

3.1 Experimental

3. Nanohybrid materials based on L-Proline immobilised in Hydrotalcite-like materials

Between the 21 natural occurring AA, Pro is the exception because it has a secondary amine forming an imino group fixed rigidly in a pyrrolidine ring. In this section, we present the synthesis of nanohybrid materials based on L-Proline (L-Pro) and Mg-Al HTs (LP/HT) by co-precipitation, anionic exchange and reconstruction methods. The materials were characterised by EA, ICP, XRD, FT-IR, Raman, ^{13}C , ^{27}Al MAS NMR and thermal evolution using TG/DTA analyses and *in situ* FT-IR under outgassing conditions at increasing temperature.

3.1 Experimental

3.1.1 Synthesis of HTs

Mg-Al hydrotalcite (HT) with Mg/Al molar ratio = 2 containing nitrates and chloride anions were synthesised by co-precipitation method according to the method exposed in section 2.1.1.

3.1.2 Synthesis of LP/HT materials

The nanohybrid materials were prepared by anionic-exchange, reconstruction and co-precipitation method using dionised-decarbonated water under Ar atmosphere as follows:

3.1.2.1 Anionic-exchange method (Method A)

Two procedures were used to synthesize LP/HT_x-Ay_z materials following the methodology described in section 2.1.2.1. Obtained materials were named: LP/HT_{rus}-A1_{0.07}, LP/HT_{rus}-A1_{0.14}, LP/HT_{Clus}-A1_{<0.01}, LP/HT_{rus}-A2_{0.57} and LP/HT_{Clus}-A2_{0.01}.

3.1.2.2 Reconstruction method (Method R)

Two procedures were used to synthesise LL/HT_x-Ry materials following the methodology described in section 2.1.2.2. The obtained materials were named: LP/HT_{rus}-R1_{0.60} and LP/HT_r-R2_{0.70}.

3.1.2.3 Co-precipitation method, LP/HT_x-Cy_z Samples

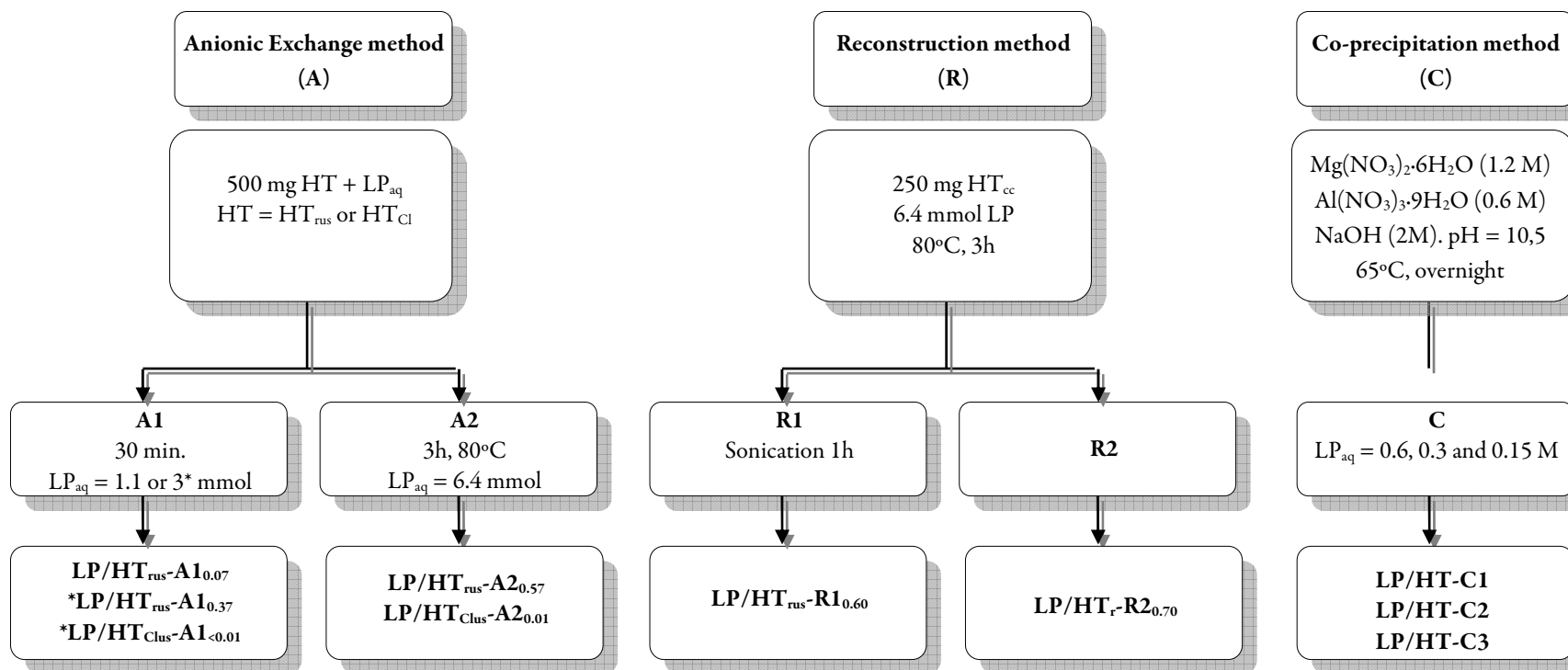
[†] LP/HT_{Cl}-A1_{0.03} material was synthesised using 3 mmol of L-Pro.

Mg-Al hydrotalcite (HT) with Mg/Al molar ratio = 2 was prepared by the conventional co-precipitation method at 65°C in the presence of a L-Pro solution as follows: two solutions containing Mg(NO₃)₂·6H₂O (1.2 M) and Al(NO₃)₃·9H₂O (0.6 M) were dissolved in 150 cm³ of water and added dropwise into a beaker containing a 150 cm³ of a L-Pro solution with known concentration (0.6, 0.3 and 0.15 M). The pH was kept at 10,5 by adding a NaOH solution (2M). After the addition of the reactants, the slurry was aged at 65°C overnight under vigorous stirring in Ar atmosphere. The obtained materials were filtered and washed with large amounts of deionised-decarbonated water to remove Na⁺, NO₃⁻ and non-immobilised L-Pro molecules. Obtained materials were denoted as LP/HT-Cy, where y is a number between 1 and 3 and indicates the initial concentration of L-Pro. Materials synthesised by this method were named: LP/HT-C1, LP/HT-C2 and LP/HT-C3 respectively.

A schematic representation of all synthesis methods is presented in Scheme 3.

3. Nanohybrid materials based on *L*-Proline and HT-like materials

3.1 Experimental



Scheme 3 Summary of the synthesis methods of LP/HT materials.

3.2 Results and discussion

Nanohybrid materials based on L-Pro and HTs were synthesised by anion-exchange, reconstruction and co-precipitation method to study: i) the role of the immobilisation time and the relationship between the immobilisation speed and the strength and kind of basic centres in the HT; ii) the role of the HT precursor in the immobilisation process and iii) the nature of the L-Pro structure in the immobilisation process. Molecular formulae of synthesised nanohybrid materials are presented in Table 4.

Table 4 Molecular formulae of HT and LP/HT materials

Entry	Material ^{a,b}	Molecular Formulae ^c
1	HT _{asym}	[Mg _{2.53} Al _{1.00} (OH) _{7.07}](CO ₃ ²⁻) _{0.85} (NO ₃ ⁻) _{3.15} ·0.70H ₂ O
2	HT _{cc}	Mg _{2.53} Al _{1.00} (O) _x (CO ₃ ²⁻) _{0.32} (NO ₃ ⁻) _{0.10}
3	HT _{rus}	[Mg _{2.53} Al _{1.00} (OH) _{7.07}](CO ₃ ²⁻) _{1.18} (NO ₃ ⁻) _{0.10} ·0.70H ₂ O
4	HT _{Cl}	[Mg _{2.31} Al _{1.00} (OH) _{6.62}](CO ₃ ²⁻) _{0.84} (Cl) _{0.52} ·0.67H ₂ O
5	LP/HT _{rus} -A1 _{0.07}	[Mg _{2.54} Al _{1.00} (OH) _{7.08}](Pro) _{0.07} (CO ₃ ²⁻) _{2.79} (NO ₃ ⁻) _{0.10} ·0.70H ₂ O
6	LP/HT _{rus} -A1 _{0.14}	[Mg _{2.54} Al _{1.00} (OH) _{7.08}](Pro) _{0.14} (CO ₃ ²⁻) _{2.27} (NO ₃ ⁻) _{0.10} ·0.70H ₂ O
7	LP/HT _{Cl} -A1 _{<0.01}	[Mg _{2.31} Al _{1.00} (OH) _{6.62}](Pro) _{<0.01} (CO ₃ ²⁻) _{1.56} (Cl) _{0.52} ·0.67H ₂ O
8	LP/HT _{rus} -A2 _{0.57}	[Mg _{2.54} Al _{1.00} (OH) _{7.08}](Pro) _{0.57} (CO ₃ ²⁻) _{1.40} (NO ₃ ⁻) _{0.10} ·0.70H ₂ O
9	LP/HT _{Cl} -A2 _{0.02}	[Mg _{2.31} Al _{1.00} (OH) _{6.62}](Pro) _{0.02} (CO ₃ ²⁻) _{1.08} (Cl) _{0.52} ·0.67H ₂ O
10	LP/HT _{rus} -R1 _{0.60}	[Mg _{2.54} Al _{1.00} (OH) _{7.08}](Pro) _{0.60} (CO ₃ ²⁻) _{2.57} (NO ₃ ⁻) _{0.10} ·0.70H ₂ O
11	LP/HT _r -R2 _{0.70}	[Mg _{2.54} Al _{1.00} (OH) _{7.08}](Pro) _{0.70} (CO ₃ ²⁻) _{2.34} (NO ₃ ⁻) _{0.10} ·0.70H ₂ O
12	LP/HT-C1	[Mg _{2.63} Al _{1.00} (OH) _{7.08}](Pro) _{0.02} (CO ₃ ²⁻) _{0.85} (NO ₃ ⁻) _{2.99} ·0.74H ₂ O
13	LP/HT _{us} -C1 ^d	[Mg _{2.63} Al _{1.00} (OH) _{7.08}](Pro) _{0.01} (CO ₃ ²⁻) _{1.21} (NO ₃ ⁻) _{2.60} ·0.74H ₂ O
14	LP/HT-C2	[Mg _{2.63} Al _{1.00} (OH) _{7.08}](Pro) _{0.01} (CO ₃ ²⁻) _{0.98} (NO ₃ ⁻) _{3.43} ·0.74H ₂ O
15	LP/HT-C3	[Mg _{2.63} Al _{1.00} (OH) _{7.08}](Pro) _{0.01} (CO ₃ ²⁻) _{0.86} (NO ₃ ⁻) _{3.04} ·0.74H ₂ O

^aSynthesis Conditions: Anionic exchange 1 (A1): HT and a solution of L-Pro were mixed and stirring for 0.5 h at r.t. Anionic exchange 2 (A2): HT and a solution of L-Pro were mixed and stirring for 3 h at 80°C. Reconstruction 1 (R1): HT_{cc} and a solution of L-Pro were mixed and sonicated during 1 h and stirred for 3 h at 80°C. Reconstruction 2 (R2): HT_{cc} and a solution of L-Leu were mixed and stirred for 3 h at 80°C. Co-precipitation (C): Mg-Al HT was precipitated in the presence of L-Pro. ^bHT = hydrotalcite. HT_{asym} = As-synthesized HT. HT_{cc} = Calcined HT. HT_{rus} = rehydrated HT under ultrasound treatment. HT_{Cl} = As-synthesized HT containing chloride anions. HT_{Clus} = HT_{Cl} after ultrasound treatment. ^cCalculated by EA and ICP analysis in materials synthesized by method A and B. Calculated by AE, TG/DTA and ICP analysis in materials synthesized by method C. Water content was calculated theoretically according with Miyata. Ref [42]. ^dUltrasound treatment (1h) was used after the material synthesis.

3.2.1 X-ray diffraction results

3.2.1.1 Anion exchange method

The XRD patterns of nanohybrid materials synthesised by anionic-exchange method are presented in Figure 18. In all cases, the obtained materials exhibit the characteristic diffraction peaks of the meixnerite structure (JCPDS 35-0965). As a reference, the XRD

3.2 Nanohybrid materials based on L-Proline and HT-like materials

3.2 Results and discussion – XRD results

patterns of precursor HTs are shown in Figure 18a and 18e. As exposed for the LL/HT materials, HT_{Clus} as precursor immobilised low amount of L-Pro indicating that L-Pro is not immobilised on the HT surface (Figure 18f and 18g). The XRD pattern of LP/HT_{rus}-A1_{0.07} and LP/HT_{rus}-A1_{0.14} nanohybrid materials (Figure 18b and 18c) show that the d_{003} basal spacing of precursor HT material remained unchanged after the immobilisation process. Nevertheless, increasing of immobilised L-Pro amount decreases the crystallinity of the HTs due to defoliation of the layers. The XRD pattern of LP/HT_{rus}-A2_{0.57} exhibits a broad band around 5.6 2 θ indicating an interlayer space of 15.8 Å. In comparison with the analogue material using L-Leu, LP/HT_{rus}-A2_{0.57} increase of the immobilised L-Pro amount is due to intercalation of the AA in the interlayer space from the HT material.

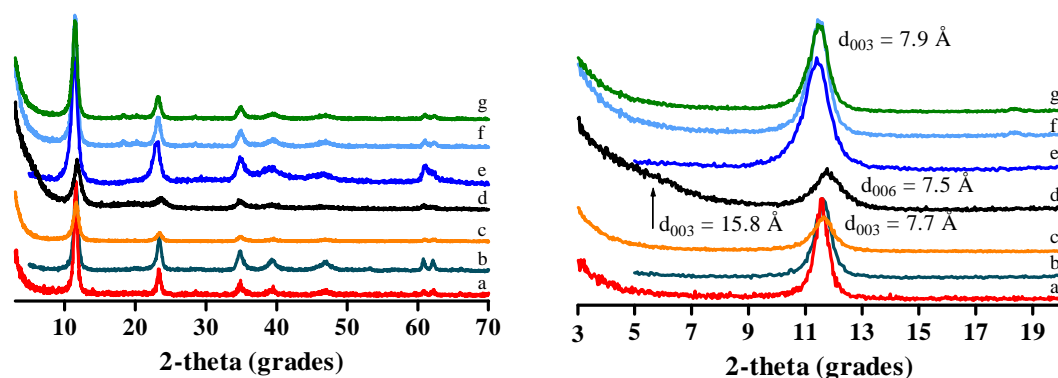


Figure 18 XRD patterns of (a) HT_{rus}, b) LP/HT_{rus}-A1_{0.07}, c) LP/HT_{rus}-A1_{0.14}, d) LP/HT_{rus}-A2_{0.57}, e) HT_{Clus}, f) LP/HT_{Clus}-A1_{<0.01} and g) LP/HT_{Clus}-A2_{0.01}. (Right) XRD pattern in the 2 θ range: 3-20°.

3.2.1.2 Reconstruction method

XRD patterns of nanohybrid materials synthesised by reconstruction method are presented in Figure 19. LP/HT_{rus}-R1_{0.60} and LP/HT_r-R2_{0.70} materials also exhibit increase in the d_{003} diffraction peak from the HT precursor to around 15 Å indicating the immobilisation of L-Pro in the interlayer space of the HT. As an approximation, the molecular size of pure L-Pro is 2.8 Å in width, 5.5 Å in length and 6.0 Å in thickness. This size, in comparison with the 3.0 Å of the interlayer space of the starting HT_{rus}, suggests that the immobilised L-Pro occurs in multi-layers even in a vertical orientation in the interlayer space, as exposed by Aisawa *et al.* for the immobilisation of Phe in HT materials [21].

* Calculated using the GaussView program implemented in the Gaussian 03

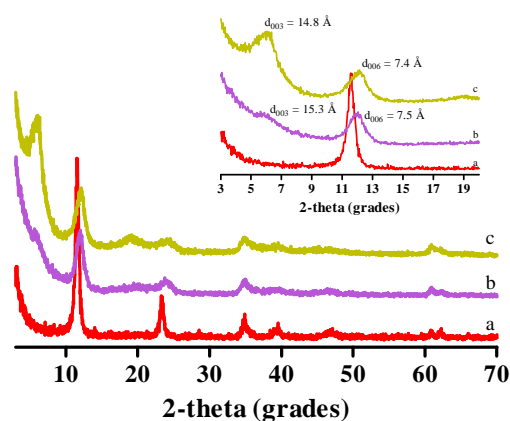


Figure 19 XRD patterns of (a) HT_{rus}, (b) LP/HT_{rus}-R1_{0.60} and (c) LL/HT_r-R2_{0.92}. Inset: XRD pattern in the 2θ range: 3-20°.

3.2.1.3 Co-precipitation method

The XRD patterns of nanohybrid materials synthesised by co-precipitation method (LP/HT-C1, LP/HT-C2 and LP/HT-C3) present a wide main diffraction peak in the d_{003} range of 8.9-7.8 Å (Figure 20).

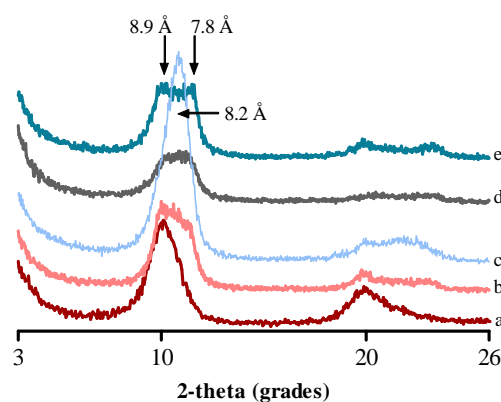


Figure 20 XRD patterns of (a) HT_{asym}, (b) LP/HT-C1, (c) LP/HT_{us}-C1, (d) LP/HT-C2 and (e) LP/HT-C3 in the 2θ range 3-26°.

Variations in the interlayer space respect to HT_{asym} suggest the immobilisation of the L-Pro occurs in the interlayer space. According to TG/DTA results (Table 4, entries 12-15) amount of L-Pro immobilised by co-precipitation method are the lowest. Increase of the interlayer space with low amount of immobilised L-Pro suggests that L-Pro is immobilised in oblique form respect to the layers through reorganisation of the water molecules and the inorganic co-intercalated anions (CO_3^{2-} , NO_3^- and OH^-) as observed Yuan *et al.* to immobilisation of Cys in HTs [16].

3.2 Results and discussion – XRD results

To evaluate the stability of the immobilised L-Pro, LP/HT-C1 was sonicated for 1 hour to obtain the LP/HT_{us}-C1 material. The XRD pattern of this nanohybrid material is showed in Figure 20c. Increases of the crystallinity of the sample as well as a shift of the 003 diffraction peak to higher 2θ angles is explained because a part of the immobilised L-Pro is way out of the material (Table 4, entries 12,13). That effect suggests most of the immobilised L-Pro mainly occurs by anionic exchange with the immobilisation of L-Pro stabilised by weak interactions.

3.2.2 FT-IR and Raman spectroscopy results

Skeletal FT-IR (left) and Raman (right) spectra of L-Pro are presented in Figure 21. FT-IR spectrum of commercially available L-Pro in KBr (Figure 21, left) show a complex group of bands due to $\nu(\text{CH})$ and $\nu(\text{NH})$ vibrations between 3200 and 1900 cm^{-1} . The typical bands at 3059, 1560 and 1169 cm^{-1} are due to the $\nu(\text{NH}_2^+)$ modes. Bands at 1624 and 1377 cm^{-1} are due to $\nu_{\text{a}}(\text{COO}^-)$ and $\nu_{\text{s}}(\text{COO}^-)$ stretching, while bands at 2367, 1408 and 1291 cm^{-1} are assigned to $\nu(\text{CH})$ and $\nu(\text{CN})$ modes. The band at 3417 cm^{-1} corresponds to the stabilisation of the L-Pro structure by either $\text{N-H}\cdots\text{O}=\text{C}$ or $\text{N}\cdots\text{H}-\text{O}$ intramolecular H-bonds showing the zwitterionic state of the pure L-Pro.

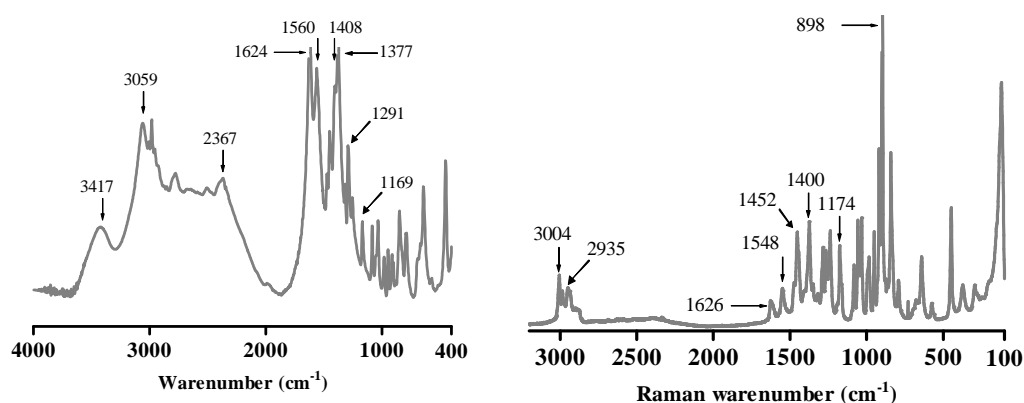


Figure 21 Skeletal FT-IR (left) and Raman (right) spectra of pure L-Pro.

Figure 22 shows the most stable structure for the pure L-Pro in solid state in accordance with Marino *et al.* [43].

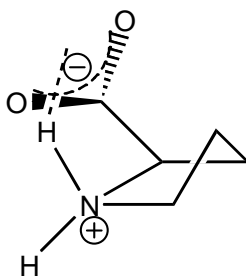


Figure 22 Schematic representation of the most stable conformation of the pure L-Pro according to reference [43].

In the Raman spectrum of pure L-Pro (Figure 21b) the bands at 1452 (complex) and 1374 cm^{-1} are due to scissoring and wagging vibrations of the CH_2 groups, while few sharp bands between 1285 and 1237 cm^{-1} are assigned to other deformation modes of the methylenic group [44]. The corresponding asymmetric and symmetric stretching bands are observed at 3004 and 2985 cm^{-1} and, at 2950, 2935 and 2900 cm^{-1} respectively [45]. In the range 1100-800 cm^{-1} the ring stretching modes fall, the most intense band at 898 cm^{-1} being assigned to symmetrical ring breathing mode. The quite complex band pattern around 1250 cm^{-1} has been assigned to stretching and deformation modes for the C-C and C-N of the L-Pro ring, partially overlapping. The weak bands at 1548 and 1174 cm^{-1} are due to NH_2^+ scissoring and N-H twisting deformation modes [44]. COO^- group is characterised by bands at 1626 (broad), and 1400 cm^{-1} , tailing towards lower frequencies and overlapping with CH_2 deformation modes, due to $\nu_{\text{a}(\text{COO}^-)}$ and $\nu_{\text{s}(\text{COO}^-)}$ vibrations [46]. Detection of the bands at 1626 and 1548 cm^{-1} shows the zwitterionic nature of the pure L-Pro.

3.2.2.1 Anion-exchange method

FT-IR and Raman spectra of nanohybrid materials of $\text{LP/HT}_{\text{Clus-A1}<0.01}$ and $\text{LP/HT}_{\text{Clus-A2}0.01}$ materials (Figures 23g, 23h, 23g and 23h) agree with the EA results due to their low quantity of immobilised L-Pro. At this point although immobilisation on surface in $\text{LL/HT}_{\text{Clus-A2}0.16}$ was observed, using L-Pro it was not detected. That effect is explained by the pKa of the L-Pro which is 10.64 while in L-Leu is 9.74. In this context, for immobilisation of L-Pro strong basic centres in the HT material are needed.

3.2 Results and discussion – FT-IR and Raman results

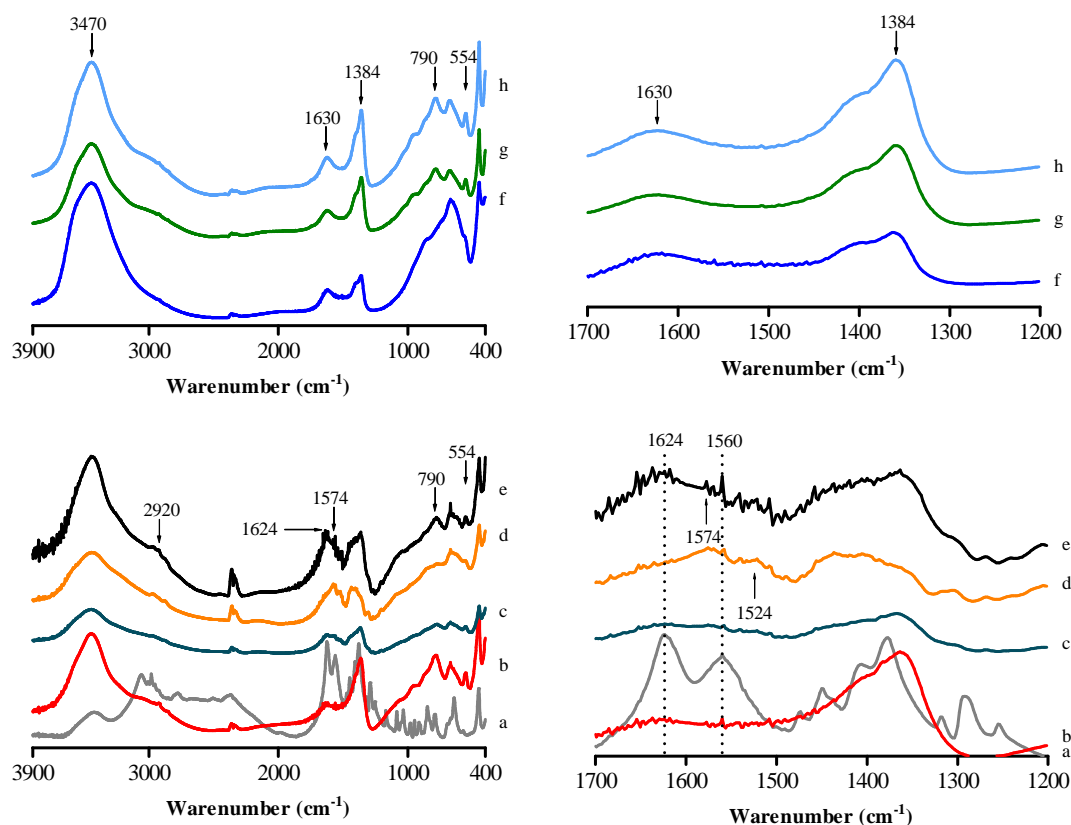


Figure 23 (left) FT-IR spectra of a) L-Pro, b) HT_{rus}, c) LP/HT_{rus}-A1_{0.07}, d) LP/HT_{rus}-A1_{0.14}, e) LP/HT_{rus}-A2_{0.57}, f) HT_{Clus}, g) LP/HT_{Clus}-A1_{<0.01} and h) LP/HT_{Clus}-A2_{0.01}. (right) FT-IR spectra in the frequency region 1700-1200 cm⁻¹.

From a general point of view, immobilised L-Pro affords signal with low intensity due to the restrictions in the freedom degree of the L-Pro molecules making difficult the correct identification. FT-IR spectrum of LP/HT_{rus}-A1_{0.14} (Figure 23d) exhibits the band around 2920 cm⁻¹ due to the $\nu(\text{CH})$ stretching of the L-Pro which shifts respect to the pure L-Pro. At lower frequency, the band due to $\nu_a(\text{COO}^-)$ shifts from 1624 to 1574 cm⁻¹ and the band due to $\nu(\text{NH}_2^+)$ mode shifts from 1560 to 1524 cm⁻¹. Shifts of these bands suggests: first, the immobilisation of the L-Pro in the HT precursor, and second, L-Pro structure changes after immobilisation possibly by formation of anionic L-Pro. Changes around 790 and 554 cm⁻¹ after immobilisation show that interaction with L-Pro also affects the Al-OH species. The Raman spectrum of LP/HT_{rus}-A1_{0.14} (Figure 24d) exhibits weakened bands from the L-Pro with significant shifts and broadening after immobilisation. In particular, at high frequency, $\nu(\text{CH})$ bands are broadened and shifted towards lower frequency. Moreover, the broad and weak component and 2900 cm⁻¹ (symmetric νCH_2 mode) is clearly shifted to 2878 cm⁻¹ and becomes the strongest band in this spectral region. These effects can be explained by the interaction of the CH₂ groups

with the HT surface and are consistent with findings of Sheena *et al.* who reported the SERS spectrum of Pro interacting parallel with Ag surface [45]. Moreover, the bands assigned to COO^- stretching and deformation modes are strongly perturbed: the high frequency component almost disappears as well as the component at 641 cm^{-1} . New broad absorption grows at 1410 and 870 cm^{-1} . The former can be assigned to $\nu_{\text{s}(\text{COO}^-)}$ stretching, whereas the latter has been reported also by Podstakwa *et al.* and assigned tentatively to $\delta_{(\text{COO}^-)}$ modes [46]. The frequency shift and the broad band shape can be taken as the evidence that COO^- groups are changing their coordination mode following intercalation, in agreement with FT-IR data. These findings confirm the interaction of COO^- groups with the HT layers. Moreover, some changes were detected in the relative intensity of the bands at 1056 cm^{-1} , due to CO_3^{2-} , and the one at 556 cm^{-1} , due to OH^- anions. Variations in these bands and detection of new bands at 1410 and 870 cm^{-1} suggest the elimination of CO_3^{2-} anions from the interlayer space due to the successful immobilisation of L-Pro [26].

FT-IR spectrum of LP/HT_{rus}-A2_{0.57} material (Figure 23e) exhibits a series of bands around 2920 cm^{-1} which are due to $\nu(\text{CH})$ from L-Pro. Shifting respect the pure L-Pro due to interactions between CH groups with HT layers. At lower frequency the band at 1560 cm^{-1} due to NH_2^+ group decreases its relative intensity while a new component was detected at 1524 cm^{-1} due to a $\nu(\text{NH})$ vibration interaction with the HT precursor. At 1624 cm^{-1} the band due to COO^- group from the L-Pro does not change after immobilisation suggesting that although a part of the L-Pro could be immobilised in the anionic form, increasing of the time and temperature during its synthesis favoured the immobilisation mostly in zwitterionic form.

Raman spectrum of LP/HT_{rus}-A2_{0.57} material (Figure 24e) also presents perturbations of the CH stretching and deformation modes possibly by interaction with the HT precursor. Moreover, the bands due to zwitterionic L-Pro are strongly reduced in intensity, while the bands assigned to $\nu_{\text{s}(\text{COO}^-)}$ stretching around 1400 cm^{-1} becomes stronger with respect to the pure L-Pro and slightly shifts in position. As in the previous case, this effect can be explained by the coordination of the COO^- group with the HT layers, which suggests the main interaction occurring through the anionic L-Pro, followed by the L-Pro interaction in its zwitterionic form, as reported in FT-IR discussion.

3. Nanohybrid materials based on L-Proline and HT-like materials

3.2 Results and discussion – FT-IR and Raman results

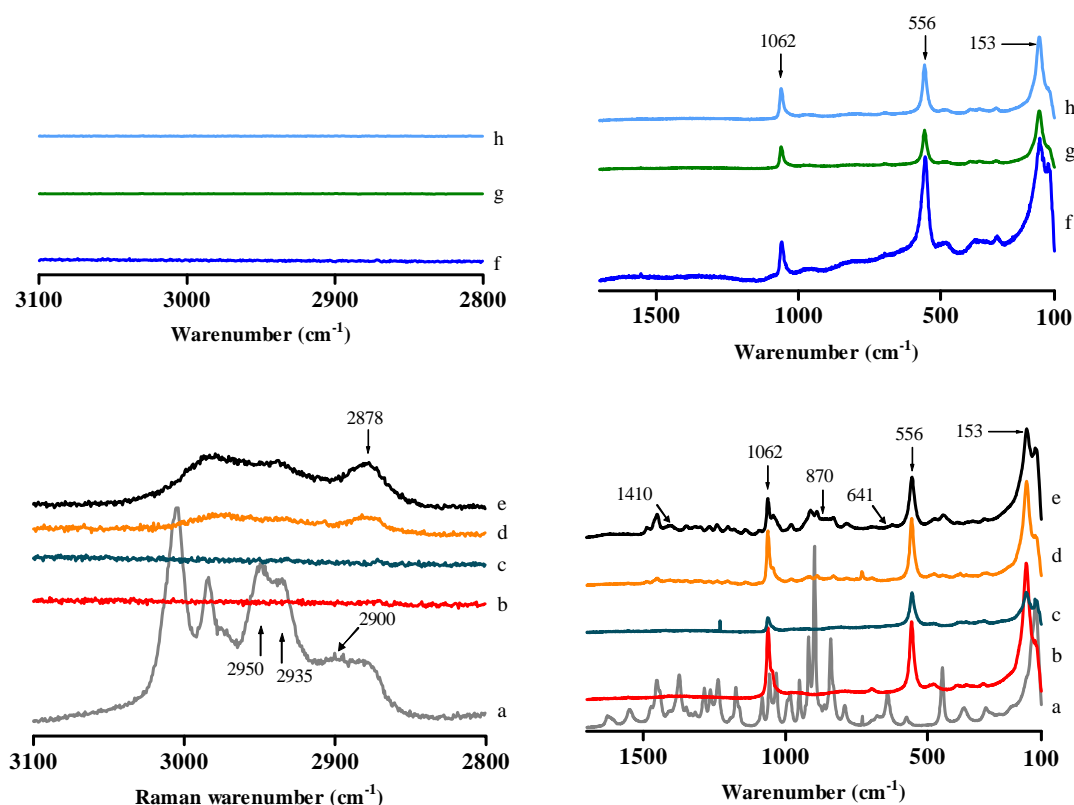


Figure 24 Raman spectra of a) L-Pro, b) HT_{rus}, c) LP/HT_{rus}-A1_{0.07}, d) LP/HT_{rus}-A1_{0.14}, e) LP/HT_{rus}-A2_{0.57}, f) HT_{Clus}, g) LP/HT_{Clus}-A1_{<0.01} and h) LP/HT_{Clus}-A2_{0.01}(left) at increased intensity scale in the frequency region 3100-2800 cm⁻¹ and (right) 1700-100 cm⁻¹.

3.2.2.2 Reconstruction method

FT-IR and Raman spectra of LP/HT_{rus}-R1_{0.60} and LP/HT_r-R2_{0.70} materials are showed in Figures 25 and 26. In FT-IR LP/HT_{rus}-R1_{0.60} spectrum (Figure 25c), the band due to $\nu(\text{CH})$ from L-Pro shifted to lower frequency for the interaction of the L-Pro with the HT layers. At lower frequency, the band due to $\nu_{\text{a}}(\text{COO}^-)$ shifted to 1577 cm⁻¹, while a component at 1524 cm⁻¹ attributed to N-H interaction was detected. Any presence of the band at 1624 cm⁻¹ due to COO⁻ group of zwitterionic L-Pro indicated that L-Pro was mainly immobilised in its anionic form. Additionally, the bands at 1050 and 790 cm⁻¹ due to Al-OH bonds were perturbed after immobilisation indicating that interaction between L-Pro and HT precursor affects the OH⁻ located in the interlayer space of the HT_{rus}. On the other hand, FT-IR spectrum of LP/HT_r-R2_{0.70} (Figure 25d) did not present variation in the $\nu_{\text{a}}(\text{COO}^-)$ or $\nu(\text{NH}_2^+)$ which remained at 1624 and 1560 cm⁻¹ respectively, indicating the immobilisation of L-Pro in its zwitterionic form. However, detection of the band at 1524 cm⁻¹ indicates the presence of L-Pro interaction with the HT precursor.

Raman spectra of LP/HT_{rus}-R1_{0.60} and LP/HT_r-R2_{0.70} materials are similar to the LP/HT_{rus}-A2_{0.57} ones. Evidence of the immobilisation by anionic interactions was found by the lower intensity of the band at 641 cm⁻¹ due to COO⁻ of the zwitterionic L-Pro and the two new bands at 1410 and 870 cm⁻¹ assigned to ν_s(COO⁻) stretching of the immobilised L-Pro.

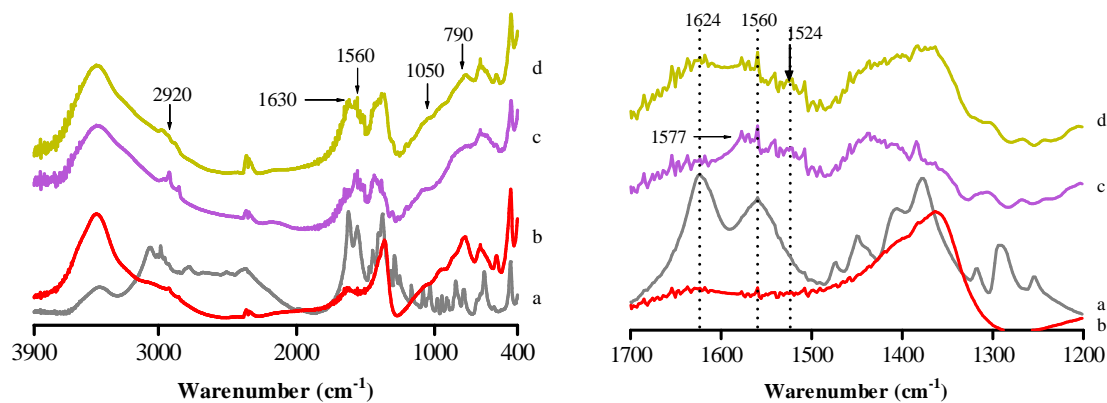


Figure 25 (left) Skeletal FT-IR spectra of a) L-Pro, b) HT_{rus}, c) LP/HT_{rus}-R1_{0.60} and d) LP/HT_r-R2_{0.70} (right) Skeletal FT-IR spectra in the frequency region 1700-1200 cm⁻¹.

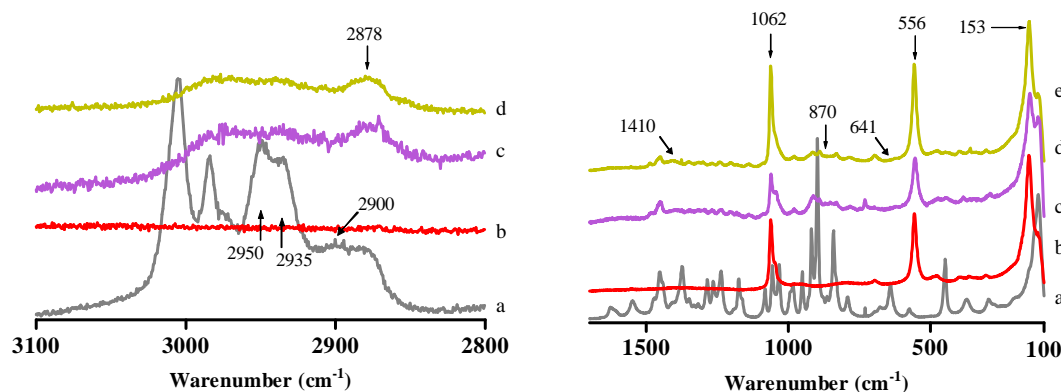


Figure 26 Raman spectra of a) L-Pro, b) HT_{rus} c) LP/HT_{rus}-R1_{0.60} and d) LP/HT_r-R2_{0.70} (left) at increased intensity scale in the frequency region 3100-2800 cm⁻¹ and (right) 1700-100 cm⁻¹.

3.2.2.3 Co-precipitation method

FT-IR spectra of nanohybrid materials synthesised by co-precipitation method are presented in Figure 27.

From a general point of view, LP/HT-C materials present practically undetectable immobilised L-Pro according to TG/DTA results (Table 4, entries 12,14-15). FT-IR spectra of all synthesised nanohybrid materials exhibit two strong bands at 1360 and 1380 cm⁻¹ which are due to the co-intercalated CO₃²⁻ and NO₃⁻ anions.

3.2 Nano hybrid materials based on L-Proline and HT-like materials

3.2 Results and discussion – FT-IR and Raman results

FT-IR observations in comparison with TG/DTA results show that increasing of the L-Pro in the initial solution did not increase the amount of immobilised L-Pro.

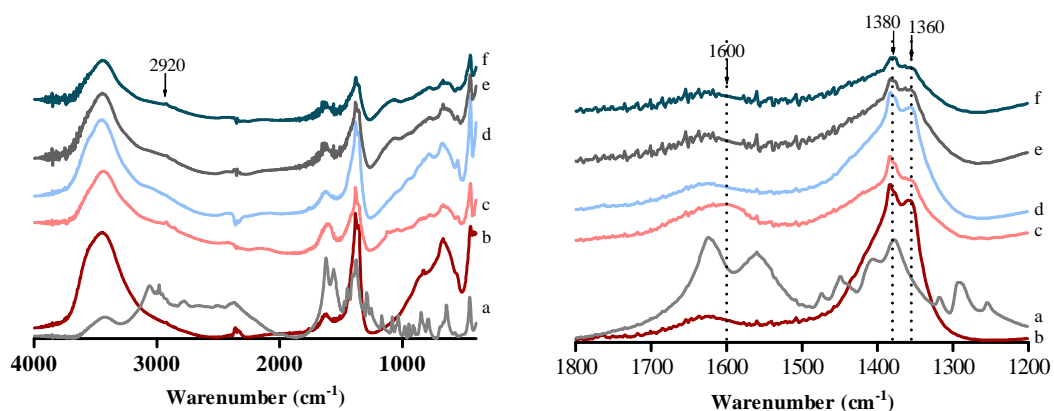


Figure 27 (left) Skeletal FT-IR spectra of (a) L-Pro, (b) HT_{asym}, (c) LP/HT-C1, (d) LP/HT_{us}-C1, (e) LP/HT-C2 and (f) LP/HT-C3. Skeletal FT-IR spectra in the frequency region 1800-1200 cm⁻¹.

Figure 27b shows the FT-IR spectrum of LP/HT-C1, where the bands around 2920 cm⁻¹ and the broad band at 1617 cm⁻¹ could indicate the presence of L-Pro. For this group of materials not much conclusions could be drawn, nevertheless the absence of a band around 1528 cm⁻¹ due to the N-H interaction with HT layers suggests that the immobilisation of L-Pro could mainly occur in its zwitterionic form, which agrees with the XRD results to oblique immobilisation. In the FT-IR spectrum of the LP/HT-C1 after ultrasound treatment (LP/HT_{us}-C1) decreasing of the band around 1600 cm⁻¹ suggests that exfoliation of the HT layers favouring the de-intercalation of the zwitterionic L-Pro (Figure 27d). Raman spectra of this group of nano hybrid materials do not present any evidence of L-Pro due to their lower immobilisation degree*

As it was explained for LL/HT materials, the difference between $\nu_a(\text{COO}^-)$ and $\nu_s(\text{COO}^-)$ gives information about the symmetry of the interaction between the COO⁻ groups with metal surfaces, which is similar to salt-like compounds [31,43]. In this context, shifting in the COO⁻ bands suggests that the immobilisation process occurred by the formation of chelating (bidentate) complexes between the anionic L-Pro and the Al-OH in the HT material. Table 5 presents a summary of the FT-IR findings and the proposed structure for the LP/HT materials according to Nakamoto and Marino's observations.

* See the Raman spectra of LP/HT-C materials in Annex 3, Figure 2.

Table 5 Summary of characterisation data for LP/HT materials

Entry	Material	Synthesis method ^a	Immobilization Location in the HT ^b	$\nu_{a(\text{COO}^-)}$ ^c	$\nu_{s(\text{COO}^-)}$ ^c	$\Delta\nu$ ^d	L-Pro structure ^e	Kind of interaction with HT ^f
5	L-Pro	-	-	1624	1378	246	Z	-
6	LP/HT _{rus} -A1 _{0.07}	A1	Edges	DD ^g	DD	-	A	DD
7	LP/HT _{rus} -A1 _{0.14}	A1	Edges	1574	1377	197	A	Bidentate
8	LP/HT _{Cl} -A1 _{<0.01}	A1	^h	-	-	-	-	-
9	LP/HT _{rus} -A2 _{0.57}	A2	Interlayer space	1624	1379	245	Z	H-bonding
10	LP/HT _{Cl} -A2 _{0.01}	A2	^h	-	-	-	-	-
11	LP/HT _{rus} -R1 _{0.60}	R1	Interlayer space	1577	1377	200	A	Bidentate
12	LP/HT _r -R2 _{0.70}	R2	Interlayer space	1624	1379	245	Z	H-bonding
13	LP/HT-C1	C	Interlayer space	1624	1378	246	Z	H-bonding
14	LP/HT _{us} -C1	C + us	DD	DD	DD	-	-	DD
15	LP/HT-C2	C	DD	DD	DD	-	-	DD
16	LP/HT-C3	C	DD	DD	DD	-	-	DD

^aImmobilisation conditions: See table 4. A=Anionic exchange method, R=Reconstruction method and C=Co-precipitation method. us = Ultrasound treatment. ^bDetermined by XRD analysis. ^cDetermined directly of the FT-IR spectra. ^d $\Delta\nu = \nu_{a(\text{COO}^-)} - \nu_{s(\text{COO}^-)}$. ^eBased on shifting of COO⁻ group by FT-IR. Z= zwitterionic and A= Anionic. ^f $\Delta\nu_{\text{L-Pro}} < \Delta\nu_{\text{nanohyb.}}$ = Bidentate interaction; $\Delta\nu_{\text{L-Pro}} \sim \Delta\nu_{\text{nanohyb.}}$ = H-bonding interaction, according to Nakamoto [31]. ^gNot immobilisation. ^hDD=Difficult to determine.

3.2.3 MAS NMR spectroscopy results

MAS NMR evaluation was performed using LP/HT_{rus}-A2_{0.57}, LP/HT_{rus}-R1_{0.60} and LP/HT_r-R2_{0.70} nanohybrid materials which have the highest amount of immobilised L-Pro. Table 6 shows the ²⁷Al and ¹³C MAS-NMR results for LP/HT_{rus}-A2_{0.57}, LP/HT_{rus}-R1_{0.60} and LP/HT_r-R2_{0.70} nanohybrid materials.

Table 6 ¹³C MAS NMR characterisation of LP/HT nanohybrid materials^a

Entry	Material	Al _{oh}	COO ⁻	C _α	C _β	C _γ	C _δ
1	HT _{rus}	9	-	-	-	-	-
2	L-Pro	-	176	63	47	33	26
3	LP/HT _{rus} -A2 _{0.57}	9	184 164*	65	49	33	28
4	LP/HT _{rus} -R1 _{0.60}	9	183	65	49	33	28
5	LP/HT _r -R2 _{0.70}	9	173 187*	66	50	34	29

^aSee ²⁷Al and ¹³C MAS-NMR spectra in Annex 3, Figures 3 and 4. ^bLess intense signal.

Any variation in the signal at 9 ppm due to the octahedral coordination of the Al atoms after immobilisation process indicates that the interaction between L-Pro and the HT layers does not occur directly in the Al atoms.

The ^{13}C MAS-NMR result for pure L-Pro (Table 6, entry 2) shows the typical signals attributed to its zwitterionic form. Shifting of the signal due to COO^- group from 176 to 187 ppm in LP/HT_r-R2_{0.70} material demonstrates the immobilisation of anionic L-Pro by anion-exchange method, nevertheless the high intensity of the signal at 173 ppm shows that using this method, the immobilisation of zwitterionic L-Pro is favoured.

In the case of LP/HT_{rus}-R1_{0.60} material, the band corresponding to COO^- group shifts from 176 to 184 ppm due to the anionic interaction with the HT precursor, while presence of two signals due to COO^- group in LP/HT_{rus}-A2_{0.57} confirmed the co-existence of both anionic and zwitterionic L-Pro in this material, where the anionic L-Pro was mainly immobilised. Additionally, shifting of the CH bands indicates that the immobilisation process allows L-Pro molecules with less freedom degree due to their interaction with the HT structure.

3.2.4 Thermal evolution of LP/HT materials

Thermal behaviour of L-Pro, LP/HT_{rus}-A2_{0.57}, LP/HT_{rus}-R1_{0.60} and LP/HT_r-R2_{0.70} materials was examined by simultaneous TG/DTA experiments and FT-IR at increasing temperature under outgassing conditions (Table 7 and Figures 28 and 29).

FT-IR spectra of L-Pro at increasing temperature (Figure 28) below 90°C and at higher frequency show changes in the band at 3417 cm^{-1} due to loss of N-H interactions by water loss contained in the pure L-Pro, while at lower frequency the bands at 1560 cm^{-1} due to $\nu(\text{NH}_2^+)$ and at 1380 cm^{-1} due to $\nu_s(\text{COO}^-)$ vibration are becoming stronger. At 130°C the relative intensity of the band at 3417 cm^{-1} decreases while a new band at 3675 cm^{-1} is evidenced. Decrease of this band is due to the progressive elimination of the H-bonding interactions of the L-Pro while new species containing a non-H-bonded O-H is forming. At lower frequencies, bands due to COO^- (1624 and 1377 cm^{-1}) and NH_2^+ (1560 and 1169 cm^{-1}) groups decreased progressively with increasing temperature. At 220°C a decomposition product is formed. According with Moldoveanu, formation of the bands at 2974, 2875 and 1442 cm^{-1} due to vibrations of CH and CH_2 groups, and the strong bands at 3675 (νOH), 1632 ($\nu\text{C}=\text{N}$) and 1377 cm^{-1} ($\nu\text{C}=\text{O}$)

suggest the formation of a tetrahydro-piperidine structure [47]. Finally above 300°C no band due to L-Pro is detected.

Table 7 TG/DTA transformation temperatures and weight losses of L-Pro, LP/HT_{rus}-A2_{0.57}, LP/HT_{rus}-R1_{0.60} and LP/HT_r-R2_{0.70} materials^a

Entry	Material	Temperature range, °C	Max. °C	Weight loss, %	Observations
1	L-Pro	30-192	-	0.1	*Loss of water absorbed in the L-Pro structure.
		192-315	270	89.8	*Decomposition of L-Pro structure.
		315-900	-	10.0	*Decomposition of remained CO, CN and CC species
2	LP/HT _{rus} -A2 _{0.57}	30-145	-	9.9	*Loss of water absorbed in the HT structure.
		145-250	216	6.3	* Loss of water, CO ₂ and NO ₂ from the HT, initial decomposition of L-Pro.
		250-900	332 405	35.1	*Decomposition of immobilized L-Pro *Deshydroxylation of HT layers
3	LP/HT _{rus} -R1 _{0.60}	30-191	-	12.7	* Loss of water absorbed in the HT structure.
		191-260	216	4.9	* Loss of water, CO ₂ and NO ₂ from the HT, initial decomposition of L-Pro.
		260-900	362 405	30.6	*Decomposition of immobilised L-Pro *Deshydroxylation of HT layers
4	LP/HT _r -R2 _{0.70}	30-178	-	10.8	* Loss of water absorbed in the HT structure.
		178-240	212	6.8	* Loss of water, CO ₂ and NO ₂ from the HT, initial decomposition of L-Pro.
		240-900	350 390	35.1	*Decomposition of immobilised L-Pro *Deshydroxylation of HT layers

^aSee TG/DTA curves in Annex 3, Figures 5 and 6.

Thermal evolution of the nanohybrid materials synthesised at 80°C and 3 hours of magnetic stirring are presented above. TG/DTA results of LP/HT_{rus}-A2_{0.57} material (Table 7, entry 2) exhibits a total weight loss higher than the HT_{rus} one (42.9%) which indicates the immobilisation of L-Pro in the material. Moreover, in all cases total decomposition of the L-Pro molecules occurs above 332°C indicating that immobilisation of L-Pro in HT_{rus} increases its thermal resistance.

FT-IR at increasing temperature of LP/HT_{rus}-A2_{0.57}, LP/HT_{rus}-R1_{0.60} and LP/HT_r-R2_{0.70} are presented in Figure 29 and Annex 3 (Figure 7).

From a general point of view, thermal evolution of this group of sample is close among themselves. Difference in the shape of the bands is due to vacuum effect. In all materials, decrease of the band at 1560 cm⁻¹ due to NH₂⁺ group decreases with increasing temperature,

3.2 Results and discussion – Thermal evolution of LP/HT materials

above 90°C this band while some changes occurs in the band at 3470 cm⁻¹ due to water loss from the HT structure. Structural changes observed above 170°C in the band at 790 cm⁻¹ are due to progressive elimination of water from the interlayer space from the HTs. At 220°C relative intensity of all bands decreases due to elimination of CO₂, NO₂, H₂O from the HT structure and NH₃ and CO₂ from the immobilised L-Pro [47]. Above 260°C, two bands at 2168 and 2157 cm⁻¹ were detected suggesting the formation of an isocyanide structure that is strongly interacting with the M-OH surface [48].

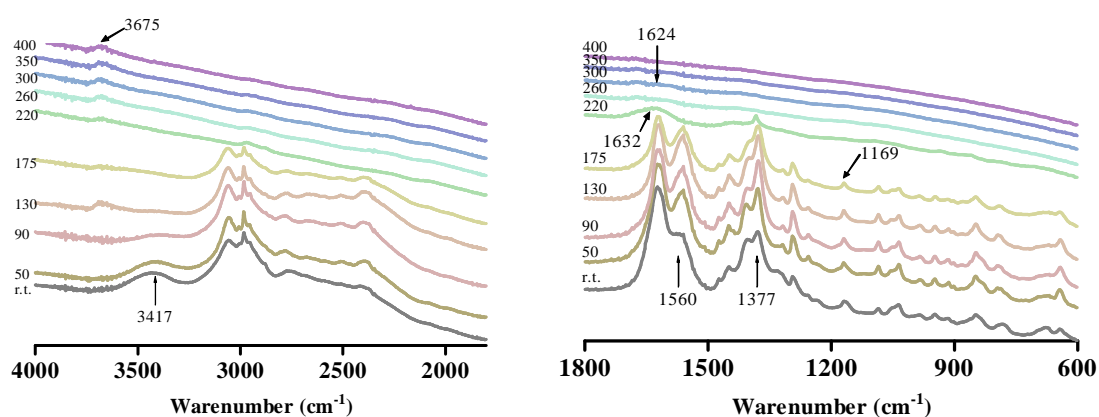


Figure 28 FT-IR spectra of L-Pro outgassing at increasing temperature in the frequency region of (left) 4000-1178 cm⁻¹ and (right) 1178-600 cm⁻¹.

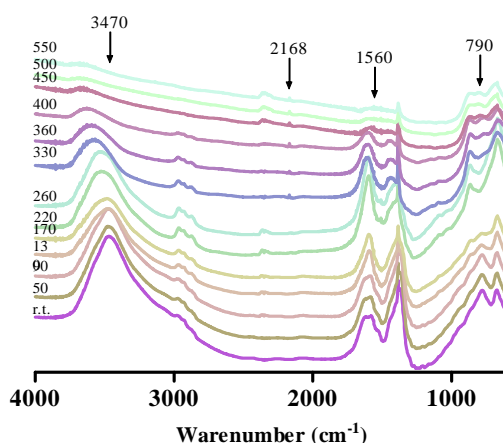
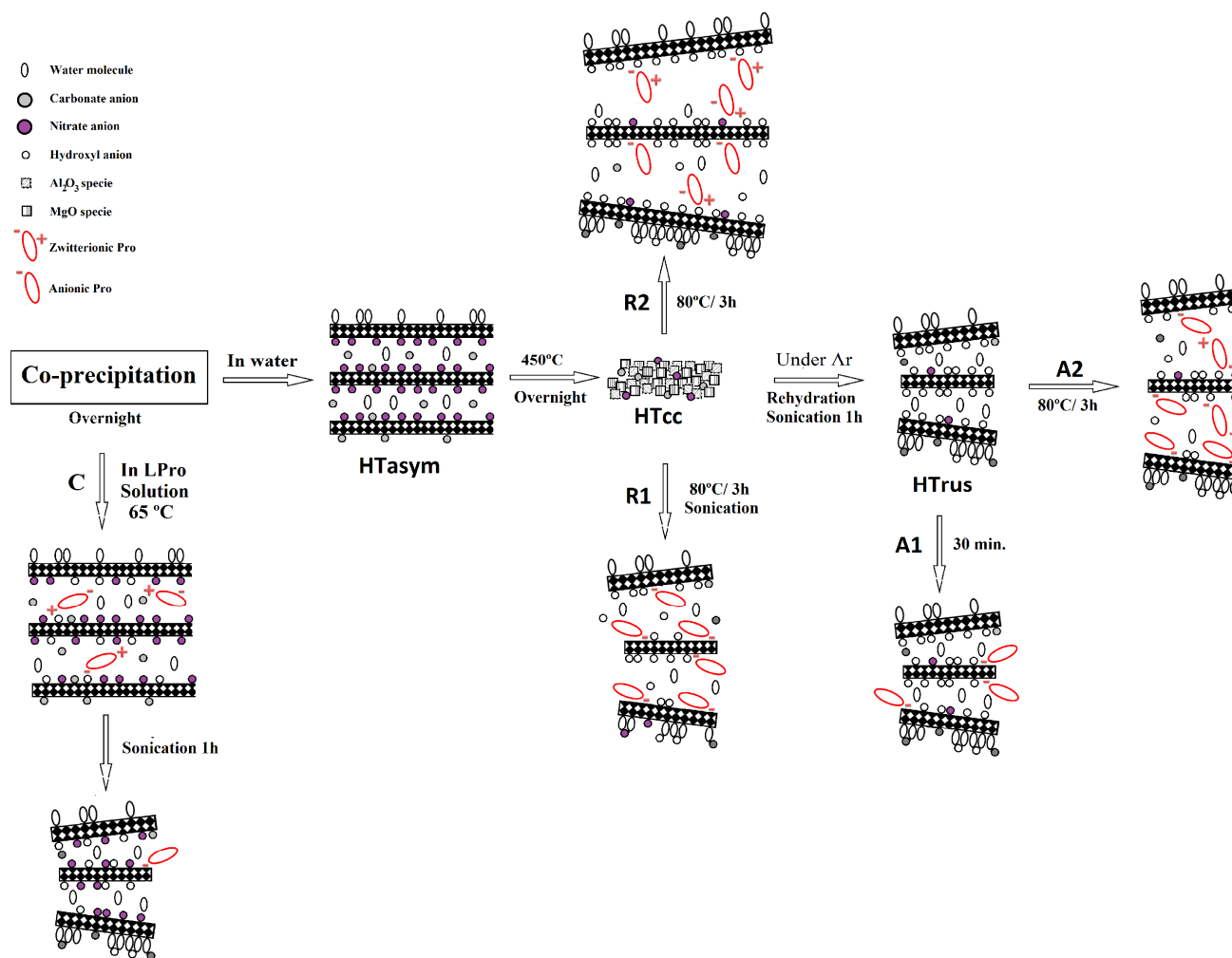


Figure 29 FT-IR at increasing temperature of LP/HT_{rus}-R1_{0.60}.

3.2.5 Nature of the organic/inorganic interaction

In general, determination of the interaction nature between L-Pro and HTs is difficult due to the rigidity of the C-C bonds of L-Pro. Nevertheless based on all characterisation data and also by comparison with LL/HT materials one reliable proposal could be done which is presented in Scheme 4. In a similar way as LL/HT materials, the high-basic active centers in the HTs were obtained by ultrasound treatment permitting the immobilisation of the L-Pro by a quick ionic exchange reaction in just 30 minutes (LP/HT_{rus}-A1_{0.07} and LP/HT_{rus}-A1_{0.44} materials). Any variation in the interlayer space from the HT_{rus} demonstrated that the immobilisation occurs on the edges of the HT_{rus}. Evidence of immobilised L-Pro in zwitterionic form in LP/HT_{rus}-A1_{0.44} and defoliation of the HT layers after immobilisation suggests that the anionic exchange occurs in a first step up to compensation of all accessible basic centres, after that, immobilisation of zwitterionic L-Pro could occur. Stabilisation of zwitterionic L-Pro occurs by H-bonding with water and/or other L-Pro molecules. Lower immobilisation ratio of L-Pro, in comparison with L-Leu, indicate that immobilisation of L-Pro requires strong basic centres located in the interlayer space on the edges of the HT layers. Practically nil amount of immobilised L-Pro in HT_{clus} material shows that immobilisation on the HT surface is not possible. Increase of the time and temperature of synthesis (LP/HT_{rus}-A2_{0.57}, LP/HT_{rus}-R1_{0.60} and LP/HT_r-R2_{0.70}) permitted the immobilisation of the L-Pro in the interlayer space from the HTs. Increase of the interlayer space in LP/HT_{rus}-R1_{0.60} up to 15.3 Å indicated the immobilisation of the L-Pro in the interlayer space. In this case the strong basic centres constantly formed in the material favour the generation of anionic L-Pro and its interaction with the HT structure. In addition, the rigidity and non-polar structure of the L-Pro limit its freedom degree after interaction with the HT (¹³C MAS NMR results). As a result of this conformation, the immobilisation occurs in a parallel orientation with respect to the HT layers stabilised by NH⁺OH interaction between the imino group and M-OH species in the HT layers, limiting also the immobilisation of most L-Pro molecules. Similar conclusions were presented by Mateo Marti *et al.* [49] to L-Pro immobilised over copper surfaces. Finally, taking into account the size of the pure L-Pro (2.8 Å in width, 5.5 Å in length and 6.0 Å in thickness) increases of the interlayer space up to 15.3 Å suggest that the immobilised L-Pro is forming a bilayer accommodation in the HT_{rus}. In the case of LP/HT_{rus}-A2_{0.57} and LP/HT_r-R2_{0.70}

materials, XRD patterns also showed increase of the interlayer space up to 15.8 and 14.8 Å respectively. Increasing of this distance and the detection of stretching modes of zwitterionic L-Pro suggest that the immobilisation of the L-Pro into the interlayer space could occur in two ways: vertical when the zwitterionic form is present and parallel respect to the layers for anionic interactions between L-Pro and M-OH species from the layers. Additionally, immobilisation of L-Pro in the interlayer space increases the thermal resistance of the L-Pro from 280 to around 350°C. Finally, co-precipitation method allows materials (LP/HT-C1, LP/HT-C2 and LP/HT-C3) where the L-Pro is immobilised in lower amount with the co-incorporation of nitrates and carbonates anions. The low amount of L-Pro in the materials makes the characterisation by most of the characterisation techniques more difficult, nevertheless XRD results showed that the 003 diffraction peak is formed by different interlayer spaces between 7.8 to 8.9 Å. This effect is explained because the incorporation of other anions reorganises the position of the zwitterionic L-Pro on the material. Moreover, the ultrasound treatment after co-precipitation showed the easy elimination of the zwitterionic L-Pro.



Scheme 4 Schematic representation of synthesised LP/HT materials

4. Conclusions

Syntheses of HTs with controllable basicity are an excellent opportunity to study the organic/inorganic interaction of AAs with anionic inorganic supports. In this context, using ultrasound treatment during the rehydration of calcined HT affords more accessible OH⁻ centres which increase the basicity of the entire material. This methodology permits the immobilisation of AAs in higher degree than similar methods previous published. Approaching the high basicity of the HT_{rus}, immobilisation of L-Leu and L-Pro was possible by a quick anionic exchange method performed in just 30 minutes (Method A1). The immobilisation occurs through anionic AAs with the OH⁻ anions from the HTs in a first moment since all accessible centres are compensated. If there is excess of AAs in the media, the immobilisation can also occurs by the interaction of AAs by H-bond with water, inorganic anions and/or other AA molecules located on the edges of the HT structure. This interaction protects the material from the CO₃²⁻ incorporation; nevertheless excessive exposition of the material to the air permitted the reaction of the M-OH on surface with atmospheric CO₂.

Increases of the time and temperature of synthesis permitted the swelling of the material and the incorporation of the AAs forming bilayers in the interlayer space (Method A2). Although using L-Leu this immobilisation occurs by anionic L-Leu, using L-Pro zwitterionic conformation was also detected. At this point, the nature of the AAs is important; L-Leu has a linear structure with a pKa of 9.74 which facilitate the interaction with basic centres. Nevertheless, L-Pro has a rigid cyclic structure which limits its freedom degree, but also has a pKa of 10.64. This property means that immobilization of anionic L-Pro only occurs though anionic exchange only with highly active basic centres.

The role of the ultrasound treatment to obtain highly active centres was evaluated by reconstruction method. Using ultrasound treatment before the immobilisation (Method R1) the nature of the nanohybrid material changed. Immobilisation of anionic L-Pro in the interlayer space is a reliable evidence of the basic strength in HT_{rus}. On the other hand, using reconstruction method without ultrasound treatment (Method R2), the immobilisation occurred mainly by H-bonding interaction between AAs with water and inorganic anions located in the interlayer space. It was also observed that the swelling effect of the HT_{rus}

permitted the immobilisation of higher amount of L-Pro. As a control probe, immobilisation of L-Leu and L-Pro was performed using HT_{clus} obtaining practically nil immobilisation degree, this experiment was indicative that AAs are immobilised in the interlayer space and/or on the edges of the HT layers, but not on the surface where the basic centers are weak in strength.

Additionally, it was demonstrated that immobilisation of L-Pro using co-precipitation method does not permit to obtain a stable nanohybrid material, because the compensation of the charges during the process occurs by the strongest NO₃⁻ anions present in the medium. Moreover, ultrasound treatment after co-precipitation permits the elimination of the immobilised zwitterionic L-Pro.

In all cases the nature of the immobilisation and also the orientation of the immobilised anionic AAs were evaluated. In this context, L-Leu interacts with M-OH species forming bridging-like coordination. According to the XRD results, the immobilisation could occur in a vertical or oblique orientation respect to the HT layers. On the other hand, L-Pro interacts by forming a bidentate-like coordination with the M-OH species. Moreover, the unfavoured steric effect was compensated by H-bonding formed between the N-H imino group and the M-OH species in the HT. This conformation suggests that the immobilisation of anionic L-Pro occurs in a parallel orientation respect to the HT layers. When the AAs were immobilised in zwitterionic form, the orientation depends on the chemical environment in the interlayer space from the HT.

In general the immobilisation of L-Leu and L-Pro allows materials with higher thermal resistance than in the pure state. Moreover, interestingly and to the best of our knowledge, we reported for the first time the polycondensation of L-Leu catalysed by HT. In this topic, it is necessary for the immobilisation of both anionic and zwitterionic L-Leu in the interlayer space of the HT increase the temperature up to around 230°C.

Finally, a part of the results presented in this section were included in two articles which are currently under revision:

- “*L-Leucine Immobilised in Hydrotalcite-like Materials. Understanding of the Immobilisation Nature*” Ronald-Alexander Miranda, Elisabetta Finocchio, Francisco Medina, Gianguido Ramis, Jesús E. Sueiras, Jordi Llorca and Anna M. Segarra

- “*Nanohybrid Materials Based on L-Proline and Hydrotalcites as Catalysts for Direct Asymmetric Aldol Reaction*” Ronald-Alexander Miranda, Elisabetta Finocchio, Francisco Medina, Gianguido Ramis, Jesús E. Sueiras and Anna M. Segarra

References

- [1] J.-H. Choy, S.-Y. Kwak, J.-S. Park, Y.-J. Jeong and J. Portier. *J. Am. Chem. Soc.* **1999**, *121*, 1399
- [2] Q. Zhenlan, Y. Heng, Z. Bin and H. Wanguo. *Colloids and Surfaces A: Physicochem. Eng. Aspects.* **2009**, *348*, 164
- [3] S. Vijaikumar, A. Dhakshinamoorthy and K. Pitchumani. *Appl. Catal. A.* **2008**, *340*, 25
- [4] B.M. Choudary, B. Kavita, N. Sreenivasa Chowdari, B. Sreedhar and M. Lakshmi Kantam. *Catal. Lett.* **2001**, *78*, 1
- [5] H. Nakayama. *Phosphorus Res. Bull.* **2009**, *23*, 1
- [6] M.B.A. Rahmana, M. Basri, M.Z. Hussein, M.N.H. Idris, R.N.Z.R.A. Rahman and A.B. Salleh. *Catal. Today.* **2004**, *93-95*, 405
- [7] J.-H. Choy, S.-Jin Choi, J.-M. Oh and T. Park. *Appl. Clay Sci.* **2007**, *36*, 122
- [8] M. Meng, L. Stievano and J. F. Lambert. *Langmuir.* **2004**, *20*, 914
- [9] M. Del Arco, E. Cebadera, S. Gutiérrez, C. Martín, M.J. Montero, V. Rives, J. Rocha and M.A. Sevilla. *J. Pharm. Sci.* **2004**, *93*, 1649
- [10] R. J. Chimentaõ, S. Abelló, F. Medina, J. Llorca, J. Sueiras, Y. Cesteros and P. Salagre. *J. Catal.* **2007**, *252*, 249
- [11] R. Morales Borgesa, G.G. Carbajal Arizaga and F. Wypych. *Biochem. Eng. J.* **2009**, *48*, 93
- [12] N.T. Whilton, P.J. Vickers and S. Mann. *J. Mater. Chem.* **1997**, *7*, 1623
- [13] T. Hibino. *Chem. Mater.* **2004**, *16*, 5482
- [14] M.X. Reinholdt and R.J. Kirkpatrick. *Chem. Mater.* **2006**, *18*, 2567
- [15] S. Aisawa, S. Takahashi, W. Ogasawara, Y. Umetsu and E. Narita. *J. Sol. Stat.* **2001**, *162*, 52
- [16] Q. Yuan, M. Wei, Z. Wang, G. wang and X. Duan. *Clay and Clay Miner.* **2004**, *52*, 40
- [17] M.X. Reinholdt, P.K. Babu and R.J. Kirkpatrick. *J.Phys.Chem.C.* **2009**, *113*, 3378
- [18] S. Aisawa, S. Sasaki, S. Takahashi, H. Hirahara, H. Nakayama and E. Narita. *J. Phys. Chem. Sol.* **2006**, *67*, 920
- [19] Á. Fudala, I. Pálinkó and I. Kiricsi. *Inorg. Chem.* **1999**, *38*, 4653
- [20] H Nakayama, N. Wada and M. Tsuhako. *Int. J. Pharm.* **2004**, *269*, 469
- [21] S. Aisawa, H. Kudo, T. Hoshi, S. Takahashi, H. Hirahara, Y. Umetsu and E. Narita. *J. Solid State Chem.* **2004**, *177*, 3987

- [22] M. Jobbágy and A.E. Regazzoni. *J. Phys. Chem. B.* **2005**, *109*, 389
- [23] F. Cavani, F. Trifirò and A. Vaccari. *Catal. Today.* **1991**, *11*, 173
- [24] P.F.F. Filho, P.T.C. Freire, K.C.V. Lima, J.M. Filho and F.E.A. Melo. *Cond. Mat. Mtrl. Sci.* **2007**, arXiv:0704.2792v1
- [25] B.J.M. Rajkumar and V. Ramakrishnan. *J. Raman Spectrosc.* **2000**, *31*, 1107
- [26] J.T. Klopogge and R.L. Frost. *J. Sol. State Chem.* **1999**, *146*, 506
- [27] S. Miyata. *Clay and Clay Miner.* **1983**, *31*, 305
- [28] J. Pérez-Ramírez, G. Mul and J.A. Moulijn. *Vibrational Spectroscopy.* **2001**, *27*, 75
- [29] A.R. García, R.B. de Barros, A. Fidalgo and L.M. Ilharco. *Langmuir.* **2007**, *23*, 10164
- [30] N.B. Colthup, L.H. Daly and S.E. Wiberley. *“Introduction to Infrared and Raman Spectroscopy”* 3rd Ed. Elsevier, Amsterdam, **1990**. ISBN-13: 978-0121825546
- [31] K. Nakamoto. *“Infrared and Raman spectra of inorganic and coordination compounds”*. 5th Ed. John Wiley & Sons, New York, **1997**. ISBN 0-471-19406-9
- [32] M. Kakihana, T. Nagumo, M. Okamoto, and H. Kakihana. *J. Phys. Chem.* **1987**, *91*, 6128
- [33] A. Béres, I. Pálikó, J.-C. Bertrand, J.B. Nagy and I. Kiricsi. *J. Mol. Struct.* **1997**, *410-411*, 13
- [34] J. Rocha, M. del Arco, V. Rives and M. Ulibarri. *J. Mater. Chem.* **1999**, *9*, 2499
- [35] F. Rey, V. Fornes and J.M. Rojo. *J. Chem. Soc. Faraday Trans.* **1992**, *88*, 2233
- [36] W. Yang; Y. Kim, P.K.T. Liu, M. Sahimi and T.T. Tsotsis. *Chem. Eng. Sci.* **2002**, *57*, 2945
- [37] V.A. Basiuk. *J. Anal. Appl. Pyrolysis.* **1998**, *47*, 127
- [38] S.-S. Choi, and J.-E. Ko. *J. Anal. Appl. Pyrolysis.* **2010**, *89*, 74
- [39] J. Bujdák and B.M. Rode. *Orig. life Evol. Bioph.* **1999**, *29*, 451
- [40] J. Bujdák and B.M. Rode. *Catal. Lett.* **2003**, *73*, 797
- [41] J. Bujdák and B.M. Rode. *J. Peptide Sci.* **2004**, *10*, 731
- [42] S. Miyata. *Clay and Clay miner.* **1975**, *23*, 369
- [43] T. Marino, N. Russo and M. Toscano. *J. Phys. Chem. B.* **2003**, *107*, 2588
- [44] S. Stewart and P.M. Fredericks. *Spectrochimica Acta Part A.* **1999**, *55*, 1641
- [45] Y.S. Mary, L. Ushakumari, B. Harikumar, H.T. Varghese and C.Y. Panicker. *J.Iran Chem. Soc.* **2009**, *6*, 138
- [46] E. Podstawka, Y. Ozaki, and L.M. Proniewicz. *Applied Spectroscopy.* **2004**, *58*, 570
- [47] Serban C. Moldoveanu, *“Pyrolysis of organic molecules with applications to health and environment issues”* in *Techniques and instrumentation in analytical chemistry - Vol 28*. Elsevier, Amsterdam, **2010**, ISBN 0167-9244
- [48] T. Montenari, E. Finocchio and G. Busca. *J. Phys. Chem. C.* **2011**, *115*, 937

- [49] E. Mateo Marti, S.M. Barlow, S. Ha and R. Raval. *Surf. Sci.* **2002**, *501*, 191

INTRODUCTION AND SCOPE

The rapid increase in the field of biohybrid materials, that exhibit improved structural and functional properties, is attracting more and more attention not only for researchers of different disciplines (biotechnology, medicine, pharmacy, nanotechnology, engineering etc.) but also for the industry. The results obtained by the scientific community offer valuable opportunities for diverse applications which cover areas as different as drug delivery systems, bio-sensing devices, green nano-composites and bio-catalysis. On the other hand, oxidation reactions are among the most significant processes in the chemical industry and epoxides are important intermediates both in bulk and fine chemical synthesis.

Using bio-hybrid materials for catalysis involve several challenges: i) the tunable system synergically enhanced by their two components must obtain deliverable properties that are unattainable from only one of the two components, ii) the catalytic systems must lead an excellent catalytic performance, iii) the processes must be designed to improve the efficiency of the chemical reaction and iv) the bio-hybrid catalyst must be designed so that they can be recovered and reused, and, in this way, ensure the environmental and economic viability of the process. Taking these factors into account, we considered various hypotheses of work focused on the synthesis, characterisation and catalytic applications of bio-nano hybrid materials. The academic challenges for this thesis were being defined in this paper where, following the hierarchy of goals to be met in any study of research, the first of which was to know the state of the art.

Therefore, this section attempts to provide the reader with a general overview of the principal concepts highlighted in this thesis.

1. Bio-nano hybrid materials

1.1 Hydrotalcite-like materials

1.2 Amino acids and poly-aminoacids

1.3 Bio-nano hybrid materials based on AAs, PAAs and HTs.

2. Bio-nano hybrid materials as catalysts in asymmetric synthesis

2.1 Juliá-Colonna asymmetric epoxidation reaction

2.2 Direct asymmetric aldol reaction

2.3 One-pot reactions

3. Scope of this thesis

References

1. Bio-nanohybrid materials

Biological systems are usually cleverly designed to combine many optimised parallel processes, which are dynamically connected to each other in harmony. Therefore, the scientists have found inspiration in nature for breakthroughs in current technologies. From the point of view of materials science, nature always creates functional optimised structures based on the self-assembly of unit materials [1]. Therefore, self-assembly processes as observed in biological systems can be a practical tool for the fabrication of advanced materials such as bio-inorganic hybrid solids.

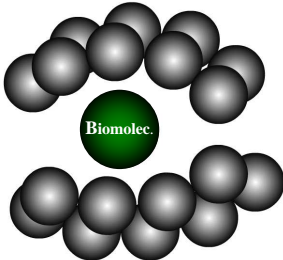
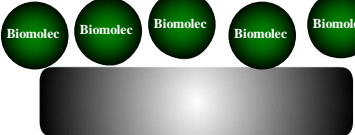
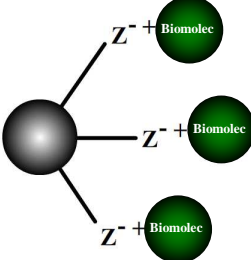
Bio-nanohybrid materials result from the combination of molecular or polymeric species of biological origin and inorganic nano-structured materials. These new solids have emerged with force in the last years as an interdisciplinary topic on the border between nanotechnology, material and life sciences. They are of great interest due to their versatile applications in diverse areas as regenerative medicine, nanocomposite materials engineering, catalysis, etc [2-5]. In addition, bio-nanohybrid materials are interesting for industrial applications since they are derived from abundant, cheap, and ecological sources. One of the most important reasons because the bio-nanohybrid materials have received attention is because they not only often exhibit high complementary properties between their assembled components but also present new and interesting properties due to a synergistic effect [6-7]. In catalysis, immobilisation of biomolecules permits to obtain solid materials which can be used as catalysts and provide numerous opportunities for recovering and recycling them from reaction environments [8].

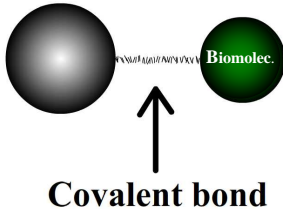
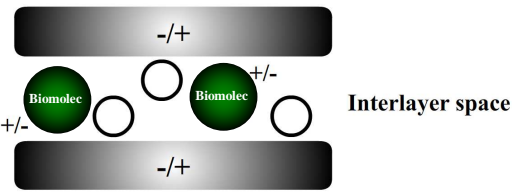
Several solid materials such as polymers [9-10], micro/mesoporous materials [11-14] and clays [3,15-16] have been employed as solid supports to biomolecules. In some cases, these bio-nanohybrid materials presented successful activity as chiral catalysts in asymmetric reactions [3,17-18]. Nevertheless, bio-nanohybrid catalysts have two principal disadvantages. First, the insufficient stability of the immobilised biomolecule due to leaching of the metal and/or the biomolecule and second, the low catalytic activity respect to the homogenous phase due to poor accessibility of the active sites for the substrate, steric effect of the matrix or deactivation of the active center.

The bottom-up self-assembly process from well-designed units is one of the best strategies for the construction of bio-nanohybrids. Usually, this approach involves routes based on soft chemistry such as the sol-gel process which permits to entrap a large number of organic and bio-organic molecules in matrixes derived from precursor monomers, intercalation between the lamella of 2D solids or inclusion in 3D nano-structures, or by the grafting to the organic counterpart through the covalent bonds on the surface of inorganic solids. Combination of two of these routes could be also required to provide the hybrid materials with the desired structural and functional properties.

Although, bio-nanohybrid materials can be synthesised under liquid media [19-20], our study was focused on the immobilisation of biomolecules onto solid supports (Table 1) specifically onto a family of naturally occurring layered clays named hydrotalcite-like materials (HTs).

Table 1 Immobilisation methods of biomolecules onto solid supports.

Immobilisation methods	Comments / troubles
<p>Biomolecules supported by physical adsorption</p> 	<p>Strict control of support porosity Diffusion troubles Limited application</p>
<p>Biomolecules supported by adsorption</p>  <p>Adsorbed layer Solid support</p>	<p>Potential competition with solvents and/or substrates Limited applications</p>
<p>Biomolecules supported by ionic interaction</p> 	<p>Anionic or cationic Potential competition with ionic substrates and/or salts</p>

<p>Biomolecules supported by covalent bond</p>  <p>Covalent bond</p>	<p>Organic, polymeric and inorganic matrixes Higher application</p>
<p>Catalysts supported by intercalation</p>  <p>Interlayer space</p>	<p>Layer materials like cationic or anionic clays Potential competition with other ions in solution</p>

1.1 Hydrotalcite-like materials

HTs are a class of synthetic two-dimensional nanostructured anionic clays whose structure can be described as containing brucite-like layers, $Mg(OH)_2$, where a fraction of the octahedrally coordinated Mg^{2+} (6-fold coordinated to OH^-) have been replaced isomorphously by trivalent cations, giving positively infinite charged hydroxyl layers. This positively charged net is compensated by CO_3^{2-} anions, which lie in the interlayer region between two brucite-like layers. In the free space of this interlayer water and other anions are randomly located with a high degree of mobility (Figure 1) [21-22].

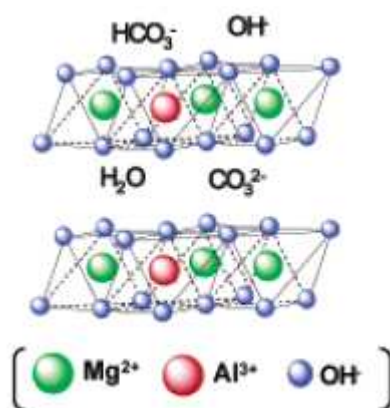


Figure 1 Structure of HT $[Mg_6Al_2(OH)_{16}CO_3]$ [23].

HTs are characterised by the general formula $[M^{2+}_{1-x}M^{3+}_x(OH)_2]^{b+}[A^{n-}]_{b/n}.mH_2O$, where M^{2+} ($M = \text{e.g. Mg, Fe, Co, Cu, Ni or Zn}$) and M^{3+} ($M = \text{e.g. Al, Cr, Ga, Mn or Fe}$) are various divalent and trivalent metal ions; A is an anion of charge n such as CO_3^{2-} , Cl^- , NO_3^- or

1.1. Hydrotalcite-like materials

organic anions. The value of x is equal to the molar ratio of the $M^{2+}/(M^{2+} + M^{3+})$ and is generally in the range 0.2 – 0.33. The x value determines the layer charge density and the anion exchange capacity. The anions can be exchanged by other inorganic, organic or metallo-organic anions and even by biologically active molecules containing ionisable acidic groups.

The most interesting properties of HTs and their mixed oxides (obtained by calcinations of HTs) may be summarised as follows [22-31]:

- *High surface area* (100-300 m²/g)
- *Homogeneous dispersion* of the thermally stable elements also in reducing conditions, with formation of very small and stable metal crystallites.
- *Cation-exchange ability of the brucite layers*, which allows synthesising different materials by ionic exchange procedures.
- *Anion-exchange ability of the interlayer*, which allows increasing or reducing the basicity of the HTs and immobilising many organic molecules in the interlayer space.
- *Swelling* as the consequence of their smooth flexible structure with relatively few interlayer bonding.
- *As host material* in order to create inorganic-organic host-guest hybrid structures with desirable physical and chemical properties, in which the brucite-like layers may impose a restricted geometry on the interlayer guests leading to enhanced control of stereochemistry, rates of reaction, and product distributions.
- *Synergistic effects* between the components, due to the intimate interdispersion, which favours, for example, the development of unusual basic or hydrogenating properties. It is worth nothing that basic properties depend significantly on composition and calcination temperature.
- *Memory effect*, which allows reconstruction of the original structure by contact with aqueous solutions containing various anions.
- *Low cost* because high technologies or expensive reagents are not necessary to their synthesis.
- *Low toxicity* due to their biocompatibility with naturally occurring molecules.

1.1.1 Synthesis of HTs

HTs can be found in nature as minerals or readily synthesised in the laboratory. In nature they are formed from the weathering of basalts or precipitation in saline water source. Unlike silicate-based clays, HTs are not found in large or commercially useful deposits. In the laboratory, there are different methods for synthesising HTs such as co-precipitation [32], urea reduction [33], salt-oxide method [34], hydrothermal [34] and sol-gel [35] methods, but the most frequently used is the co-precipitation method.

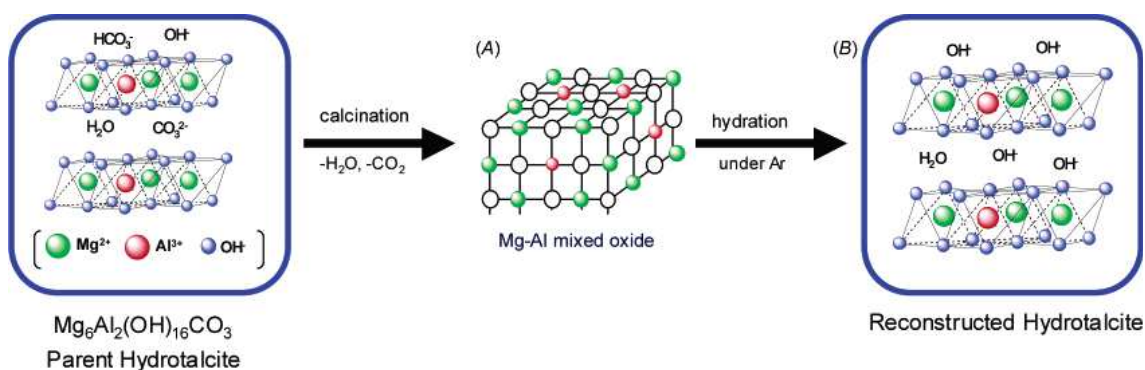
The co-precipitation method is based on the slow addition of a mixed solution of divalent and trivalent metal salts to an alkaline solution which leads to the co-precipitation of the two metallic salts. Formation of the HTs is based on the condensation of hexa-aqua complexes in solution that form the brucite-like layers containing both metallic cations [22]. Interlayer anions either arise from the counter-anions of the metallic salts, or anions from the alkaline solution. At high pH, hydroxyl ions are prevalent and therefore can be intercalated [36]. At low pH the synthesis proceeds by a more complex pathway and is not complete. This effect is indicated by the formation of an amorphous compound which has different chemical composition than its starting materials. In order to obtain well organized phases, the preparation conditions have to be optimised for the desired product. In general to form well ordered HT structures a pH range between 8 and 10 is required [37].

One of the advantages of this method is the precipitation occurs at lower pH than in the absence of M^{2+} , thus there is less risk of the incorporation of unwanted CO_2 by the reaction mixture. Such uptake of CO_2 is a major nuisance in HT synthesis because it gives rise to carbonate, which is the most strongly held anion within the HT interlayer region.

Thermal decomposition of Mg-Al HTs leads to a well dispersed mixture of magnesium and aluminium oxides ($MgAlO_x$). These mixed oxides are formed with very small crystal size and are stable to thermal treatments. Moreover, calcined oxides show the *memory effect*, a property by which they can recover the original layered structure if they come into contact with water vapor or are immersed in water under decarbonated atmosphere (rehydration or reconstruction method). This leads to meixnerite [$Mg_6Al_2(OH)_{18}$] which is a

1.1. Hydrotalcite-like materials

more basic material because that is HTs intercalated with OH^- as compensating anions in the interlayer (Scheme 1).



Scheme 1 Synthesis of meixnerite [Mg₆Al₂(OH)₁₈] [23].

1.1.2 Accesibility of the Brönsted-Base sites in rehydrated hydrotalcites

Accesibility of the OH^- groups in rehydrated HTs has been determined by its activity as solid base catalysts. Nowadays, it is well-known that active sites in HTs are located on the edges of the layers, which are only a minor part of the Brönsted-base groups present in the HTs. de Jong *et al.* reported that the activity of the rehydrated HTs involves both the counteranion OH^- between the layers and the reconstructed layers of the HT. Several characterisation data demonstrated that rehydration of a previously calcined HT allows more active and accessible basic centres than by other methods [38,39]. Moreover, Medina *et al.* studied the rehydration of the mixed oxide *via* three methods demonstrating that rehydration process under ultrasound treatment was an effective method to maximise the accessibility and utility of the OH^- anions [40]. They explained that phenomena because ultrasound treatment permits the formation of small HT nanolayers with irregularities along the platelets. In general, a common problem using more active HTs is the competition between anions and the incorporation of CO_2 in their structure, for this reason, manipulation of the materials under an inert atmosphere is usually crucial.

1.1.3 Ion-exchange properties

The HTs can modify their chemical structure and their physic-chemical properties by exchange of the anions located in the interlayer space. In this context, the anion-exchange is

the most common method for the incorporation of organic anions into the HT structure. Monovalent anions can be exchanged easily in the follow order: $\text{OH}^- > \text{F}^- > \text{Cl}^- > \text{Br}^- > \text{NO}_3^-$. However, divalent anions such as SO_4^{2-} and CO_3^{2-} have higher selectivity than monovalent ones. Due to the relatively easy capacity of the NO_3^- to be exchanged, HTs containing NO_3^- are the most suitable precursors for anion exchange syntheses. In general, the anion-exchange reaction of organic molecules is carried out by simply dispersing the precursor HT in aqueous solution containing an excess of the organic anion to be incorporated. The organic anion of interest must be stable at the pH of exchange [37].

So, biocompatibility, variable chemical composition, ability to intercalate organic anions, nanosize and alkaline character of the HTs have permitted the generation of a new kind of nanohybrid materials with pharmaceutical, biochemical and catalytic applications [1-4,41-42]. Particularly, nanohybrid materials based on Mg/Al HT allow the design and synthesis of a large number of hybrid materials by changing the interlayer anions *via* anion exchange procedures. Anionic biomolecules such as DNA [43-44], ATP [30], nucleotides [43-44], vitamins [42], drugs [45-48], pesticides [41,49], amino acids [3,16,50-54], enzymes [55-56] and polymers [52,57-59] are some examples of organic and bio-organic molecules immobilised in HTs.

1.2 Amino acids and poly-amino acids

Amino acids (AAs) are carboxylic acids that contain at least an amine group. AAs play central roles as building blocks of proteins and as intermediates in metabolism. AAs are classified as α , β , γ , and so on, according to the location of the amine group on the carbon chain that contains the carboxylic acid function. (Fig. 2)

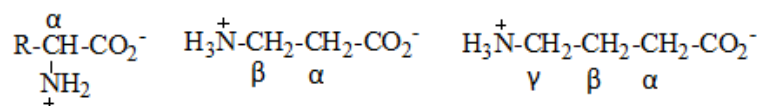
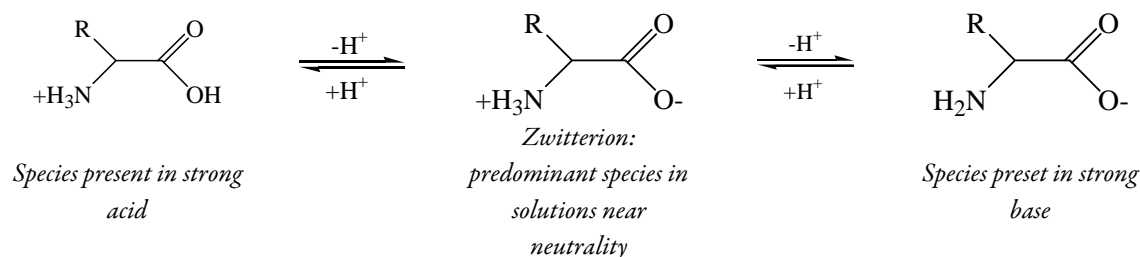


Figure 2 α , β and γ amino acids.

Although more than 700 different AA are known to occur naturally, a group of 20 of them demand special attention. All the AAs precursors of proteins are α -AAs, and all of them contain a primary amino function and conform to the general structure, the unique exception

1.2 Amino acids and poly-amino acids

is proline (Pro), which is a secondary amine with an amino nitrogen into a five-membered ring. AAs are amphoteric substances, meaning they contain an acidic functional group and a basic functional group. This bifunctionality allows AAs to have amphiprotic properties. The carboxylic acid group (-COOH) can be deprotonated to become a negative carboxylate (-CO₂⁻), an α-amino group (NH₂-) can be protonated to become a positive α-ammonium group (⁺NH₃-). Each AA has a characteristic isoelectric point (pI) which is the pH value at which the AA bears no net charge and the zwitterionic specie is the predominant form adopted by the AA; and two pK values (pK_{a1} for deprotonation of the -COOH and pK_{a2} for a second deprotonation from the α-ammonium groups) (Scheme 2) [60]. In solid state AAs exist as zwitterions as presented in Annex 1.



Scheme 2 Amphoteric behaviour of amino acids in acid, neutral and base solution.

The most important behaviour of AAs is that under certain conditions the amine group of one molecule and the carboxyl group of a second one can react together joining the two AAs by an amide bond (peptidic bond) to form peptides or poly-amino acids (PAAs).

Natural PAA (proteins) are copolymers of α-AA linked together, through amide bonds, in a well-defined sequence, which characterises their primary structure. Intra- and intermolecular interactions between the functional groups of the residual AAs lead to organised higher order (secondary, tertiary, and quaternary) 3D structure, which are responsible for the extremely selective and quantitative catalytic properties as well as the mechanical performance of proteins [60].

* A complete list of the nature occurring amino acids is included in Annex 1, Table 1.

1.2.1 Synthesis of poly-amino acids

Biological systems produce proteins that possess the ability to self-assemble into complex, yet highly ordered structures [61]. These remarkable materials are PAA copolymers that derive their properties from precisely controlled sequences and compositions of their constituent AA monomers. There has been recent interest in developing synthetic routes for preparation of mimics of these natural polymers as well as wholly artificial PAA sequences for applications in catalysis [62-64] and biotechnology [65-66]. Although there are different methods to synthesize PAA [67], ring-opening polymerisation (ROP) of α -amino acid-N-carboxyanhydrides (NCA) is the most economic and common technique used even for large scale preparation of PAA [68].

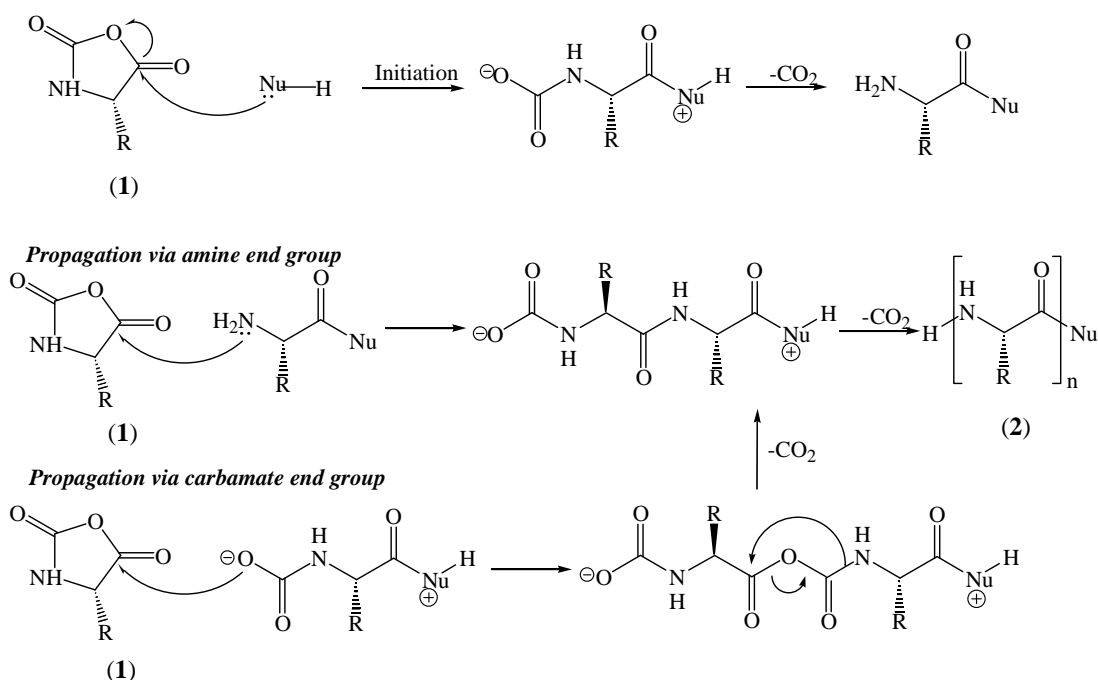
1.2.1.1 Ring opening polymerisation

ROPs are traditionally initiated using many different nucleophiles and bases, the most common being primary amines and alkoxides anions [69]. Primary amines, being more nucleophilic than basic, are good general initiators for ROP of NCA monomers (**1**). Tertiary amines, alkoxides, and other initiators that are more basic than nucleophilic, have found use since they are, in some cases, able to prepare polymers of high molecular weight where primary amine initiator cannot. Optimal polymerisation conditions have often been empirically determined for each NCA and thus there have been no universal initiator or conditions by which to prepare PAAs (**2**) from any monomer [65]. This is in part due to the different properties of individual NCAs and their polymers (e.g. solubility) but is also strongly related to the side reactions that occur during polymerisation.

The most likely pathways of ROP from NCAs are known as “*amine mechanism*” and the “*active monomer mechanism*” [69-71]. In amine mechanism (Scheme 3) the initiation occurs by nucleophilic attack of the initiator at the anhydride carbonyl carbon, followed by opening of the NCA ring. The resulting carbamate endgroup may lose carbon dioxide, after which the resulting amino endgroup propagates the polymerisation. When the decarboxylation is slow, the propagation may proceed *via* the carbamate mechanism. Both

1.2 Amino acids and poly-amino acids

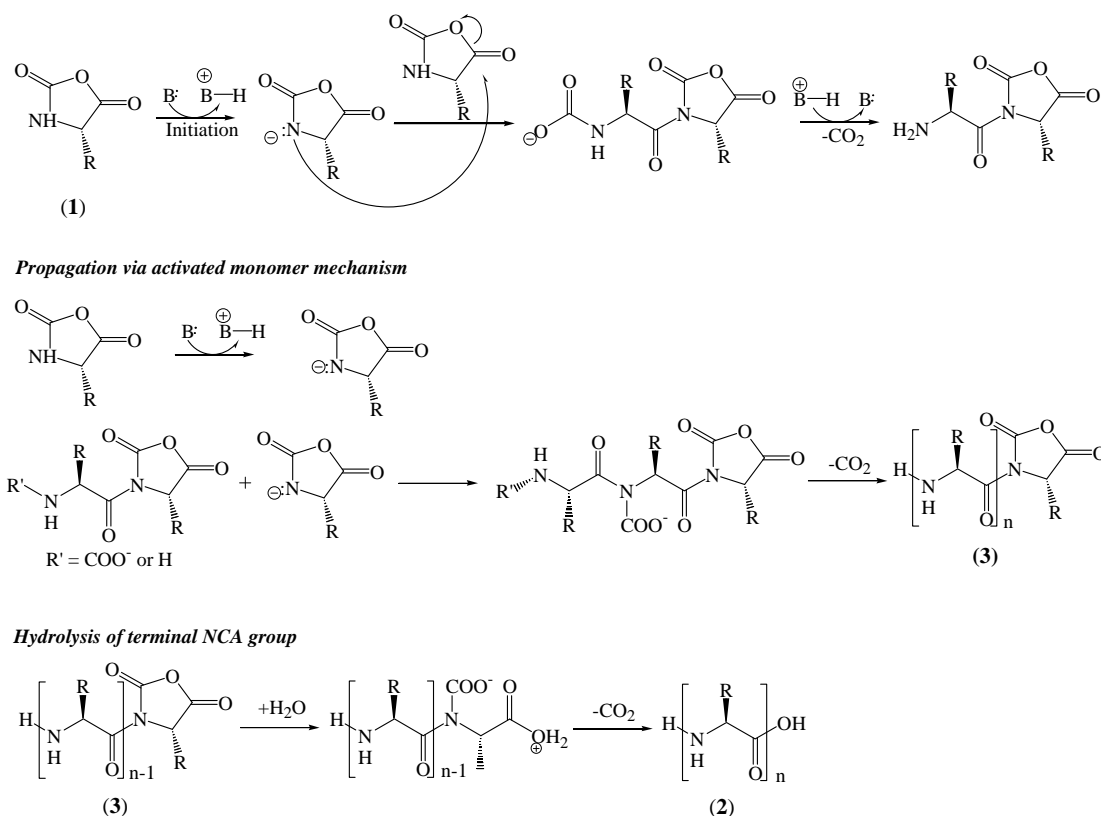
propagation mechanisms yield the same polymer with one amino group and one initiator such as endgroups of the chain.



Scheme 3 Amine mechanism for NCA polymerisation (Nu-H = nucleophilic initiator) [69].

On the other hand, in the monomer mechanism (Scheme 4) the initiation occurs by deprotonation of an NCA by a base, which then becomes the nucleophile that initiates the chain growth. Propagation can proceed *via* either the amine mechanism (Scheme 3), or *via* nucleophilic attack of a newly formed NCA anion on the *N*-acyl NCA endgroup (3) (Scheme 4). In the second case, polymer chains are obtained without incorporation of the initiator with an amino group at one end and *N*-acyl NCA group at the other end of the chain [65,69].

One inherent problem in conventional ROP is that there is no control over the reactivity of the growing polymer chain-end during the course of the polymerisation. Once an initiator reacts with a NCA monomer, it is no longer active in the polymerisation and the resulting primary amine, carbamate, or NCA anion endgroup is free to undergo a variety of undesired side reactions as should be cyclic-PAA chains [72-73].



Scheme 4 Activated monomer mechanism for NCA polymerisation (B = Base initiator) [69].

Another problem is the one of purity. Although most NCA are crystalline compounds, they typically contain traces of acid, hydrochloric acid, or isocyanates that can quench propagating chains. The presence of other adventitious impurities, such as water, can cause problems by acting as chain transfer agents or even as catalysts for side-reactions. Overall, the sheer abundance of potential reactions present in reaction media makes it difficult to achieve a living polymerisation system where only chain propagation occurs [68].

Moreover, on the top of these inconvenients, ROP is an useful route to synthesise PAA with potential catalytic and biological applications since 1) PAAs are readily, and reproducibly, produced in large (multigram to kilogram) quantities, 2) chain length, AA sequence, and composition are predictably varied in the PAAs by straightforward adjustment of monomer and initiator concentration and order of addition, 3) the desired endgroup can be modified by the use of different kind of initiators, 4) PAAs are obtained in high purity with complete removal of the solvent, bases or other chemicals employed during the synthesis, 5) PAAs are free from biological contaminants and 6) the reaction conditions can be modified

1.2 Amino acids and poly-amino acids

(initiator, monomer/initiator ratio, temperature, solvent and kind of NCA) to improve the desired properties of the synthesised PAA.

1.2.1.2 Thermal polycondensation

In general, clays are known as minerals with particular suitability for adsorption and catalytic processes. They were probably present on the primitive earth crust after weathering products of volcanic rocks [74]. Clay minerals could, therefore, have played a crucial role in the molecular evolution of bio-organic compounds (AAs, PAAs, sugars, nucleosides and nucleic acids) in chemical evolution [76-77]. The catalytic activity of some clay minerals to promote oligomerisation of PAA precursors was confirmed [78]. Nowadays, it is well known that clay minerals catalysed PAA formation in a rather complex combination of various reactions (AA dimerization, cyclic anhydride formation and PAA chain elongation), mechanism and reaction conditions.

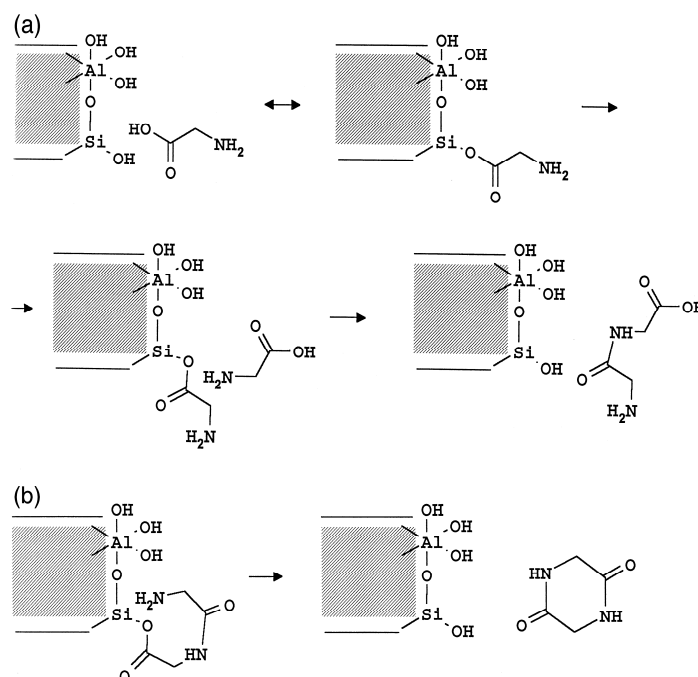


Figure 3 Glycine activation on clay particle edge leading to a) Gly₂ formation and b) formation of DKP from Gly₂ activated on clay particle edge [79].

Bujdák and Rode have reported several works about the role of the clay minerals in the peptide bond formation catalysis. Using different kind of clays and glycine (Gly) as the model molecule, they detected two main products: diglycine (Gly₂) and diketopiperazine (DKP), the cyclic anhydride of Gly₂ with yields up to 5% using talc and hectorite [79]. In both cases, the

principal product was DKP which is formed from the biomolecular reaction after the activation of one reactant species on the edge of the clay material (Figure 3) [79].

1.3 Bio-nanohybrid materials based on AAs, PAAs and HTs.

As it is exposed below, HTs are excellent guest materials to a large variety of inorganic and organic molecules [36]. Particularly, the interaction of organic and biological species with HTs is critical in such diverse fields as catalysis, drug delivery, and geochemical transport [80-84]. Some of these nanohybrid materials including AAs, carboxylic species, PAAs, large proteins and natural organic matter molecules, occur as anions at neutral to basic pH values. They are thus expected to interact strongly with solids materials having positive structural or pH dependent charges [31]. In this context, the intercalation of AAs and PAAs in HTs has been investigated because the resulting compounds are nanostructured materials with new functional properties. These bio-nanohybrid materials are attractive to industrial application because they are both environmentally and economically interesting.

1.3.1 Synthesis of AAs immobilised in HTs (AA/HTs)

Although there are few studies about the immobilisation of AAs in HTs, they described the synthesis of nanohybrid materials by three main methods: 1) anion-exchange of a precursor HT; 2) direct synthesis by co-precipitation and 3) reconstruction of a calcined HT precursor. In the case of the immobilisation of PAA in HTs, to the best of our knowledge, just four articles have been published. In there, immobilisation process was performed by two main methods: thermal polycondensation and co-precipitation.

1.3.1.1 Anionic exchange method

Anion exchange method consists in a suspension of HTs in a solution of the salt of AA to be intercalated and stirring during a determinate time. Inert atmosphere is necessary to prevent the contamination with atmospheric CO₂. Although this method is the most common for preparation of organo-HTs, to the best of our knowledge, there are just two examples in the literature using this protocol in the immobilisation of AAs. Fudala *et al.*

1.3 Bio-nanohybrid materials based on AAs, PAAs and HTs

immobilised L-Tyrosine (L-Tyr) and L-Phenylalanine (L-Phe) in Zn/Al-HT ratio 3:1 during 24 hours of synthesis at 60°C. Their results showed that the AAs were located in the interlayer space of the HT. They reported the shift of the d(003) reflection of HT from 8.9 Å for the as-synthesised HT up to 17.5 Å for L-Tyr/HT or 18 Å for L-Phe/HT (Figure 4) [16].

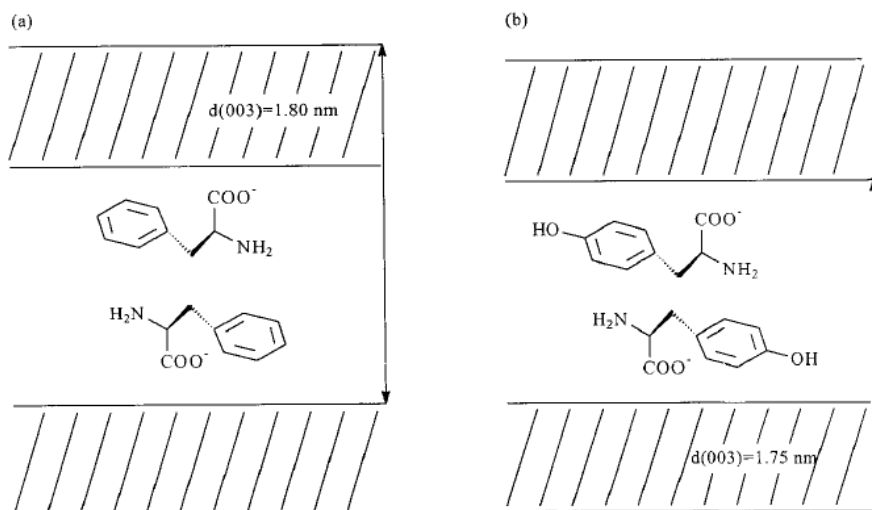


Figure 4 Spatial arrangement of the intercalated ions of a) L-Phe and b) L-Tyr in HTs according to reference [16].

In addition, Choudary *et al.* studied the immobilisation of the sodium salt of L-Pro with Mg/Al-HT ratio 2:1 during 24 hours at r.t. obtaining a material without any variation in the d(003) reflection and with a content of L-Pro calculated as 0.06 mol L-Pro/mol Al³⁺. No variation in the d(003) reflection was attributed to the location of the L-Pro molecules on the edge of the HT structure [53].

1.3.1.2 Direct synthesis – Co-precipitation method

Co-precipitation method for the direct synthesis of HT containing simple inorganic anions has been developed over a number of years [29,37,85] and a similar procedure is used for organo-HTs: the M²⁺ and M³⁺ hydroxide layers are nucleated and grown from an aqueous solution containing the anion that is to be incorporated into the HT. This anion must have an affinity for the hydroxide layers, otherwise the counter anions of the metal salts may also be incorporated, thus contaminating the HT. For this reason, metal nitrate is commonly utilised because of the low selectivity of HTs towards this anion [85]. As exposed below, the control over the pH of the forming HTs layers is important. Moreover, the pH value should be

adjusted around the value at which M^{2+} and M^{3+} hydroxides precipitate and where the organic species are in anionic form. The usual direct synthesis procedure involves crystallisation of the co-precipitation product for about 18 hours at temperatures in the range of 25-100°C.

To the best of our knowledge, there are 13 works reporting that, including the immobilisation of AAs in HTs by co-precipitation method. Table 2 summarises the co-precipitation conditions of all these works.

Table 2 Synthesis condition of AAs immobilised in HTs by direct synthesis method.

HT (M^{2+}/M^{3+} ratio)	AA	pH	Time (h)	Temperature (°C)	Immobilisation degree (mol AA/mol Al^{3+})	Ref.
Mg/Al 2:1	Asp Glu	12	24	65	0.70	[58]
					0.65	
Mg/Al 2:1		10			0.42	
Mn-Al 2:1		9			0.80	
Ni/Al 2:1	Phe	8	DS	40	1.00 ^a	[54]
Zn/Al 2:1		8			0.83	
Zn/Cr 2:1		9			0.64	
Mg/Al 2:1	Pro	11.5	24	65	0.06	[53]
Mg/Al 3:1	Several	10	DS	DS	DS	[86]
Mg/Al 2:1	Asp	10	6	100	0.47	[87]
		12			0.32	
Mg/Al 2:1	Asp	12.5	6	100	0.43	[88]
Mg/Al 3:1	Ala, Try	10	14	80	DS	[89]
Ni/Al 3:1		8				
Zn/Al 2:1	Phe Gly	9	DS	25	0.70	[52]
					0.27	
Mg/Al 2:1	Cys	10	24	65	0.90 and 0.98 ^b	[90-91]
		8			0.68	
		9			0.68	
Mg/Al 2:1	Glu	10	DS	50	0.70	[92-93]
		11			0.48	
		12			0.30	
Mg/Al 2:1	Met	10	24	80	DS	[94]

DS = Does not specified. ^aHydroxy double salt was presented in the obtained material. ^bReported in two articles.

In 2001, Aisawa *et al.* reported one important advance in the understanding of the organic/inorganic interaction by co-precipitation method. They investigated the formation process of Phe/HTs nanohybrid materials. Using Mg/Al-HT they found that at the end of

the co-precipitation process the $d(003)$ reflection had increased from 7.9 \AA to 8.6 \AA . This expansion in the interlayer space indicated that the anionic Phe was arranged by electrostatic force of attraction inside of the lamellar HT structure. Moreover, they also found that during the co-precipitation process the anionic Phe substituted the NO_3^- and/or OH^- ions by ion-exchange reaction being temporarily oriented vertically with respect to the basal layer [54] (Figure5).

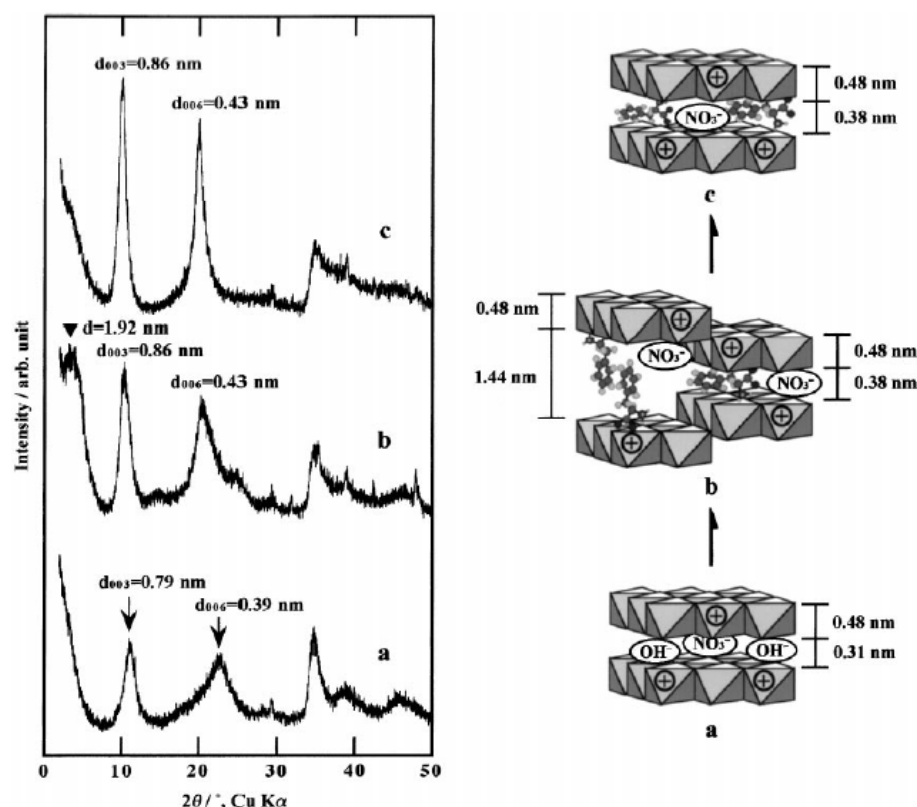


Figure 5 XRD pattern and schematic models of the formation process of Phe/Mg-Al HT (pH 10) precipitate. a) Precipitate after 3 min, b) 10-25 min and c) final precipitate [54].

A similar behaviour was found for Mn/Al, Zn/Al and Zn/Cr HT based nanohybrid materials. In all cases the $d(003)$ reflection increased respect to the HT precursor indicating the incorporation of the Phe in the interlayer space but also that Phe anions could adopt a bilayer-like arrangement oriented in an approximately perpendicular direction with respect to the HT layers (Figure 6). These observations were confirmed five years later by Aisawa's group [52].

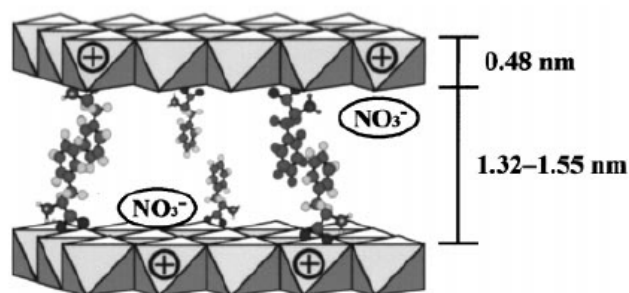


Figure 6 Schematic model of the intercalation of Phe into various HTs: Mn/Al (pH 9), Zn/Al (pH 8) and Zn/Cr (pH 9) according with reference [54].

Yuan *et al.* reported the immobilisation of L-aspartic acid (L-Asp) and L-cysteine (L-Cys) in Mg/Al-HT by co-precipitation at different pH values (See the AA structures in Annex 1). They found that orientation, structure and nature of the AA immobilised depend on the pH. In their case, increasing the pH from 10 to 12, increases the interlayer space of the HT from 9.3 Å to 12.4 Å. The L-Asp exists principally such as a monovalent anion at pH 10 and such as a bivalent anion at pH 12.5. Therefore, they explained this phenomenon due to the oblique orientation of L-Asp influenced for the attraction $-\text{NH}_3^+$ and the adjacent $-\text{COO}^-$, as well as, the repulsion between $-\text{NH}_3^+$ and the HT layers at pH 10. The remaining positive charge of the HT layers was neutralised by the coexistent NO_3^- ion within the interlayer space. In the case of the nanohybrid synthesised at pH 12, the existence of two negative charges permitted the vertical orientation of the L-Asp molecules in the interlayer space due to the electrostatic forces between the carboxylic groups and the host layers [87-88].

In addition, Reinholdt's group using Glutamate (Glu) [69,92] and Duan's group using Cys [90-91] reached the same conclusion and now it is well known that pH and temperature, during the aging process, play an important role in the immobilisation of AAs in HTs.

1.3.1.3 Reconstruction method

Miyata reported that a HT can be regenerated after thermal decomposition in the presence of the anion to be incorporated [85]. This so-called *memory effect* property of HTs provides an effective synthetic route for immobilising organic and inorganic anions into HTs. An advantage of this method is to avoid the incorporation of competing inorganic counter

anions into the HTs layers. However, the inclusion of carbonate anions from atmospheric CO₂ into the interlayer space of HTs remains as a problem.

In this context, reconstruction method is the easier methodology to immobilise AAs in HT. Nevertheless, to the best of our knowledge, there are only three works which report this methodology. In 2004, Aisawa *et al.* immobilised Phe and other AAs in Zn/Al-HT using time of synthesis up to 14 days at different pH values. Their results indicated that the amount of the AA intercalated depends on the structure of the AA and the carbon number of the side-chain. In agreement with Newman *et al.* [72], Aisawa explained that AA was oriented vertically in a bilayer way in the interlayer space from the HTs and stabilised by hydrophobic interactions at pH 7.0 increasing the interlayer distance up to 13.8 Å [51].

In the same year, Nakayama *et al.* reported that although L-Leucine (L-Leu) exists as an anion in the reaction solution at pH 10, the intercalation could be performed in their zwitterionic form also favouring the co-intercalation of anions such as OH⁻ and CO₃²⁻. To prove this, they presented the ¹³C NMR chemical shift values of different forms of the L-Leu in aqueous solution, and they compared them with the resulted chemical shift values from the ¹³C MAS NMR spectra of the biohybrid material (Table 3). Based on the chemical shift values and line width of the ²⁷Al MAS NMR spectra, which are very sensitive to the environment of Al, they also suggested that the intercalation of Leu occurs without the deformation of the HTs layers after the reconstruction method [33].

Finally, Pitchumani *et al.* reported the synthesis of L-Proline (L-Pro)/HT nanohybrid material in 24 hours. Although they did not allow important information about the nature of the immobilisation, they used this material as the catalyst for the asymmetric Michael addition [3].

The literature shows that either the synthetic conditions or the methodology used are of capital importance for the nature and properties of the final biohybrid material affecting the orientation and the location of the AAs and the structural properties of the layered double hydroxide support. However, there are not any in-depth study that related different synthetic procedure with the nature of interactions between the AAs and the HTs solid support.

Table 3 ^{13}C NMR chemical shift values of Leu at different ionic state and HT/Leu [32]

		Leu in aqueous solution				
		COOH	C_α	C_β	C_γ	C_δ
$ \begin{array}{c} \text{H} \quad \beta \\ \quad \\ +\text{H}_3\text{N}-\text{C}-\text{C}-\text{CH} \\ \quad \quad \\ \text{COOH} \quad \text{H}_2 \quad \gamma \quad \text{CH}_3 \\ \delta \\ \text{CH}_3 \\ \delta \end{array} $	176.5	54.9	41.9	26.6	23.5	
	$ \begin{array}{c} \text{H} \quad \beta \\ \quad \\ +\text{H}_3\text{N}-\text{C}-\text{C}-\text{CH} \\ \quad \quad \\ \text{COO}^- \quad \text{H}_2 \quad \gamma \quad \text{CH}_3 \\ \delta \\ \text{CH}_3 \\ \delta \end{array} $	178.1	56.0	42.4	26.8	23.5
		$ \begin{array}{c} \text{H} \quad \beta \\ \quad \\ \text{H}_2\text{N}-\text{C}-\text{C}-\text{CH} \\ \quad \quad \\ \text{COO}^- \quad \text{H}_2 \quad \gamma \quad \text{CH}_3 \\ \delta \\ \text{CH}_3 \\ \delta \end{array} $	184.7	57.1	46.4	27.0
			Biohybrid Leu/HT			
		COOH	C_α	C_β	C_γ	C_δ
$ \begin{array}{c} \text{H} \quad \beta \\ \quad \\ +\text{H}_3\text{N}-\text{C}-\text{C}-\text{CH} \\ \quad \quad \\ \text{COO}^- \quad \text{H}_2 \quad \gamma \quad \text{CH}_3 \\ \delta \\ \text{CH}_3 \\ \delta \end{array} $	176	55	42	25	24	

1.3.2 Synthesis of PAAs immobilised in HTs (PAA/HTs)

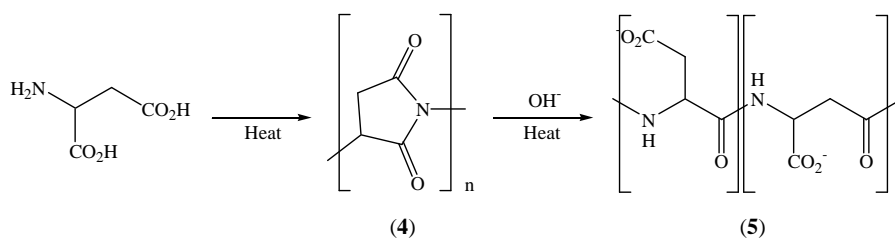
The biohybrid materials can be also derived from the combination at the nanometre scale of naturally occurring polymers (biopolymers) with inorganic solids. In the bionanohybrid context, nature can supply an abundant and wide range of biomacromolecules from renewable sources for the preparation of a large variety of materials. For example, the biopolymers can be extracted directly from the biomass (cellulose, starch, pectin, etc), synthesised from one or more bio-derivative monomers (polylactic acid, polyamino acid), or produced by microorganisms (polyhydroxybutirate). And also, nature can provide with bio-inspiration in how the structural control provides diverse functionalities. Therefore, we can find in the literature a large number of synthesised bio-nanocomposites considered as bio-inspired materials because they try to mimic the hierarchical arrangement of the components in nature to achieve similar properties [95].

The singular properties of the HTs [96] favour the incorporation of small, negatively charged organic molecules into the gallery spaces between the brucite layers. They can

incorporate successfully not only AAs but also terephthalate [97], long chain fatty acids[98], organic dyes [99], BINOL [3] and sulfonate-like intercalants [100] among many others. Although studied for many years [101], HTs have not been used as much in polymers or biopolymers and their influence on such matrices is quite poorly known. They show some advantages compared to the cationic ones such as montmorillonite clays (MMT) due to a more versatile chemical composition and tunable charge density, allowing multiple interactions with the polymer [102]. By that reason, it is possible to incorporate into HTs a wider variety of polymers and biopolymers [103]. The introduction, as in the rest of the thesis, focuses on the PAAs as biopolymers for the synthesis of nanobiohybrid materials mainly by two methodologies: Thermal polycondensation and co-precipitation.

1.3.2.1 Thermal polycondensation

The thermal polycondensation of the AAs permits the *in situ* polymerisation of the intercalated AA monomers. To the best of our knowledge, Mann *et al.* reported the unique example in the literature for the synthesis of PAA-HTs [58]. The protocol consisted in heating a previously synthesised Asp/HT nanohybrid material up to 220°C for 48 hours in air. As the result, they observed the formation of Poly(α,β -Asp) (5) which proceeded *via* a polysuccinimide intermediate (4) (Scheme 5).



Scheme 5 Thermal polycondensation of Asp to poly(α,β -Asp) [58].

1.3.2.2 Co-precipitation method

Although different kinds of biopolymers have been immobilised in HTs (proteins [57,104], DNA [43-44,104], enzymatic extracts [105] and lipids [106]) there are few examples of the PAAs immobilisation. In this context, poly(α,β -Asp) [58], Phe₂ [52], Gly₂, Gly₃ [50,52] and Gly₄ [50] are the PAA immobilised in HTs. The two most important findings in the immobilisation of PAAs in HTs were first, Gly₂₋₄ were immobilised in their zwitterionic form without any change in the interlayer space from the Mg/Al-HT [50] and

second, Gly₂₋₃ could be immobilised in the interlayer space from Zn/Al-HT in a horizontal orientation respect to HT layers [52].

The poly(α,β -Asp)/HTs synthesised by Mann *et al.* by coprecipitation method gave a laminated nanocomposite with an average interlayer separation of 15.1 Å as denoted the XRD data and with Mg/Al molar ratio of 1.2. This material also presented irregularly shaped aggregates of plate-like particles with very smooth surface textures. The presence of the biopolymer was determined by FT-IR spectra [58].

On the other hand, the works of Nakayama [50] and Aisawa [52] *et al.*, where intercalated di-, tri- and oligo-AAs into HTs, are much easier to characterise than PAAs, showed two important findings that could be extended to the PAA-HT biohybrids. Nakayama *et al.* observed by ¹³C NMR data that the oligo glycines, Gly₂₋₄, immobilised in the HTs were in their zwitterionic form without observing any change in the interlayer space from the Mg/Al-HT precursor [50]. And Aisawa *et al.* proposed that the disposition of the oligo-glycine, Gly₂₋₃, in the interlayer space of the Zn/Al-HT solid follows a horizontal orientation respect to the HTs layers [52]. However, it is important to take into account that these facts can not be generalised to the other poly-AAs due to the intrinsic structural differences and diverse properties of the constituents AAs (Annex 1). Any study of the immobilisation in HTs of oligo-AAs derived of other AAs such as Leu have been found.

2. Bio-nanohybrid materials as catalysts

Many enzymes are remarkable asymmetric catalysts, performing highly efficient and selective reactions. Aspiring to imitate enzymatic efficiency, chemists have transformed AAs into countless auxiliaries, ligands and catalysts. In the majority of examples, the AA is used purely as a source of chirality and both the amine and acid functionality are altered or eliminated. Unmodified AAs and PAAs have been used much less frequently as asymmetric organocatalysts. Early studies of PAA-based catalysis appear to have been focused on two ends of a spectrum of possible catalysts: First, small conformationally rigid AAs and cyclic di-

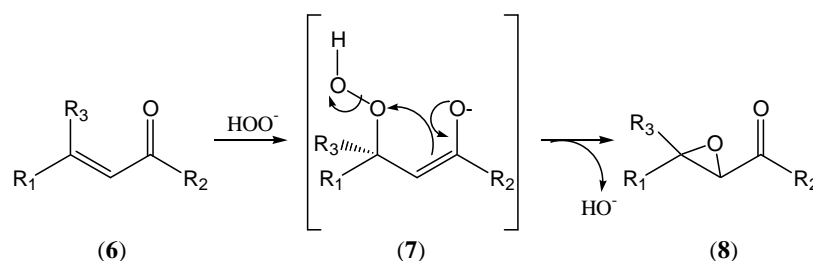
PAA (DKP), and second, we can find large PAA which, thanks to their increased size, likely adopt a specific tertiary structure in solution. Hajos and Wiechert reported the use of Pro as a catalyst for the Robinson annulations as early as 1970 [64]. Inoue used DKP as catalysts in the Strecker reaction in early 1980s [107] while, Juliá and Colonna employed PAA (>10 AAs in length) as epoxidation catalysts [108]. In this context, in many cases AAs and PAA act as chemo-, regio- and enantioselective catalysts, nevertheless, they have the same disadvantage than the conventional homogeneous catalysts: the difficult encountered when trying to separate the reaction product from the catalyst and from any reaction solvent. This problem arises because the most commonly used separation method, distillation, requires elevated temperatures unless the product is very volatile. AAs and PAA are thermally sensitive, usually decomposing below 200°C. Moreover, other conventional processes such as chromatography or extraction also lead to catalyst loss.

On the other hand, solid bio-catalysts are rather limited in the nature of their active sites and thus the scope of reactions that they can accomplish. In general, although solid catalysts present lower conversions and selectivities than homogeneous catalysts, they are interesting from an economic and environmental (“green”) point of view, because they can be quickly and easily handled, stabilised and separated from the products and often recycled several times [8]. Thus, the motivation factors for creating recoverable bio-catalysts are large. Silica, alumina, clays, ionic liquids and highly cross-linked polymers are the standard support to create a bio-hybrid catalyst from AAs and PAA. At this point, the goal is not only use the organic moiety as the active site and the solid to provide avenues to recovery and possibly recyclability of the organic active site [17,109], but also take advantage of potential synergies between host-guest interactions to improve the properties of the biohybrid catalyst.

2.1 Juliá-Colonna asymmetric epoxidation reaction

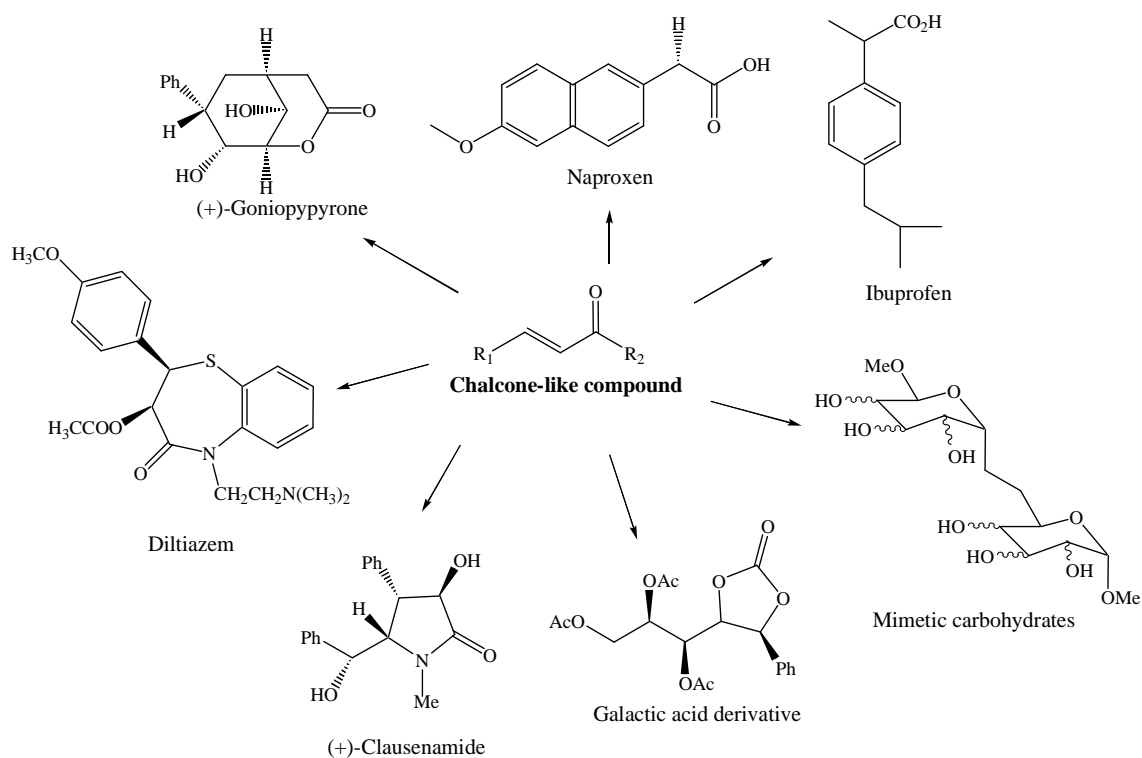
α,β -Unsaturated ketone also called chalcones belong to the flavonoid families which are synthesized in plants performing diverse physiological functions such as attractants of pollinators, UV protectors, and insect repellents [110]. They have found numerous applications as pesticides, food additives, photoprotectors in plastics, sunscreen agents, and a plethora of interesting biological activities (antimalarial [111], ant-inflammatory [112],

cytotoxic [113], anticancer [114-115], diuretic, and choleric [116]) have been reported. In this context, treatment of α,β -unsaturated ketones with hydrogen peroxide under basic conditions yield epoxy ketones, although a transformation known as the Weitz-Scheffer reaction. Weitz-Scheffer reaction begins with conjugate addition of the peroxide (or other *O*-nucleophilic species) to the C_α of the α,β -unsaturated ketone (6) forming an hydroperoxy enolate (7). Attack of the enolate on the peroxide oxygen generates the epoxide product (8) and releases a leaving group (Scheme 6) [117].



Scheme 6 Weitz-Scheffer reaction.

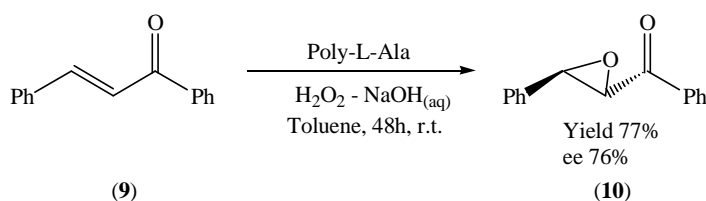
In the last decades, Weitz-Scheffer and the later developed Juliá-Colonna epoxidation reaction have been very interesting reactions since chiral, non-racemic epoxides may serve as building blocks for the synthesis of a wide variety of optically active compounds. Several examples have been published to illustrate the value of such building blocks (Scheme 7).



Scheme 7 Pharmaceutical products obtained by chiral epoxy-ketones [118-122].

2.1 Juliá-Colonna asymmetric epoxidation reaction

Asymmetric Juliá-Colonna epoxidation reaction of α,β -unsaturated ketones, such as chalcone (**9**), using a synthetic PLA as catalyst was reported by first time in 1980 [123]. Few years later, Poly-L-Leucine (PLL) proved to be a most efficient catalyst [21,124]. The original reaction conditions consisted in a triphasic system: aqueous hydrogen peroxide containing sodium hydroxide, a water immiscible organic solvent such as hexane or toluene, and the solid PLL (Scheme 8).



Scheme 8 Juliá-Colonna epoxidation reaction of chalcone [123].

However, “Three-phase” Juliá-Colonna reaction did not gain more popularity for three main reasons. Firstly, the optimum catalyst was not commercially available in large quantities. Secondly, the transformation appeared to be limited to enones of the type (*E*)-Ar¹CH=CHCOAr², i.e. close relative chalcone. Thirdly, the catalyst forms a gel in the reaction mixture, which filters very slowly making difficult the recovery of the catalyst after completion of the reaction [108,124]. To overcome some of these limitations improved conditions for the enantioselective epoxidation were developed by Roberts *et al.*: biphasic conditions [125], PaaSiCat (PaaSiCat = PAAs anchored onto Silica as Catalyst) [126] and the addition of percarbonate as co-catalyst [127]. Using the biphasic or the PaaSiCat conditions it is even possible to epoxidise substrates with active hydrogen atoms adjacent to the carbonyl group. Nevertheless, activation of the used catalyst is needed to maximise both rate and stereoselectivity. This activation consisted of stirring the PAAs in a mixture of NaOH_(aq) and toluene for 1–5 days and PLL had to be recovered by adsorption over silica (PaaSiCat protocol) [126,128]. Roberts *et al.* also reported the polyethylene glycol (PEG)-bound PLLs as catalyst under the biphasic conditions obtaining conversions up to 80% with ee 98% in 24 h of reaction [129]. Despite of all progress, from an economical point of view the various improved procedures of the Juliá-Colonna epoxidation reaction are still hampered.

Most of the problems are related to the PAAs used as catalyst, especially the necessity of rather large quantities of the catalyst, the time-consuming of the catalyst, which has to be carried out separately [130] and difficulties in the work-up process due to the gel-like nature of the catalyst [131]. Beside these problems related to the method the availability of highly active catalyst is limited.

Inspired by Robert's works, Tang *et al.* reported one series of PLLs easy handling as catalyst of (*E*)-chalcone under biphasic conditions. Using immobilised PLL to silica gel functionalised with primary 3-aminopropyl groups (AMPSi) (Figure 7), the enantioselectivity increased with the degree of polymerisation of PLL, reaching 93% ee and 90% yield when $n=45$. Moreover, the enantioselectivity was not affected by changing the reaction conditions, such as oxidants and solvents. Attempts to recycle the catalyst were made. And washing PLL with MeOH after each consecutive run, the organocatalyst was successfully reused 10 times keeping similar activity and selectivity [132,133].

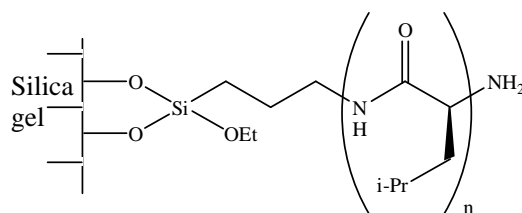
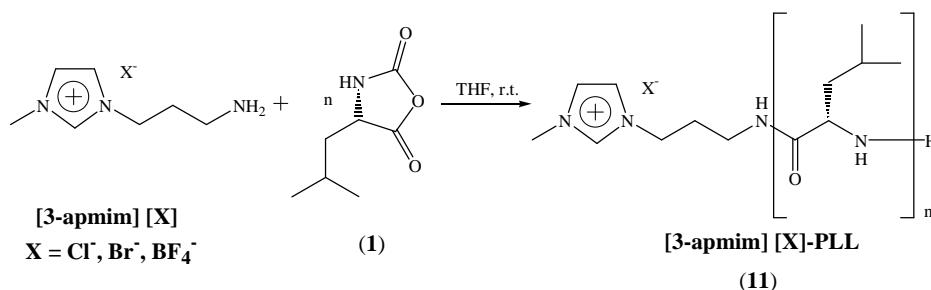


Figure 7 Silica gel-AP-PLL.

More recently, Tang *et al.* also reported the synthesis and application of a novel PLL catalyst called [3-apmim][X]-PLL with an imidazolium group in one side of the chain (11) (Scheme 9) [134]. Using this new recyclable catalyst, yields of 99% with ee up to 96% in 15 min. of reaction were reported.

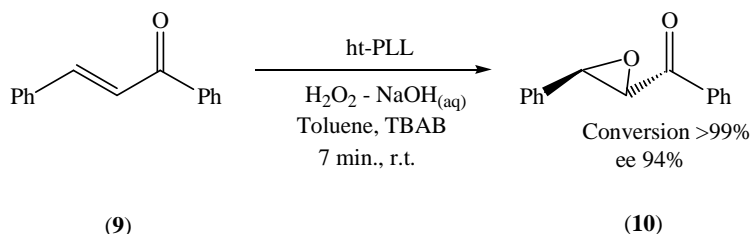


Scheme 9 Preparation of 1-(3-aminopropyl)-3-methylimidazolium-PLL [134].

2.1 Juliá-Colonna asymmetric epoxidation reaction

2.1.1 Three-phase system for Juliá-Colonna epoxidation using a phase-transfer co-catalyst (PTC)

Geller *et al.* reported an improved preparation of the PLL catalyst by a non-specified high-temperature polymerisation of L-Leu-NCA (**1**). With this ht-PLL in combination with tetrabutylammonium bromide (TBAB) as a phase transfer co-catalyst (PTC), no preactivation of the PAA was unnecessary [135-137]. The reaction time could be reduced dramatically and in some cases even the enantioselectivity was increased. Using chalcone as substrate, the reaction was finished after 7 min. with conversion to (**10**) over 99% and ee of 94% (Scheme 10). Using other substrates that were previously difficult to epoxidise, conversions to of 40-99% and ees of 68-94% were obtained after 2-18 h.



Scheme 10 Three-phase System for Juliá-Colonna Epoxidation Using a PTC [137].

2.1.2 Mechanistic considerations

The Weitz-Scheffer epoxidation of electro-deficient alkenes by alkaline hydrogen peroxide is the achiral progenitor of Juliá-Colonna epoxidation. Early studies of Weitz-Scheffer epoxidation showed that the rate had a first order dependency on the concentration of both hydroperoxide ion (HOO^-) and the electron-deficient alkene [117]. Roberts and Kelly *et al.* also reported kinetic studies of the Juliá-Colonna reaction [64,138-139]. They exposed that Juliá-Colonna epoxidation reaction occurs by and steady-state random bireactant mechanism, which implicates alternative pathways to the ternary complex and, importantly, postulates that the pathway A, where the complex PLL: HOO^- formed in the first instance, is kinetically preferred to the pathway B (Figure 8) [140].

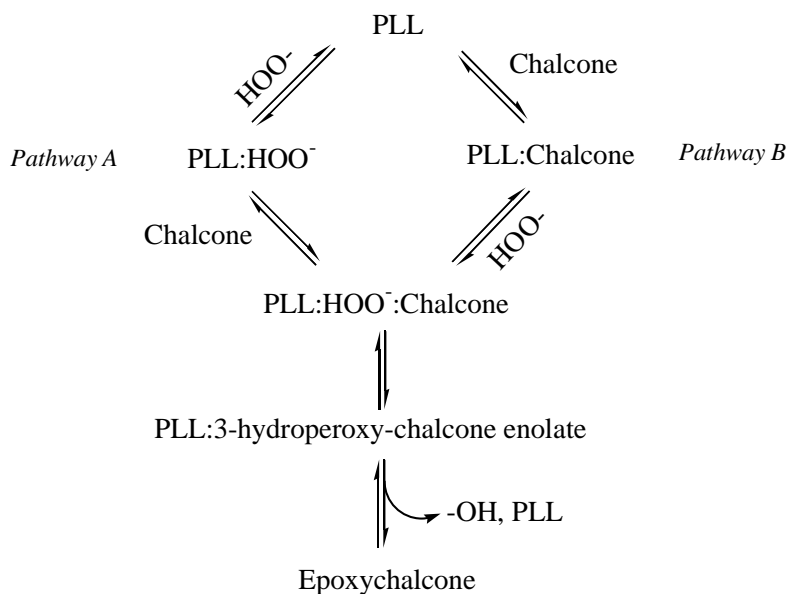


Figure 8 Kinetic scheme for chalcone oxidation by hydrogen peroxide anion catalysed by PLL [140].

This type of mechanism is sequential; that is, all substrates must bind to the catalyst to form a central complex (PLL-HOO⁻:Chalcone) before the formation of the hydroperoxide enolate of chalcone which eventually forms epoxychalcone. Moreover, in Kelly-Roberts model enone binding is carried out by the NH groups of two adjacent AAs, whereas the third one is involved in the binding/delivery of the hydroperoxide.

These three NHs implicated in catalysis do not need to include the *N*-terminus, but may as well be derived from residues 2, 3 and 4 (Figure 9). In these studies Roberts and Kelly indicated that the reaction proceeds *via* a fast reversible addition of hydrogen peroxide anion to form the final non-racemic epoxide (Scheme 11).

Thus, the role of the catalyst is the stabilisation of the initially formed enolate through the oxi-anion hole formed by the amidic groups located near to the *N*-terminus of PAA. This stabilisation is higher for one of the two enantiomeric enolate intermediates, favouring kinetic resolution of the racemic mixture.

2.1 Juliá-Colonna asymmetric epoxidation reaction

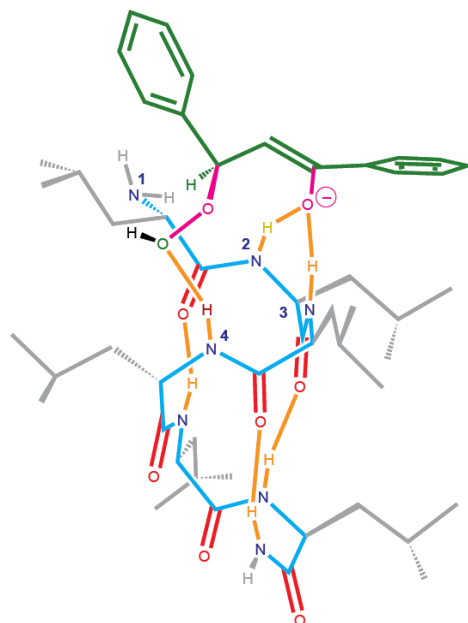
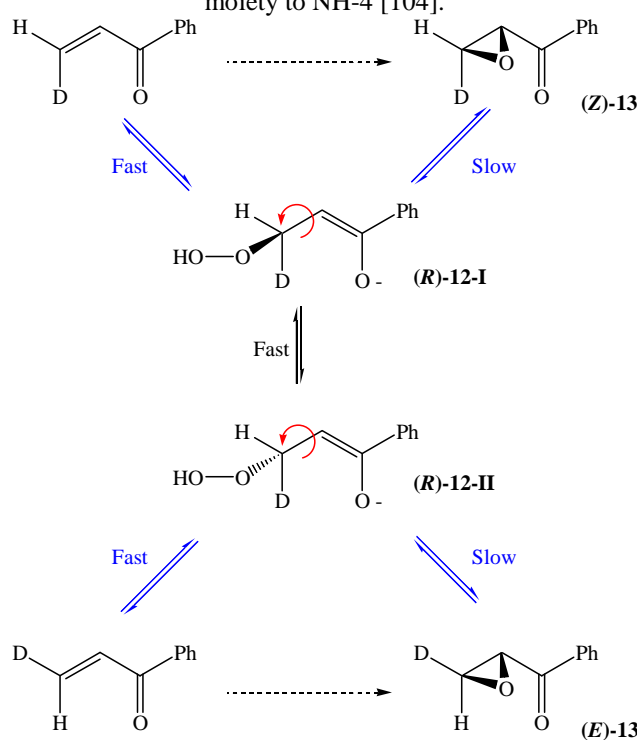


Figure 9 Model for the binding of the chalcone peroxyenolate to NH-2 and NH-3 and of the peroxide moiety to NH-4 [104].



Scheme 11 Mechanism scheme for Weitz-Scheffer and Juliá-Colonna epoxidation: fast hydroperoxide addition to chalcone, followed by fast rotation of enolate (**12**) and slow ring closure to the epimeric epoxides (*E*)- and (*Z*)-**13** [138].

2.2 Direct asymmetric aldol reaction

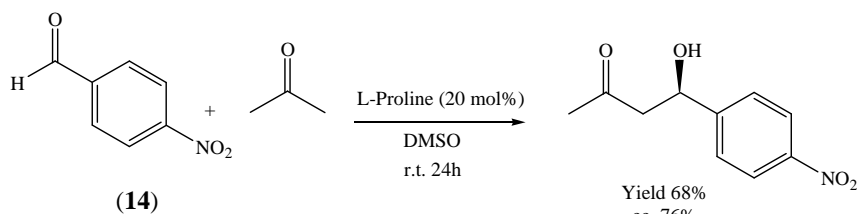
Aldol reaction is one of the most powerful methods of forming C-C bonds. The ability to control the absolute configurations of the newly formed estrogenic centre is of paramount importance for the synthesis of natural products. In general, control of

stereochemistry has been accomplished diastereomerically through the use of chiral aldehyde as starting materials, stoichiometric chiral auxiliaries attached to the donor enolate [141], chiral metal catalysts and chiral bio-organocatalysts [142].

In this context, L-Pro can be regarded as the simplest “enzyme” and, in addition to the aldol reaction, it has been successfully applied to many other reactions such as Robinson annulations, Mannich reactions, Michael reactions, direct electrophilic α -aminations, Diels-Alder reactions, Baylis-Hillman reactions, aza-Morita-Baylis-Hillman reactions, α -selenenylation, oxidation, chlorination and others [142-146]. Taking into account that there are much information about different kind of aldol reactions this section will be focused just in the intramolecular aldol reaction using L-Pro and their nanohybrid materials as catalysts.

2.2.1 Intramolecular asymmetric aldol reaction

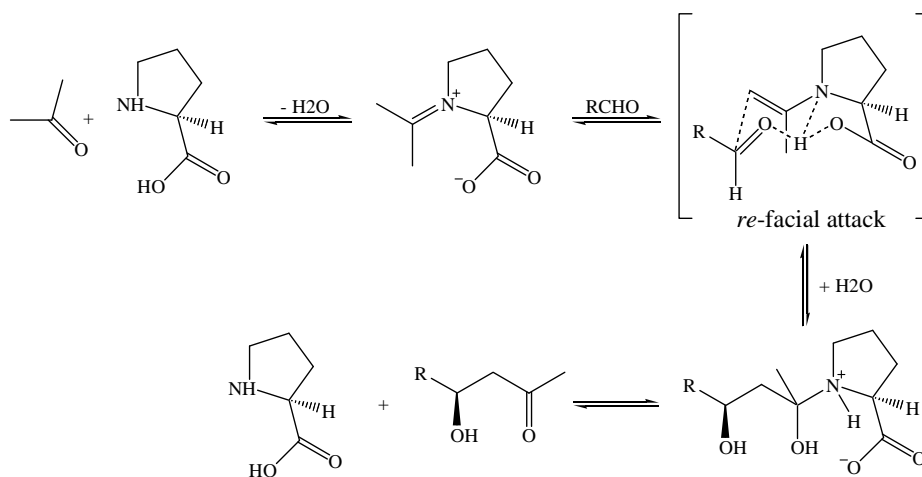
Catalytic antibodies that mediate asymmetric aldol reactions in a fashion similar to Type I aldolases have been reported by Lerner and Barbas III's groups. Based on these studies and the Hajos-Wechert reaction, List and Barbas III *et al.* investigated the use of Pro as a catalyst for the intermolecular aldol reaction between acetone, 4-nitrobenzaldehyde (**14**) [147] and other aldehydes [148] (Scheme 12).



Scheme 12 Intermolecular Asymmetric Aldol Reaction catalysed by L-Pro [147].

In Lerner, List, Barbas III and subsequent works, there have found that 5-membered ring and carboxylate of the catalyst is required to maintain good activity and enantioselectivity. Moreover, nowadays is well known that aldol reaction occurs *via* an enamine mechanism (Scheme 13), where the L-Pro provides two “active centres” the nucleophilic amino group and the carboxylate group which acts as an acid/base co-catalyst. In the preferred transition state the large R group takes the position away from the enamine substituents, leading to *re*-facial selectivity.

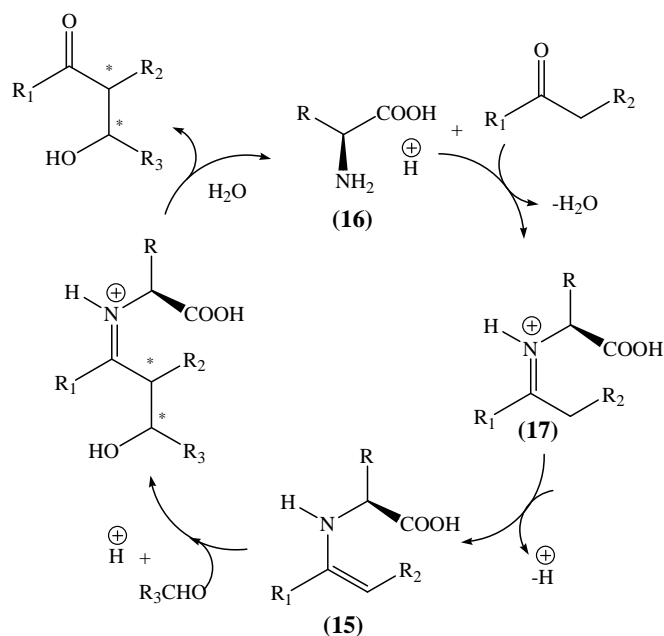
2. Bio-nanohybrid materials as catalysts
 2.2 Direct asymmetric aldol reaction



Scheme 13 Enamine mechanism for the asymmetric direct aldol reaction [148].

Although L-Pro is arguably the most efficient and versatile small organic molecule that catalyses direct aldol reaction, the rather poor solubility of L-Pro in organic solvents limits its applications as catalyst [149]. To overcome this limitation, two mainly improvements have been reported; the first, the synthesis of new L-Pro derivatives more soluble in common organic solvents [142] and the second, the anchoring of L-Pro or L-Pro derivatives on insoluble materials such as alumina [18], clays [3,53,150], ionic liquids [151-152], silica [153] or organic polymers [154-156] obtaining new non air-sensitive, easy handling, recovering and reusable catalytic systems.

L-Pro and its structural analogues have been demonstrated to be powerful catalysts for a large variety of reactions. However, primary AAs-promoted enamine catalysis is rather limited. List and Barbas III reported that in the direct intramolecular asymmetric aldol reaction of acetone and (**14**) [147-148], unlike L-Pro, primary AAs such as Val and Phe were poor catalysts. Scheme 14 shows the catalytic cycle of the intermolecular aldol reaction catalysed by primary AAs. It has long been thought that a secondary enamine (**15**) is better stabilized by hyperconjugation, whereas a primary amine (**16**) gives the predominant imine form (**17**). For primary AAs to serve as efficient catalysts in enamine catalysis, effective tautomerization of their imine (**17**) form to the enamine form (**15**) is absolutely essential [97].



Scheme 14 Primary AA-promoted intermolecular aldol reactions *via* the enamine mechanism [7]

For example, L-Ala induces excellent levels of diastereoselectivity and enantioselectivity in the aldol reaction between cyclic ketones as aldol donor and aromatic aldehydes as aldol acceptor [157]. L-Try in water media shows the highest activity and selectivity in the aldol reaction of acetones. Lu *et. al.* reported yields up to 91% with enantioselectivities up to 96% using L-Try as the organocatalyst [158] and they demonstrated the high potential of some primary AAs in the aldol reactions [159]. On the other hand, PLAs and PLLs also are able to perform efficiently asymmetric aldol reaction, but the selectivity and yield obtained decreases as the length of the PAAs increases and it is necessary very long reaction time (upper to 96 h) [160-161].

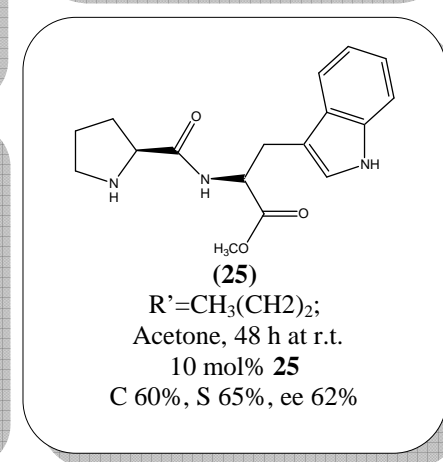
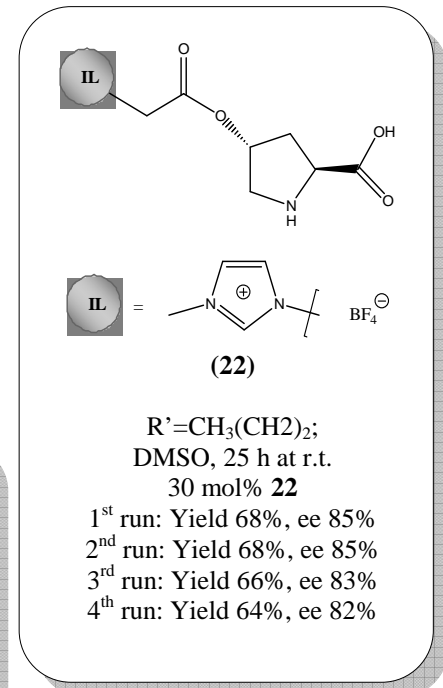
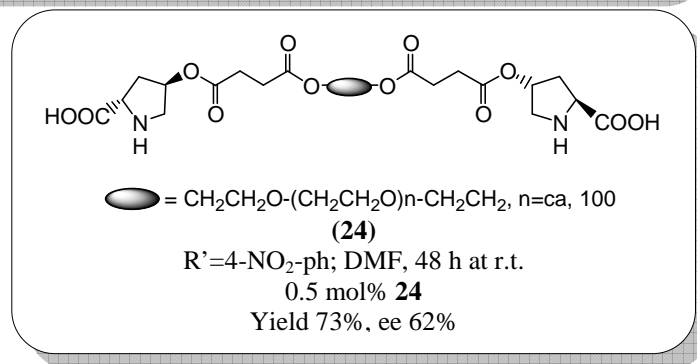
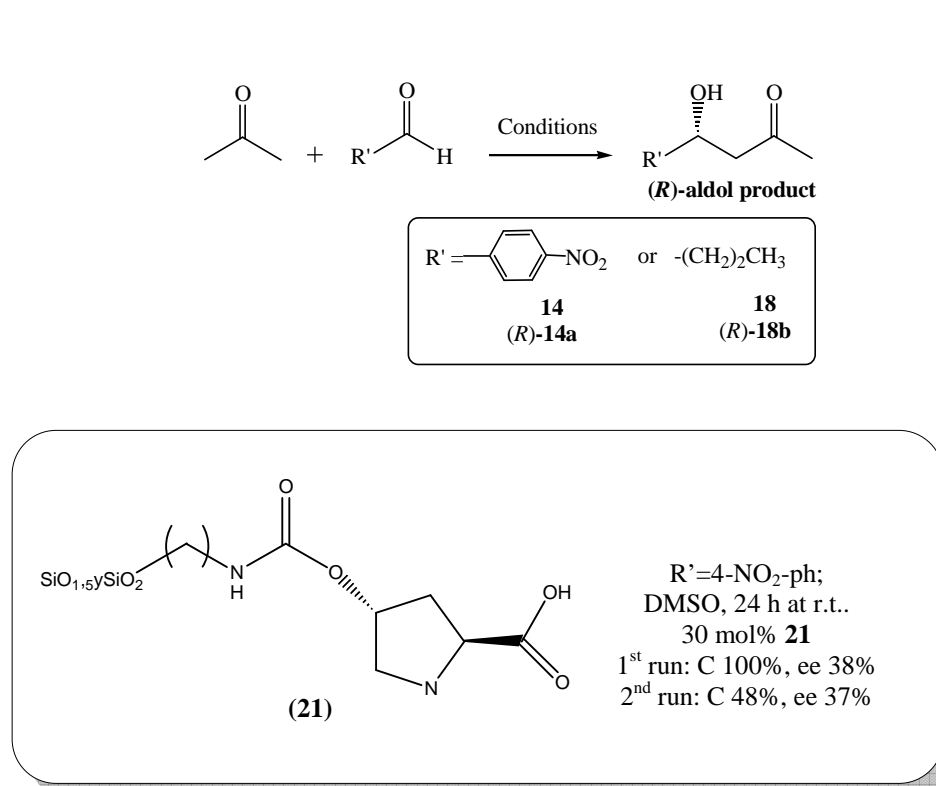
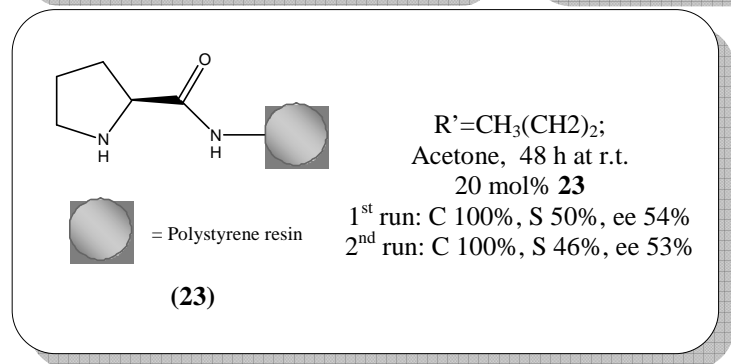
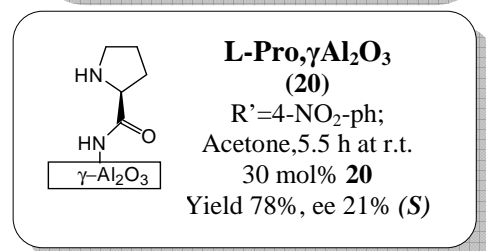
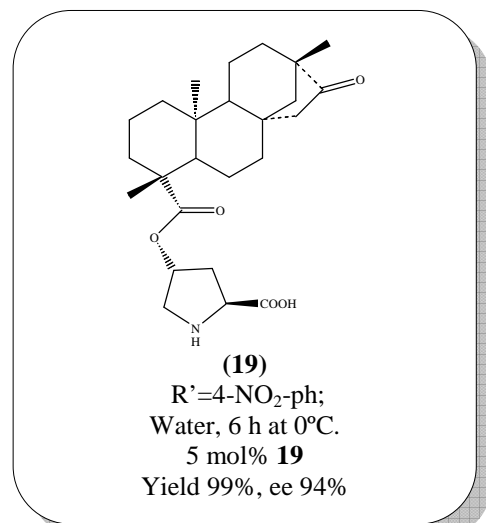
2.2.1.1 Aldol reaction catalysed by supported L-Pro

During several years, increasing efforts have been devoted to immobilisation, recovery and reuse of L-Pro after the reaction occurs [148]. L-Pro is inexpensive and available in both enantiomeric forms, so its immobilisation could be considered useless. It should be noted that immobilisation of Pro is expensive, because a Pro derivative is used as precursor material, usually a hydroxyl-*N*-substituted-L-Proline, and several synthetic steps may be necessary for its immobilisation. To counterbalance this point, the immobilisation of pure L-Pro onto solid materials should be a solution from an economical point of view, nevertheless the

2.2 Direct asymmetric aldol reaction

immobilisation occur by one of the active amino or carboxylic group which are responsible of the activity and enantioselectivity. For this reason, the supported derivative Pro material should be easily recovered and reused many times with unchanged reactivity and selectivity. However, at least two “driving forces” for Pro immobilisation may be considered. The first one is that Pro is used up to 30 mol%, which can be regarded as a large amount of catalyst, especially if the reaction is carried out on multigram scale. Moreover immobilisation of Pro may enhance its activity and stereoselectivity. The second “driving force” is that an improved Pro immobilisation strategy may be then applied to a more expensive organocatalyst and, hence, its recovery and re-use could be of still higher value, from an economical point of view, so increasing the greenness of the process. Finally, immobilisation gives the possibility to explore modifications in the properties of the supported catalysts by employing specific characteristics of the support.

Scheme 15 summarises some effective hybrid materials based on Pro for asymmetric aldol reaction between acetone and the aldehyde (**14**) and (**18**). There are three general concepts behind these catalysts. The first is that replacement of the carboxylic acid functionality present in Pro modulates the acidity and/or solubility of the catalyst, for example (**23**) and (**25**) [162]; the second is that a catalyst with C₂ symmetry reduces the number of stereoisomeric transition states available, for example (**19**) [163], (**21**) [153], (**22**) [152], (**24**) [154] and thereby potentially increasing the enantioselectivity [164], and the third is that permits the immobilisation of non modified L-Pro on inorganic materials, for example (**20**) [18].

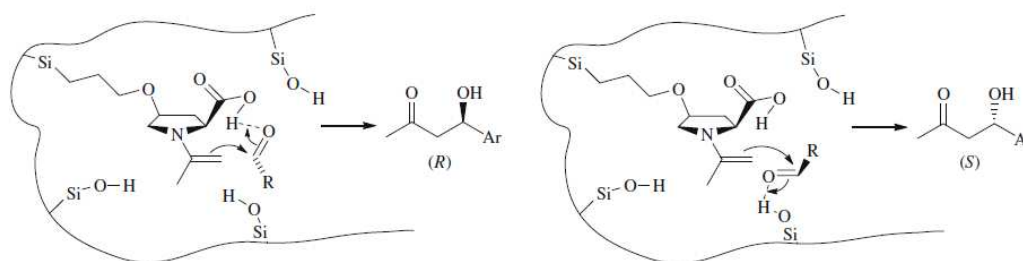


Scheme 15 Pro and Pro derivatives catalysing aldol additions of acetone with 14 and 18.

2.2 Bio-nanohybrid materials as catalysts

2.2 Direct asymmetric aldol reaction

The results of the Scheme 15 show the critical role of both amino and carboxylate group not only in the activity but also in the asymmetric induction of the aldol products. The variation in activity or enantioselectivity in the asymmetric aldol reaction respect to the pure L-Pro (68 and 76%, respectively [147]) can be also due to involvement of the support in the mechanism of the reaction. Zamboulis *et al.* observed that the derivatives of L-Pro anchored on silica by a covalent bond as catalyst followed the usual enamine mechanism of the pure L-Pro because both NH- and COOH-Pro moieties remained free after the immobilisation process. However, the activity and selectivity decreased because of acidic silanol groups present on the surface of the pores interfere, competed with the carboxylic acid group of Pro for the oxygen of the aldehyde (scheme 16) [153].



Scheme 16 Simplified presentation of the competition between the silanol and COOH groups of L-Pro according to reference [153].

Li *et al.* also observed a direct effect of the support in the selectivity of the aldol reaction of acetone with (14) [18]. They anchored the L-Pro on γ - Al_2O_3 as catalyst. The inversion in the enantioselectivity showed by the hybrid catalyst was explained because the carboxylic group of the immobilised L-Pro participates interacts with the support.

Thus while the amine group of the immobilised L-Pro activates acetone, the hydroxyl groups on γ - Al_2O_3 activates the carbonyl of (14) through H-bonding instead of the carboxylic group of the immobilised L-Pro (Figure 10).

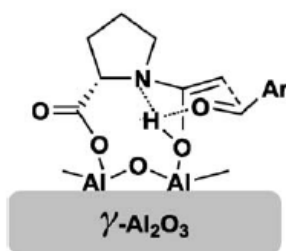
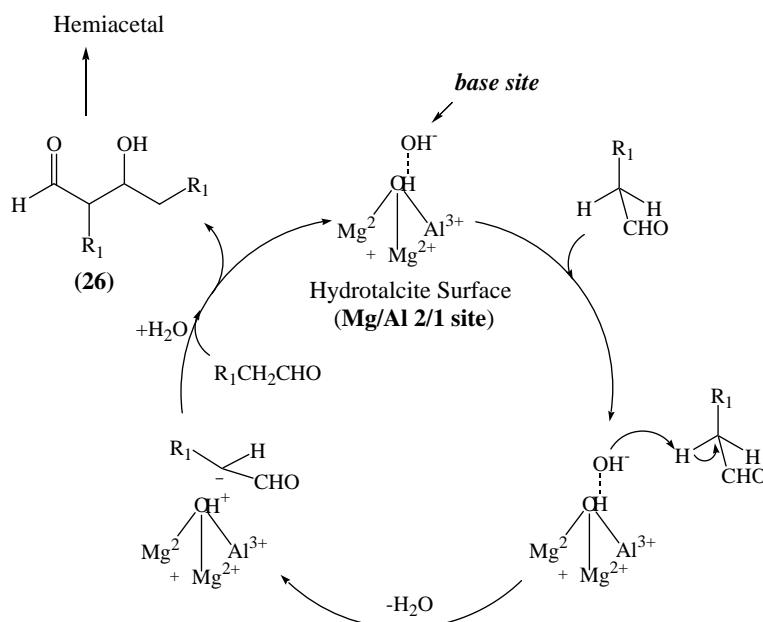


Figure 10 Assumed intermediate complex of the asymmetric aldol reaction catalysed by L-Pro immobilised on γ - Al_2O_3 [18].

This conformation favors the *Si* face attack of enamine on the pro-chiral aldehyde resulting in formation of the corresponding (*S*)-product [18].

2.2.2 Aldol reaction catalysed by HTs

Many works have been reported using non-calcined HTs in a large number of base-catalytic reactions [21,165-166]. Particularly, HTs have been used as catalyst in aldol reaction under aqueous media [23]. Under aqueous conditions, surface OH⁻ species abstracts the acidic hydrogen of an aliphatic aldehyde as a pro-nucleophile to generate a carbanion intermediate, which can be paired with the cationic surface of the HTs. According with Figueras and Corma *et al.* HTs have base sites with a p*K*_a value of at least 11 [167-168], which depressed the dehydration of the aldol products, leading to high selectivity for the putative 3-hydroxy aldehydes (**26**). 3-Hydroxy aldehydes can react with another aldehyde to afford the corresponding hemiacetal compounds by a base-catalysed mechanism (Scheme 17) [169].



Scheme 17 Proposed mechanism for rehydrated HTs catalysing aldol reaction of aliphatic aldehydes in aqueous media [23].

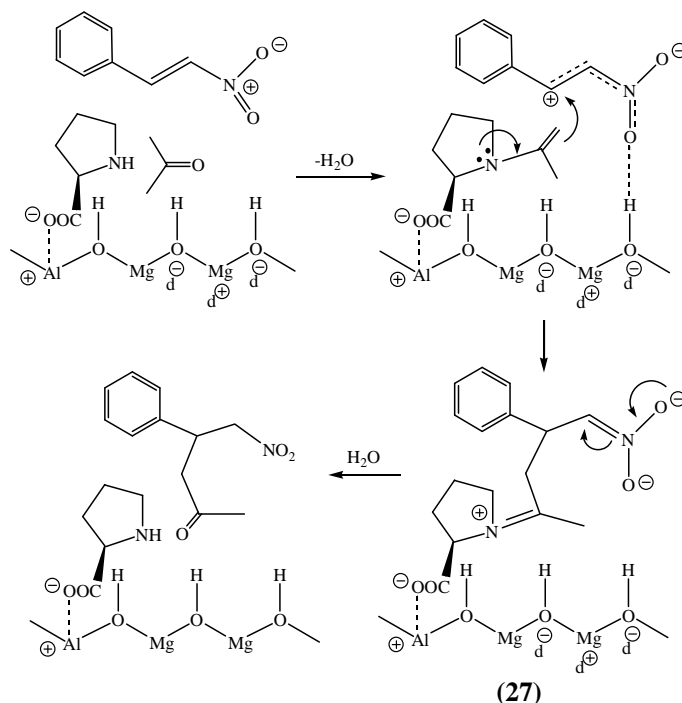
In general, although activity and selectivity of aldol condensations of aliphatic and aromatic compounds depend of the nature on reagents and catalysts, the solvent used during the synthesis plays an important role in both activity and selectivity.

2.2 Direct asymmetric aldol reactions

2.2.3 Aldol reaction catalysed by L-Pro immobilised on HTs

To the best of our knowledge, there are three examples using L-Pro immobilised on HTs as catalysts in Aldol reaction. Choudary *et al.* reported the synthesis of L-Pro immobilised in Mg/Al-HT (3:1) as catalyst in Aldol, Henry, Michael and cyanosilylation reactions obtaining high conversions but with poor enantioselectivities. However they did not study the nature of the immobilisation or the host-guest interactions. So, they did not propose any mechanistic interpretation [53].

Pitchumani *et al.* developed the asymmetric Michael reaction between β -nitrostyrene and nitromethane catalyzed by the same biohybrid catalyst than Choudary *et al.* [3]. They concluded that the synergistic effect of the host-guest interaction between L-Pro and the HTs allowed increasing conversion but with inversion of the asymmetric induction. In a similar way than Zamboulis *et al.* [153], Pitchumani interpreted their results because of the hydroxyl groups of the HTs activates the alkene by polarizing the double bond and a nucleophilic attack of the enamine to alkene takes place to form intermediate (27), which undergoes subsequent hydrolysis to yield the Michael adduct (Scheme 18).



Scheme 18 Enamine-type mechanism for L-Pro/HT-catalysed Micheal addition of acetone to β -nitro styrene proposed by Pitchumani *et al.* [3].

2.3 One-pot reactions

Multireaction in a single pot is considered as an ideal chemical process due to operational simplicity and the minimisation of energy input, time, solvents and reagents which translate to substantial economic and environmental benefits [170]. A significant problem in one-pot synthesis is the mutual destruction of reagents. To overcome this problem, several attractive methods, for example, the anchoring active gel materials have been developed [171]. However, solid reagents still suffer from deactivation by interaction between opposing anchored reagents and require expensive dopants as active sites as well as a tedious preparation method. Particularly, although synthesis of α,β -epoxy ketones has been studied since 1980, there are few examples using one-pot process.

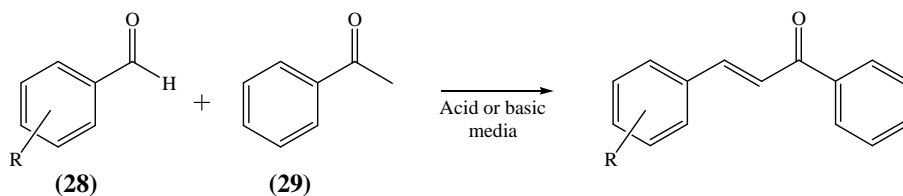
Shi *et al.* reported the one-pot synthesis of α,β -epoxy ketones using acetophenones and arylaldehydes [172]. Under their reaction conditions yields up to 92% were obtained. Nevertheless, the protocol included use of methanol as solvent and long time of synthesis (24 h) as well as the formation of complex side-products. Although two of the problems (toxic solvent and long time of synthesis) of the Shi *et al.* protocol were minimised by use of ultrasound treatment [173], the low reactivity of some arylaldehydes and the not complete reaction of the formed chalcone were still present.

2.3.1 Claisen-Schmidt reaction

Claisen-Schmidt reaction between benzaldehyde derivatives (**28**) and acetophenone (**29**) is a valuable C-C bond-forming reaction to obtain α,β -unsaturated ketones (Scheme 19). This reaction is catalysed by acids and bases under homogenous conditions [174-176]. Homogeneous reactions present several hurdles, such as catalyst recovery and waste disposal problems. In this respect, heterogeneous catalysts are considered as an eco-friendly alternative [177-181].

To the best of our knowledge, there are just three examples using rehydrated HTs as catalysts in Claisen-Schmidt reaction. López *et al.* reported the synthesis of chalcone using (**28**) and (**29**) in a protocol that included DMF as solvent at 0°C during 6 hours of reaction [182]. Under their reaction conditions 80% of yield was obtained.

2.3 One-pot reactions



Scheme 19 Claisen-Schmidt condensation between benzaldehyde and acetophenone.

Hargrove-Leak *et al.* using Li-Al rehydrated HTs achieved conversion around 55% in 1 hour of reaction between 2-hydroxyacetophenone and benzaldehyde [177]. Moreover, one complete study was developed by Corma *et al.* who studied the synthesis of chalcones of pharmaceutical interest through the Claisen-Schmidt condensation between benzaldehydes and acetophenones [183]. They found that Mg/Al (3:1) mixed oxide with water content of 35 wt% was the optimised solid-base catalyst, and could be used in the synthesis of several chalcones with anti-inflammatory, antineoplastic, and diuretic activities; in all cases excellent activity and selectivity were reported.

2.3.2 Claisen-Schmidt-Juliá-Colonna asymmetric one-pot reactions

As exposed below, asymmetric epoxidation is a remarkably powerful organic transformation, which can efficiently establish two stereogenic centres in one simple operation. About asymmetric one-pot synthesis of α,β -epoxy ketones, Choudary *et al.* developed a bifunctional nanocrystalline aerogel-MgO catalyst for synthesising chiral epoxy ketones using (+)-diethyl tartrate as chiral auxiliary and toluene as solvent [184]. The synthesis was evaluated in a tandem reaction starting with the Claisen-Schmidt reaction of benzaldehydes and ketones followed by asymmetric epoxidation to afford chiral epoxy ketones with moderate yields and moderate to high enantioselectivities. However, although the time of synthesis was increased up to 36 h, they demonstrated that one-pot reaction allowed better results permitting the recycling of the catalyst fifth times without any appeared deactivation. Ling *et al.* reported the first example of a combination of condensation and epoxidation process for the synthesis of chiral epoxy ketones using cinchona as catalyst [185]. However, the enantioselectivity varied from moderate to high while the yields are generally just moderate, furthermore, the expensive chiral catalyst may be difficult to isolate from the reaction system and to be reused. Recently, Yang *et al.* reported the use of imidazolium-

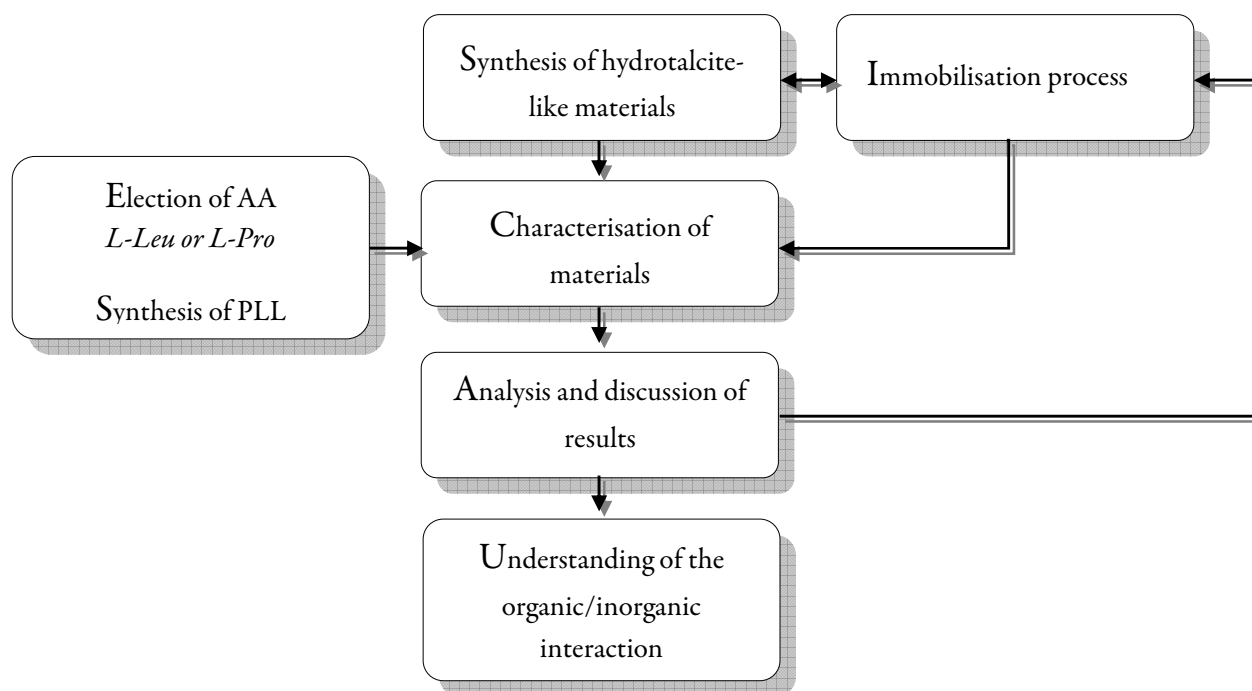
modified PLLs (Scheme 9) as catalyst in one-pot reaction of **(28)** and **(29)** [181]. Using the biphasic epoxidation conditions, they could obtain high enantioselectivity with satisfactory yields in 72 h of reaction. The most important contribution of Yang *et al.* protocol was the possibility of recovering and recycling catalysts tenth times with slight decrease of yield since 70 up to 64% and the enantioselectivity since 97 to 93% [186].

3. Scope of this thesis

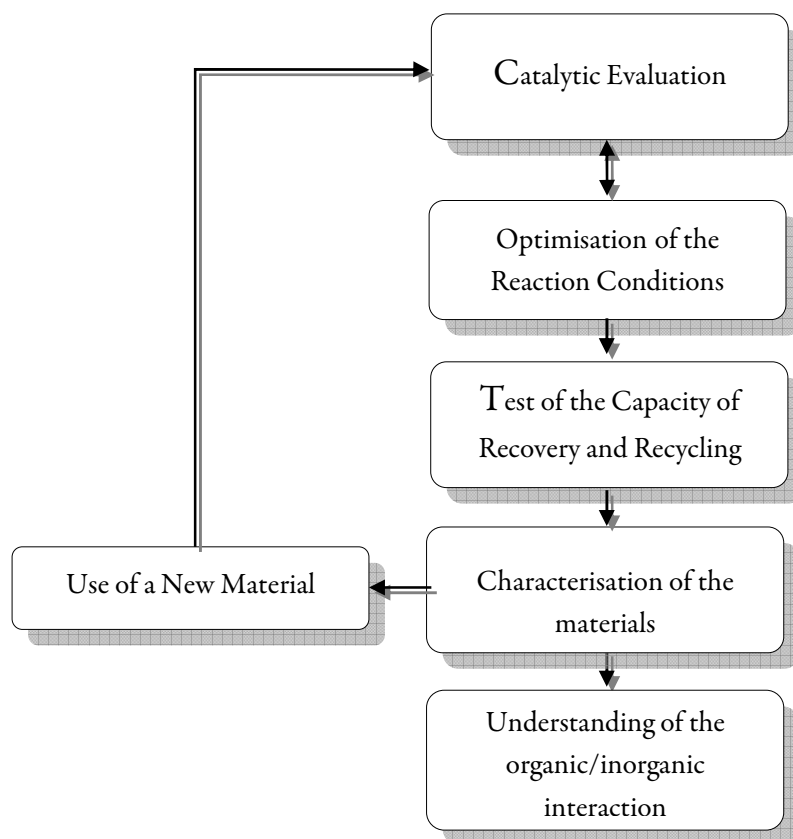
This introduction clearly shows the interest in the synthesis of bio-nanohybrid materials which have been used in different fields. In this context, our hypotheses were focused on design, synthesis and characterisation of novel bio-nanohybrid materials as catalysts in enantioselective reactions of interests to the fine-chemical and pharmaceutical industries. One in-depth study of the physical and chemical properties of the synthesised bio-nanohybrid materials could allow novel materials with desirable stability used as catalyst permitting the easy and clean separation of the reaction media. Moreover, the complete understanding of the interactions between the biomolecules and the hydrotalcite support would permit the synthesis of more complex bio-nanohybrid materials with versatile applications in different fields.

At this point, we planned to develop in this thesis the following aspects:

1. Investigate the nature of the immobilisation organic/inorganic in bio-nanohybrid materials based on L-Leu, L-Pro and PLL immobilised in hydrotalcite-like materials



- 2. Evaluate catalytically synthesised bio-nano hybrid materials in aldol condensations and/or asymmetric Juliá-Colonna epoxidation reactions. Design of a chiral catalytic system that can be easily recovered from the products and reused.**



References

- [1] E. Ruiz-Hitzky, M. Dader, P. Aranda and K. Ariga. *Adv. Mater.* **2010**, *22*, 323
- [2] S.P. Newman and W. Jones. *New J. Chem.* **1998**, 105
- [3] S. Vijaikumar, A. Dhakshinamoorthy and K. Pitchumani. *Appl. Catal. A.* **2008**, *340*, 25
- [4] A.I. Khan and D. O'Hare. *J. Mater. Chem.* **2002**, *12*, 3191
- [5] A.H. Yuwono, B. Liu, J. Xue, J. Wang, H.I. Elim, W. Ji, Y. Lic and T.J. Whitec. *J. Mater. Chem.* **2004**, *14*, 2978; E. Ruiz-Hitzky, K. Ariga and Y. Lvov. *Bio-inorganic hybrid nanomaterials*. Wiley, Germany, **2008**. ISBN 978-3-527-31718-9
- [6] G. Lagaly and K. Beneke, *Colloid Polym. Sci.* **1991**, *269*, 1198; B.K.G. Theng, *The Chemistry of Clay-Organic Reactions*, Wiley, New York, **1974**. ISBN 978-0470858523; G. A. Ozin, *Adv. Mater.* **1992**, *4*, 612; Y. Lvov, K. Ariga, I. Ichinose and T. Kunitake. *J. Am. Chem. Soc.* **1995**, *117*, 6117; U. Constantino, M. Casciola, G. Pani, D. M. Jones and J. Rozière. *J. Solid State Ionics*, **1997**, *97*, 261
- [7] Z.-C. Xing, Y. Chang and I.-K. Kang. *Sci. Technol. Adv. Mater.* **2010**, *11*, 14101
- [8] N. End and K.-U. Schöning. *Topics in Current Chem.* **2004**, *242*, 241
- [9] S. Laib and B.D. MacCraith. *Anal. Chem.* **2007**, *79*, 6264
- [10] I.-T. Hwang, D.-K. Kim, C.-H. Jung, J.-S. Lee, J.-H. Choi, Y.-C. Nho, D.-H. Suh and K. Shin. *J. Nanosci. Nanotechnol.* **2011**, *11*, 4562
- [11] X. Zhou, T. Yu, Y. Zhang, J. Kong, Y. Tang, J.-L. Marty and B. Liu. *Electrochem. Commun.* **2007**, *9*, 1525
- [12] T.B. Goriushkina, B.A. Kurç, A. Sacco Jr., S.V. Dzyadevych. *Sensor Electronics and Microsystem Technologies.* **2010**, *1*, 36
- [13] G.J.de A.A. Soler-Illia, C. Sanchez, B. Lebeau and J. Patarin. *Chem. Rev.* **2002**, *102*, 4093
- [14] F. Calderón, R. Fernández, F. Sánchez and A. Fernández-Mayoralas. *Adv. Synth. Catal.* **2005**, *347*, 1395
- [15] H. Nakayama. *Phosphorus Res. Bull.* **2009**, *23*, 1
- [16] Á. Fudala, I. Pálinkó and I. Kiricsi. *Inorg. Chem.* **1999**, *38*, 4653
- [17] A.P. Wight and M.E. Davis. *Chem. Rev.* **2002**, *102*, 3589
- [18] L. Zhong, J. Xiao and C. Li. *J. Catal.* **2006**, *243*, 442; J.M. Fraile, J.I. García, C.I. Herrerías, J.A. Mayoral and E. Pires. *Chem. Soc. Rev.* **2009**, *38*, 695
- [19] M. Camplo, M. Wathier, J. Chow and M.W. Grinstaff. *Chem. Commun.* **2011**, *47*, 2128
- [20] E. Ruiz-Hitzky, P. Aranda, M. Darder and M. Ogawa. *Chem. Soc. Rev.* **2011**, *40*, 801
- [21] F. Li and X. Duan. *Struct Bond.* **2006**, *119*, 193
- [22] A. Viccari. *Catal. Today.* **1998**, *41*, 53

- [23] K. Ebitani, K. Motokura, K. Mori, T. Mizugaki and K. Kaneda. *J. Org. Chem.* **2006**, *71*, 5440
- [24] H. Gorzawski, W.F. Hoelderich. *J. Mol. Catal. A.* **1999**, *144*, 181
- [25] S.P. Paredes, G. Fetter, P. Bosch and S. Bulbulian. *J. Nuclear Mat.* **2006**, *359*, 155
- [26] J.-C. Dupin, H. Martínez, C. Guimon, E. Dumitriu, I. Fechete. *Appl. Clay Sci.* **2004**, *27*, 95
- [27] I. Kirm, F. Medina, X. Rodriguez, Y. Cesteros, P. Salagre and J. Sueiras. *Appl. Catal. A.* **2004**, *272*, 175
- [28] C. Del Hoyo. *Appl. Clay Sci.* **2007**, *36*, 103
- [29] J.M. Fraile, N. García, J.A. Mayoral, E. Pires and L. Roldán. *Appl. Catal. A.* **2010**, *387*, 67; S. Abelló, F. Medina, D. Tichit, J. Pérez-Ramírez, J.C. Groen, J.E. Sueiras, P. Salagre and Y. Cesteros. *Chem. Eur. J.* **2005**, *11*, 728
- [30] J.-H. Choy, S.-Y. Kwak, J.-S. Park, Y.-J. Jeong. *J. Mater. Chem.* **2001**, *11*, 1671
- [31] U. Costantino, V. Ambrogio, M. Nocchetti and L. Perioli. *Microporous and Mesoporous Mater.* **2008**, *107*, 149
- [32] R.L. Frost and A.W. Musumeci. *J. Colloid Interface Sci.* **2006**, *302*, 203
- [33] K.L. Erickson, T.E. Bostrom and R.L. Frost. *Mater. Lett.* **2005**, *59*, 226
- [34] N. Gutmann, B. Müller and H.-J. Tiller. *J. Solid State Chem.* **1995**, *119*, 331
- [35] S.P. Paredes, G. Fetter, P. Bosch and S. Bulbulian. *J. Mater. Sci.* **2006**, *41*, 3377
- [36] D. Tichit. *Langmuir.* **1998**, *14*, 2086
- [37] F. Cavani, F. Trifirò and A. Vaccari. *Catal. Today.* **1991**, *11*, 173
- [38] J. C. A. A. Roelofs, D. J. Lensveld, A. J. van Dillen and K. P. de Jong. *J. Catal.* **2001**, *203*, 184
- [39] F. Winter, X. Xia, B.P.C. Hereijgers, J.H. Bitter, A. J. van Dillen, M. Muhle and K.P. de Jong. *J. Phys. Chem. B.* **2006**, *110*, 9211
- [40] R. J. Chimentao, S. Abelló, F. Medina, J. Llorca, J. Sueiras, Y. Cesteros and P. Salagre. *J. Catal.* **2007**, *252*, 249
- [41] Q. Zhenlan, Y. Heng, Z. Bin and H. Wanguo. *Colloids and Surfaces A: Physicochem. Eng. Aspects.* **2009**, *348*, 164
- [42] S. Aisawa, N. Higashiyama, S. Takahashi, H. Hirahara, D. Ikematsu, H. Kondo, H. Nakayama and E. Narita. *Appl. clay Sci.* **2007**, *35*, 146
- [43] J.-H. Choy, S.-Y. Kwak, J.-S. Park, Y.-J. Jeong and J. Portier. *J. Am. Chem. Soc.* **1999**, *121*, 1399
- [44] H. Nakayama, A. Hatakeyama and M. Tshako. *Int. J. Pharm.* **2010**, *393*, 104
- [45] H. Nakayama, K. Huwano and M. Tshaki. *J. Phys. Chem. Sol.* **2008**, *69*, 1552
- [46] M. Del Arco, E. Cebadera, S. Gutiérrez, C. Martín, M.J. Montero, V. Rives, J. Rocha and M.A. Sevilla. *J. Pharm. Sci.* **2004**, *93*, 1649
- [47] L. Parioli, T. Posati, M. Nocchetti, F. Bellezza, U. Costantino and A. Cipiciani. *Appl. Clay Sci.* **2010**, doi:10.1016/j.clay.2010.06.028

- [48] A.I. Khan, L. Lei, A.J. Norquist and D. O'Hare. *Chem. Commun.* **2001**, 2342
- [49] F. Bruna, I. Pavlovic, R. Celis, C. Barriga, J. Cornejo and M.A. Ulibarri. *Appl. Clay Sci.* **2008**, *42*, 194
- [50] H Nakayama, N. Wada and M. Tshako. *Int. J. Pharm.* **2004**, *269*, 469
- [51] S. Aisawa, H. Kudo, T. Hoshi, S. Takahashi, H. Hirahara, Y. Umetsu and E. Narita. *J. Solid State Chem.* **2004**, *177*, 3987
- [52] S. Aisawa, S. Sasaki, S. Takahashi, H. Hirahara, H. Nakayama and E. Narita. *J. Phys. Chem. Sol.* **2006**, *67*, 920
- [53] B.M. Choudary, B. Kavita, N. Sreenivasa Chowdari, B. Sreedhar and M. Lakshmi Kantam. *Catal. Lett.* **2001**, *78*, 1
- [54] S. Aisawa, S. Takahashi, W. Ogasawara, Y. Umetsu and E. Narita. *J. Sol. Stat.* **2001**, *162*, 52
- [55] R. Morales Borgesa, G.G. Carbajal Arizaga and F. Wypych. *Biochem. Eng. J.* **2009**, *48*, 93
- [56] M.B.A. Rahmana, M. Basri, M.Z. Hussein, M.N.H. Idris, R.N.Z.R.A. Rahman and A.B. Salleh. *Catal. Today.* **2004**, *93-95*, 405
- [57] A. Yasutake, S. Aisawa, S. Takahashi, H. Hirahara and E. Narita. *J. Phys. Chem. Sol.* **2008**, *69*, 1542
- [58] N.T. Whilton, P.J. Vickers and S. Mann. *J. Mater. Chem.* **1997**, *7*, 1623
- [59] F. Kovanda, E. Jindová, K. Lang, P. Kubát and Z. Sedláková. *Appl. Clay Sci.* **2010**, *48*, 260. F. Leroux, P. Aranda, J.-P. Besse, E. Ruiz-Hitzky. *Eur. J. Inorg. Chem.* **2003**, *6*, 1242
- [60] F.A. Carey "*Aminoacids, peptides and proteins. Nucleic acids*" in *Organic Chemistry*, 5th Ed. McGraw-Hill, United States of America, 2003. p1051-1107
- [61] K. Tamura and R.W. Alexander. *Cell. Mol. Life Sci.* **2004**, *61*, 1317
- [62] P. Coffey, K.-H. Drauz, S.M. Roberts, J. Skidmore and J. Smith. *Chem. Commun.* **2001**, 2330
- [63] E.R. Jarvo and S.J. Miller. *Tetrahedron.* **2002**, *58*, 2481
- [64] D. Kelly and S.M. Roberts. *Biopolymers.* **2006**, *84*, 74
- [65] T.J. Deming. *Adv. Mater.* **1997**, *9*, 299
- [66] T.J. Deming. *Prog. Polym. Sci.* **2007**, *32*, 858
- [67] W. Kim, J. Thévenot, E. Ibarboure, S. Lecommandoux and E.L. Chaikof. *Angew. Chem. Int. Ed.* **2010**, *49*, 4257
- [68] H.R. Kricheldorf. *Angew. Chem. Int. Ed.* **2006**, *45*, 5752
- [69] W.N. E. van Dijk-Wolthuis, L. van de Water, P. van de Wetering, M. van Steenberghe, J.J.K. van den Bosch, W. Schuyl and W.E. Hennink. *Macromol. Chem. Phys.* **1997**, *198*, 3893
- [70] H. Sekiguchi. *Pure Appl. Chem.* **1981**, *53*, 1689
- [71] T. Deming. *Adv. Polym. Sci.* **2006**, *202*, 1
- [72] H.R. Kricheldorf, C.V. Lossow, N. Lomadze and G. Schwarz. *J. Polymer Sci. Chem.* **2008**, *46*, 4012
- [73] H.R. Kricheldorf, C. von Lossow and G. Schwarz. *J. Polymer Sci. A.* **2005**, *43*, 5690

- [74] F. Bergaya, B.K.G. Theng and G. Lagaly "Clay minerals and the origin of life" in Handbook of Clay Science, Elsevier Ltd, The Netherlands, 2006. P379-391
- [75] D.A.M. Zaia. Aminoacids. **2004**, 27, 113
- [76] J. Bujdák and B.M. Rode. Catal. Lett. **2003**, 73, 797
- [77] J. Bujdák and B.M. Rode. J. Peptide Sci. **2004**, 10, 731
- [78] J. Bujdák and B.M. Rode. Orig. life Evol. Bioph. **1999**, 29, 451
- [79] J. Bujdák and B.M. Rode. J. Molec. Catal. A. **1999**, 144, 129
- [80] M. Darder, M. López-Blanco, P. Aranda, F. Leroux and E. Ruiz-Hitzky. Chem. Mater. **2005**, 17, 1969
- [81] K. Ladewig, Z.P. Xu and G.Q. Lu. Expert Opin. Drug Deliv. **2009**, 6, 907
- [82] J.-H. Choy, S.-Jin Choi, J.-M. Oh and T. Park. Appl. Clay Sci. **2007**, 36, 122
- [83] J.-M. Oh, T.T. Biswick and J.-H. Choy. J. Mater. Chem. **2009**, 19, 2553
- [84] A.R. Hill Jr., C. Böhrer and L.E. Orgel. Origin life evol. Bioph. **1998**, 28, 235
- [85] S. Miyata. Clay and Clay miner. **1975**, 23, 369
- [86] T. Hibino. Chem. Mater. **2004**, 16, 5482
- [87] Q. Yuan, M. Wei, Z. Wang, G. wang and X. Duan. Clay and Clays Miner. **2004**, 52, 40
- [88] Q. Yuan, M. Wei, D.G. Evans, and X. Duan. J. Phys.Chem.B. **2004**, 108, 12381
- [89] E.M. Seffel, E. Dvininov, D. Lutic, E. Popovici and C. Ciocoiu. J.optoel.Adv.Mater. **2005**, 7, 2869
- [90] M. Wei, Z. Shi, D.G. Evans, X. Duan. J. Mater. Chem. **2006**, 16, 2102
- [91] M. Wei, J. Guo, Z. Shi, Q. Yuan, M. Pu, G. Rao and X. Duan. J. Mater. Sci. **2007**, 42, 2684
- [92] M.X. Reinholdt and R.J. Kirkpatrick. Chem. Mater. **2006**, 18, 2567
- [93] M.X. Reinholdt, P.K. Babu and R.J. Kirkpatrick. J.Phys.Chem.C. **2009**, 113, 3378
- [94] A. Dhakshinamoorthy, A. Sharmila and K. Pitchumani. Chem. Eur. J. **2010**, 16, 1128
- [95] G. Oxin and A. Arsenault, Biomaterials and Bioinspiration in nanochemistry: A Chemical Approach to nanomaterials, Royal Society of Chemistry, London **2005**, 473; A. Sellinger, P.M. Weiss, A. Nguyen, Y. Lu, R. A. Assink, W. Gong and C. J. Brinker, Nature **1998**, 394, 256; Z. Tang, N.A. Kotov, S. Magonov and B. Ozturk, Nature mater. **2003**, 2, 413
- [96] M. Meyn, K. Beneke and G. Lagaly, Inorg. Chem., **1990**, 29, 5201
- [97] M. A. Drezdon, Inorg. Chem. **1988**, 27, 4628
- [98] L. Raki, D.G. Rancourt, C. Detellier. Chem. Mater. **1995**, 7, 221; N.Nhlapo, T. Motumi, E. Landman, S. M:C. Verryyn and W.W.Focke. J. Mater Sci, **2008**, 43, 1033
- [99] I.Y. Park, K.Kurado and C. Kato. J. Chem. Soc., Dalton Trans., **1990**, 3071, Z. Sun, L. Jin, W. Shi, M. Wei, D.G Evans, and X. Duan. Langmuir, **2011**, 27, 7113
- [100] N.Iyi, Y. Ebina and T. Sasaki. J. Mater, Chem., 2011, **21**, 8085

- [101] E. Kanezaki. *Mater. Res. Bull.* **1998**, *33*, 773; F. Leroux, M. Adachi,-Pagano, M. Intissar, S.Chauviere, C. Foranoand and J. Besse. *J.Mater. Chem.* **2001**, *11*, 105; F. Leroux, and J.-P. Besse. *Chem. Mater.* **2001**, *13*, 3507; R. Anbarasan, W. Lee, S. Im, *Bull. Mater. Sci.* **2005**, *28*, 145; L.C.Du and B.J.Qu. *Polym. Comp.* **2007**, *28*, 131; F.R. Costa, A. Leuteritz, U. Wagenknecht, D. Jehnichen, L. Hausslerand and G. Heinrich. *Appl. Clay Sci.* **2008**, *38*, 153
- [102] F. Leroux. *J. Nanosci. Nanotechnol.* **2006**, *6*, 303
- [103] F. Leroux, P. Aranda, J-P. Besse and E. Ruiz-Hitzky. *Eur. J. Inorg. Chem.* **2003**, 1242; W. Lee; S. IM, K. Kim. *Polymer* **2006**, *47*, 1364; P. Ding and B. Qu. *Poly. Eng. Sci.* **2006**, *46*, 1153; C. Nyambo, D. Wang and C.A. Wilkie. *Poly. Adv. Technol.* **2009**, *20*, 332; A. Doménech, E. Coronado, N. Lardiés, C.M. Gastaldo, M. T. Doménech-Carbó and A. Ribera. *J. Electroanal. Chem.* **2008**, *624*, 275; K. Hongliang, H. Gailling, M. Shulan. *J. Phys. Chem. C*, **2009**, *21*, 9157
- [104] J.-H. Choy, S.-Y. Kwak, Y.-J. Jeong and J.-S. Park. *Angew. Chem. Int. Ed.* **2000**, *39*, 4042
- [105] R. Morales Borgesa, G.G. Carbajal Arizaga and F. Wypych. *Biochem. Eng. J.* **2009**, *48*, 93
- [106] M.R. Berber, I.H. Hafez, K. Minagawa, T. Mori and M. Tanaka. *Pharm. Res.* **2010**, *27*, 2394
- [107] J.-I. Oku and S. Inoue. *J. Chem. Soc. ChemCommun.* **1981**, 229
- [108] S. Juliá, J. Guixer, J. Masana, J. Rocas, S. Colonna, R. Annuziata and H. Molinari. *J. Chem. Soc. Perkin Trans. 1.* **1982**, 1317
- [109] A. Baiker. *Curr. Opin. Solid St. Mater. Sci.* **1998**, *3*, 86
- [110] N.C. Veitch and R.J. Grayer. *Nat. Prod. Rep.* **2008**, *25*, 555
- [111] R. Li, G.L. Kenyon, F.E. Cohen, X. Chen, B. Gong, J.N. Dominguez, E. Davidson, G. Kurzban, R.E. Miller, E.O. Nuzum, P.J. Rosenthal and J.H. McKerrow. *J. Med. Chem.* **1995**, *38*, 5031
- [112] J. F. Ballesteros, M. J. Sanz, A. Ubeda, M.A. Miranda, S. Iborra, T.M. Paya and M. J. Alcaraz. *J. Med. Chem.* **1995**, *38*, 2794
- [113] J.R. Dimmock, N.M. Kandepu, M. Hetherington, J.W. Quail, U. Pugazhenthii, A.M. Sudom, M. Chamankhah, P. Rose, E. Pass, T.M. Allen, S. Halleran, J. Szydowski, B. Mutus, M. Tannous, E.K. Manavathu, T.G. Myers, E. De Clercq and J. Balzarini. *J. Med. Chem.* **1998**, *41*, 1014
- [114] R.J. Anto, K. Sukumaran, G. Kuttan, M.N.A. Rao, V. Subbaraju and R. Kuttan. *Cancer Lett.* **1995**, *97*, 33
- [115] A.T. Dinkova-Kostova C. Abeygunawardana and P. Talalay. *J. Med. Chem.* **1998**, *41*, 5287
- [116] T. Akihisa, H. Tokuda, M. Ukiya, M. Iizuka, S. Schneider, K. Ogasawara, T. Mukainaka, K. Iwatsuki, T. Suzuki and H. Nishino. *Cancer Lett.* **2003**, *201*, 133
- [117] Q.-H. Xia, H.-Q. Ge, C.-P. Ye, Z.-M. Liu and K.-X. Su. *Chem. Rev.* **1995**, *105*, 1603
- [118] M.W. Cappi, W.-P. Chen, R.W. Flood, Y.-W. Liao, S.M. Roberts, J. Skidmore, J.A. Smith and N.M. Williamson. *Chem. Commun.* **1998**, *10*, 1159

- [119] B.M. Adger, J.V. Barkley, S. Bergeron, M.W. Cappi, B.E. Flowerdew, M.P. Jackson, R. McCague, T.C. Nugent and S.M. Roberts. *J. Chem. Soc. Perkin Trans. 1.* **1997**, 3501
- [120] L. Carde, D.H. Davies and S.M. Roberts. *J. Chem. Soc. Perkin Trans. 1.* **2000**, 2455
- [121] P. Ray and S.M. Roberts. *Chem. Commun. J. Chem. Soc. Perkin Trans. 1.* **2001**, 149
- [122] W.-P. Chen and S.M. Roberts. *J. Chem. Soc. Perkin Trans. 1.* **1999**, 103
- [123] S. Juliá, J. Masana, J. C. Vega. *Angew. Chem. Int. Ed. Engl.* **1980**, 19, 929
- [124] S. Banfi, S. Colonna, H. Molinari, S. Juliá and J. Guixer. *Tetrahedron.* **1984**, 40, 5207
- [125] P.A. Bentley, S. Bergeron, M.W. Cappi, D.E. Hibbs, M.B. Hursthouse, T.C. Nugent, R. Pulido, S.M. Roberts and L.E. Wu. *Chem. Commun.* **1997**, 8, 739
- [126] A. Dhanda, K.-H. Drauz, T. Geller and S.M. Roberts. *Chirality.* **2000**, 12, 313
- [127] J.V. Allen, K.-H. Drauz, R.W. Flood, S.M. Roberts and J. Skidmore. *Tetrahedron Lett.* **1999**, 40, 5417
- [128] T. Geller and S.M. Roberts. *J. Chem. Soc. Perkin Trans. 1.* **1997**, 1397
- [129] L. Christelle and S.M. Roberts. *Aldrichimica.* **2002**, 35, 47
- [130] R.W. Flood, T.P. Geller, S.A. Petty, S.M. Roberts, J. Skidmore and M. Volk. *Org. Lett.* **2001**, 3, 683
- [131] S. Itsuno, M. Sakakura and K. Ito. *J. Org. Chem.* **1990**, 55, 6047
- [132] H. Yi, G. Zou, Q. Li, Q. Chen, J. Tang and M.-Y. He. *Tetrahedron Lett.* **2005**, 46, 5665
- [133] F. Yang, L.-M. He, H. Yi, G. Zou, J. Tang and M.-Y. He. *J. Mol. Catal. A.* **2007**, 273, 1
- [134] W. Qiu, L. He, Q. Chen, W. Luo, Z. Yu, F. Yang, J. Tang. *Tetrahedron Lett.* **2009**, 50, 5225
- [135] T. Geller, C.M. Krügerb and H.-C. Militzer. *Tetrahedron Lett.* **2004**, 45, 5069
- [136] T. Geller, A. Gerlach, C.M. Krügerb and H.-C. Militzer. *Tetrahedron Lett.* **2004**, 45, 5065
- [137] T. Geller, A. Garlach, C.M. Krüger and H.-C. Militzer. *J. Mol. Catal. A.* **2006**, 251, 71
- [138] D. Kelly, A. Meek and S.M. Roberts. *Chem. Commun.* **2004**, 2021
- [139] D. Kelly, A. Meek and S.M. Roberts. *Chem. Commun.* **2004**, 2021. D. Kelly and S.M. Roberts. *Chem. Commun.* **2004**, 2018
- [140] T. Kawasaki and Y. Yamamoto. *J. Org. Chem.* **2002**, 67, 5138
- [141] P.M. Pihko, K.M. Laurikainen, A. Usano, A.I. Nyberg and J.A. Kaavi. *Tetrahedron.* **2006**, 62, 317
- [142] L.M. Geary and P.G. Hultin. *Tetrahedron: Asym.* **2009**, 20, 131
- [143] G. Guillena, C. Nájera and D.J. Ramón. *Tetrahedron: Asym.* **2007**, 18, 2249
- [144] T.D. Machajewski and C.-H. Wong. *Angew. Chem. Int. Ed.* **2000**, 39, 1352
- [145] T. Hoffmann, G. Zhong, B. List, D. Shabat, J. Anderson, S. Gramatikova, R.A. Lerner and C.F. Barbas III. *J. Am. Chem. Soc.* **1998**, 120, 2768
- [146] M. Gruttadauria, F. Giacalone and R. Noto. *Chem. Soc. Rev.* **2008**, 37, 1666 and references therein.
- [147] B. List, R.A. Lerner and C.F. Barbas III. *J. Am. Chem. Soc.* **2000**, 122, 2395
- [148] K. Sakthivel, W. Notz, T. Bui and C.F. Barbas III. *J. Am. Chem. Soc.* **2001**, 123, 5260

- [149] Y.-Q. Fu, Y.-J. An, W.-M. Liu, Z.-C. Li, G. Zhang and J.-C. Tao. *Catal. Lett.* **2008**, *124*, 397
- [150] V. Srivastava, K. Gaubert, M. Pucheault and M. Vaultier. *Chem.Cat.Chem.* **2009**, *1*, 94
- [151] C. Zhuo, D. Xian, W. Jian-Wei and X. Hui. *ISRN Org. Chem.* **2011**, doi 10,5402/2011/676789
- [152] W. Miaoa and T.H. Chana. *Adv. Synth. Catal.* **2006**, *348*, 1711
- [153] A. Zamboulis, N.J. Rahier, M. Gehringer, X. Cattoën, G. Niel, C. Bied, J.J.E. Moreau and M.W.C. Man. *Tetrahedron:Asym.* **2009**, *20*, 2880
- [154] M. Benaglia, M. Cinquini, F. Cozzi, A. Puglisi and G. Celentano. *Adv. Synth. Catal.* **2002**, *5*, 344
- [155] F. Giacalone, M. Gruttadauria, A. Mossuto Marculescu and R. Noto. *Tetrahedron Letters.* **2007**, *48*, 255
- [156] J. Li, G. Yang and Y. Cui. *J. Appl. Polym. Sci.* **2011**, *121*, 1506
- [157] A. Córdova, W. Zou, I. Ibrahim, E. Reyes, M. Esgqvist and W.-W. Liao. *Chem. Commun.* **2005**, 3586
- [158] Z. Jiang, Z. Liang, X. Wu and Y. Lu. *Chem. Commun.* **2006**, 2801
- [159] For more examples of AA and PAA see: P. Dziejdzic, W. Zou, I. Ibrahim, H. Sudén and A. Córdova. *Tetrahedron letters.* **2006**, *47*, 6657; M. Lei, L. Shi, G. Li, S. Chen, W. Fang, Z. Ge, T. Cheng and R. Li. *Tetrahedron.* **2007**, *63*, 7892; J.D. Revell and H. Wennemers. *Tetrahedron.* **2007**, *63*, 8420; V. D'Elia, H. Zwicknagl, O. Reiser. *J. Org. Chem.* **2008**, *73*, 3262
- [160] A. Córdova, W. Zou, P. Dziejdzic, I. Ibrahim, E. Reyes and Y. Xu. *Chem. Eur. J.* **2006**, *12*, 5383
- [161] G. Carrea, G. Ottolina, A. Lazcano, V. Pironti and S. Colonna. *Tetrahedron. Asym.* **2007**, *18*, 1265
- [162] G. Szöllösi, G. London, L. Balásipiri, C. Somlai and M. Bartók. *Chirality.* **2003**, *15*, S90
- [163] Y.-J. An, Y.-X. Zhang, Y. Wu, Z.-M. Liu, C. Pi and J.-C. Tao. *Tetrahedron:Asym.* **2010**, *21*, 688
- [164] Q. Gu, X.-F. Wang, L. Wang, X.-Y. Wua and Q.-L. Zhou. *Tetrahedron. Asymm.* **2006**, *17*, 1537
- [165] R. J. Chimentaó, S. Abelló, F. Medina, J. Llorca, J. Sueiras, Y. Cesteros and P. Salagre. *J. Catal.* **2007**, *252*, 249
- [166] K. Kaneda, K. Ebitani, T. Mizugaki and K. Mori. *Bull. Chem.Soc.Jpn.* **2006**, *79*, 981 and references therein.
- [167] A. Corma, V. Fornés, R.M. Martín-Aranda and F. Rey. *J. Catal.* **1992**, *134*, 58
- [168] D. Tichit, M.H. Lhouty, A. Guida, B.H. Chiche, F. Figueras, A. Auroux, D. Bartalini and E. Garrone. *J. Catal.* **1995**, *151*, 50
- [169] I.K. Mangion, A.B. Northrup and D.W.C. MacMillan. *Angew. Chem. Int. Ed.* **2004**, *43*, 6722
- [170] T. Kawasaki and Y. Yamamoto. *J. Org. Chem.* **2002**, *67*, 5138. R.A. Sheldon. *Chem. Commun.* **2008**, 3352
- [171] F. Gelman, J. Blum and D. Avnir. *J. Am. Chem. Soc.* **2000**, *122*, 11999
- [172] L.-Z. Dai and M. Shi. *Tetrahedron Lett.* **2009**, *50*, 651
- [173] J.-T. Li, Y. Yin and M.-X. Sun. *Ultrasonic Sonochem.* **2010**, *17*, 363

- [174] F. Toda, K. Tanaka and K. Hamai. *J. Chem. Soc. Perkin Trans 1*. **1990**, 3207
- [175] E.V. Stoyanov, Y. Champavier, A. Simon and J.-P. Basly. *Bioorg. Med. Chem. Lett.* **2002**, *12*, 1685
- [176] S. Chandrasekhar, K. Vijeender and K.V. Reddy. *Tetrahedron Lett.* **2005**, *46*, 6991
- [177] D. French, P. Schifano, J. Cortés-Concepción and S. Hargrove-Leak. *Catal. Commun.* **2010**, *12*, 92
- [178] X. Wang and S. Cheng. *Catal. Commun.* **2006**, *7*, 689
- [179] M.T. Drexler and M.D. Amiridis. *J. Catal.* **2003**, *214*, 136
- [180] V. Calvino, M. Picallo, A.J. López-Peinado, R.M. Martín-Aranda and C.J. Durán-Valle. *Appl. Surf. Sci.* **2006**, *252*, 6071
- [181] J. Shen, H. Wang, H. Liu, Y. Sun and Z. Liu. *J. Mol. Catal. A*. **2008**, *280*, 24
- [182] J. López, R. Jacquot and F. Figueras. *Stud. Surf. Sci. Catal.* **2000**, *130*, 491
- [183] M.J. Climent, A. Corma, S. Iborra and A. Velty. *J. Catal.* **2004**, *221*, 474
- [184] B.M. Choudary, M.L. Kantam, K.V.S. Ranganath, K. Mahendar and B. Sreedhar. *J. Am. Chem. Soc.* **2004**, *126*, 3396
- [185] Y. Wang, J. Ye and X. Liang. *Adv. Synth. Catal.* **2007**, *349*, 1033
- [186] W. Luo, Z. Yu, W. Qiu, F. Yang, X. Liu and J. Tang. *Tetrahedron*. **2011**, *67*, 5289

NANOHYBRID MATERIALS BASED ON AAs AND HTs AS CATALYSTS IN FINE CHEMISTRY REACTIONS

Biohybrid nanostructured materials based on the combination of laminar inorganic solids such as HTs and naturally occurring AAs have received considerable attention due to their importance in regenerative medicine, nanocomposite materials engineering and catalysis. In addition, they find industrial interest since they are derived from abundant, cheap, and ecological sources. The biohybrids not only often exhibit high complementary properties between their assembled components but also present new and interesting properties due to a synergistic effect. These new materials, easily recovered, may represent a big breakthrough in the pharmaceutical industry and fine chemistry compared to currently used homogeneous catalysts which are difficult to separate causing that the purification of the products requires several stages. This chapter attempts to use LL/HT and LP/HT nanohybrid materials as catalysts and to rationalise how the synthesis protocol influence their catalytic activity.

-
- 1. Initial considerations**
 - 2. LL/HT nanohybrid materials as catalysts in asymmetric Juliá-Colonna epoxidation reaction**
 - 2.1 Experimental
 - 2.2 Results and discussion
 - 2.3 Preliminary conclusions
 - 3. LP/HT nanohybrid materials as catalysts in direct asymmetric aldol reaction**
 - 3.1 Experimental
 - 3.2 Results and discussion
 - 3.3 Preliminary conclusions
 - 4. Conclusions**
 - References**
-

1. Initial Considerations

Fine chemistry and enantioselective organocatalysis has received much attention in recent years and has become increasingly important in the production of novel catalytic systems and chiral molecules. In this context, enzymes are highly efficient biocatalysts in living systems so that chemists around the world have been inspired in these bio-systems to synthesise, modify or functionalise biomolecules to imitate Nature. AAs form complex bio-structures such as peptides and have a chiral carbon in their structure. These characteristics have been used to design catalytic systems which are efficient and selective. The most important findings in the use of AAs or AA derivatives as organocatalysts were published by Wierchert and Hajos's groups who reported the use of L-Pro as the catalyst of Robinson annulations [1,2], Inoue *et al.* who used diketopiperazines as catalysts in Strecker reactions [3] and Juliá-Colonna's groups who employed PAAs as epoxidation catalysts [4]. Since these findings several improvements to the initial catalytic systems have been reported [5-8].

Particularly, although some reports have been published about the immobilisation of unmodified AAs in HTs, to the best of our knowledge, just three publications have reported the use of AA/HT materials as catalysts. In 2002, Choudary *et al.* reported the synthesis of L-Pro immobilised in HTs (LP/HT) as catalysts for C-C bond-forming reactions (Aldol, Henry and Cyanosilylation reactions), nevertheless any relation between catalysts structure and catalytic results were performed, moreover the nature of the interaction was not studied [9]. Pitchumani *et al.* in 2008 reported the synthesis of LP/HT and its use as catalyst in Michael reaction between β -nitrostyrene and acetone obtaining total conversions with lower enantioselectivities [10]. In 2010, they reported the synthesis of Methionine immobilised in HT as the catalyst in chemoselective *O*-methylation of phenols and esterification of carboxylic acids with dimethyl carbonate obtaining total conversion after 6 h of reaction [11]. This chapter is focused in the catalytic evaluation of LL/HT and LP/HT nanohybrid materials as a part of the understanding of the organic/inorganic interaction nature. LL/HT materials were used for the first time as the catalyst in Juliá-Colonna epoxidation reaction where the disposition of the AAs in the support and the hindered environment provided to the AAs by the support itself confers catalytic properties to the inactive pure AAs. Moreover, LP/HT materials were used as catalysts in direct

2.1 Experimental

asymmetric aldol reaction where the synergistic effect of the obtained nanohybrid was the responsible of the high activity and selectivity.

2. LL/HT nanohybrid materials as catalysts in asymmetric Juliá-Colonna epoxidation reaction

Asymmetric Juliá-Colonna epoxidation reaction of chalcone catalysed by PAAs (See Scheme 10 in Chapter 1, Section 2.1.1) has a relevant importance since its obtained epoxide products are needed reagent in the synthesis of important chiral drugs (eg. Taxol, cancer chemotherapy [12]; (+)-Clausenamide, antiemetic agent [13]; Statin, cholesterol-lowering drug [14]; or (+)-Fenoprofen, treatment of rheumatoid arthritis [15]).

Although the Juliá-Colonna epoxidation mechanism is not clear at all, experimental works and molecular modelling suggest that the α -helicity of the PLL determines the epoxide configuration through face-selective delivery of a hydroperoxide anion. Five L-Leu residues were found sufficient to catalyse the Juliá-Colonna epoxidation of chalcone with 96-98% ee [16]. In addition, the COOH-terminal group of the PLL seems not participate in the catalytic process.

Taking all this into consideration, we explored the possibility to use the LL/HT nanohybrid materials which have different physical properties as catalysts in asymmetric Juliá-Colonna epoxidation reaction. The obtained results show that design of nanohybrid materials with specific physical properties helps achieving higher activity and selectivity in the catalytic reaction of interest than the pure PLL.

2.1 Experimental

2.1.1 Synthesis of LL/HT materials

Synthesis of LL/HT nanohybrid materials was performed by anionic exchange (A) and reconstruction (R) method as was described Chapter 2, section 2.1.2.1 and 2.1.2.2. Table 1 shows a list of the nanohybrid materials used in this section.

Table 1 LL/HT nanohybrid materials used as catalysts in asymmetric Juliá-Colonna epoxydation reaction

Entry	Material ^{a,b}	Synthesis	Main	Molecular formulae ^d
-------	-------------------------	-----------	------	---------------------------------

		method	Location in the HT ^c	
1	L-Leu	-	-	C ₆ H ₁₃ NO ₂
2	HT _{rus}	-	-	[Mg _{2.53} Al _{1.00} (OH) _{7.07}](CO ₃ ²⁻) _{1.18} (NO ₃ ⁻) _{0.10} •1.10H ₂ O
3	LL/HT _{rus} -A1 _{0.08} ^e	A1	Edges	[Mg _{2.63} Al _{1.00} (OH) _{7.25}](Leu) _{0.08} (CO ₃ ²⁻) _{1.70} (NO ₃ ⁻) _{0.10} •1.11H ₂ O
4	LL/HT _{rus} -A1 _{0.22}	A1	Edges	[Mg _{2.63} Al _{1.00} (OH) _{7.25}](Leu) _{0.22} (CO ₃ ²⁻) _{2.36} (NO ₃ ⁻) _{0.10} •1.34H ₂ O
5	LL/HT _{rus} -A1 _{0.44}	A1	Edges	[Mg _{2.63} Al _{1.00} (OH) _{7.25}](Leu) _{0.44} (CO ₃ ²⁻) _{2.30} (NO ₃ ⁻) _{0.10} •1.34H ₂ O
6	LL/HT _{rus} -A2 _{1.09}	A2	Interlayer space	[Mg _{2.39} Al _{1.00} (OH) _{6.79}](Leu) _{1.09} (CO ₃ ²⁻) _{1.19} (NO ₃ ⁻) _{0.10} •1.34H ₂ O
7	LL/HT _{rus} -R1 _{0.95}	R1	Interlayer space	[Mg _{2.63} Al _{1.00} (OH) _{7.25}](Leu) _{0.95} (CO ₃ ²⁻) _{3.34} (NO ₃ ⁻) _{0.10} •2.03H ₂ O
8	LL/HT _r -R2 _{0.92}	R2	Interlayer space	[Mg _{2.63} Al _{1.00} (OH) _{7.25}](Leu) _{0.92} (CO ₃ ²⁻) _{2.99} (NO ₃ ⁻) _{0.10} •1.80H ₂ O

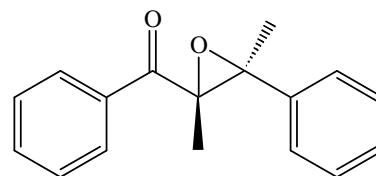
^aSynthesis Conditions: Anionic exchange 1 (A1): HT and a solution of L-Leu were mixed and stirring for 0.5 hour at r.t. Anionic exchange 2 (A2): HT and a solution of L-Leu were mixed and stirring for 3 h at 80°C. Reconstruction 1 (R1): HT_{cc} and a solution of L-Leu were mixed and sonicated during 1 h, following by stirring for 3 h at 80°C. Reconstruction 2 (R2): HT_{cc} and a solution of L-Leu were mixed and stirred for 3 h at 80°C. ^bHT = hydrotalcite. HT_{rus} = rehydrated HT under ultrasound treatment, HT_r = rehydrated HT. ^cDetermined by XRD. ^dCalculated by EA and ICP analyses. Water content was calculated by TG/DTA. ^eLL/HT_{rus}-A1_{0.08} was synthesised by method A1 using 75 mg (0.57 mmol) of L-Leu.

2.1.2 Asymmetric Juliá-Colonna epoxidation reaction

Typical asymmetric Juliá-Colonna epoxidation reaction was performed in a tube of 10 mL where synthesisd LL/HT containing 0.44 mmol of L-Leu, tetrabutylammonium bromide, TBAB, (0.042 mmol), NaOH 5 M (0.43 ml) and hexane (3 ml) were mixed. Subsequently H₂O_{2(aq)} (0.19 ml) and chalcone (**1**) (0.24 mmol) were added. The mixture was stirred during 90 minutes at room temperature. After that time, the mixture was diluted in 1 ml of ethylacetate to work-up the reaction. The catalyst (solid phase) was washed several times with hexane and separated by centrifugation. The organic fraction was dried with MgSO₄. Then, the solvent in the organic phase was evaporated. The product was identified by ¹H NMR:

trans-(2R,3S)-Epoxy-1,3-diphenyl-propan-1-one (**2**)

¹H NMR (400 MHz, CDCl₃): δ = 4.01 (s, 1H), 4.23 (s, 1H), 7.32-7.45 (m, 7H), 7.54 (d, 1H), 7.94 (d, 2H) ppm. The enantiomeric excess (ee) determined by chiral HPLC



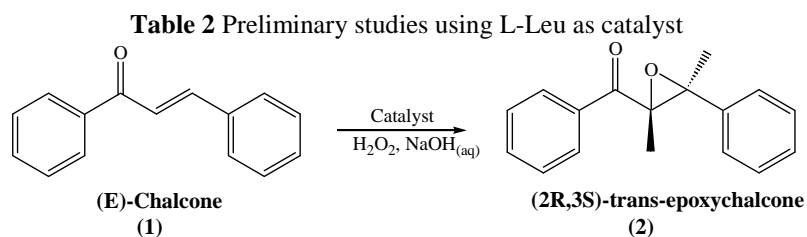
(ChiralPak IA column, EtOH/ hexane = 25/75, UV 254 nm, flow rate 1 mL/min. (S,R)-isomer, *t*_(S,R) = 7.6 min and (R,S)-isomer, *t*_(R,S) = 10.6 min.

2.1 Results and discussion

2.2 Results and discussion

2.2.1 Preliminary studies

To the best of our knowledge, we were the first to employ pure L-Leu in the Juliá-Colonna asymmetric epoxidation reaction, although with low activity and no enantioselectivity (Table 2).



Entry ^a	Catalyst L-Leu (mg)	Co- catalysts	Solvent	t (h)	%C ^b	%ee ^c
1	58	-	Acetone	48	-	-
2	58	-	Acetonitrile	48	-	-
3	58	-	Dichloromethane	48	3.0	ND ^d
4	58	-	Toluene	48	5.5	ND
5	58	-	Hexane	48	60.1	0.5
6	-	-	Hexane	48	8.0	-
7	58	TBAB	Hexane	3	9.4	ND
8	58	-	Hexane	3	3.7	ND
9	-	TBAB	Hexane	3	<1.0	ND
10	116	TBAB	Hexane	3	14.4	0.3

^aReaction Conditions: L-Leu as catalyst, 0.43 ml NaOH 5M, 0.19 ml H₂O₂ (30 wt%), 0.24 mmol **1**, 0.042 mmol TBAB and 3 ml solvent at r.t. Total diastereoselectivity towards *trans*-epoxychalcone.

^b%C calculated by ¹H NMR. ^c%ee determined by chiral HPLC. ^dND= not determined.

Entries 1-5 in Table 2 show the direct relation between solvent polarity and conversion. In this case decrease of the polarity allows higher conversions at 48 hours of reaction. According with Carrea *et al.* asymmetric Juliá-Colonna epoxidation reaction requires the formation of the hydroperoxide anion by deprotonation using NaOH. The hydroperoxide anion is stabilised by the catalysts before the reaction with the chalcone to form the epoxychalcone [17]. In this context, formation of hydroperoxide anion and stabilisation with the catalyst occurs in the aqueous phase, so the use of polar solvent prevents this stabilisation decreasing the total conversion. As showed in Table 2, entry 5, the use of hexane which has nil dipolar moment permitted the formation of the epoxychalcone in 60%. Moreover, presence of two phases (aqueous and organic) limits the time of contact between the chalcone, soluble in organic phase, and the hydroperoxide-L-Leu complex, formed in aqueous phase, increasing the time of reaction.

In that context, following the methodology published by Geller *et al.* we use tetrabutylammonium bromide (TBAB) [18] as a phase transfer co-catalysts to reduce the time of synthesis. Although the activity of the pure L-Leu in hexane and using TBAB as the co-catalyst was not so high (9.4 % of conversion of chalcone in 3 hours), it improved significantly the 3.7% of conversion obtained without TBAB in the same reaction conditions (Table 2, entries 7 and 8). In order to know whether the reaction requires stabilisation by interaction of hydroperoxide anion with the L-Leu, two experiments were performed: the first experiment carried out without the presence of L-Leu afforded practically nil conversion (Table 2, entry 9). In the second experiment the quantity of L-Leu employed was 116 mg instead of the usual 58 mg and the conversion increased to 14.4% (Table 2, entry 10). The L-Leu showed moderate activity in the epoxidation reaction. In all cases, the diastereoselectivity was towards *trans*-epoxychalcone but no enantioselectivity was observed. According with Kelly *et al.* the enantioselectivity is due to the binding of a complex specie PLL-HOO:chalcone which is stabilised and orientated although interaction with the five L-Leu terminal monomer of the PLL [19-20]. In that context, pure L-Leu cannot orientate the chalcone to form a specific enantiomer.

2.2.2 Catalytic Results

Figure 1 shows the catalytic results using LL/HT materials as catalysts. In the heterogenised reaction using LL/HT_{rus}-A1_{0,22} as catalyst the presence of TBAB also improved notably the conversion from 5% to 41% of conversion towards *trans*-1,2-epoxy-1,3-diphenylpropan-1-one. Moreover, the asymmetric Juliá-Colonna epoxidation reaction requires a strong base such as NaOH to activate the hydrogen peroxide generating the hydroperoxide anion. The HT_{rus} contains stronger and accessible -OH interlayer anions, as was exposed in Chapter 2. Therefore, HT_{rus} support could also work as a base of the reaction after immobilisation of L-Leu. Nevertheless, the low conversion (7 %) shows that the basic centers still present in the HT_{rus} are not enough or not accessible at all to deprotonate the hydrogen peroxide.

As it was reported in the preliminary part, pure L-Leu showed a low activity toward the *trans*-1,2-epoxy-1,3-diphenylpropan-1-one (9%) with nil enantioinduction capacity. In the case of HT_{rus} the conversion was also low (6%). Our results contrast together with thus obtained by Fraile *et al.* [21] and Kaneda *et al.* results [22]. They used the Mg₁₀Al₂(OH)₂₄CO₃

2.2. Results and discussion – Catalytic results

material as the catalyst in the α,β -ketone isophorone epoxidation obtaining a 99% conversion. The Kaneda's work exposed two main findings: first, decreases of the Mg/Al molar ratio in HT decrease the catalytic activity. And second, the hydroxyls of the synthesised materials play an important role in the conversion; nevertheless they reported one experiment using Na_2CO_3 as catalyst which allows catalytic activity (53%). This result suggests that the interlayer carbonate anions also contribute significantly to the epoxidation reaction.

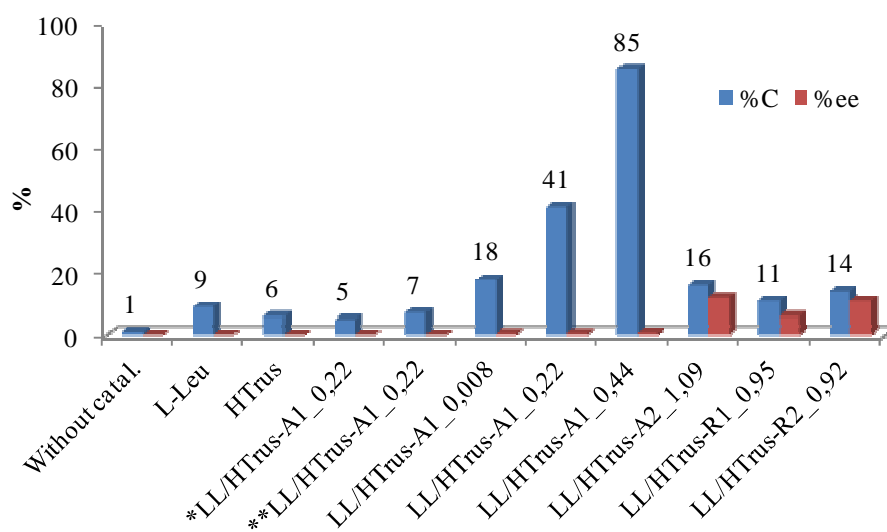


Figure 1 LL/HT-catalyzed epoxidation of chalcone

Reaction Conditions: 0.44 mmol L-Leu contained in LL/HT material, 0.43 ml NaOH 5M, 0.19 ml H_2O_2 (30 wt%), 0.24 mmol **1**, 0.042 mmol TBAB and 3 ml hexane, 90 minutes at r.t. Total diastereoselectivity towards *trans*-epoxychalcone. %C calculated by ^1H NMR. %ee determined by chiral HPLC. *In the absence of TBAB. **In the absence of NaOH.

In our case, using LL/HT materials, increases in the immobilised L-Leu amount on the edges from the HT (Method A1), also increased the conversion from 18% obtained using LL/HT_{rus}-A1_{0,08} up to 85% using LL/HT_{rus}-A1_{0,44}. These results are explained by the formation of the complexes L-Leu:chalcone and/or L-Leu:HOO⁻ in neighbouring positions on the HT_{rus}. This fact facilitates the nucleophilic attack by the hydroperoxide anion on the chalcone double bond to generate the peroxy-enolate [20]. However, due to the location of the L-Leu in this group of materials the chiral induction was nil. On the other hand, LL/HT_{rus}-A1_{1,09} presented enantioselectivity toward the product *trans*-(R,S)-epoxy-1,3-diphenyl-propan-1-one (12%). Taking into account that the immobilisation of the L-Leu occurs in the interlayer space of the HTs, the enantioselectivity is attributed to the synergistic effect between HT_{rus} and the immobilised L-Leu, where L-Leu distributed in a more restricted space between the layers

favour the chiral induction as the PLL. However, the moderate conversion (16%) is attributed to the lower accessibility of the chalcone up to immobilised L-Leu molecules.

One interesting but slight effect was found using LL/HT_{rus}-R1_{0.95} and LL/HT_{rus}-R2_{0.92} as catalysts. In the case of LL/HT_{rus}-R1_{0.95} the conversion decreased to 11% while in LL/HT_{rus}-R2_{0.92} this decreased was to 14%. As it was extensive explained in Chapter 2, A2 method allows materials where the L-Leu immobilisation occurs in both anionic and zwitterionic form; by R1 method the immobilisation mainly occurs through anionic L-Leu, while by R2 method the immobilisation is mostly in its zwitterionic form. These differences could be affected by the catalytic behaviour. In LL/HT_{rus}-A2_{1.09} the high amount of immobilised L-Leu created an environment in the interlayer space, where the chalcone molecules that can access to the immobilised L-Leu can be converted. Moreover, the material also contains zwitterionic L-Leu molecules stabilised by H-bonding, which could be working together with the anionic ones permitting the chiral induction. In the case of LL/HT_{rus}-R1_{0.95} the material not only has lower amount of immobilised L-Leu but also the immobilisation mostly occur through anionic L-Leu. The most separate distribution of L-Leu in the interlayer space impairs both conversion and chiral orientation. Finally, using LL/HT_{rus}-R2_{0.92} the not organised immobilisation of zwitterionic L-Leu in the interlayer space reduces the catalytic activity, increasing slightly the enantioselectivity in comparison with LL/HT_{rus}-R1_{0.95} which has a similar immobilisation degree.

As a summary, this section shows the catalytic behaviour of LL/HT nanohybrid materials using as the model reaction the asymmetric Juliá-Colonna epoxidation reaction of chalcone. The results showed that both L-Leu and HT_{rus} are poor active catalysts in our reaction condition, nevertheless the synthesised nanohybrid exhibited an excellent synergistic effect reflected by the activity towards the epoxy-chalcone product (85%). The catalytic results also showed the importance of the immobilisation location. L-Leu immobilised on the edges of the HT precursor, bringing to an increase in the activity with increasing of the immobilised amount of L-Leu but without any induction. Nanohybrid materials where the L-Leu was immobilised in the interlayer space showed a decrease in the conversion due to the lower accessibility of the chalcone molecules into the interlayer space, nevertheless, this kind of location of the L-Leu restricted the freedom degree permitting the asymmetric induction. Moreover, the presence of

2.2. Results and discussion – Catalytic results

both anionic and zwitterionic immobilised L-Leu favours the conversion and the enantioselectivity.

3. LP/HT nano hybrid materials as catalysts in direct asymmetric aldol reaction

L-Pro is a secondary cyclic, pyrrolidine-based AA which catalyzes C-C bond-forming reactions. In that context, Aldol reaction is arguably one of the most important C-C bond-forming reactions in nature, by imitating the class I aldolase enzyme through an enamine mechanism [23]. The reaction generally produces moderate to good enantioselectivity in an efficient way. In the Chapter 1, section 2.2, Scheme 3, it has been shown the bifunctional effect of the L-Pro acting as the catalyst. While the amine group acts as a Lewis base catalyst that facilitates iminium- and enamine-base transformations, the carboxyl group further contributes to stabilise a 6-membered ring by acting as a general Brønsted co-catalyst (Figure 2) [24].

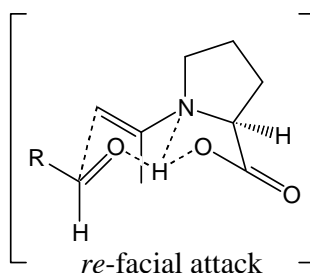


Figure 2 6-membered transition state in direct asymmetric aldol reaction using L-Pro as catalyst.

As explained in Chapter 2, immobilisation of L-Pro in HT precursors occurs through an anionic exchange reaction between the carboxylate group and OH's located in the interlayer and/or on the edges position from on the HTs. In that context, our interest was focused on the study and understanding of the catalytic behaviour of immobilised L-Pro which does not have the carboxylic group accessible to act as the co-catalyst in the direct asymmetric aldol reaction.

3.1 Experimental

3.1.1 Synthesis of LP/HT materials

Synthesis of LP/HT nanohybrid materials was performed by anionic exchange (A), reconstruction (R) and co-precipitation (C) methods as it described Chapter 2, sections 3.1.2.1, 3.1.2.2 and 3.1.2.3. Table 3 lists the nanohybrid materials used in this section.

Table 3 LP/HT nanohybrid materials used as catalysts in asymmetric Juliá-Colonna epoxydation reaction

Entry	Material ^{a,b}	Synthesis method	Main Location in the HT ^c	Molecular formulae ^d
1	L-Pro	-	-	C ₅ H ₉ NO ₂
2	HT _{asym}	-	-	[Mg _{2.53} Al _{1.00} (OH) _{7.07}](CO ₃ ²⁻) _{0.85} (NO ₃ ⁻) _{3.15} ·0.89H ₂ O
3	HT _{rus}	-	-	[Mg _{2.53} Al _{1.00} (OH) _{7.07}](CO ₃ ²⁻) _{1.18} (NO ₃ ⁻) _{0.10} ·1.10H ₂ O
4	LP/HT _{rus} -A1 _{0.14}	A1	Edges	[Mg _{2.54} Al _{1.00} (OH) _{7.08}](Pro) _{0.46} (CO ₃ ²⁻) _{2.27} (NO ₃ ⁻) _{0.10} ·0.70H ₂ O
5	LP/HT _{rus} -A2 _{0.57}	A2	Interlayer space	[Mg _{2.54} Al _{1.00} (OH) _{7.08}](Pro) _{0.57} (CO ₃ ²⁻) _{1.40} (NO ₃ ⁻) _{0.10} ·0.70H ₂ O
6	LP/HT _{rus} -R1 _{0.60}	R1	Interlayer space	[Mg _{2.54} Al _{1.00} (OH) _{7.08}](Pro) _{0.60} (CO ₃ ²⁻) _{2.57} (NO ₃ ⁻) _{0.10} ·0.70H ₂ O
7	LP/HT _r -R2 _{0.70}	R2	Interlayer space	[Mg _{2.54} Al _{1.00} (OH) _{7.08}](Pro) _{0.70} (CO ₃ ²⁻) _{2.34} (NO ₃ ⁻) _{0.10} ·0.70H ₂ O
8	LP/HT-C1	C	Interlayer space	[Mg _{2.63} Al _{1.00} (OH) _{7.08}](Pro) _{0.02} (CO ₃ ²⁻) _{0.85} (NO ₃ ⁻) _{2.99} ·0.74H ₂ O
9	LP/HT _{us} -C1 ^e	C + us	ND ^f	[Mg _{2.63} Al _{1.00} (OH) _{7.08}](Pro) _{0.01} (CO ₃ ²⁻) _{1.21} (NO ₃ ⁻) _{2.60} ·0.74H ₂ O

^aSynthesis Conditions: Anionic exchange 1 (A1): HT and a solution of L-Pro were mixed and stirring for 0.5 hours at r.t. Anionic exchange 2 (A2): HTs and a solution of L-Pro were mixed and stirring for 3 hours at 80°C. Reconstruction 1 (R1): HT_{cc} and a solution of L-Pro were mixed and sonicated for 1 h and stirred for 3 h at 80°C. Reconstruction 2 (R2): HT_{cc} and a solution of L-Pro were mixed and stirred for 3 hours at 80°C. Co-precipitation (C): Mg-Al HT was precipitated in the presence of L-Pro. ^bHT = hydrotalcite. HT_{asym} = As-synthesised HT. HT_{rus} = rehydrated HT under ultrasound treatment. ^cDetermined by XRD. ^dCalculated by EA and ICP analysis in materials synthesised by method A and B. Calculated by AE, TG/DTA and ICP analysis in materials synthesised by method C. Water content was calculated theoretically according to Miyata. Ref [25]. ^eUltrasound treatment (1 h) was used after the material synthesis. ^fND = Not determined.

3.1.2 Direct asymmetric aldol reaction

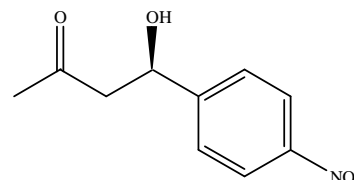
Typical direct asymmetric aldol reaction was performed in a tube of 40 mL under Ar atmosphere. A given amount of LP/HT nanohybrid material containing 15 mg of immobilised L-Pro (0.13 mmol) was added to the tube containing acetone (**3**) (13 mmol, 0.6 mL) and the indicated solvent. The mixture was stirred during 10 min and 4-nitrobenzaldehyde (**4**) (0.30 mmol, 45.4 mg) was added. The resulting mixture was stirred at room temperature for the indicated time and then worked up using ethylacetate. The reaction product was separated by centrifugation, and the catalyst (solid phase) was washed with ethylacetate. The aldol product was dried with anhydrous MgSO₄ and concentrated under reduced pressure. The crude aldol

3.1 Experimental

product was purified by silica-gel column chromatography with a 3:1 hexanes:EtOAc mixture as eluent to give the product. The obtained aldol product was determined by ^1H NMR:

(4R)-(4-Nitrophenyl)-4-hydroxy-2-butanone (5)

^1H NMR (400 MHz, CDCl_3): δ = 2.21 (s, 3H), 2.84 (m, 2H), 3.69 (d, 1H), 5.26 (m, 1H), 7.52 (d, 2H), 8.20 (d, 2H) ppm. The ee determined by chiral HPLC (ChiralPak IA column, EtOH/i-

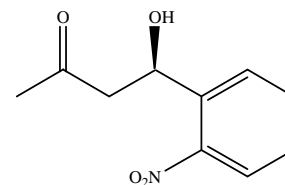


PrOH/Hexane = 33/17/50), UV 254 nm, flow rate 0.8 mL/min. R-isomer, t_R = 8.5 min and S-isomer, t_S = 8.1 min.

Other aldol products were determined as follow:

(4R)-(2-Nitrophenyl)-4-hydroxy-2-butanone (6)

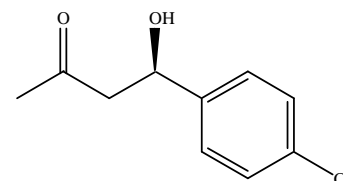
^1H NMR (400 MHz, CDCl_3): δ = 2.23 (s, 3H), 2.73-3.1 (m, 2H), 3.79 (brs, 1H), 5.65-5.67 (m, 1H), 7.41 (t, 2H), 7.66 (t, 1H), 7.87-



7.96 (dd, 2H) ppm. The ee determined by HPLC (ChiralPak IA, i-PrOH/Hexane = 30/70), UV 254 nm, flow rate 1.0 mL/min. R-isomer, t_S = 13.1 min and S-isomer, t_S = 9.5 min.

(4R)-(4-chlorophenyl)-4-hydroxy-2-butanone (7)

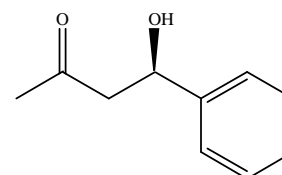
^1H NMR (400 MHz, CDCl_3): δ = 2.18 (s, 3H), 2.82 (m, 2H), 3.46 (brs, 1H), 5.11 (m, 1H), 7.29 (m, 4H) ppm. The ee determined by HPLC (ChiralPak IA, i-PrOH/Hexane = 10/90),



UV 254 nm, flow rate 1.0 mL/min. R-isomer, t_R = 16.9 min and S-isomer, t_S = 20.9 min.

(4R)-(4-phenyl)-4-hydroxy-2-butanone (8)

^1H NMR (400 MHz, CDCl_3): δ = 2.18 (s, 3H), 2.82 (m, 2H), 3.37 (brs, 1H), 5.15 (m, 1H), 7.28-7.35 (m, 5H) ppm. The ee determined by HPLC (ChiralPak IA, i-PrOH/Hexane = 15/85),

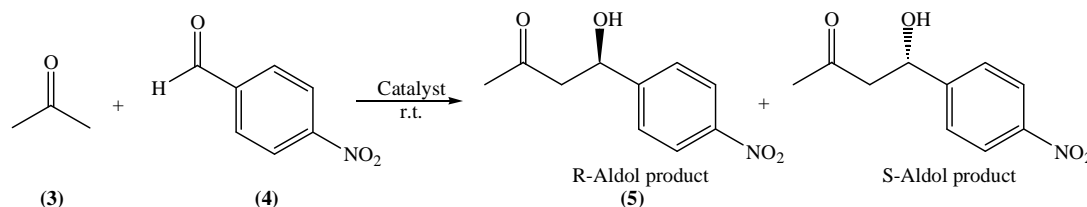


UV 254 nm, flow rate 1.0 mL/min. R-isomer, t_R = 10.7 min and S-isomer, t_S = 11.4 min.

3.2 Results and discussion

3.2.1 Preliminary studies

The catalytic properties of LP/HT nanohybrid materials were evaluated in the direct asymmetric aldol reaction between **3** and **4** (Scheme 2).



Scheme 1 Direct aldol reaction between 4-nitrobenzaldehyde and acetone.

In order to understand the role of the immobilisation of L-Pro in HTs, the preliminary study was focused in to find the reaction conditions where L-Pro had good activity and selectivity, but HT_{rus} was inactive. These results are summarised in Table 5.

Table 4 Asymmetric direct aldol reaction of 4-nitrobenzaldehyde and acetone. Influence of the solvent

Entry ^a	Catalyst	Solvent ^b	%C ^c	%S ^d	%ee ^c
1	L-Pro	-	97.4	97.7	63.0
2	L-Pro	Water	99.0	99.6	4.0
3	L-Pro	DMF	97.7	98.1	70.8
4	L-Pro	THF	99.2	89.2	63.6
5	HT _{rus}	-	98.5	96.1	-2.6
6	HT _{rus}	THF	3.5	ND	ND

^aReaction condition: 13 mmol (**3**), 0.30 mmol (**4**), Catalyst (15 mg L-Pro or 50 mg HT_{rus}). T: 25°C. Time: 24 h. ^b2.5 mL of solvent was used. ^cDetermined by ¹H NMR.

^dSelectivity towards to 4-Nitrophenyl-4-hydroxy-2-butanone. ^eDetermined by chiral HPLC, enantiomer excess of (R)-Enantiomer (**5**). ND = Not Determined

In agreement with several authors, we found that the use of organic solvents achieves high activity and enantioselectivity [26-27]. Using large amount of water declines the enantioselectivity to 4.0% because water molecules prevent the efficient stabilisation of the 6-membered transition state necessary to the formation of the chiral enamine [28]. Under neat conditions both conversion and enantioselectivity were high (97.4 and 63.0% respectively). In all cases the selectivity towards the aldol product was high and the α,β -unsaturated ketone was determined as the unique side-product.

In contrast, using HT_{rus} as catalysts in the presence of THF the activity was practically nil, while under neat conditions the conversion increased up to 98.5%. The high catalytic

3.2 Results and discussion – Preliminary studies

activity under water conditions was reported by Kaneda *et al.*, who explained this effect because, the OH⁻ groups in the rehydrated HT act efficiently as Brønsted base sites initialising the aldol reaction [29]. Moreover, the role of the solvent is crucial in this reaction. As explained Tichit *et al.*, the acidity of the solvent reduces the activity of the HT by poisoned of the strong basic centres [30]. In front of these results, our aim was to evaluate the catalytic behaviour of the immobilised L-Pro and the synergistic effect of the synthesised nanohybrid materials; for this reason, we selected THF as the solvent in order to eliminate the activity of the HT_{rus} maintaining the high enantioselectivity of the L-Pro.

2.2.2 Catalytic results

Table 5 summarises the results obtained using LP/HT nanohybrid materials as catalysts. From a general point of view immobilized L-Pro in HTs conserved its high activity and selectivity. As explained below, direct asymmetric aldol reaction is catalysed by a nucleophile group and co-catalysed through a carboxylate group. This demonstrated that using LP/HT materials, the reaction is initialised through the amine group of the immobilised L-Pro and co-catalysed by the HT layers. In a first moment, the L-Pro starts the reaction by the nucleophilic attack of the amino group on the carbonyl carbon of (3); the dehydration of (3) generates the enamine intermediate while the aldehyde carbonyl group of (4) is activated by one OH⁻ group on the HT layers. After these interactions, the subsequent deprotonation, C-C bond formation and hydrolysis take place to obtain the aldol product.

Using LP/HT_{rus}-A1_{0.14} as the catalyst (Table 5, entries 6,7) the activity is as high as using free L-Pro even at 12 hours of reaction. In this case, the immobilised L-Pro is located on the edges of the HT layers facilitating the accessibility of the substrate to the nucleophilic amino group. However, in LP/HT_{rus}-A2_{0.57} materials, the substrate needs to penetrate in the HT structure increasing the time necessary for that the reaction occurs (Table 5, entries 9).

Interestingly, differences in the nature of the immobilisation afforded variation at 12 hours of reaction. LP/HT_{rus}-R1_{0.60} material which contain mainly anionic L-Pro presented conversion of 21.8% in comparison to LP/HT_r-R2_{0.70} where the immobilisation mainly occurs through zwitterionic L-Pro, which presented conversion of 9.5% at 12 hours of

reaction (Table 5, entries 11, 13, respectively). Decreasing of the conversion shows the important role of the electron lone pair of the amino group in reaction initiation. In the case of LP/HT_r-R2_{0.70} material, the zwitterionic L-Pro does not have any lone pair available to the nucleophilic attack decreasing the conversion at 12 hours of reaction. This observation was confirmed using LP/HT-C1 material, which has low conversion at 24 hours (37.3%) attributed to three factors: low amount of immobilised L-Pro, presence of zwitterionic L-Pro and difficult accessibility up to immobilised L-Pro molecules; nevertheless after ultrasound treatment, the conversion increase up to 81.8% indicating that both, elimination of zwitterionic L-Pro and defoliation in the material favoured the accessibility to the active centers from the material which were located on the edges of the HT structure after ultrasound treatment (Table 5, entry 15).

Table 5 LP/HT nanohybrid materials-catalysed Asymmetric direct aldol reaction of 4-nitrobenzaldehyde and acetone.

Entry ^a	Catalyst	Reaction time (h)	%C ^b	%S ^{b,c}	%ee ^d
1	-	24	-	-	-
2	L-Pro	24	99.2	89.2	66.5
3	L-Pro	12	84.1	91.9	66.4
4	L-Pro	6	30.3	87.0	66.5
5	HT _{rus} ^c	24	3.5	ND	ND
6	LP/HT _{rus} -A1 _{0.14}	24	95.6	83.3	5.7
7	LP/HT _{rus} -A1 _{0.14}	12	85.8	94.0	4.9
8	LP/HT _{rus} -A2 _{0.57}	24	99.9	92.4	-12.8
9	LP/HT _{rus} -A2 _{0.57}	12	17.5	95.8	ND
10	LP/HT _{rus} -R1 _{0.60}	24	84.2	94.9	-15.0
11	LP/HT _{rus} -R1 _{0.60}	12	21.8	92.5	ND
12	LP/HT _r -R2 _{0.70}	24	78.5	94.5	-11.2
13	LP/HT _r -R2 _{0.70}	12	9.5	94.7	ND
14	LP/HT-C1	24	37.3	89.7	-13.9
15	LP/HT _{us} -C1	24	81.8	93.0	6.9

^aReaction condition: 13 mmol (3), 0.30 mmol (4), Catalyst (containing 15 mg L-Pro) in THF during the indicated time at r.t.. ^bDetermined by ¹H NMR. ^cSelectivity towards 4-Nitrophenyl-4-hydroxy-2-butanone. ^dDetermined by chiral HPLC. Enantiomer excess towards (R)-Enantiomer (5). ^e50 mg HT_{rus} was used.

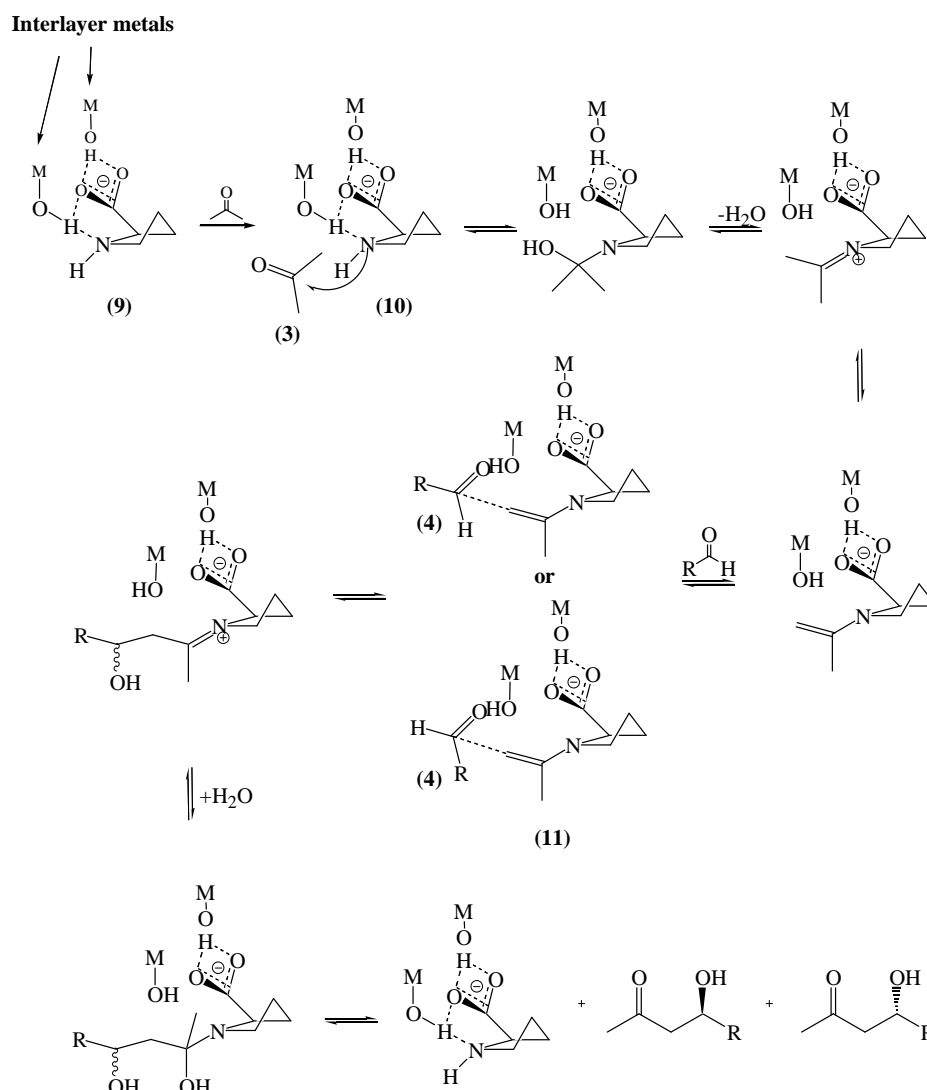
From the point of view of the asymmetric induction, the low enantioselectivity using LP/HT_{rus}-A1_{0.14} materials is explained by the stabilisation of the enamine intermediate occurs by OH⁻ groups located on the edges from the HT structure (9) preventing the stabilisation of

3.2 LP/HT as catalysts in direct asymmetric aldol reaction

3.2 Results and discussion – Catalytic results

the 6-membered transition state, but also because the orientation of the aromatic aldehyde depends of the repulsion with the hydrophilic HT layers [30].

When the L-Pro is immobilised in the interlayer space from the HTs, the interaction between substrate and OH⁻ groups located in the interlayer space stabilises the interaction permitting the increase of the enantioselectivity and even the inversion of this parameter (11) [31] as was also observed by Li *et al.* using L-Pro immobilised on γ -Al₂O₃ [32]. In comparison with List [26], Pitchumany [10] and Li's [32] works, we propose a mechanism for the aldol reaction catalysed by LP/HT materials in Scheme 2 where the amino group of the L-Pro activates the acetone while the carbonyl group of the aldehyde is stabilised by the hydroxyl groups on the HT layers (10).



Scheme 2 Proposed mechanism for the LP/HT_{rus}-catalysed Direct Asymmetric Aldol Reaction between acetone and aromatic aldehydes.

In order to evaluate the stability of the immobilised L-Pro, the recovery of the material was performed during four consecutive runs and the results are summarised in Table 6. The results showed the low stability of the immobilised L-Pro during four consecutive runs. This behaviour was expected according to the characterisation data which indicated that interaction between L-Pro and HT layers requires strong basic centres. In this case, each run was performed for 24 hours, so the time of synthesis favours the swelling of the HT and also the deintercalation of the L-Pro, thus reducing the activity of the material after four consecutive runs.

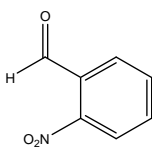
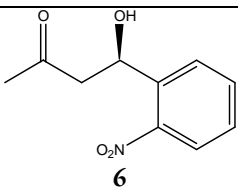
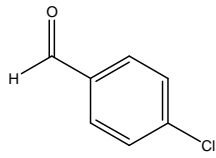
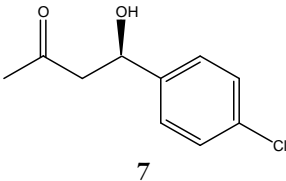
Table 6 Stability of the LP/HT_{rus}-A2_{0.57} nanohybrid material.

Run	%C ^b	%S ^{b,c}	%ee ^d
1	99.9	94.4	-12.8
2	83.2	98.4	-10.9
3	51.0	84.6	-15.8
4	42.9	86.7	-13.5

^aReaction condition: 13 mmol (3), 0.30 mmol (4), LP/HT_{rus}-A2_{0.57} as catalysts, 2.5 mL THF, 24 h at r.t. ^bDetermined by ¹H NMR. ^cSelectivity towards 4-Nitrophenyl-4-hydroxy-2-butanone. ^dDetermined by chiral HPLC. Enantiomer excess towards (R)-Enantiomer (5).

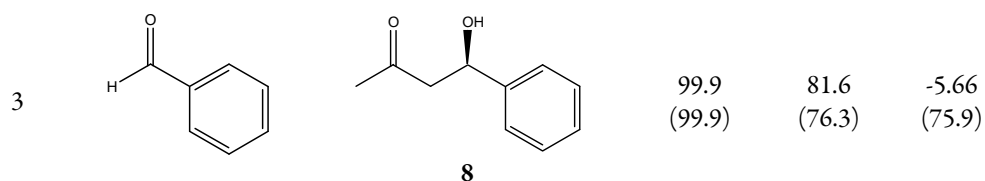
In order to evaluate the effect of the aromatic substitution in the enantioselectivity, LP/HT_{rus}-A2_{0.57} nanohybrid material was also evaluated as the catalyst using three different aldehydes (6), (7), (8) and (3) under the same reaction conditions and the results are showed in Table 7.

Table 7 Asymmetric direct aldol reaction of acetone with aldehydes catalysed by free L-Pro and L-Pro immobilised on HTs.

Entry ^{a,b}	Aldehyde	Product	%C ^{b,c}	%S ^{c,d}	%ee ^e
1			99.9 (67.9)	99.9 (99.9)	-11.3 (82.2)
2			99.9 (50.1)	85.8 (99.9)	-18.0 (81.0)

3.2 LP/HT as catalysts in direct asymmetric aldol reaction

3.2 Results and discussion – Catalytic results



^aReaction condition: 13 mmol **3**, 0.30 mmol of (**6**), (**7**) or (**8**), Catalyst (containing 15 mg L-Pro) and 2.5 mL THF. T: 25°C. Time: 24 h. ^bValues in brackets correspond to results in homogenous phase. ^cDetermined by ¹H NMR. ^dSelectivity towards to aldol products. ^eDetermined by chiral HPLC, enantiomer excess of (R)-Enantiomers.

Results in Table 7 show that the L-Pro immobilised in HT_{rus} permitted to obtain the aldol products with higher conversions than using pure L-Pro, as also shown Table 5. From a general point of view, increase of the conversion is explained because in LP/HT_{rus}-A2_{0.57} material, the swelling property of the HT layers favoured the accessibility of the substrates up to the immobilised L-Pro molecules. Moreover, increasing and inversion of the enantioselectivity using (**6**) and (**7**), respect to (**8**), could be explained because the electrophilic nature of the substituted group in the aromatic aldehyde favours its interaction with the positively charged HT layers.

As a summary, this section helped us d understands the nature of the immobilisation between L-Pro and HT through the catalytic activity of the synthesised nano hybrid materials. Under our reaction conditions, the synthesised nano hybrid materials showed an excellent synergistic effect over both activity and enantioselectivity of the aldol product. In a similar way than as the LL/HT materials, location of L-Pro plays an important role in the catalytic results. Immobilisation of the L-Pro on the edges of the HTs (LP/HT_{rus}-A1_{0.14} material) favours the accessibility permitting to reduce the reaction time in a similar way as with pure L-Pro. On the other hand, when the L-Pro is immobilised in the interlayer space (LP/HT_{rus}-A2_{0.57}, LP/HT_{rus}-R1_{0.60} and LP/HT_r-R2_{0.70} materials) the required reaction time increased due to the necessity of the reagents to penetrate in the HT structure. In this aspect, the parallel immobilisation of the anionic L-Pro in the HT layers increases slightly the activity due to the proximity with the M-OH which act as co-catalysts. This kind of immobilisation increased the conversion causing also the inversion of the enantioselectivity. When zwitterionic L-Pro was presented in the material, the activity decreased suggesting that zwitterionic L-Pro cannot act as catalyst because it does not have the electron lone pair on the amino group to do it. The catalytic activity of nano hybrid materials synthesised by co-

precipitation method (LP/HT-C1) was also evaluated. The results confirmed the previous discussion, L-Pro immobilised by co-precipitation method does not permit to obtain a stable nanohybrid material, because the compensation of the charges is mostly due to strongest NO_3^- anions present in the medium. On the other hand, ultrasound treatment after co-precipitation permitted the elimination of zwitterionic L-Pro present in the nanohybrid material and the defoliation of the layers exposing the immobilised L-Pro on the edges of the HT structure.

The stability of the LP/HT_{rus}-A2_{0.57} material was evaluated in four consecutive runs showed that slight changes in the basicity of the HT_{rus} de-immobilised the L-Pro losing its activity during all the process. On the other hand, LP/HT nanohybrid material also exhibits synergistic effect towards other kind of aromatic aldehydes, where the catalytic results showed higher activity and comparable selectivity in contrast with pure L-Pro.

4. Conclusions

The catalytic results presented in this section provide an example of the potential of the synergistic effect between AAs and HTs. Where the nature of the host-guest interaction is the key to: i) Improve the catalytic properties of the L-Pro biohybrid nanostructured solids. Nevertheless, this effect is unique to each nanohybrid material. LL/HT materials showed that the presence of anionic and zwitterionic L-Leu in the interlayer space of the HTs creates a chemical environment comparable to the α -helical conformation of PLL favouring the asymmetric induction. On the other hand, the zwitterionic form of L-Pro in the L-Pro biohybrid materials can not provide the electron lone pair necessary for activation of the acetone. As a consequence and due to the mechanistic requirements the activity in the direct aldol reaction of acetone decreases significantly. ii) Ensure the success of the recovery and reuse of the catalyst. The zwitterionic form of the AAs has demonstrated to interact more weakly with the HT type supports than the anionic form of the AAs. As a result, the AAs in the zwitterionic form are lost under ultrasonic treatment of the biohybrid material or during the different consecutive runs in the catalytic reaction.

As a general trend, the immobilisation of AAs into lamellar anionic clays such as HTs favours the conversion of the reactants in different types of catalytic reactions and facilitates the separation and washes after reaction by simple centrifugation or filtration.

The control over the immobilization process has also an important role in the obtention of the desired properties of the bionanohybrid material. For example, the immobilisation in the edges of the HT layers facilitate the interaction with the reagents increasing the conversion, while although immobilisation in the interlayer space from the HT makes the accesibility of the reagents to the catalyst more difficult, the enantiomeric induction was slightly increased.

- “*Novel nanohybrid materials based on L-Leucine on hydrotalcite clays: Asymmetric epoxidation reaction of chalcone*” Ronald-Alexander Miranda, Jordi Llorca, Elisabetta Finocchio, Gianguido Ramis, Francisco Medina, Jesús E. Sueiras, Anna M. Segarra. *Catal. Today*. **2011**, 172, 48.
- “*Nanohybrid Materials Based on L-Proline and Hydrotalcites as Catalysts for Direct Asymmetric Aldol Reaction*” Ronald-Alexander Miranda, Elisabetta Finocchio, Francisco Medina, Gianguido Ramis, Jesús E. Sueiras and Anna M. Segarra

References

- [1] U. Eder, G. Sauer and R. Wierchert. *Angew. Chem. Int. Ed. Engl.* **1971**, 10, 496
- [2] Z.G. Hajos and D.R. Parrish. *J. Org. Chem.* **1974**, 39, 1615
- [3] J.-I. Oku and S. Inoue. *J. Chem. Soc. Chem. Commun.* **1981**, 229
- [4] S. Juliá, J. Guixer, J. Masana, J. Rocas, S. Colonna, R. Annuziata and H. Molinari. *J. Chem. Soc. Perkin Trans. 1.* **1982**, 1317
- [5] E.R. Jarvo and S.J. Miller. *Tetrahedron.* **2002**, 58, 2481
- [6] S. Colonna, D. Perdicchia and E. Di Mauro. *Tetrahedron: Asymmetric.* **2009**, 20, 1709
- [7] L.-W. Xu and Y. Lu. *Org. Biomol. Chem.* **2008**, 6, 2047
- [8] G. Guillena, C. Nájera and D.J. Ramón. *Tetrahedron. Asym.* **2007**, 18, 2249
- [9] B.M. Choudary, B. Kavita, N. Sreenivasa Chowdari, B. Sreedhar and M. Lakshmi Kantam. *Catal. Lett.* **2001**, 78, 1
- [10] S. Vijaikumar, A. Dhakshinamoorthy and K. Pitchumani. *Appl. Catal. A.* **2008**, 340, 25
- [11] A. Dhakshinamoorthy, A. Sharmila and K. Pitchumani. *Chem. Eur. J.* **2010**, 16, 1128

- [12] B.M. Adger, J.V. Barkley, S. Bergeron, M.W. Cappi, B.E. Flowerdew, M.P. Jackson, R. McCague, T.C. Nugent and S.M. Roberts. *J. Chem. Soc. Perkin Trans. 1*. **1997**, 3501
- [13] M.W. Cappi, W.-P. Chen, R.W. Flood, Y.-W. Liao, S.M. Roberts, J. Skidmore, J.A. Smith and N.M. Williamson. *Chem. Commun.* **1998**, 10, 1159
- [14] P. Verdié, G. Subra, P. Chevallet, M. Amblard and J. Martinez. *Int. J. Peptides and Therapeutics*. **2007**, 13, 337
- [15] L. Carde, D.H. Davies and S.M. Roberts. *J. Chem. Soc. Perkin Trans. 1*. **2000**, 2455
- [16] A. Berkessel, N. Gasch, K. Glaubitz and Christoph Koch. *Org. Lett.* **2001**, 3, 3839
- [17] G. Carrea, S. Colonna, D.R. Kelly, A. Lazcano, G. Ottolina and S. M. Roberts. *Trends in Biotech.* **2005**, 23, 507
- [18] T. Geller, A. Garlach, C.M. Krüger and H.-C. Militzer. *J. Mol. Catal. A*. **2006**, 251, 71
- [19] D. Kelly, A. Meek and S.M. Roberts. *Chem. Commun.* **2004**, 2021
- [20] D. Kelly and S.M. Roberts. *Chem. Commun.* **2004**, 2018
- [21] J.M. Fraile, J.I. García, J.A. Mayoral, S. Sebti and R. Tahir, *Green Chemistry*, **2001**, 3, 271
- [22] K. Yamaguchi, K. Mori, T. Mizugaki, K. Ebitani and K. Kaneda. **2000**, 65, 6897
- [23] T.D. Machajewski and C.-H. Wong. *Angew. Chem. Int. Ed.* **2000**, 39, 1352
- [24] K. Sakthivel, W. Notz, T. Bui and C.F. Barbas III. *J. Am. Chem. Soc.* **2001**, 123, 5260
- [25] S. Miyata. *Clay and Clay miner.* **1975**, 23, 369
- [26] B. List, R.A. Lerner and C.F. Barbas III. *J. Am. Chem. Soc.* **2000**, 122, 2395
- [27] X. Zhu, F. Tanaka, Y. Hu, A. Heine, R. Fuller, G. Zhong, A.J. Olson, R.A. Lerner, C.F. Barbas III and I.A. Wilson. *J. Mol. Bio.* **2004**, 343, 1269
- [28] N. Mase, Y. Nakai, N. Ohara, H. Yoda, K. Takabe, F. Tanaka and C.F. Barbas III. *J. Am. Chem. Soc.* **2006**, 128, 734
- [29] W. Qiu, L. He, Q. Chen, W. Luo, Z. Yu, F. Yang and J. Tang. *Tetrahedron lett.* **2009**, 50, 5225
- [30] A. Guida, M.H. Lhouty, D. Tichit, F. Figueras and P. Geneste. *Appl. Catal. A*. **1997**, 164, 251
- [31] A. Zamboulis, N.J. Rahier, M. Gehringer, X. Cattoën, G. Niel, C. Bied, J.J.E. Moreau and M.W.C. Man. *Tetrahedron:Asym.* **2009**, 20, 2880
- [32] L. Zhong, J. Xiao and C. Li. *J. Catal.* **2006**, 243, 442

SYNTHESIS AND CHARACTERISATION OF POLY-L-LEUCINE INITIALISED AND IMMOBILISED BY REHYDRATED HYDROTALCITE

Knowledge of the physical properties and characteristics of the different PLLs, makes it possible to understand the activity and selectivity of the bioorganocatalytic system and also the selection and design of the biohybrid catalyst. For this reason, it is necessary to make an effort to find the conditions of synthesis that permit to improve the catalytic properties of the PLL and also to facilitate a controlled immobilisation in the support. Unfortunately, this is not an easy task and it is sometimes difficult to acquire data, partly because of the limitations in the usual characterisation techniques. This chapter attempts to rationalise-connections between molecular structure and physical properties of the PLL and the nature of the interaction between PLLs and HT_{rus}. To accomplish these goals two points were further investigated: first synthesis of PLLs by ROP reaction and second immobilisation of the synthesised polymers in the rehydrated hydrotalcite.

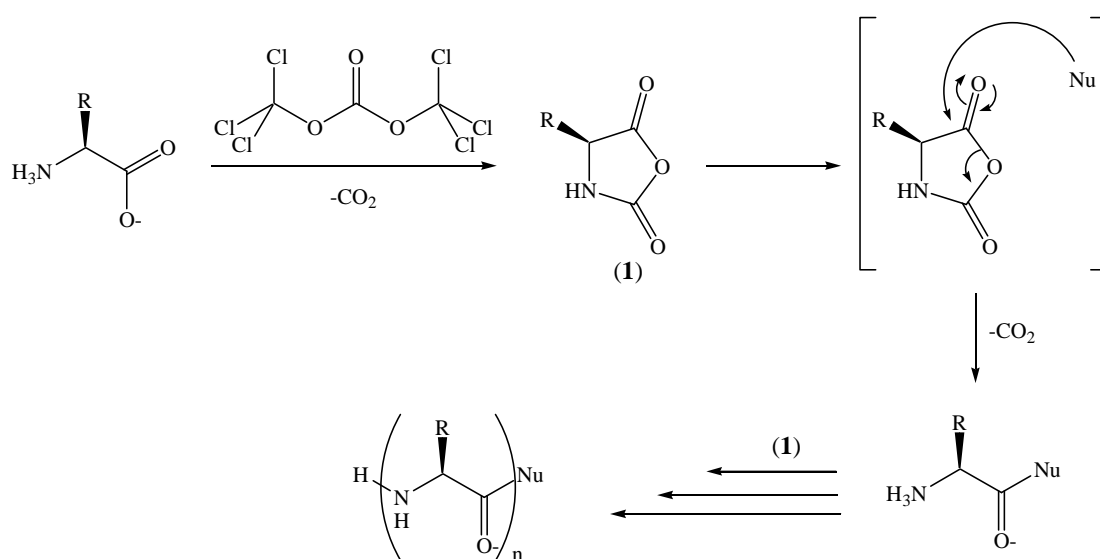
-
- 1. Initial Considerations**
 - 2. Synthesis of PLL materials using triethylamine as initiator**
 - 2.1 Experimental
 - 2.2 Results and discussion
 - 3. Immobilisation of synthesised PLL in HT_{rus}**
 - 1.1 Experimental
 - 1.2 Results and discussion
 - 2. Synthesis of PLL using green initiators: water and HT_{rus}**
 - 2.1 Experimental
 - 2.2 Results and discussion
 - 5. Thermal evolution of the synthesised materials**
 - 6. Conclusions**
 - References**
-

1. Initial considerations

Nanohybrid materials based on PAAs immobilised onto inorganic materials are interesting for their potential applications in protein engineering, biomedicine and catalysis [1,2]. Particularly, PAAs are excellent organocatalysts in epoxidation reaction of α,β -unsaturated ketones due to their excellent activity, selectivity and enantioselectivity [3]. Nevertheless, use of pure PAA as the catalyst presents two important limitations: the lengthy reaction time and the difficulty of recovering the gel- or paste-like catalyst formed after reaction [4]. In this context synthesis of novel nanohybrid materials based on designed PAAs presents an important contribution to the fine chemical/pharmaceutical industries.

It has been mentioned above that the three NHs implicated in the asymmetric Juliá-Colonna epoxidation reaction are located near to the N-terminus of PLLs. In addition, although three NHs do not need to include the N-terminus, higher activities and selectivities were observed when the PLLs used as catalyst had a NH₂ as an N-terminus. In addition, the C-terminal group does not participate in the catalytic process [5-8]. These features have to be taken into account for the correct design and synthesis of the immobilised PAAs.

PAAs are mostly synthesised by ring-opening polymerisation (ROP) [9-10] of α -amino acid N-carboxyanhydrides (NCA) (**1**) initialised by nucleophilic species or bases [11-13] (Scheme 1).



Scheme 1 Synthesis of PAA by ring-opening polymerisation of NCA

Trialkyl amines used as initiators are able to activate the NCA and to initiate the synthesis of PAAs with high molecular weight (M_w) [14] without incorporation of the initiator in the polymer structure [13]. However, due to their basic nature triethylamines, such as triethylamine (pK_a of 10.9), cause the cyclisation of the endgroups of the PAAs [13,15]. On the other hand, rehydrated HTs are strong basic material ($pK_a \sim 11$) [16-17]. They are potential candidates to be used as initiators in ROP to carry out the synthesis of nano hybrid materials in just one step. In addition, nano hybrid materials based on PAAs and rehydrated HTs could be synthesised by immobilisation of the appropriate synthetic PAA exploiting the intercalation properties from the HTs.

In this context and in the view to future industrial applications, the present Chapter describes the synthesis by ROP and in-depth characterisation of suitable PLLs. Time of synthesis, kind of basic initiator and M/I ratio were modified to achieve the desired physical properties in the synthesised PLLs. The obtained PLLs were immobilised by anionic-exchange method and compared with the immobilisation by simple ROP of NCA using HT_{rus} as initiator. We focused all our discussion on the nature of the synthesised PLLs and also on the nature of the organic/inorganic interaction with the HT_{rus} based on the characterisation results using EA, ICP, XRD, Raman, MALDI-TOF, ESI-TOF, FTIR at increasing temperature and TG/DT analyses.

2. Synthesis of Poly-L-Leucine materials using triethylamine

2.1 Experimental

2.1.1 Synthesis of α -Leucine-*N*-carboxy anhydride (NCA)

NCA was synthesised according to the method published by Ahn *et al.* as follows [18]: L-Leu (931 mg, 7.1 mmol) was suspended in anhydrous THF (10.5 ml, 10 wt.%) at increasing temperature to 55°C. Separately, triphosgene (2.1 g, 7.1 mmol) was dissolved in anhydrous THF and added dropwise to the reaction mixture. The reactor was closed with a freshly prepared $CaCl_2$ drying tube and vigorously stirred for 2 h. The obtained liquid was condensed by rotoevaporation and poured into a 10-fold excess amount of anhydrous *n*-

heptane to precipitate NCA. NCA was separated by filtration, dried under vacuum at r.t. during 3h and characterized by ¹H NMR (400 MHz, CDCl₃): δ = 0.94-1.05 (m, 6H), 1.66-1.78 (m, 1H), 1.80-1.86 (m, 2H), 4.33-4.38 (m, 1H), 7.05 (s, 1H) ppm.

2.1.2 Synthesis of PLLs

PLL materials were synthesised by ROP immediately after NCA synthesis as follows: NCA (0.4 g, 2,55 mmol) was dissolved in dry 1,4-dioxane (7 mL) under Ar atmosphere at indicated temperature. Triethylamine was added according with the M/I ratio after 15 min of magnetic stirring. The reactor was closed with a freshly prepared CaCl₂ drying tube and stirred during 3 or 4 days. MQ-water was added as work-up solvent and the mixture was stirred for 2 h more. Finally, the obtained solid was filtered and dried at 60°C under vacuum.

2.2 Results and discussion

In this section the synthesis and characterisation of PLL using triethylamine as the initiator of ROP are presented. A complete list of synthesised PLL materials using triethylamine as initiator, including degree of polymerisation (DP), molecular weight (M_w) and poly-dispersion (PD) data are summarised in Table 1.

Table 1 Synthesis of PLLs using triethylamine as initiator.

Entry	material	Synthesis time (days)	Temperature (°C)	M/I ratio ^a	DP ^{b,c}	M _w ^c	PD ^c
1	PLL1 ₆₀	4	60	10	5-42	2456	1.43
2	PLL2 ₆₀	4	60	5	5-38	2303	1.49
3	PLL1	4	25	10	5-42	2212	1.57
4	PLL2	4	25	5	2-39	2405	1.51
5	PLL3	4	25	2.5	2-33	2249	1.46
6	PLL1 _{3d}	3	25	10	4-42	2347	1.45
7	PLL2 _{3d}	3	25	5	3-40	2469	1.48
8	PLL3 _{3d}	3	25	2.5	3-40	2125	1.40

^aM/I= mmol NCA/mmol triethylamine. ^bDetermined by ESI-TOF MS analyses. ^cDetermined by MALDI-TOF analyses.

PLL obtained after 3 days of synthesis presented similar characteristics as PLL synthesised during 4 days but the obtained amount were significantly lower, indicating that the reaction were incomplete. For this reason all our discussion was centered on PLLs synthesised in 4 days. However, if the reader is interested in the characterisation of the

2.2 Results and discussion – MALDI TOF results

PLL1_{3d}, PLL2_{3d} and PLL3_{3d}, Annex 3 (Figure 8) attaches the corresponding MALDI-TOF spectra.

2.2.1 MALDI-TOF results

MALDI-TOF MS is a powerful technique to identify PLL structure, nevertheless, the intensity of the peaks in the MALDI-TOF spectrum depends on the efficiency of the ionisation, type of apparatus, abundance of the ions, solubility of the sample, etc. For this reason, determination of polydispersion (PD) and molecular weight (Mw) with exactitude is a difficult task. In our case, synthesised polymers are similar among themselves, all of them are homopolymers synthesised by ROP under closely similar conditions, and so although physical properties of the obtained PLL are difficult to define with exactitude, some qualitative comparison could be done among them. PLL1, PLL2 and PLL3 were synthesised with variations in the M/I ratio as presented in Table 1. MALDI-TOF spectrum of PLL1 exhibits a regular series of peaks ranging from m/z values of 500 to around 5000 (Figure 1). The spectrum shows a bimodal frequency distribution which is attributed to the low solubility of the PLL chains in dioxane. As Kricheldorf explained, low solubility of the growing PLL prevents the formation of β -sheets PLL structures [19]. The inset spectrum shows that the entire spectrum is a repetition of a series of three peaks where the difference between each series is 113 Da due to a Leu residue.

The first peak at 735 Da, in the inset spectrum, corresponds to a polymer of six monomers adducted with potassium, while the second peak at 773 Da corresponds to a dipotassium adduct after elimination of a proton (Table 2). High intensity of these two adducted peaks along the entire spectrum suggests that the obtained polymer is conformed mainly by linear PLL containing both carboxylic and amino endgroups also called *living groups*. A small peak at 779 Da is due to the presence of polymer chains containing an L-Leu-NCA (NCA) endgroup in low quantity [13,20].

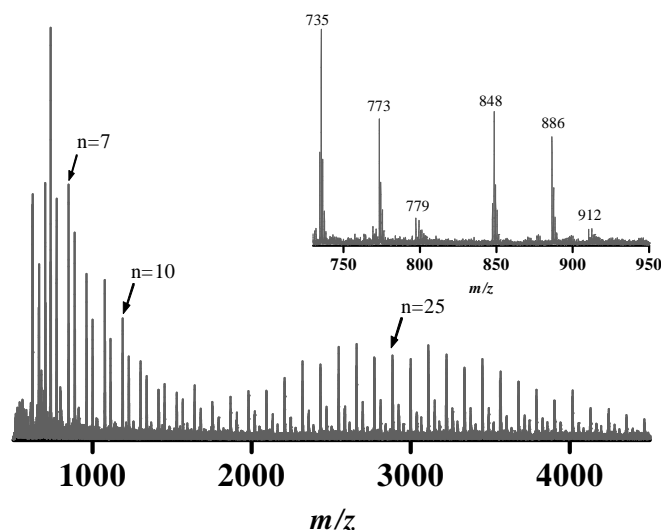


Figure 1 MALDI TOF spectrum of PLL1. Inset: MALDI-TOF spectra in the m/z range: 730-950.

Table 2 Mass of doped PLLs using ESI-TOF and MALDI-TOF MS

Entry	DP	MALDI-TOF MS (Da)			
		ESI-TOF MS (Da) ^a PLL + H/OH + H ⁺	PLL + H/OH + K ⁺ ^a	PLL + H/OH – H ⁺ + 2K	PLL + H/NCA – H ⁺ + 2K ⁺ ^b
1	2	244	OR ^c	OR	OR
2	3	357	OR	OR	OR
3	4	470	OR	547	OR
4	5	583	622	661	ND
5	6	697	735 ^d	773	779
6	7	810	848	886	912
7	8	923	961	999	1025
8	9	1036	1074	1112	1138
	...				
9	18	OR	2093	2130	2270
10	19	OR	2206	2243	2383

^aH/OH corresponds to PLL containing living groups. ^bNCA corresponds to NC₇H₁₀O₃. ^cOR = Out of detection range. ^dExample of calculation: 735 = 6*113 + (1 + 17) + 39

Although kinetic studies were not included in this thesis, some conclusions around of NCA polymerisation could be drawn in comparison with Kricheldorf *et al.* findings [9,21]. Synthesis of PLL chains with molecular weight up to 4770 Da (42 monomers) and PD of 1.57 suggest that the initiation step is not faster than the growing step. This means that not quick initiation step favours the growing of the polymer chain preventing both the formation of cyclic polymers and also the precipitation of PLL in a β -sheet structure [15]. Nevertheless, detection of polymer chains with low molecular weight suggests that under our reaction conditions, initiation and growing steps spend similar time reducing the length of the PLL

2.2 Results and discussion – MALDI TOF results

chains without formation of high amount of PLL containing NCA endgroups (Table 1, entry 3).

Figure 2 shows the MALDI-TOF spectra of PLL2 and PLL3. The spectra also present a bimodal frequency distribution similar to the PLL1 one. Both spectra are formed by a repetition of a series of three peaks with differences of 113 Da due to Leu residues. Peaks assignation is the same as PLL1 material which was described in Table 2. Detection of PLL containing NCA endgroup confirms the role of the triethylamine in the initiation step.

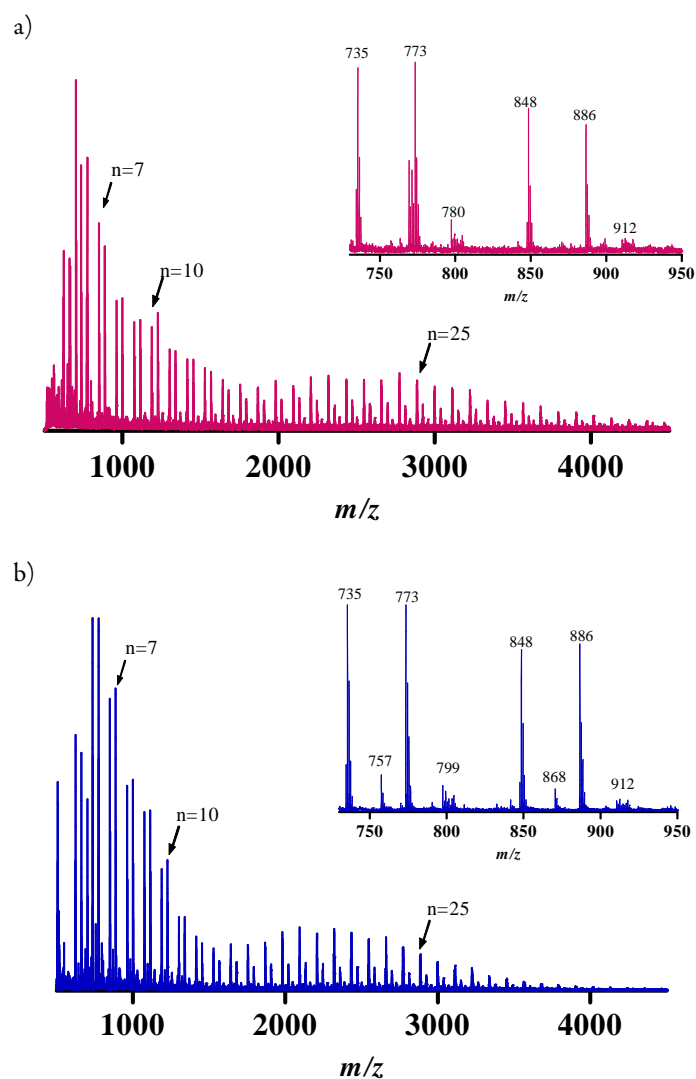
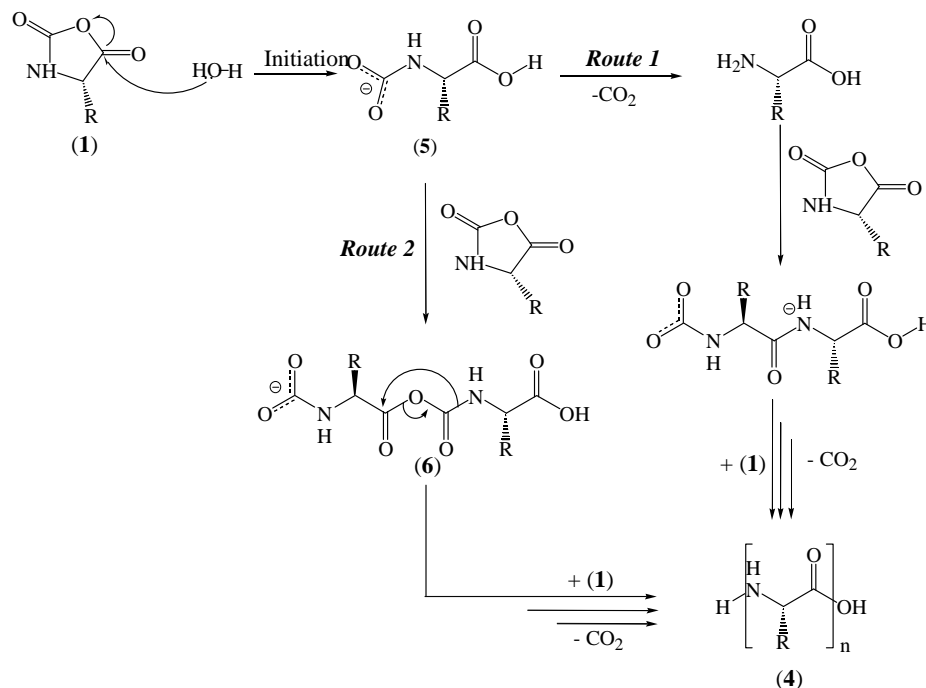


Figure 2 MALDI-TOF MS spectra of a) PLL2 and b) PLL3. Inset: MALDI-TOF spectra in the m/z range: 730-950.

Triethylamine as the initiator starts the ROP through deprotonation of NCA (1) forming a dimer (2) with a highly electrophilic *N*-acyl NCA endgroup and a nucleophilic carbamate group. Chain propagation can take place either through the carbamate mechanism

2.2 Results and discussion – MALDI TOF results

H/OH + K⁺ + Na⁺ - H⁺), and the other hand could due a cyclic-PLL chain detected by loss of a water molecule (e.g. 757 = 6*L-Leu + H/OH + 2K⁺ - H⁺ - H₂O) [9,22]. Though, MALDI TOF MS is not enough to clarify these assignments.



Scheme 4 ROP to synthesise PLLs containing living groups *via* (route 1) enamine mechanism and (route 2) carbamate mechanism [13,19]. R=CH₂CH(CH₃)₂

About cyclisation of PLL chains, Kricheldorf *et al.* reported the thermal polymerisation of NCA at 120°C obtaining cyclic-PAA as the main product [20]; however no observation was reported by Geller *et al.* who used a primary amine as the initiator under unspecified high temperature of synthesis [23]. In that context, we wanted to obtain PLL containing living groups preventing the cyclisation of the chains. For these reasons, we chose to perform the reaction at 60°C to investigate the effect of temperature in ROP reaction. Two PLL materials were synthesised at 60°C and named PLL₁₆₀ and PLL₂₆₀ respectively. MALDI-TOF spectra of both PLL are quite similar. Figure 3 shows the MALDI-TOF spectrum of PLL₂₆₀. MALDI-TOF results show that increases of the reaction temperature from 25°C to 60°C during the synthesis of PLLs at the same conditions does not affect, apparently, the structural properties of PLLs which mainly contain living groups and a small quantity of PLL with NCA endgroups.

* MALDI-TOF spectrum of PLL₁₆₀ is shown in Annex 3, Figure 10.

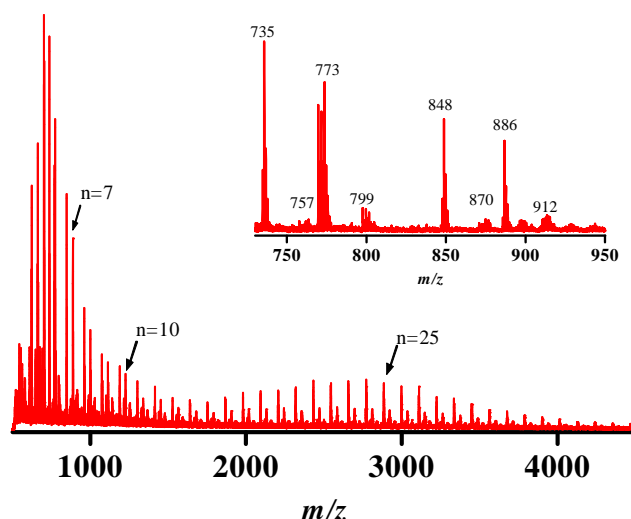
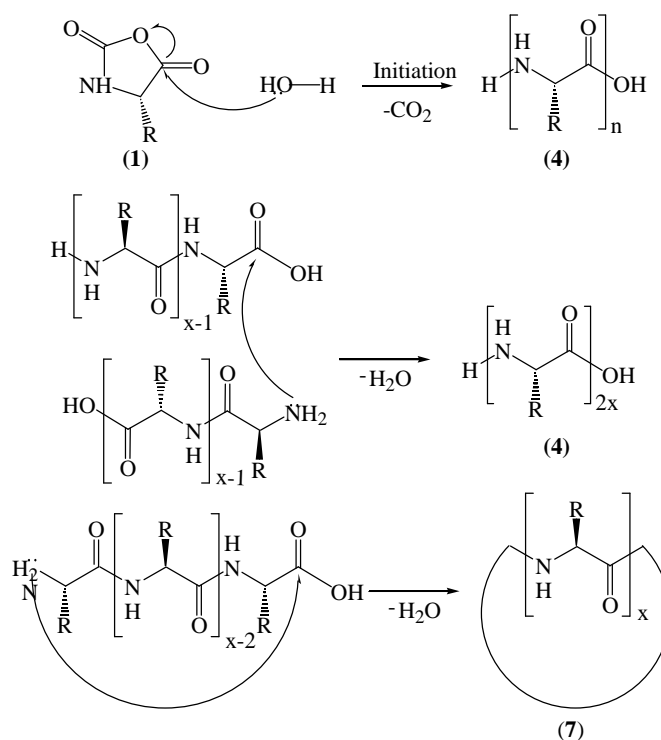


Figure 3 MALDI-TOF MS spectrum of PLL₂₆₀. Inset: MALDI-TOF spectra in the m/z range: 730-950.

In this case, the peak at 757 Da was also observed. The plausible assignation for this peak is PLL chains containing living groups after water loss (e.g. $757 = 6 \cdot \text{L-Leu} + \text{H}/\text{OH} + 2\text{K}^+ - \text{H}^+ - \text{H}_2\text{O}$) which indicates the cyclisation of the PLL containing living groups (7) as observed Kricheldorf [20] to PLL synthesised a high temperature. A feasible mechanism for the synthesis of cyclic-PLL was reported by Kricheldorf *et al.* and it is showed in Scheme 5.



Scheme 5 Proposal mechanism to the synthesis of cyclic-PLL [20].

2.2 Results and discussion – MALDI TOF results

2.2.2 FT-IR and Raman Spectroscopy results

Skeletal FT-IR (left) and Raman (right) spectra of PLL1, PLL2 and PLL3 are shown in Figure 4. FT-IR spectrum of PLL1 in KBr (Figure 4a, left) shows the alkyl C-H stretching and deformation bands at 2953, 2937, 2871 and 1467 cm^{-1} . The band due to N-H stretching vibration and Fermi resonance is observed at 3300 cm^{-1} , while the band at 3060 cm^{-1} is due to overtones and/or combinations of amide I modes. The characteristic bands of the peptidic bond are evidenced at 1654 and 1542 cm^{-1} . The band at 1654 cm^{-1} is mainly associated with C=O stretching vibration and the backbone conformation of the α -helical structure (amide I) [24] and the band at 1542 cm^{-1} is mainly associated to N-H bending and C-N stretching vibrations (amide II). Detection of amide I and II bands around 1650 and 1550 cm^{-1} agrees with literature to peptide chains with α -helical conformations [25]. Broad effect in amide I band at higher frequency, in comparison with PLL2 and PLL3 FT-IR spectra, could be attributed to segments of PLL are not involved in H-bond interaction [26].

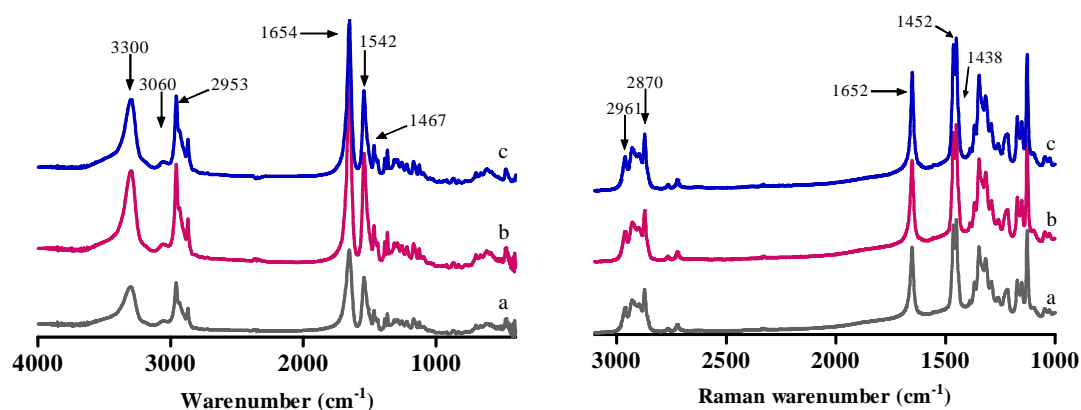


Figure 4 Skeletal FT-IR (left) and Raman (right) spectra of a) PLL1, b) PLL2 and c) PLL3.

This observation agrees with MALDI-TOF analyses to PLLs containing NCA endgroups and strongly suggests that at room temperature cyclisation of the PLL chains was not observed. Interpretation of the spectrum below 1400 cm^{-1} is complex due to the presence of deformation bands from the C-N, C-C, C-N, C-O and N-H bonds. Raman spectrum of PLL1 (Figure 4a, right) shows bands between 2870 to 2961 cm^{-1} due to CH_2 and CH_3 stretching vibrations. Amide I and II bands were detected at 1652 and 1452 cm^{-1} respectively. The bands below 1388 cm^{-1} correspond to deformations of C-N, C-C, C-N, C-O and N-H bonds. FT-IR and Raman spectra of PLL2 and PLL3 (Figure 4b,c) do not present any difference respect to PLL1 ones.

Figure 5 (left) shows FT-IR spectra of PLL1₆₀ and PLL2₆₀ which are similar to PLL synthesised at room temperature. At low frequency two new bands at 1778 (very small) and 1719 cm^{-1} were detected. In order to further investigate the nature of these two bands, subtraction FT-IR spectrum of PLL1₆₀ minus PLL1 is presented in Figure 5c (left). Presence of a very intense band at 1719 cm^{-1} in comparison with amide I and II bands suggests the formation of cyclic structures in the polymer chain which possibly affects the growth of the chains. Moreover, the absence of a band at 3300 cm^{-1} indicates that these kinds of PLL chains are not forming N \cdots H interaction among themselves and they are probably affecting the stability of α -helical conformation either. These findings are totally complementary to MALDI-TOF results for the presence of PLL containing NCA endgroups, and in agreement with Kricheldorf *et al.* who explained that thermal polymerisation of Poly-Sar is a complex process yielding numerous low molar mass species together with cyclic polypeptide structures [20]. It is not clear the presence of the band at 1778 cm^{-1} in the subtracted spectrum, but it could be due to a C=O specie forming secondary PLL structures. Assignment of other bands in spectra 5a and b agrees with the assignment presented for PLLs synthesised at room temperature. Raman spectrum of PLL1₆₀ (Figure 5b, right) also presents bands due to secondary polymeric structures at 1780 and 1668 cm^{-1} . Nevertheless no band at those frequencies was detected for PLL2₆₀.

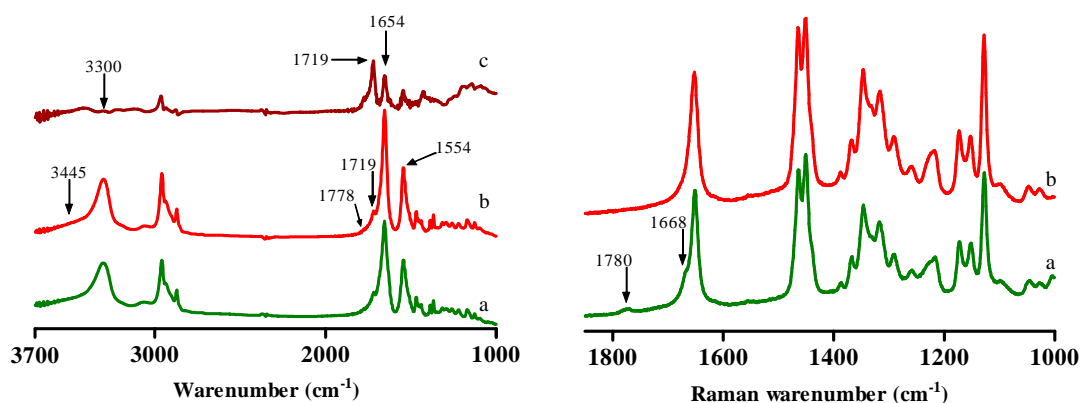


Figure 5 Skeletal FT-IR spectra (left) of a) PLL1₆₀, b) PLL2₆₀, c) Subtracted spectrum [PLL1₆₀ – PLL1] and Raman spectra in the frequency range 1850-1000 cm^{-1} of a) PLL1₆₀ and b) PLL2₆₀.

3. Immobilisation of synthesised PLL in HT_{rus}

3.1 Experimental

3.1.1 Synthesis of rehydrated hydrotalcite (HT_{rus})

Rehydration of Mg-Al hydrotalcite (HT) with Mg/Al molar ratio = 2 was performed according with the method exposed in Chapter 2, section 2.1.1.

3.1.2 Synthesis of Poly-L-Leu/HT materials

Under Ar atmosphere, 5 mL of deionised-decarbonated water was added to a solid mixture containing 300 mg of freshly synthesised HT_{rus} and 100 mg of the indicated PLL. The obtained mixture was sonicated during 30 min. After that time, the slurry was washed with THF for three times. The obtained solid was dried at 60°C and named: IPL3 and IPL2₆₀.

3.2 Results and discussion

Based on the results obtained for the immobilisation of AAs in HT_{rus} (Chapter 2) and taking into account the high catalytic activity of LL/HT and LP/HT nanohybrid materials synthesised by anion-exchange method (Chapter 3), in this section we discuss the synthesis and characterisation of nanohybrid materials based on the synthesised PLL immobilised on HT_{rus} following this methodology. All our discussion was focused in the further investigation about the nature of organic/inorganic interactions between these two components.

To evaluate the immobilisation properties of the PLL two materials were selected: PLL3 and PLL2₆₀. According with characterisation data presented below, PLL3 and PLL2₆₀ have closer physical properties and lower DP values than their PLL materials homologues. All conclusions are drawn on the basis of the characterisation by AE, ICP, XRD, FT-IR, Raman, MALDI, ESI-TOF and thermal evolution using TG/DTA analyses and *in situ* FT-IR under outgassing conditions at increasing temperature. Molecular formulae of all nanohybrid materials synthesised in this report are presented in Table 3.

Table 3 Molecular formulae of HT and PLL/HT materials

Entry	PLL precursor	Material ^{a,b}	Molecular Formulae ^c
1	-	HT _{rus}	[Mg _{2.39} Al _{1.00} (OH) _{6.79}](CO ₃ ²⁻) _{1.13} (NO ₂ ⁻) _{0.10} ·1.10H ₂ O
2	PLL3	IPL3	[Mg _{2.39} Al _{1.00} (OH) _{6.79}](Leu*) _{2.73} (CO ₃ ²⁻) _{2.28} (NO ₂ ⁻) _{0.10} ·0.70H ₂ O
3	PLL ₂₆₀	IPL ₂₆₀	[Mg _{2.39} Al _{1.00} (OH) _{6.79}](Leu*) _{1.68} (CO ₃ ²⁻) _{5.20} (NO ₂ ⁻) _{0.10} ·0.70H ₂ O

^aSynthesis Conditions: HT_{rus} and PLL were suspended in 5 mL of deionised-decarbonated water and stirring for 0.5 hour at room temperature. ^bHT_{rus} = HT rehydrated under ultrasound treatment. ^cCalculated by EA and ICP analysis. Water content was calculated theoretically according with Miyata Ref [27]. Leu* = monomeric unit.

3.2.1 X-ray diffraction and High Resolution TEM results

XRD patterns of nanohybrid materials synthesised using PLL3 and PLL₂₆₀ are presented in Figure 6. In all cases, the obtained materials exhibit the characteristic d_{003} , d_{006} and d_{009} diffraction peaks of the meixnerite structure (JCPDS 35-0965).

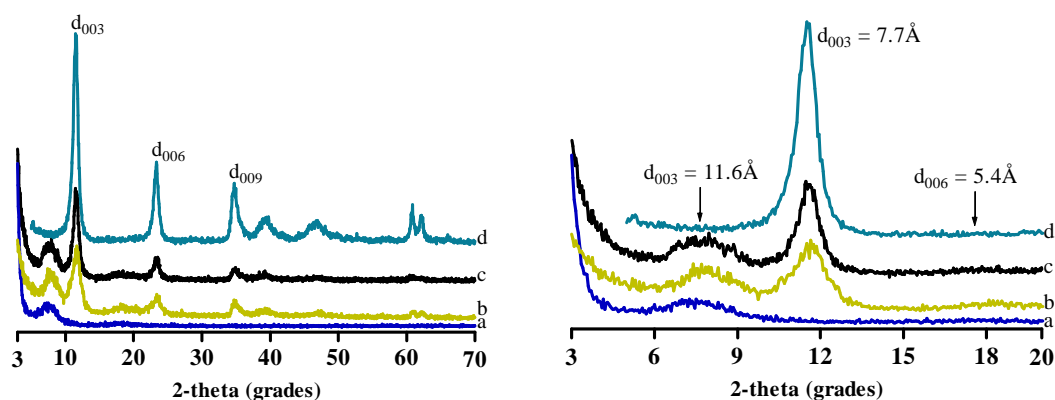


Figure 6 (left) XRD patterns of a) PLL3, b) IPL3, c) IPL₂₆₀ and d) HT_{rus}. (Right) XRD pattern in the 2θ range: 3-20°

In agreement with Cavani *et al.*, HT_{rus} which mainly contain hydroxyl anions presented the main diffraction peak at $11.4 \text{ } 2\theta$ corresponding to a $d_{003}=7.7 \text{ \AA}$ [28] (Figure 6d). XRD pattern of IPL3 and IPL₂₆₀ (Figure 6b and 6c) showed new diffraction peaks corresponding to d_{003} at $7.5 \text{ } 2\theta$ and d_{006} at $18.0 \text{ } 2\theta$ reflection planes of HTs with immobilised PLLs. The two types of HT structure showed different interlayer spaces. While the interlayer space remained unchanged with respect to the meixnerite in one structure (7.7 \AA), the space increased in size in the other one (11.2 \AA) (Figure 6b and 6c, respectively). XRD pattern of PLL3 (Figure 6a) has a diffraction peak at $7.3 \text{ } 2\theta$ and no present of any diffraction peak around $18.0 \text{ } 2\theta$ was observed. So, the presence of significant amounts of non-intercalated PLLs in samples IPL3 and IPL₂₆₀ was discarded. Figure 7 shows the HRTEM images of HT_{rus} and IPL materials.

3. Immobilisation of synthesised PLL in HT_{rus}

3.2 Results and discussion – XRD and HRTEM results

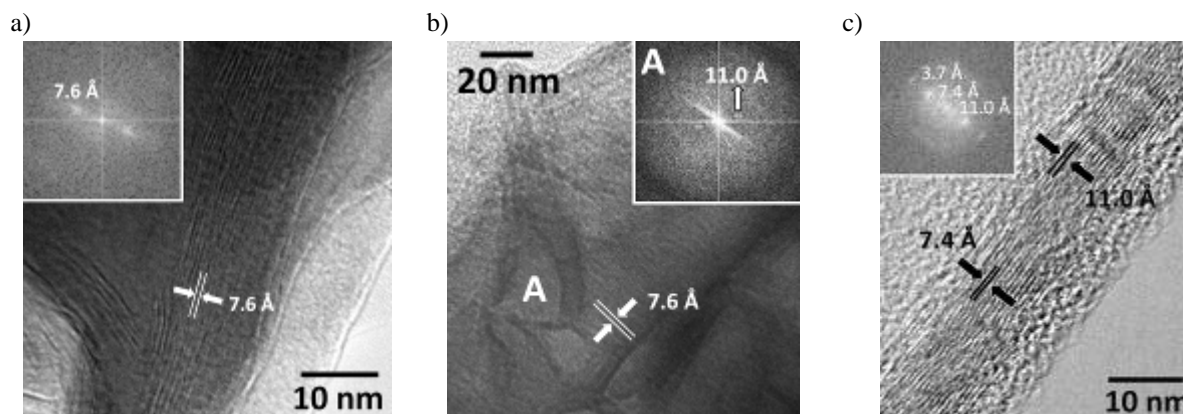
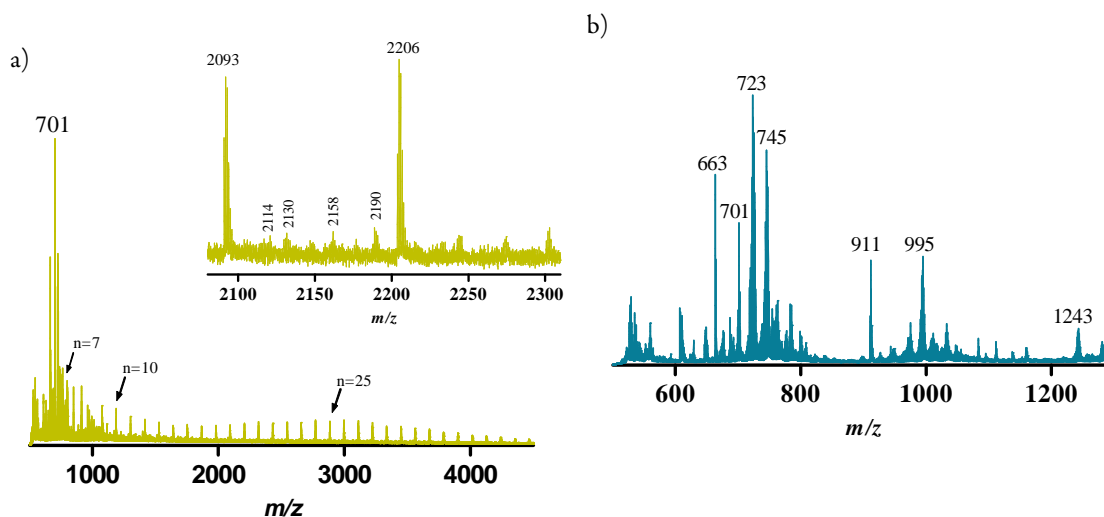


Figure 7 HRTEM images of a) HT_{rus}, b) IPL3 and c) IPL2₆₀.

HRTEM image of HT_{rus} (Figure 7a) shows aggregated layers up to 100 nm in length with interlayer space around 7.6 Å as it was deduced by FT analysis. Additionally, HRTEM images of IPL3 and IPL2₆₀ (Figure 7b and 7c) exhibit a morphology constituted by two types of mixed agglomerates, one of them containing disordered layers with interlayer space of 7.6 Å and the other one containing fine-grained structure poorly resolved with an interlayer space of 11.0 Å. Taking into account the morphology and interlayer space values, disordered layers in the sample were identified with the HT_{rus} precursor, whereas fine-grained aggregates confirmed the incorporation of PLL in the HT structure.

3.2.2 MALDI-TOF results

To identify the nature of the PLL structure immobilised in the HT_{rus}, MALDI-TOF analyses were performed on IPL3 and IPL2₆₀ materials, and they are shown in Figure 8.



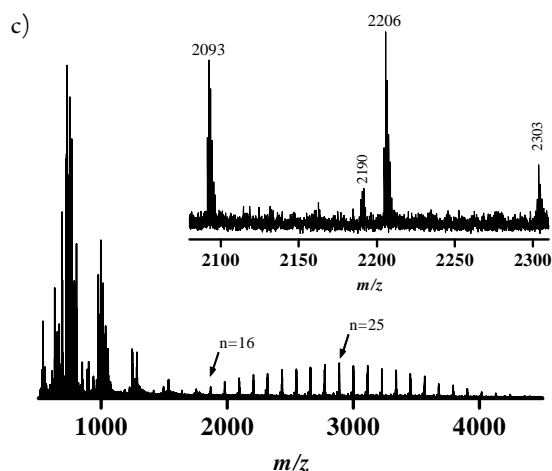


Figure 8 MALDI-TOF MS spectra of a) IPL3 and b) HT_{rus} and c) $IPL2_{60}$. Inset: MALDI-TOF spectra in the m/z range a) 1180-1400 and c) 2080-2310

From a general point of view, ionisation of both IPL3 and $IPL2_{60}$ is lower than the pure PLLs. This effect could be attributed to immobilisation of PLL in HTs which have low solubility and made the analysis more difficult. The peak at 701 Da in IPL3 spectrum is due to the α -ciano-4-hydroxycinnamic acid used as the matrix, while the peak at 723 Da in $IPL2_{60}$ spectrum is due to presence of HT_{rus} , like other peaks detected between 660 and 1243 Da (Figure 8b).

We proposal that presence of PLL containing living groups is because the immobilisation process occurs through an anionic/exchange reaction between the OH^- anions located in the interlayer space and the carboxylate endside of the PLL. Moreover, presence of a small peak due to PLL containing NCA endgroups in IPL3 spectrum suggests that during the immobilisation process, HT_{rus} can attack PLL chains containing NCA group *via* activated monomer mechanism (Scheme 2) immobilising the PLL chain conserving the NCA endgroup. Nevertheless relative intensity of this band suggests that living groups are favored to be immobilised in HT_{rus} . To clarify this point, the non-immobilised PLLs of the liquid fraction obtained after separation by centrifugation of the nanohybrid solid was also characterised by MALDI-TOF (Figure 9).

The inset spectrum of the non-immobilised fraction shows a series of eight main peaks, which were assigned as follows: 2093 and 2116 Da due to PLL containing living groups, 2147 and 2189 Da due to cyclic-PLL from PLL containing living groups, 2103 and 2189 Da due to cyclic-PLL from PLL chains containing NCA endgroups, 2132 Da due to

3.2 Results and discussion – MALDI TOF results

PLL chains containing a C₁₂H₂₁N₂O₂ group and 2161 Da due PLL chains containing an excess of 46 Da in their structure.

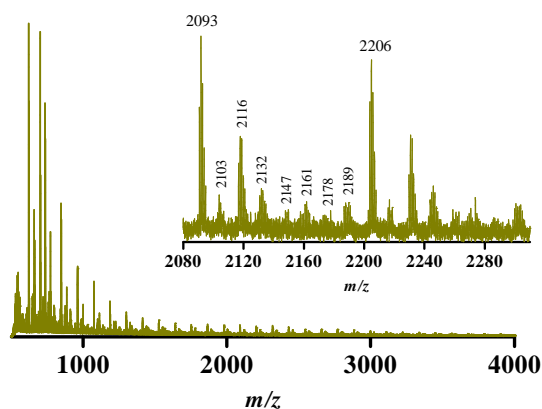
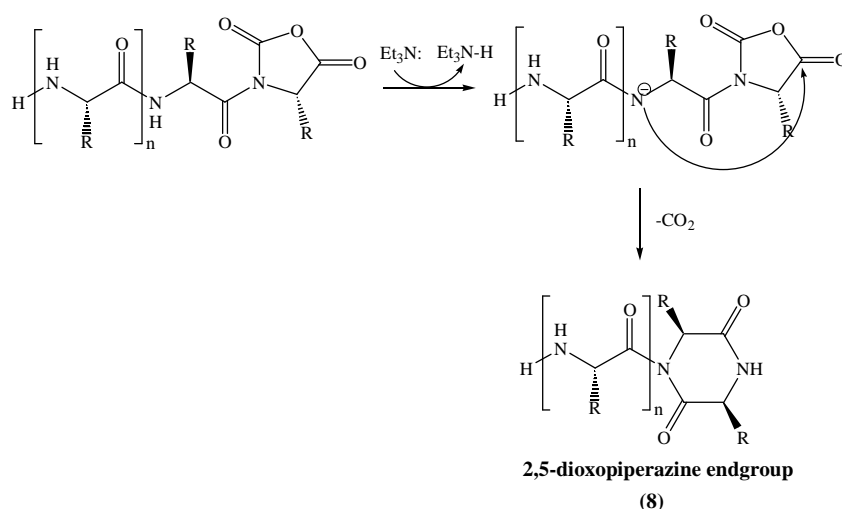


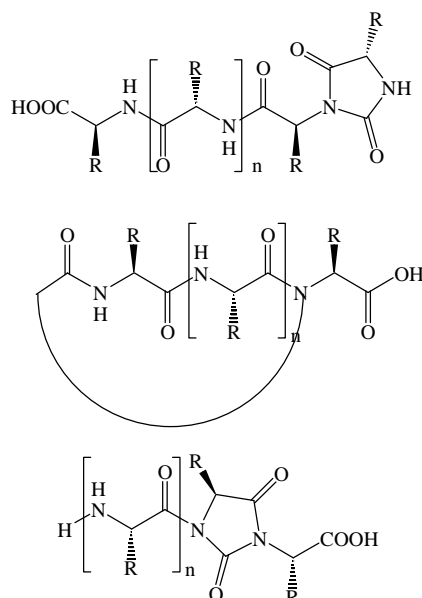
Figure 9 MALDI-TOF MS spectra of none immobilised fraction of IPL2₆₀. Inset: MALDI-TOF spectra in the m/z range: 2080-2310.

Comparison between spectrum showed in Figure 9 and assignation of pure PLL3 (Table 2, entry 9) demonstrated that the immobilisation process occurs through PLL chains containing living groups. Less PLL containing living groups in the sample permitted to detect other PLL chains forming during the ROP. In this case detection of PLL containing a C₁₂H₂₁N₂O₂ cyclic group or PLL containing NCA endgroup with a additional mass of 46 Da show that ROP occurs by different routes obtaining a high number of different PLL chains. Presence of C₁₂H₂₁N₂O₂ cyclic group agrees with Dijk-Wolthuis *et al.* who proposed the formation of a 2,5-dioxopiperazine endgroup (**8**) using triethylamine as the initiator in the synthesis of poly-Lysine [13] (Scheme 6).



Scheme 6 Formation of a 2,5-dioxopiperazine (C₁₂H₂₁N₂O₂) endgroup according to Ref [13].
 R=CH₂CH(CH₃)₂.

Additionally, detection of PLL containing NCA endgroup plus 46 Da could be due to the formation of a secondary PLL structure containing an uracil-type group (Scheme 7). Kricheldorf *et al.* also detected the formation of secondary cyclic-PLL structures in the synthesis of poly-L-Phenylalanine using *N,N*-dimethylaminopyridine as the initiator [15]. Nevertheless, the detection of none of these peaks in the pure PLL3 (MALDI-TOF and FT-IR spectra) also shows that ROP under our evaluated conditions allows mainly PLL chains containing living groups.



Scheme 7 Some possible uracil-kind PLL structure formed during the ROP reaction according to Ref [15]. $R = \text{CH}_2\text{CH}(\text{CH}_3)_2$

Taking into account that the obtained PLL were washed several times with THF and chloroform after immobilisation, PLL remaining in the materials should be stabilised through H-bonds or anionic interactions. Nevertheless, it is not possible to determine through MALDI-TOF MS the nature of the interaction between PLLs and HT materials because the sample preparation is performed in trifluoroacetic acid where the HT structure is destroyed.

3.2.2 FT-IR and Raman spectroscopy results

Under a general point of view, FT-IR spectra of IPL3 and IPL2₆₀ (Figure 10b left and 10c left) show the characteristic bands of both HT_{rus}* and PLL materials. Moreover, any

* A complete characterisation of HT_{rus} material by FT-IR and Raman spectroscopy is showed in Chapter 2, section 2.2.3

3.2 Results and discussion – FT-IR and Raman results

detected change in the shape of Fermi N-H (3060 cm^{-1}), amide I (1654 cm^{-1}) and amide II (1542 cm^{-1}) bands suggests that the immobilisation process does not affect the α -helical conformation of the PLL after immobilisation. Differences in the relative intensity of the band at 3300 cm^{-1} in both IPL materials reflect the amount of immobilised PLL, being higher in IPL3 (Figure 10b) than IPL2₆₀. This observation agrees with the EA results (Table 3, entries 2 and 3).

About the nature of the immobilisation, FT-IR spectrum of IPL3 (Figure 10b) shows that H-interactions of both HT_{rus} and PLL3 were slightly affected. The band at 3000 cm^{-1} in free PLL3 shifts to 3307 cm^{-1} when it is immobilised, while the band at 3470 cm^{-1} in HT_{rus} shifts to 3446 cm^{-1} after immobilisation. Comparison of the relative intensity between amide I and II after immobilisation, shows that α -helical PLL3 is stabilised in the HT by H-bonding between the N-H and C=O groups from the backbone structure and the M-OH of the HT [29]. Moreover, changes at 790 cm^{-1} after immobilisation of PLL suggest that the interaction between the HT_{rus} and PLL3 occurs by displacement of the OH⁻ groups in the HT as it has been reported for less complex anionic organic molecules [30].

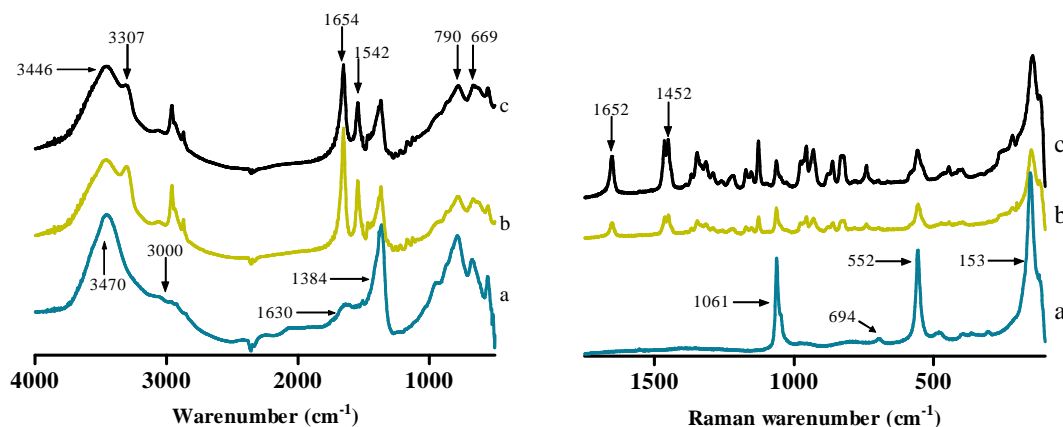


Figure 10 Skeletal FT-IR (left) and Raman (Right) spectra of a) HT_{rus}, b) IPL3 and c) IPL2₆₀ in the frequency range $1700\text{-}100\text{ cm}^{-1}$.

Finally, the strong band observed at 1384 cm^{-1} is due to adsorbed CO_3^{2-} anions in the HT structure during its manipulation. Furthermore, FT-IR spectrum of IPL2₆₀ (Figure 10c) does not present the band at 1719 cm^{-1} due to cyclic-PLL observed in the pure PLL2₆₀. Comparison of the relative intensities of the amide I and II bands after immobilisation of PLL2₆₀ also shows that the stabilisation of the α -helical PLL occurs by H-bonding interactions. Some changes in the lattice region after immobilisation also indicate that the

interaction between PLL and the HTs affects the M-OH bonds. All these findings agree with MALDI-TOF results which suggested that immobilisation process occurs through PLL chains containing living groups. Raman spectra of both IPL materials (Figures 10a and 10b right) do not present any change in the PLL structure after immobilisation.

4. Synthesis of Poly-L-Leucine using green initiators: water and HT_{rus}

4.1 Experimental

4.1.1 Synthesis of PLL materials

PLL were synthesised according with the methodology described in section 2.1.2 during 4 days at r.t. PLL4 material was synthesised using 91.6 µl of water as the initiator (M/I = 10). PLL5 and PLL6 materials were synthesised using 33.8 mg (M/I = 10) and 715 mg (M/I = 0.5) respectively.

4.2 Results and discussion

As it was explained before, presence of water traces during ROP allows PLL chains containing living groups. It also was exposed above that the HTs has basic and nucleophile properties that could permit its role as the initiator of the polymerisation reaction. The next step is to extend the synthesis and, also, the immobilisation process to other initiators such as water and HT_{rus} and alternative immobilisation procedures to those discussed in the previous section. These ones have been chosen for their optimal synthetic properties but also to develop a more sustainable process under the environmental point of view. The list of all the PLL materials used in this section, including some of their properties like: Degree of polymerisation (DP), Molecular weight (Mw) and Poly-dispersion (PD) data are summarised in Table 4.

Table 4 Synthesis of PLL using water and HT_{rus} as initiator.

Entry	material	M/I ratio ^a	DP ^{b,c}	Mw ^c	PD ^c	Molecular formulae ^d
1	PLL4	10	5-42	2456	1.43	
2	PLL5	10	5-38	2303	1.49	[Mg _{2.53} Al _{1.00} (OH) _{7.07}](Leu*) _{11.14} (CO ₃ ²⁻) _{0.38} (NO ₂ ⁻) _{0.10} ·1.10H ₂ O
3	PLL6	0.5	5-42	2212	1.57	[Mg _{2.53} Al _{1.00} (OH) _{7.07}](Leu*) _{3.00} (CO ₃ ²⁻) _{1.96} (NO ₂ ⁻) _{0.10} ·1.10H ₂ O

^aM/I = mmol NCA/mmol OH⁻ available to act as initiator (1 mmol OH⁻/1 mmol HT_{rus}). ^bDetermined by ESI-TOF MS analyses. ^cDetermined by MALDI-TOF analyses. ^dCalculated by EA and ICP analysis. Water content was calculated theoretically according with Miyata Ref [27]. Leu* = monomeric unit

4.2.1 MALDI-TOF results

MALDI-TOF spectrum of PLL4 (Figure 11) shows a monomodal frequency distribution with a distinct maximum around 950 Da (8 monomers). According to Kricheldorf *et al.* monomodal distribution and decreasing of the Mw values is indicative of low solubility and/or precipitation of PLL chains during the synthesis [13]. The inset spectrum in Figure 11 shows that the entire spectrum is a repetition of a series of seven peaks separated by 113 Da. Peaks at 1073, 1112 Da and possibly the one at 1171 Da are due to adducts of PLL chains containing living groups.

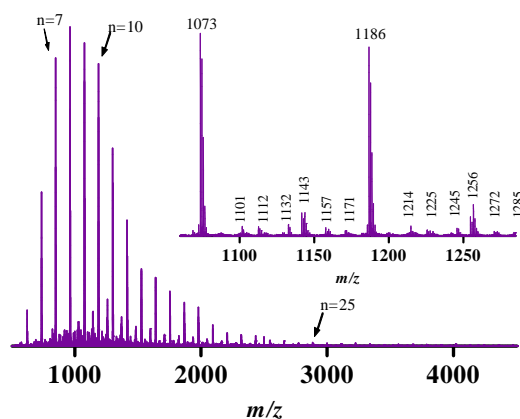


Figure 11 MALDI-TOF MS spectrum of PLL4. Inset: MALDI-TOF spectra in the m/z range: 1050-1285.

Presence of the other peaks is explained since a mechanistic point of view. PLL synthesised using water as the initiator has a similar behaviour than to those obtained through polymerisation using primary amines as the initiators. Presence of PLL containing living groups in PLL4 were formed *via* enamine and/or carbamate mechanism (Scheme 4) where water acts as a nucleophile and the initiation step is faster than the growing one. Moreover, low DP in PLL4 (Table 4, entry 1) demonstrated that water can also act as a base and initiate the ROP *via* the activated monomer mechanism (Scheme 2) forming PLL containing NCA endgroups.

Peaks due to PLL containing NCA endgroups are evidenced at 1132, 1143 and 1157 Da, respectively. On the other hand, although enamine mechanism allows PLL chains with high Mw, detection of the peak at 1132 Da shows the formation of cyclic-PLL chains which prevent the growth of the lengths by precipitation [9,22] (Scheme 6). The peak at 1171 Da could be also due to cyclic-PLL, though the assignment is no clear because has the same mass

as the PLL containing living groups dopped with sodium. Competition between all these reactions allowed polymers with lower Mw than PLLs synthesised using triethylamine as the initiator. The list of all peaks with their dopped correspondences are shown in table 5.

Table 5 Calculated Masses (Da) of PLL4 by MALDI-TOF SM.

Endgroup	H/OH			H/NCA + 46Da	H/NCA		Cyclic
	+ K ⁺	+ 2K ⁺ - H ⁺	+ Na ⁺ ^a	+ K ⁺	+ K ⁺	+ H ⁺ - H ₂ O	+ H ⁺
7	847	886	833	1030	988	931	793
8	960	999	946	1143	1101	1044	906
9	1073	1112	1058	1256	1214	1157	1019
10	1186	1125	1171	1369	1327	1270	1132
11	1299	1339	1284	1483	1441	1384	1245
12	1413	1452	1397	1596	1554	1497	1358

^aMass at 1171.8 is calculated as 10*Leu + H/OH + Na⁺; nevertheless, it could be due to a cyclic polymer chain and calculated as 10*Leu + H/OH + K⁺ - H₂O.

PLL5 and PLL6 were synthesised using HT_{rus} as the precursor in M/I ratios of 10 and 0.5 respectively. The MALDI-TOF spectrum of PLL5 is shown in Figure 12a. In a similar way as the non immobilised PLL4, the PLL5 spectrum exhibits a series of five peaks. The intense peak at 1073 Da corresponds to PLL containing living groups dopped with potassium, while the peak at 1171 is due to a sodium adduct. The small peak detected at 1143 Da corresponds to PLLs containing a NCA endgroup plus 46 Da which is similar to the PLL chains observed in the non immobilised aqueous fraction of IPL3 (Figure 9 and Scheme 7). While the peaks at 1101 and 1132 Da are due to PLL containing NCA endgroup and cyclic-PLL, respectively. In comparison with other authors [12-13,31], we may infer that the presence of several kinds of PLL structures is due to the basic nature of HT_{rus} which initiates the polymerisation *via* a monomer activated mechanism (Scheme 2). Nevertheless, intensity of the peaks in the inset spectrum suggests that ROP was mainly directed by enamine/carbamate mechanism.

Figure 12b shows the MALDI-TOF spectrum of PLL6. In this case, PLL6 was synthesised using excess of HT_{rus} in M/I ratio of 0.5. MALDI-TOF spectrum of PLL6 is formed by a series of four main peaks at 1073, 112, 1143 and 1186 Da as they are represented in the inset spectrum. The representative peaks at 1073 Da and the one at 1112 Da are due to potassium adducts of PLL chains containing living groups. The peak at 1143 Da is due to uracil-kind PLL and PLL containing NCA endgroups, which are formed *via* activated

4. Synthesis of Poly-L-Leucine using green initiators, water and HT_{rus}

4.2 Results and discussion – MALDI TOF results

monomer mechanism without incorporation of the HT in the final structure. Moreover, characterisation data suggest that formation of PLLs containing living groups and cyclic-PLLs occurs in two steps: first, the ROP is initiated *via* enamine mechanism obtaining polymer chains with an amino and a carboxylate-HT endgroup and second, remnant PLLs containing NCA endgroups are hydrolysed after ROP as exposed in Scheme 3.

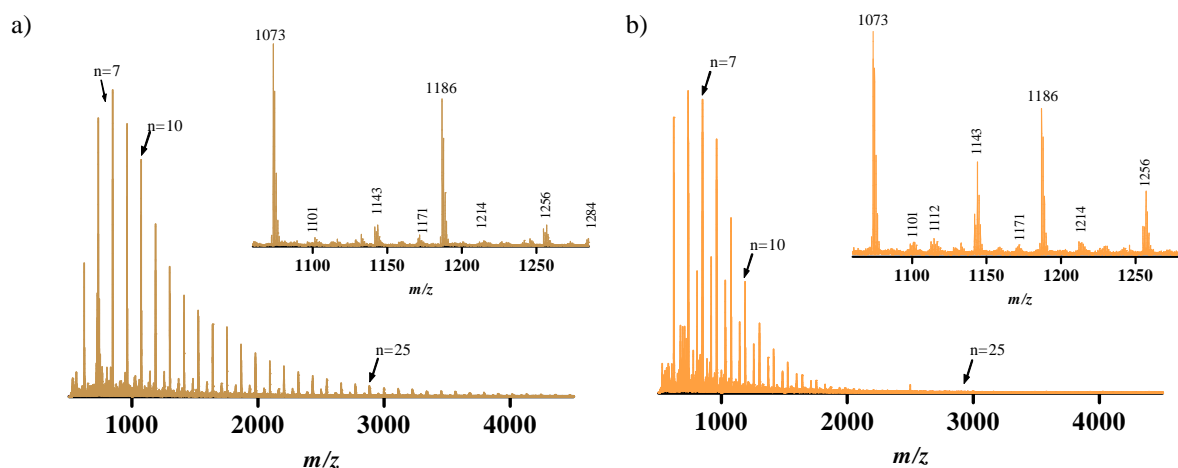


Figure 12 MALDI-TOF MS spectrum of a) PLL5 and b) PLL6. Inset: MALDI-TOF spectra in the m/z range 1060-1285.

4.2.2 FT-IR and Raman spectroscopy results

FT-IR spectra of PLLs synthesised using water (PLL4) and HT_{rus} (PLL5 and PLL6) as initiators are presented in Figure 13 and 15. FT-IR spectrum of PLL4 (Figure 13) exhibits a complex group of bands in comparison with the other synthesised PLLs. To further investigate the difference in the PLL structure, subtractions spectra were performed and presented in Figure 13.

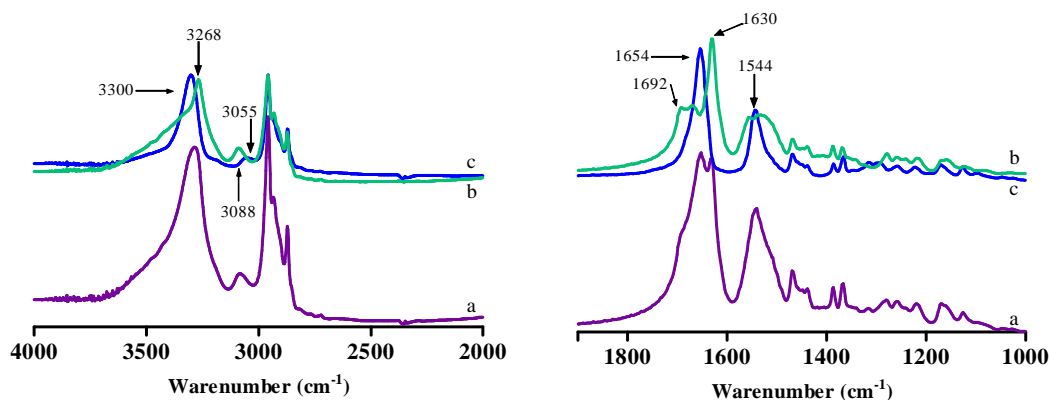


Figure 13 Skeletal FT-IR spectra of a) PLL4, b) Subtracted spectrum [PLL4 – PLL3] and c) PLL3 in the frequency region of (left) 4000-2000 cm^{-1} and (right) 1900-1000 cm^{-1} .

Figure 13b corresponds to subtraction spectrum of PLL4 minus PLL3 to obtain the bands due to new PLL chains, while Figure 13c corresponds to PLL3 spectrum. At higher frequency bands due to N-H stretching vibration and Fermi resonance shift to 3285 and 3088 cm^{-1} indicating differences in the H-bonding between PLL chains. At lower frequency, the amide I band centered at 1654 cm^{-1} exhibits new components at 1630 and around 1690 cm^{-1} . Presence of the band at 1630 cm^{-1} with a second component around 1533 cm^{-1} agrees with Barlow *et al.* who exposed that shift of amide I and II bands at lower frequency is due to formation of β -sheet conformations [25]. Moreover, the possible formation of β -sheet PLL agrees with the low PD presented in Figure 3 and also with Kricheldorf who exposed that precipitation of β -sheet PLL increases the probability of parallel reactions to obtain cyclic polymeric structures [19]. The bands around 1690 cm^{-1} are due to C=O stretching vibrations of secondary PLL structures containing cyclic groups.

In contrast with the FT-IR results, Raman spectrum of PLL4 (Figure 14) exhibits shifts of most of the bands below 1300 cm^{-1} as well as a complex series of new bands. An important change in the amide I band was detected as the appearance of a band at 1670 cm^{-1} which is related with the band detected at 1669 cm^{-1} in FT-IR spectrum. Shifts of the band at 1282, 1215, 1148, 1087 and 1040 cm^{-1} as well as the appearance of new bands at 1555, 1242, 1112 and 1003 cm^{-1} are due to complex changes in the PLL structure, which according with FT-IR and MALDI-TOF results is formed by several PLL structures.

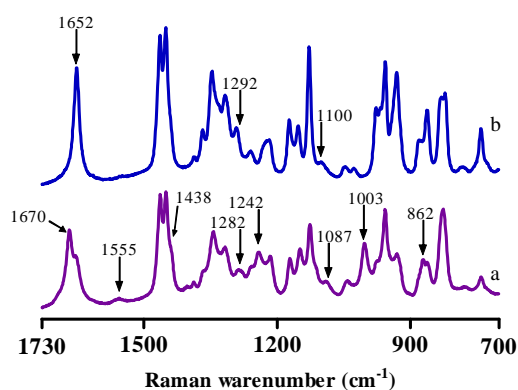


Figure 14 Raman spectra of a) PLL4 and b) PLL3 in the frequency range 1730-700 cm^{-1} .

FT-IR spectra of PLL5 and PLL6 are shown in Figure 15. FT-IR spectrum of PLL5 presents the characteristic bands of PLL4. These results agree with MALDI-TOF observations which suggested that polymerisation using HT_{rus} allows different kinds of PLL

4. Synthesis of Poly-L-Leucine using water or HT_{rus} as initiator

4.2 Results and discussion – FT-IR and Raman results

structures where the main ones are due to PLLs containing living groups. Although the results are very similar between the ROP initiated by water and that initiated by HT_{rus} ($M/I = 10$), two differences were detected: first, the band due to N \cdots H interactions shifts to higher frequency respect to PLL4 and it is centered at 3292 cm^{-1} . Second, the amide I and II bands centered at 1654 and 1542 cm^{-1} due to PLLs containing living groups have higher relative intensity than the other amide I band centered at 1633 cm^{-1} . These two differences demonstrated that using HT_{rus} as initiator, in small quantity, the formation of β -sheet polymers decrease, because the ROP is mainly directed *via* the enamine mechanism (Scheme 4, route 1) where the initiation occurs by the highly reactive OH^- anions located in the interlayer space of the HT. The Raman spectrum of PLL5 does not present any difference respect to the PLL4 one and any band due to HT_{rus} was detected (Figure 15b, right). Subtraction FT-IR spectrum of PLL6 (Figure 15c, left) shows that ROP reaction allows a PLL of similar properties to PLL5, while Raman spectrum of PLL6 (Figure 15a, right) shows a new band at 1766 cm^{-1} associated to PLL chains containing NCA endgroups. Finally, the bands due to HT_{rus} initiator are detected at 1062 , 553 and 153 cm^{-1} , respectively.

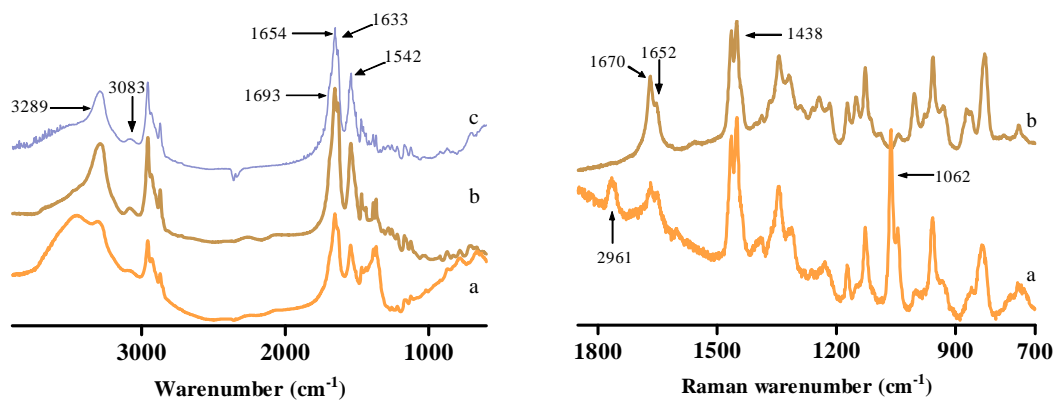


Figure 15 Skeletal FT-IR (left) and Raman (right) spectra of a) PLL5 and b) PLL6 in the frequency range $1830\text{--}700\text{ cm}^{-1}$. c) corresponds to Subtracted FT-IR spectrum [PLL6 – HT_{rus}].

In general, these results explain the appearance of MALDI-TOF spectra of PLL4, PLL5 and PLL6. According with Kricheldorf, less formation of β -sheet PLL prevents the arrangement of cyclic secondary structures and also decreases the Mw of the final polymer [19]. In other words, using water and HT_{rus} as the initiator, the kinetics of the reaction are different. Water permits a faster initiation step than the propagation. As a result of the faster initiation, it is favoured the precipitation of β -sheets and formation of a cyclic secondary

structure is favoured. On the other hand, HT_{rus} favours the propagation step. Using excess of HT_{rus} ROP is highly favoured *via* activated monomer mechanism afforded higher amount of cyclic ended PLLs.

4.2.3 X-ray diffraction and High Resolution TEM results

XRD patterns PLL4, PLL5 and PLL6 are shown in Figure 16a. The XRD pattern of PLL6 exhibits the typical signals due to HT structure with a new band at 7.6 2 θ which could indicate the increasing of the interlayer space up to 11.6 Å in a similar way as the IPL materials (Figure 6). For this reason HRTEM experiments were also performed with these materials and they are shown in Figures 16b and 16c.

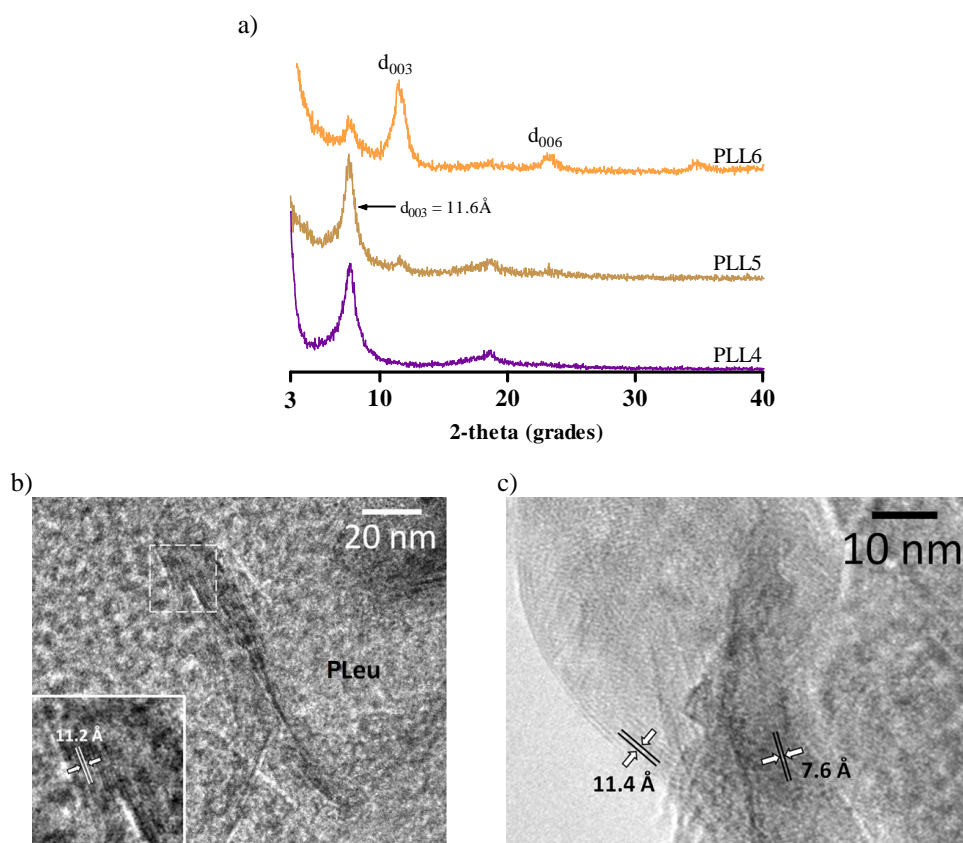


Figure 16 a) XRD patterns of PLL4, PLL5 and PLL6. b) HRTEM images of PLL5 and c) PLL6.

HRTEM analysis to PLL5 (Figure 16b) exhibits two kind of morphologies similar to those observed for IPL3 and IPL2₆₀ materials (Figures 7b and 7c). On one hand, a fine-grained fraction that likely corresponds to PLL, which is the most abundant. On the other hand, a more crystalline phase with a layered morphology, less abundant is ascribed to HT layers with lattice fringes at about 11.2 Å (inset figure). Increase of the interlayer space

indicates that intercalation of PLL into HT has likely occurred. HRTEM image of PLL6 are similar to the IPL3 and IPL2₆₀ ones, where HT in the sample has two kinds of interlayer spaces, one at 7.6 and the other at 11.4 Å indicating the intercalation of the PLL in the HT structure. Moreover, both the lattice fringes are recorded over well crystalline parts of the PLL6 material and it was no observed any free PLL.

5. Thermal Evolution of the synthesised materials

5.1 Thermal evolution of synthesised PLL

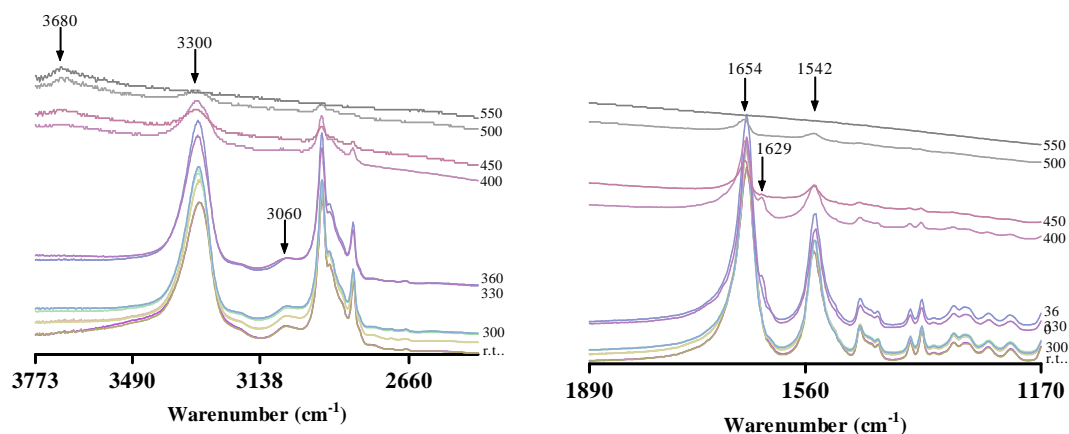
In situ FT-IR at increasing temperature and simultaneous TG/DTA analyses were examined to investigate the thermal stability of PLL materials before and after immobilisation and also PLL materials initialised by water and HT_{rus}. Figure 17 shows the FT-IR spectra of PLL3 under outgassing conditions at increasing temperature. As shown MALDI-TOF analysis, PLL3 are mainly formed by PLL containing living groups, so comparison of the relative intensity between amide I and II allows important information about the thermal stability of the α -helical conformation. Between 25 and 260°C, spectra of PLL3 do not present any important structural changes. At higher frequency, the band at 3300 cm⁻¹ shifts to 3306 cm⁻¹ due to progressive loss of water retained in the PLL structure, while at lower frequency, amide I band at 1654 cm⁻¹ becomes narrower with increasing temperature. Relationship in the relative intensity between amide I and II ratio of the spectra shows that constant loss of water increases the intermolecular N-H interactions in the α -helical conformation making it more stable*. Above 300°C progressive decreasing of the bands around 2900 cm⁻¹ and small changes in the amide II band at 1542 cm⁻¹ suggests loss of N-H, C-C and C-N bonds, possibly by elimination of CO, C₄H₈, NH₃ and HNCO species [32]. At 360°C, intensity of the amide II band decreases and shifts to 1541 cm⁻¹, while new bands are formed at 3680 and 1629 cm⁻¹, these changes suggest the formation of keto-enolic structures containing N-H bonds as decomposition products. At 450°C the α -helical conformation collapses and the PLL is decomposed above 500°C.

FT-IR spectra at increasing temperature of PLL2₆₀ (Figure 17b) show some differences respect to the PLL3 one. From a general point of view the PLL structure is stable

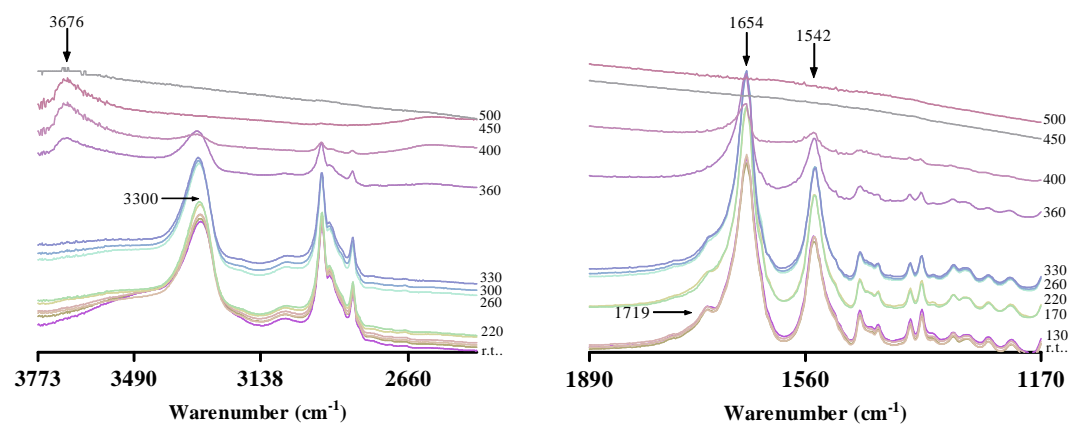
* See relationship between amide I and II bands at increasing temperature in Annex 3, Table 2.

below 400°C , while in PLL3 the PLL structure is conserved up to 450°C . In the temperature region of 25°C - 220°C , spectra show a decrease of the bands around 3480 cm^{-1} and at 3300°C , indicating a constant loss of water, CO , C_4H_8 , NH_3 and HNCO species. At lower frequency, a decrease in the intensity of the component at 1719 cm^{-1} decrease is due to the loss of thermal stability of the secondary PLL structures.

a)



b)



c)

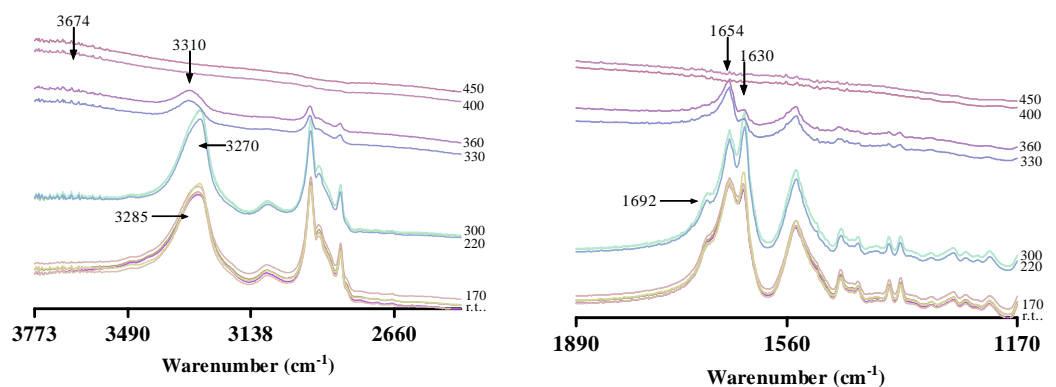


Figure 17 FT-IR spectra under outgassing conditions at increasing temperature in KBr of a) PLL3, b) PLL₂₆₀ and c) PLL4 in the frequency region of (left) 3773 - 2300 cm^{-1} and (right) 1890 - 1170 cm^{-1} .

Comparison between relative intensity of the amide I and II is complex, because amide I band in PLL₂₆₀ is attributed to the α -helical PLL and other secondary components, however, this relationship shows destabilisation of the PLL structure during all thermal evolution. Between 220 and 360°C formation of a band at 3676 cm⁻¹, shifting of the band at 3300 to 3310 cm⁻¹ and total loss of the component at 1719 cm⁻¹, are due to decomposition of secondary PLL structures formed during the synthesis. At 360°C a small shoulder band was detected around 1629 cm⁻¹ due to the formation of decomposition structures. Between 360 and 400°C a widening of the amide I band and its shift to higher frequency is due to the formation of C=O species which are not parts of the α -helical PLL. PLL structure is decomposed above 400°C.

FT-IR spectra of PLL₄ at increasing temperature are shown in Figure 17c. In the temperature range 25-220°C, the band at 3285cm⁻¹ shifts to 3270 cm⁻¹, while the band due to amide I at 1630 cm⁻¹ increases its intensity. As explained below, loss of water increases the intermolecular N-H interactions, in this case of the β -sheet conformation. The component observed at 1692 cm⁻¹ between 220 and 300°C is due to secondary structures formed during the synthesis of PLL₄. Above 330°C the band at 3270 cm⁻¹ shifts to 3310 cm⁻¹, a small band is formed at 3674 cm⁻¹ while the amide I band at 1692 cm⁻¹ drastically decreases. This finding agrees with Kricheldorf who suggested that PLL containing β -sheet conformations are less stable than the α -helical ones [3]. In our observations, decomposition of β -sheet PLL occurs around 330°C while α -PLL structure decomposition occurs above 400°C. In the same way as PLL₂₆₀, a relationship in the relative intensity of amide I and II bands at increasing temperature, shows destabilisation during all thermal treatment (See Annex 3, Table 2).

Simultaneous TG/DTA analyses of PLL₃, PLL₂₆₀ and PLL₆ were also evaluated in order to confirm the results obtained by FT-IR. Table 6 summarises the TG/DTA results. TG/DTA results are totally consistent with FT-IR findings.

Table 6 TG/DTA transformation temperatures and weight losses of PLL₃, PLL₂₆₀ and PLL₄^a

Entry	Material	Temperature range, °C	Max. °C	Weight loss, %	Observations
1	PLL ₃	25-319	-	7.79	*Loss of water absorbed in the PLL structure.
		319-478	451	91.45	*Decomposition of α -PLL structure.
		478-900	-	0.76	*Decomposition of remained CO, CN and CC species

2	PLL ₂₆₀	25-287	255	6.14	*Loss of water absorbed in the PLL structure.
		287-328	-	3.28	*Decomposition of secondary PLL structures.
		328-900	374	91.01	*Decomposition of remained species from secondary PLL structure
			435		*Total decomposition of α -PLL structure.
3	PLL4	25-430	397	70.33	*Decomposition of β -sheet PLL structure.
		430-900	445	25.43	*Mainly decomposition of α -PLL structure.

^aSee TG/DTA curves in Annex 3, Figure 11.

PLL4 material exhibits two closer main weight losses centered at 397 and 445°C (Table 6, entry 3). Although very close weight losses make the quantification difficult, this finding shows that ROP initialised by excess of water allows higher quantity of cyclic and complex PLL than α -helical PLL conformations.

5.2 Thermal evolution of PLL/HT_{rus} nanohybrid materials

Thermal behaviour of the nanohybrid materials synthesised by immobilisation of PLL in HT_{rus} and nanohybrid materials synthesised using HT_{rus} as the initiator are presented in this section.* FT-IR spectra at increasing temperature of IPL3 and IPL₂₆₀ materials are showed in Figure 18. Figure 18a shows the FT-IR spectra of IPL3 material at increasing temperature. From 25°C to 260°C the band at 3378 cm⁻¹ decreases and shifts to 3513 cm⁻¹ due to water loss from the HT structure. Relationship between the relative intensities of the amide I and II bands at increasing temperature shows that the α -helical conformation increases its stability up to 170°C, and above that temperature, the water eliminated from the HT structure interacts with the PLL structure destabilising its α -helical conformation". This behaviour was also confirmed by the shift of the band due to N-H stretching from 3303 cm⁻¹ to 3308 cm⁻¹. At lower frequency, the bands at 1336 and 669 cm⁻¹ decrease due to elimination of CO₂ from the HT structure. Below 1000 cm⁻¹, changes in the bands at 780 and 925 cm⁻¹ are due to changes in the Al-OH bonds by loss of the inorganic anions located in the interlayer space, but it also could be due to changes in the interaction between PLL and HT structures. From 260 to 360°C the band at 3308 cm⁻¹ shifts back at 3304 cm⁻¹ indicating stabilisation of the PLL structure, while the band at 3513 cm⁻¹ shifts to 3568 cm⁻¹ due to continue loss of water

* A complete description of the thermal behaviour of HT_{rus} is presented in Chapter 2, section 2.2.5.

** See relationship between areas of amide I and II bands at increasing temperature in Annex 3, Table 2.

5.2 Thermal evolution of the synthesized materials

5.2 Thermal evolution of PLL/HT_{rus} nanohybrid materials

since the OH⁻ anions from the HT. In this temperature range the relative intensity of the amide I and II bands does not present any variation indicating stability of the α -helical PLL. Finally, in the temperature range 360-550°C and centered around 400°C the decomposition of the PLL is evident by the disappearance of the amide I and II bands. At 2167 cm⁻¹ a new band is formed after decomposition of PLL structure, indicating the formation of C=O species interacting strongly with the oxide surface formed by the thermal treatment. Decrease of the decomposition temperature of the PLL3 after immobilisation is because the excessive presence of water from the HT during the thermal evolution destabilises the α -helical conformation by forming new N-H and O-H bonding between the AA residues and the water molecules.

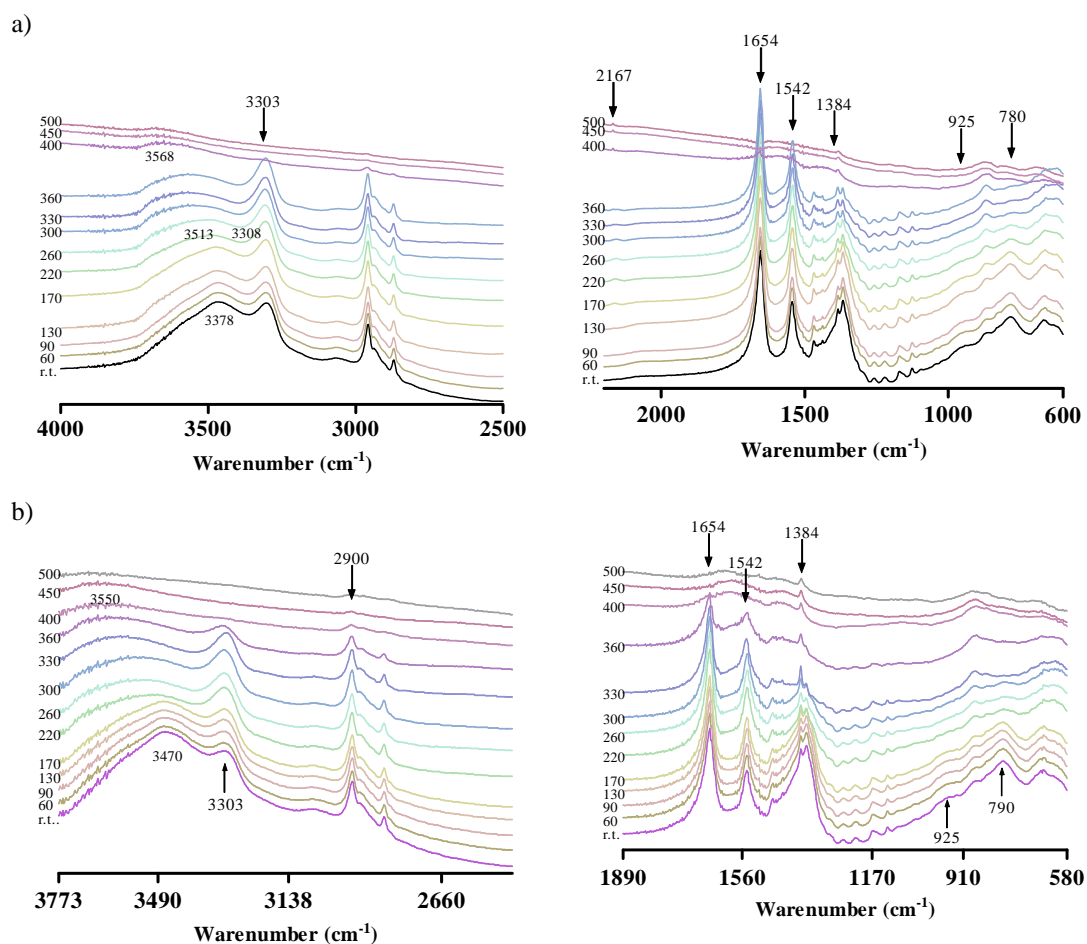


Figure 18 Skeletal FT-IR at increasing temperature of a) IPL3 and b) IPL2₆₀ in the frequency region of (left) 3773-2300 cm⁻¹ and (right) 1890-1170 cm⁻¹.

FT-IR spectra at increasing temperature of IPL2₆₀ are shown in Figure 18b. The thermal evolution of this material is also divided into three main temperature ranges. In the temperature range of 25-170°C the N-H interactions become stronger by elimination of

water from the PLL structure. These changes were observed by an increase of the intensity of the band at 3303 cm⁻¹ and narrow amide I and II bands. Elimination of CO₂ from the HT material is also observed at this temperature through a decrease in intensity of the band at 669 cm⁻¹. Comparison of the relative intensity of the amide I and II bands in this temperature range confirms a similar behaviour for the free PLL3 material, confirming that HT_{rus} only immobilises PLL containing living groups. Moreover, below 170°C the α-helical conformation is perturbed by water from the HT structure. In the temperature range of 170-300°C the band at 3470 cm⁻¹ shifts at higher frequency and it is stabilised at 3550 cm⁻¹. Decrease of the intensity of the bands around 2900 cm⁻¹ indicates loss of species containing C-H bonds, nevertheless the absence of any detectable change in amide I and II bands suggests decomposition of secondary PLL structures obtained in low quantity. Changes at 790 and 925 cm⁻¹ are due to elimination of OH group from the HT structure.

Finally, in the temperature range of 330-500°C the PLL decomposes. TG/DTA results of IPL3 and IPL2₆₀ (Table 7) are in agreement with all FT-IR results. Nevertheless, although no band due to PLL structure was detected above 400°C, TG/DTA results from IPL2₆₀ material exhibit a heat flow at 455°C which is attributed to the CO₂ left in the sample according to the EA results (Table 3, entry 3). In the same way as PLL3, a decrease of the decomposition temperature of the PLL2₆₀ after immobilisation is due to the presence of water during the thermal evolution.

Table 7 TG/DTA transformation temperatures and weight losses of PLL3, PLL2₆₀ and PLL4^a

Entry	Material	Temperature range, °C	Max. °C	Weight loss, %	Observations
1	IPL3	25-240	168 220	13.70	*Loss of water, CO ₂ and NO ₂ from the HT
		240-900	422	43.23	*Dehydroxylation of the HT and decomposition of the PLL structure.
		30-272	234	9.84	*Loss of water absorbed in the PLL structure.
2	IPL2 ₆₀		408		*Dehydroxylation of the HT and decomposition of the PLL structure.
		272-900	455	44.92	*Elimination of CO ₂ remained from the HT structure.

^aSee TG/DTA curves in Annex 3, Figure 12.

Thermal evolution of PLL materials synthesised using HT_{rus} as the initiator (PLL5 and PLL6) are presented in Figures 19 and 20. FT-IR spectra at increasing temperature of

5. Thermal evolution of the synthesized materials

5.2 Thermal evolution of PLL/HT_{rus} nanohybrid materials

PLL5 are shown in Figure 19a. From a general point of view, FT-IR spectra of PLL5 are similar to the PLL4 ones (Figure 15c), nevertheless some changes at increasing temperature were observed. At 330°C, the band due to N-H stretching was stable at 3290 cm⁻¹ while in PLL4 it was detected at 3312 cm⁻¹ at the same temperature. At low frequency the amide I band at 1654 cm⁻¹ was more intense than the one at 1630 cm⁻¹ showing the higher stability of the α -helical PLLs. Above 360°C the PLL decomposes. This result, in comparison with PLL4 and TG/DT analyses, suggests that spectrum at 360°C in PLL5 is not dependable and the total decomposition occurs around 400°C.

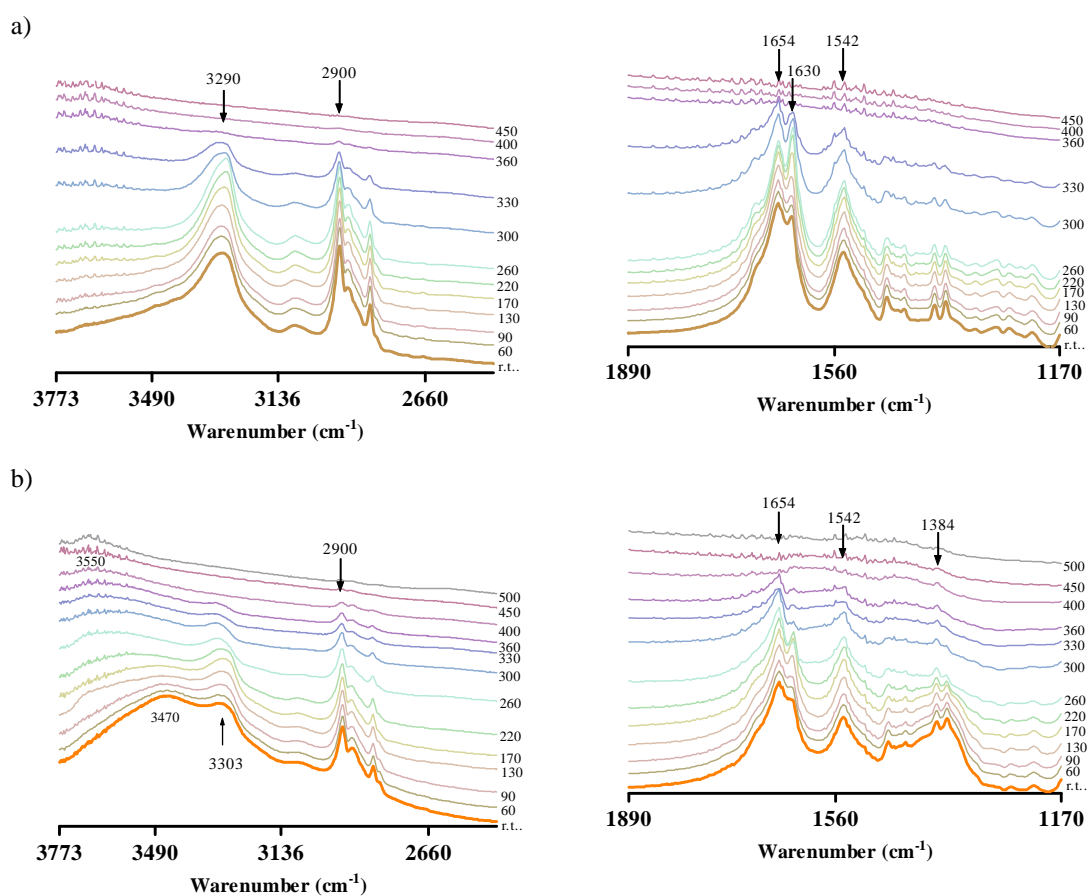


Figure 19 Skeletal FT-IR at increasing temperature of a) PLL5 and b) PLL6 in the frequency region of (left) 3773-2300 cm⁻¹ and (right) 1890-1170 cm⁻¹.

TG/DT analysis (Figure 20) exhibits a total weight loss of 91.56% indicating that 8.48% of the total weight is due to HT_{rus}. Theoretical content of HT_{rus} value is 12.42% which is in agreement with the TG results and suggests that around 70% of the HT_{rus} contribute with the formation of PLL containing living groups *via* enamine mechanism. The part of the HT_{rus} that does not form PLL with living groups is because ROP reaction can also occur *via* activated monomer mechanism forming PLL with NCA endgroups. DTA results show that

the main weight loss presents two heat flows. According with FT-IR results, the first heat flow centered at 388°C is mostly due to decomposition of PLL containing NCA endgroups while the second one at 440°C is due to decomposition of PLL containing living groups.

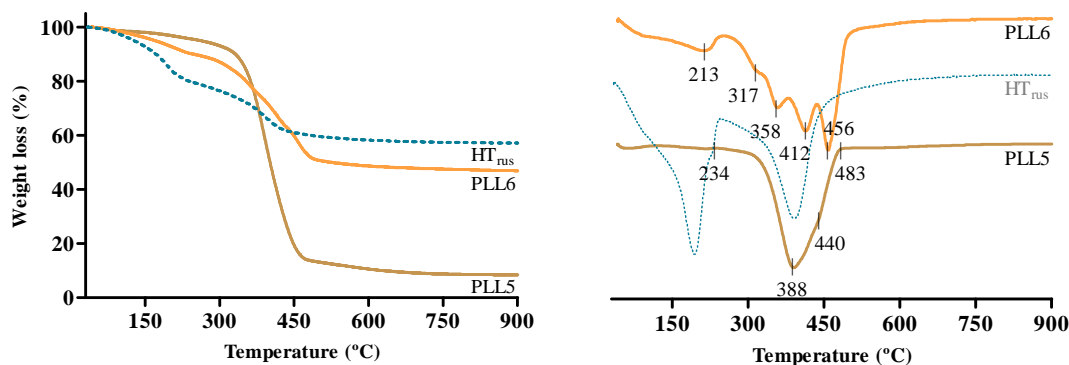


Figure 20 TG (left) and DT (right) experiments of PLL5 and PLL6. TG/DTA curves of HT_{rus} is showed as a reference.

6. Conclusions

Synthesis and characterisation of PLL using triethylamine, water and HT_{rus} as initiators were further investigated together with an extensive investigation of the thermal stability of the synthesised materials. ROP reaction using triethylamine as the initiator allows PLL chains containing NCA endgroups as the main product *via* a monomer activated mechanism, nevertheless under our synthesis conditions, traces of water in the NCA monomer and hydrolysis after PLL synthesis permitted to obtain PLL chains containing living groups as the main product. Rising in the temperature synthesis up to 60°C increased the length of PLL *via* enamine mechanism, producing cyclisation of PLL chains; moreover, high temperatures also gave high reactivity to the ROP which could produce high amount of PLL containing NCA endgroups *via* monomer activated mechanism. We also used water as the initiator to further understand the role of water in the ROP reaction and to compare it with the synthesis of PLL using triethylamine and HT_{rus} as the initiator. Characterisation data confirmed the double effect of water in ROP: water acts as a nucleophile attacking the NCA

monomer and starting the reaction *via* enamine mechanism, nevertheless, water also acts as a base deprotonating NCA monomer starting a secondary ROP *via* activated monomer mechanism. Competition of both mechanisms allowed a complex series of PLL structures containing living and NCA endgroups, but also the possible formation of β -sheet structures and other cyclic species which reduced the Mw of the obtained PLL. Thermal evolution of PLL synthesised using triethylamine as the initiator shown temperature resistance up to 500°C, while PLL synthesised using water as initiator showed lower thermal resistance due to presence of secondary PLL structures which descomposed below 400°C.

We also presented here, the synthesis of PLL using HT_{rus} as the initiator. Two materials were synthesised to understand the role of the HT_{rus} used as initiator in ROP, one of them using lower amounts of HT_{rus} (M/I = 10) and the second one using excess of initiator. Similar to PLL synthesised using water, ROP of PLL using lower amount of HT_{rus} was directed by three possible mechanisms: enamine, carbamate and monomer activated, producing different PLL structures. Our results show that around of 70% of the used HT_{rus} produces PLL containing an amino and a HT-carboxylate endgroups. Using HT_{rus} in excess (M/I = 0.5), ROP enamine and monomer activated mechanism were favoured and several secondary PLL structures were obtained in a similar way as using water as the initiator. In both cases, obtained PLL were immobilised in the interlayer space of the HT and stabilised by H-bonding interaction between the PLL structures and the HT layers.

Further investigation about the nature of the PLL after immobilisation in HT_{rus} indicates that the cationic nature of the HT layers permitted the immobilisation of PLL containing living groups by an anionic exchange reaction through OH⁻ anions located in the interlayer space and the carboxylate group of the PLL. This means that the immobilisation process is favoured only for PLL containing living groups as it was evaluated by MALDI-TOF and FT-IR experiments. The results also indicated that immobilisation of PLL occurs in the interlayer space from the HT_{rus} without destabilisation of the α -helical conformation. Moreover, the PLL chains were stabilised by H-bonding between the backbone α -helical PLL structure and the M-OH from the HT structure. Detection of cyclic-PLL immobilised in HT_{rus} could due to nucleophile attack of the OH⁻ from the HT_{rus} to the NCA ended group of PLL chains. That attack favors the growing of PLL chains and also induces the cyclisation of

the synthesised PLLs. This attack favours the growth of PLL chains and also induces the cyclisation of the synthesised PLLs. Further investigation on the role of the initiator in the synthesis of PLL allows a better understanding of the immobilisation nature of PLL in HT precursor, which could be escalated to more complex structures such as proteins and enzymes immobilised in other inorganic supports. Moreover, bio-nanohybrid materials based on complex biomolecules and HT supports allow an interesting topic about the use of these kinds of materials in several fields.

Finally, synthesis and characterisation of PLL and PLL/HT materials presented in this section was included in one article which is currently under revision:

- “*Synthesis and Characterisation of Poly-L-Leucine Initialised and Immobilised by Rehydrated Hydrotalcite. Understanding of the Stability and Interaction Nature*”. Ronald-Alexander Miranda, Elisabetta Finocchio, Francisco Medina, Gianguido Ramis, Jesús E. Sueiras, Jordi Llorca and Anna M. Segarra

References

- [1] J.C.M. van Hest and D.A. Tirrell. *Chem. Commun.* **2001**, 19, 1897
- [2] T.J. Deming. *Prog. Polym. Sci.* **2007**, 32, 858
- [3] S. Juliá, J. Guixer, J. Masana, J. Rocas, S. Colonna, R. Annuziata and H. Molinari. *J. Chem. Soc. Perkin Trans. 1.* **1982**, 1317
- [4] L. Christelle and S. Roberts. *Aldrichimica.* **2002**, 35, 47
- [5] A. Berkessel, N. Gasch, K. Glaubitz and C. Koch. *Org. Lett.* **2001**, 3, 3839
- [6] D. Kelly and S. Roberts. *Chem. Commun.* **2004**, 2018
- [7] G. Carrea, S. Colonna, D.R. Kelly, A. Lazcano, G. Ottolina and S.M. Roberts. *Trends in Biotech.* **2005**, 23, 507
- [8] D. Kelly and S. Roberts. *Biopolymers.* **2006**, 84, 74
- [9] H.R. Kricheldorf. *Angew. Chem. Int. Ed.* **2006**, 45, 5752
- [10] N.N.M.B. Smeets, P.L.J. van der Weide, J.Meuldijk, J.A.J.M. Vekemans and L.A. Hulshof. *Org. Process. Res. Dev.* **2005**, 9, 757
- [11] H. Sekiguchi. *Pure Appl. Chem.* **1981**, 53, 1689
- [12] T. Deming. *Adv. Polym. Sci.* **2006**, 202, 1

6. Conclusions
- [13] W.N. E. van Dijk-Wolthuis, L. van de Water, P. van de Wetering, M. van Steenberghe, J.J.K. van den Bosch, W. Schuyl and W.E. Hennink. *Macromol. Chem. Phys.* **1997**, *198*, 3893
- [14] E.R. Blout and R.H. Karlson. *J. Am. Chem. Soc.* **1956**, *78*, 941
- [15] H. R. Kricheldorf, C. von Lossow and G. Schwarz. *J. Polym. Sci. A.* **2006**, *44*, 4680
- [16] A. Corma, V. Fornés, R.M. Martín-Aranda and F. Rey. *J. Catal.* **1992**, *134*, 58
- [17] D. Tichit, M.H. Lhouty, A. Guida, B.H. Chiche, F. Figueras, A. Auroux, D. Bartalini and E. Garrone. *J. Catal.* **1995**, *151*, 50
- [18] J. Lee, S.-J. Lee, J.-Y. Choi, J.Y. Yoo and C.-H. Ahn. *Eur. J. Pharm. Science.* **2005**, *24*, 441
- [19] H. R. Kricheldorf. *Macromol. Rapid Commun.* **2009**, *30*, 1371
- [20] H.R. Kricheldorf, C.V. Lossow, N. Lomadze, G. Schwarz. *J. Polymer Sci. Chem.* **2008**, *46*, 4012
- [21] H. R. Kricheldorf, C. von Lossow and G. Schwarz. *Macromol. Chem. Phys.* **2005**, *206*, 282
- [22] H.R. Kricheldorf, C. von Lossow and G. Schwarz. *J. Polymer Sci. A.* **2005**, *43*, 5690
- [23] T. Geller, A. Garlach, C.M. Krüger and H.-C. Militzer. *J. Mol. Catal. A.* **2006**, *251*, 71
- [24] E.R. Blout, C. de Lozé, S.M. Bloom and G.D. Fasman. *J. Am. Chem. Soc.* **1960**, 3787
- [25] S. M. Barlow, S. Haq, and R. Raval. *Langmuir.* **2001**, *17*, 3292
- [26] E.S. Manas, Z. Getahun, W.W. Wright, W.F. DeGrado and J.M. Vanderkooi. *J. Am. Chem. Soc.* **2000**, *122*, 9883
- [27] S. Miyata. *Clay and Clays miner.* **1980**, *28*, 50
- [28] F. Cavani, F. Trifirò and A. Vaccari. *Catal. Today.* **1991**, *11*, 173
- [29] E.S. Manas, Z. Getahun, W.W. Wright, W.F. DeGrado and J.M. Vanderkooi. *J. Am. Chem. Soc.* **2000**, *122*, 9883
- [30] S. Aisawa, S. Sasaki, S. Takahashi, H. Hirahara, H. Nakayama and E. Narita. *J. Phys. Chem. Sol.* **2006**, *67*, 920
- [31] T.J. Deming. *Adv. Mater.* **1997**, *9*, 299
- [32] K.-M. Hansson, L.-E. Amand, A. Habermann and F. Winter. *Fuel.* **2003**, *82*, 653

NANOHYBRID MATERIALS BASED ON PLL AND HTs AS CATALYSTS IN FINE CHEMISTRY REACTIONS

Industry favours heterogeneous catalytic processes over the homogeneous ones. Many reports have shown that it is possible to design and produce new chiral catalytic systems that have obvious advantages over their homogeneous counterparts: they are easy handling, they can induce asymmetry, they can be removed from the reaction mixture by simple separation methods and, in many cases, they can be recycled and reused. The asymmetric epoxidation of α,β -unsaturated ketones is an important organic transformation since the resulting chiral epoxy ketones are versatile precursors to many natural products and drug molecules. In the direction of heterogenisation, PAAs immobilised on naturally occurring clay minerals, designed and synthesised by simple process of anchoring, can be considered as a potential effective and efficient solution.

This chapter describes, for the first time, the used of the synthesised PLLs/HTs as a truly recyclable bionanohybrid catalyst in the asymmetric Juliá-Colonna epoxidation reaction of α,β -unsaturated ketones and, as a step beyond, in the one-pot production of chiral α,β -epoxides from benzaldehydes and acetophenones.

-
- 1. Initial Considerations**
 - 2. PLL/HT Nanohybrid Materials as Catalyst in Asymmetric Juliá-Colonna Epoxidation Reaction**
 - 2.1 Experimental
 - 2.2 Results and discussion
 - 3. PLL/HT Nanohybrid Materials as Catalyst in Claisen-Schmidt-Juliá-Colonna- Reaction**
 - 3.1 Experimental
 - 3.2 Preliminary results and discussion
 - 4. Conclusions**
 - References**
-

1. Initial Considerations

The catalytic asymmetric epoxidation provides a way of transforming unsaturated molecules into optically enriched epoxides. Through different synthetic routes the chiral epoxide can be also transformed in a wide number of symmetric and asymmetric drugs of industrial interest [1-11].

Synthetic PAAs like PLLs are known as excellent catalysts for the asymmetric Juliá-Colonna epoxidation reaction [12,13], obtaining enantiomerically enriched α,β -epoxy ketones. Nevertheless, the original triphasic protocol (PAA-aqueous phase-organic phase) had two important problems, the lengthy reaction time and the difficulties in recovering the gel or paste-like catalyst obtained after reaction. To overcome these limitations Roberts *et al.* reported a non-aqueous biphasic system using organic bases and anhydrous urea-hydrogen peroxide [14] and a PAA on Silica as the catalyst (PaaSiCat) protocol [15]. Under PaaSiCat protocol the reaction time was reduced to 4 hours and yielded optically active epoxydes with enantioselectivity up to 97 % ee. Roberts *et al.* also reported the synthesis of PLLs immobilised on polyethylene glycol (PEG)-PLL obtained conversions up to 80% with enantioselectivities of 98% in 24 hours of reaction [16]. In spite of these improvements, the potential industrial application of these protocols have still some problems related with the time consuming catalyst pre-activation, which has to be carried out separately and difficulties in the work-up process. Other important improvements were achieved by Geller *et al.* who presented a modified triphasic protocol, in which addition of a phase transfer co-catalyst (PTC) improved the reaction rates up to 30 minutes using Poly-L-leucine-1,3-diaminopropane as the catalyst [17]. Using that protocol no separate pre-activation of the catalyst was required. The heterogenised catalysts shown in the literature permitted the recovery and reuse of the catalytic system, making the heterogenised PLL catalyst preferred over the non immobilised PLL ones. However, the catalytic epoxidation required long reaction times or the PLL was functionalised by long synthetic protocols. Additionally, although Juliá-Colonna epoxidation mechanism is not clear in all its aspects, several studies suggest that the five terminal L-Leu residues of the α -helical PLL play an important role in its catalytic activity and

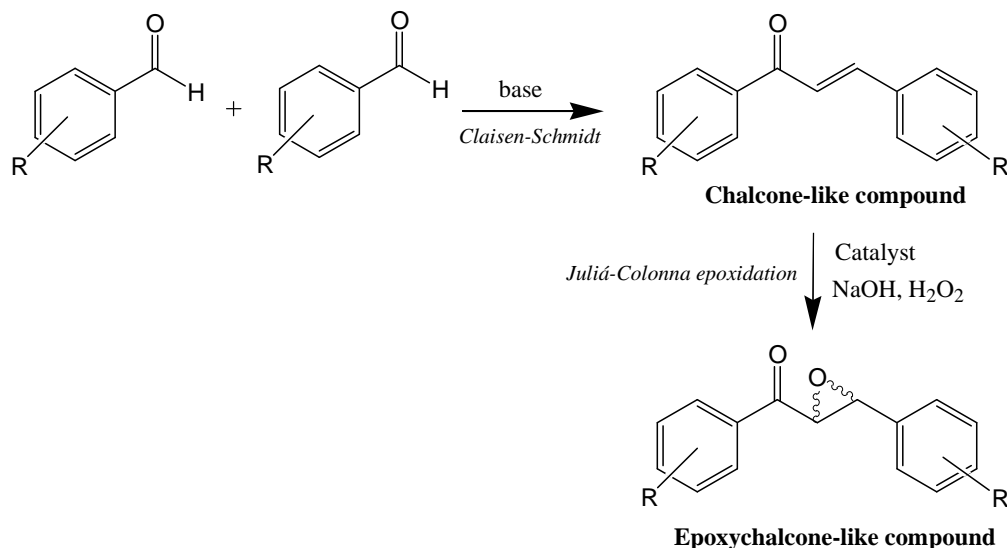
enantioselectivity. These results also suggest that COOH-terminal group does not participate in the catalytic process [13, 18].

On the other hand, Claisen-Schmidt condensation is a kind of aldol condensation which provides a way to obtain α,β -unsaturated ketones. α,β -Unsaturated ketones also called chalcones are synthesised in Nature by plants and have many uses in pharmaceutical and fine chemical industries [5, 19-23]. Artificially, synthesis of chalcones is usually performed through Claisen-Schmidt condensation using alkaline hydroxides or sodium ethoxide with reaction times of 12-15 hours (Scheme 1) [24].

Nowadays, environment-friendly solid base materials such as HTs have been used as catalysts in Claisen-Schmidt reaction to replace soluble bases and hydroxides, preventing also collateral reactions [25-26]. In that context, several authors have published different protocols for the synthesis of chalcones. Tichit *et al.* reported the kinetic study on the synthesis of chalcone using MgO and rehydrated HTs [27]. Rehydrated HTs showed better conversion and selectivity than MgO. Tichit explained this behaviour because the hydroxyl anions located on the edges of the HTs play an important role in the initial activation by deprotonation of acetophenone. Moreover, the role of the solvent in this reaction was also investigated confirming that acidity in solvents reduces the activity of the HTs by poisoning of the strong basic centers. De Jong *et al.* and Medina *et al.* reported the synthesis of different more active HT materials showing that variations in the rehydration process leads to materials with more or less amounts of active basic centers and with different basic strength [28-29]. Specifically Medina *et al.*, developed a new hydrotalcite type by rehydration of the mixed oxides under ultrasounds, which contains stronger and more accessible OH interlayer anions as active basic sites [30]. One disadvantage of using HTs as the catalyst in C-C bond-forming reactions is the acid-base character of the layers. Both, strong basic centers and metals located on the surface are able to catalyse side-reactions such as self-condensation of ketones or condensation between the reagent and the formed chalcone [27]. Regrettably not much information about secondary products has been reported.

In this context, it seemed interesting to apply the immobilised PLL catalysts (Chapter 4) in the Juliá-Colonna epoxidation reaction under PTC/triphasic conditions. And also, in the Claisen-Schmidt-Juliá-Colonna one-pot reaction (Scheme 2). Moreover, the immobilised

catalytic reactions would provide excellent stability of the bionanohybrid catalysts, complementary host-guest synergistic effect and a clean economic methodology for synthesising chiral epoxide compounds.



Scheme 1 Claisen-Schmidt-Juliá-Colonna one-pot reaction

2. PLL/HT Nanohybrid Materials as Catalyst in Asymmetric Juliá-Colonna Epoxidation Reaction

2.1 Experimental

2.1.1 Synthesis of PLL and PLL/HT materials

PLL materials were synthesized by ROP using triethylamine as the initiator in accordance with the protocol presented in Chapter 4, sections 2.1.1 and 2.1.2. Rehydrated Hydrotalcite under ultrasound treatment (HT_{rus}) was obtained in accordance with the protocol exposed in Chapter 2, section 2.1.1 [30]. PLL/HT nanohybrid materials were prepared by anion-exchange method as described in Chapter 4, section 3.1.2. Table 1 shows a list of the PLLs and PLL/HT nanohybrid materials used in this section. One additional PLL/HT materials was synthesised following the protocol exposed in Chapter 4, section 3.1.2 using commercially available PLL supplied by Acros Organics (Ref. 327580010) whose synthesis was reported by Geller *et al.* in reference [22]. A schematic representation of

2.2 Results and results

synthesised PLL (PLL_S) containing living groups and commercially available PLL (PLL_C) is presented in Figure 1.

Table 1 Synthesis of PLLs used as catalysts

Entry ^a	Material	T / °C	M/I ratio	Monomer Distribution ^{b,c}	Mw ^c	PD ^c
1	PLL _C ^d	-	-	5-39	2343	1.26
2	PLL1	25	10	2-39	2212	1.57
3	PLL2	25	5	2-39	2405	1.51
4	PLL3	25	2.5	2-37	2249	1.46
5	PLL1 ^d	25	10	5-42	2275	1.47
6	PLL1 ₆₀	60	10	5-42	2456	1.43
7	PLL2 ₆₀	60	5	5-38	2303	1.49

^aSee details for synthesis conditions in Chapter 3, sections 2.1.1 and 2.1.2. ^bDeterminate by ESI-TOF MS analyses. ^cDeterminate by MALDI-TOF analysis. ^dSee details of synthesis in Ref [22] ^ePLL was washed several times with chloroform after synthesis.

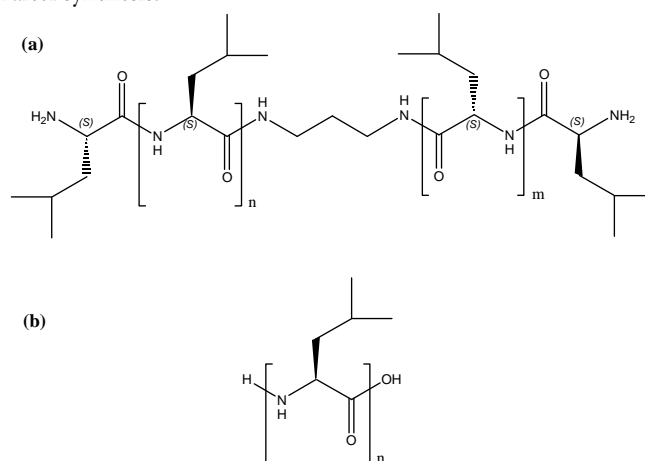


Figure 1 Molecular structures of poly-amino acids a) PLL_C from Acros Organics and b) synthesised PLL_S

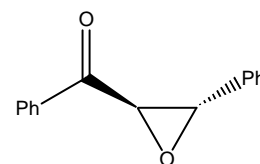
2.1.2 Asymmetric Julia-Colonna epoxidation reaction

The asymmetric epoxidation reaction was performed in a tube of 10 mL where synthesised PLL or PLL/HT_{rus} (200 wt.% of PLL, 100 mg), tetrabutylammonium bromide, TBAB, (0.004 mmol, 1.3 mg), NaOH 2M and toluene (0.5 mL) were mixed. Subsequently, H₂O_{2(aq)} (30 wt%, 40.6 μL) and chalcone (0.036 mmol, 7.7 mg) were added. The mixture was stirred at room temperature for the indicated time. The mixture was then diluted in 1 mL of ethylacetate for work-up. The liquid phase was separated by centrifugation and extracted into ethyl acetate. The catalyst (solid phase) was washed several times with toluene. The organic fraction was dried with MgSO₄ and separated by

filtration. Then, the solvent in the organic phase was evaporated. The reusability of the catalysts was assessed by reusing them for five consecutive runs. The products were identified by ^1H NMR.

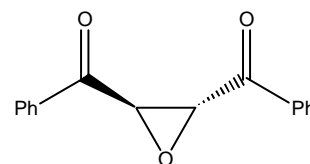
***trans*-(2R,3S)-Epoxy-1,3-diphenyl-propan-1-one (1)**

^1H NMR (400 MHz, CDCl_3) δ = 4.01 (s, 1H), 4.23 (s, 1H), 7.32-7.45 (m, 7H), 7.54 (d, 1H), 7.94 (d, 2H) ppm. The ee of *trans*-(2R,3S)-(1) was determined by chiral HPLC (ChiralPak IA column, EtOH/hexane = 25/75), UV 254 nm, flow rate of 1 mL/min.. (S,R)-isomer, $t_{(R,S)}$ = 7.6 min. and (R,S)-isomer, $t_{(R,S)}$ = 10.6 min.



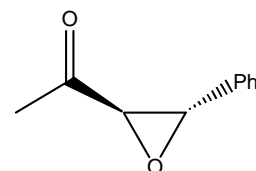
***trans*-(2R,3S)-Epoxy-1,4-diphenylbutan-1,4-one (2)**

^1H NMR (400 MHz, CDCl_3) δ = 4.49 (s, 2H), 7.52 (m, 4H), 7.65 (m, 2H), 8.06 (m, 4H) ppm. The ee determined by HPLC (ChiralPak IA column, i-prOH/hexane = 10/90), UV 254 nm, flow rate of 1 mL/min. (S,R)-isomer, $t_{(R,S)}$ = 18.8 min. and (R,S)-isomer, $t_{(R,S)}$ = 29.6 min.



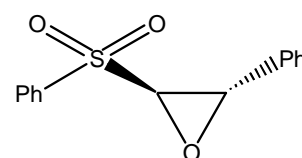
***trans*-(3R,4S)-Epoxy-4-phenyl-2-butanone (3)**

^1H NMR (400 MHz, CDCl_3) δ = 2.16 (s, 1H), 3.47 (d, 1H), 3.98 (d, 1H), 7.35-7.24 (m, 5H) ppm. The ee determined by HPLC (ChiralPak IA column, i-prOH/hexane = 10/90), UV 254 nm, flow rate of 1 mL/min. (S,R)-isomer, $t_{(R,S)}$ = 24.5 min. and (R,S)-isomer, $t_{(R,S)}$ = 32.5 min.



***trans*-(2R,3S)-1-phenyl-3-phenylsulfonyl-oxirane (4)**

^1H NMR (400 MHz, CDCl_3) δ = 4.19 (d, 1H), 4.59 (d, 1H), 7.28-7.24 (m, 2H), 7.38-7.32 (m, 3H), 7.65-7.60 (m, 2H), 7.76-7.71 (m, 1H), 8.02-7.98 (m, 2H) ppm. The ee determined by HPLC (ChiralPak IA column, i-prOH/hexane = 10/90), UV 254 nm, flow rate of 0.4 mL/min. (S,R)-isomer, $t_{(R,S)}$ = 45.3 min. and (R,S)-isomer, $t_{(R,S)}$ = 20.9 min.



2.2 Results and results

2.2 Results and discussion

2.2.1 Asymmetric catalytic Juliá-Colonna epoxidation with non immobilised PLLs

As explained in Chapter 4, differences in the synthesis conditions (temperature, M/I ratio) do not affect structural properties and the Mw of the PLL_{Syn} which in all cases are similar to those of the commercial PLL_C (Table 1). PLL_S synthesised at room temperature presented monomer distributions with oligomers from two residues (Table 1, entries 2-4). For the catalytic application, the more soluble oligomers were removed after washing with chloroform (Table 1, entry 5). One study about the influence of the solvent in the immobilisation process was also reported in this section and the results are summarised in Annex 3, Table 3 and Figures 13-15.

The methodology used for PLL synthesis turned out to be of crucial importance for all the developed Juliá-Colonna protocols [24]. The different PLL synthesised were therefore tested using the standard test reaction of chalcone (**5**). The results were compared with those of PLL under the same conditions (Table 2).

Table 2 Asymmetric epoxidation reaction catalysed by PLL

Entry ^a	Catalyst	Conversion (%) ^b	e.e. (%) ^b
1	-	< 2	-
2	L-leu	< 2	-
3	NCA	< 2	-
4	PLL _C	85	95
5	PLL1	27	87
6	PLL2	45	85
7	PLL3	37	91
8 ^d	PLL1	99	93
9	PLL1 ₆₀	91	94
10	PLL2 ₆₀	90	92

^aStandard conditions: Chalcone 7.7 mg (0.036 mmol), catalyst 100 mg (200 wt.% of PLL#), H₂O₂ 97.2 μL (30 wt.%, 28.5 equiv.), NaOH 2 M 75.6 μL (4.2 equiv.), TBAB 1.3 mg (0.004 mmol) in toluene (0.5 mL); 1.5 h reaction time, room temperature. Total diastereoselectivity towards *trans*-(**1**). ^bDetermined by ¹H NMR. ^cEnantiomeric excess towards the *trans*-(2R, 3S)-(1) determined by chiral HPLC. ^dUsing PLL previously washed with chloroform.

In agreement with Geller's studies, polymers synthesised at increasing temperature (PLL₁₆₀ and PLL₂₆₀) were considerably more active in the asymmetric epoxidation than those synthesised at room temperature and slightly more active than the PLL_C. PLL_S synthesised at room temperature showed lower activity due to the presence of oligomers with a smaller sized chain (<5 monomers). Nevertheless, after the dimmers, trimmers and tetramers were eliminated by means of chloroform washing, the conversion rate and enantioselectivity increased significantly, up to 99% and 93%, respectively (Table 2, entry 8).

This is because the oligomers with less than five monomers do not have any catalytic properties, as proposed by Berkessel *et al.* [31]. In order to optimise the reaction conditions, further epoxidation reactions were carried out to maximise the activity of all PLL_S. Table 3 shows the results.

Table 3 Optimisation of asymmetric epoxidation reaction conditions catalysed by PLL

Entry ^a	Catalyst	Conversion (%) ^b	ee (%) ^c
1	-	< 4	-
2	L-leu	< 4	-
3	NCA	< 4	-
4	HT _{rus}	6	-
5	PLL _C	97	92
6	PLL ₁	98	90
7	PLL ₂	98	92
8	PLL ₃	98	93
9	PLL ₁₆₀	94	94
10	PLL ₂₆₀	95	93

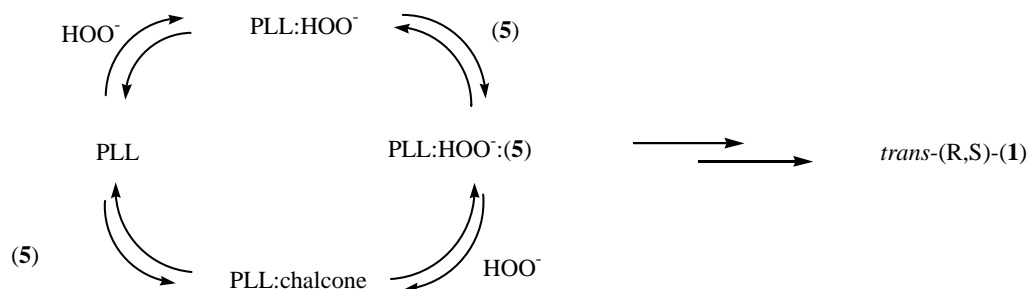
^aStandard conditions: (*E*)-(5) 7.7 mg (0.036 mmol), catalyst 100 mg (200 wt.% of PLL#), H₂O₂ 40.6 μL (30 wt.%, 11.9 equiv.), NaOH 2 M 0.18 mL (10 equiv.), TBAB 1.3 mg (0.004 mmol) in toluene (0.5 mL); 0.5 hour reaction time, room temperature. Total diastereoselectivity towards *trans*-(1).

^bDetermined by ¹H NMR. ^cEnantiomeric excess towards the *trans*-(2R, 3S)-(1) determined by chiral HPLC.

Interestingly, for all PLL_S, the optimised methodology reduced the reaction time to 30 min. In addition, the synthesised catalysts were highly active yet did not require previous chloroform washing. These interesting results can be explained according to the mechanistic studies of Colonna *et al.* (Scheme 2) [32]. Colonna *et al.* found that both hydrogen peroxide and the substrate exhibit inhibitory behaviour due to the competition of different pathways. Nevertheless, under our conditions, kinetic saturation could be overcome by decreasing

2.2 Results and results

competition and favouring the formation of the PLL:HOO⁻:chalcone complex which leads to the formation of *trans*-(2R,3S)-(1).



Scheme 2 Mechanism of PLL-catalysed asymmetric epoxidation reaction

To widen the scope of the new catalysts (PLL₂₆₀ and IPL₂₆₀), some further epoxidation reactions were carried out to broaden the substrate range using the same conditions as chalcone (Table 4). As the test substrates were chosen those exhibited low reactivity under standard triphasic conditions [7,15,32] and much faster conversions under new triphasic/PTC conditions [17].

Table 4 Epoxidation of different enones

Entry ^a	Product	Conversion (%) ^d	ee (%) ^e	Time referent experiment (min.)
1 ^b	(R,S)-(2)	> 99 (> 99)	62 (92)	8
2 ^c		99	61	
3 ^b	(R,S)-(3)	39 (65)	62 (64)	60
4 ^c		32	64	
5 ^b	(R,S)-(4)	30 (82)	19 (68)	120
6 ^c		22	13	

^aStandard conditions: 0.036 mmol substrate, 200 wt.% of catalyst, H₂O₂ 40.6 μL (30 wt.%, 11.9 equiv.), NaOH 2 M 0.18 mL (10 equiv.), TBAB 1.3 mg (0.004 mmol) in toluene (0.5 mL); 0.5 hour reaction time, r.t. ^bPLL₂₆₀. ^cIPL₂₆₀. ^dDetermined by ¹H NMR. ^eEnantiomeric excess towards the *trans*-(2R,3S)-epoxide determined by chiral HPLC and ¹H NMR; results of Ref. [17] experiments are given in brackets.

The new catalysts in the triphasic/PTC conditions showed slightly higher activity when the reaction was performed using the non immobilised catalyst. Also, they show similar enantioselectivities in either PLL₂₆₀ or IPL₂₆₀ catalysts. On the other hand, the *trans*-1,4-diphenyl-2-butene-1,4-dione shows activities comparable with to those reported in Geller and coworker's results, but the enantioselectivities are significantly lowers (Table 4, entries 1 and

2). It is important take into account that the reaction times in the epoxidation of phenyl *trans*-styryl sulfone (Table 4, entries 3 and 4) and phenyl *trans*-4-phenyl-3-buten-2-one (Table 4, Entries 5 and 6) are two and four time lower, respectively, than in Geller's experiment. In addition, the NaOH/TBAB ratio is different. Taken together these facts could explain the poorer activity observed with the PLL₂₆₀ and IPL₂₆₀ catalysts.

Due to the similar catalytic properties in the optimised conditions of the differents synthesised catalysts showed in Table 3, the polymer PLL₂₆₀ and the immobilised counterpart, IPL₂₆₀, were selected the model catalysts.

2.2.2 Asymmetric catalytic Juliá-Colonna epoxidation with nanohybrid PLLs: reusability of nanohybrid materials

We studied the potential of IPL₂₆₀ and IPL_C nanohybrid materials in the asymmetric epoxidation reaction of (5) in which both materials were synthesised following the same immobilisation procedure. We evaluated the new nanohybrid catalyst or synzymes under optimised conditions for 1 hour of reaction (Figure 2). The activity of the basic catalyst Mg/Al 2:1 rehydrated under ultrasounds (HT_{rus}) was also tested in the epoxidation reaction of (5) in Chapter 3 presenting a very poor activity (6%).

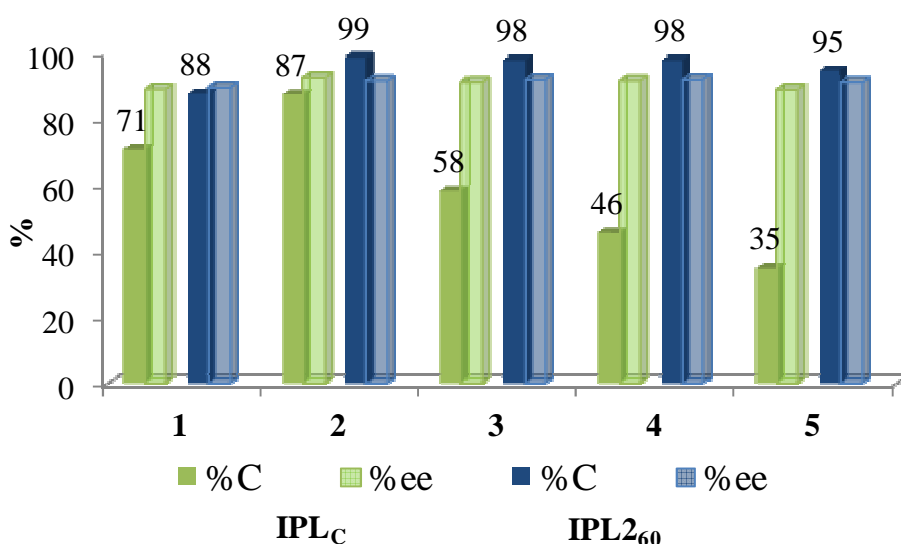


Figure 2 Reusability of IPL_C (green) and IPL₂₆₀ (blue). Reaction conditions: 10 equiv. NaOH 2M, 11.9 equiv. H₂O₂ (30 wt.%), during 1 hour at r.t. Total diastereoselectivity and enantioselectivity towards *trans*-(R,S)-(1).

2.2 Results and results

Figure 2 shows that the activity and selectivity of the IPL_C and IPL₂₆₀ nanohybrid materials decreases slightly in the first run if compared to the corresponding non immobilised PLL_C and PLL₂₆₀. In the case of the nanohybrid based on synthesised PLL, PLL₂₆₀, comparable values for activity and stereoselectivity were obtained from the second run. These remained constant after the organic phase was removed by simple centrifugation, and the epoxidation-recycling cycle was repeated for at least five consecutive runs.

A remarkable difference in reusability was observed when the nanohybrid material was prepared from PLL_C. The conversion rate and enantiomeric excess decreased significantly upon reuse. This was due to leaching of the PLL_C because no basal peaks of the (003) and (006) planes of the PLL intercalated into HT_{rus} were observed in the XRD pattern of the IPL_C after five consecutive runs (Figure 3). The decrease in activity using IPL_C as the catalyst confirmed the poor stabilisation of PLL_C onto HT_{rus}, because of the absence of C-terminal groups in the PLL_C.

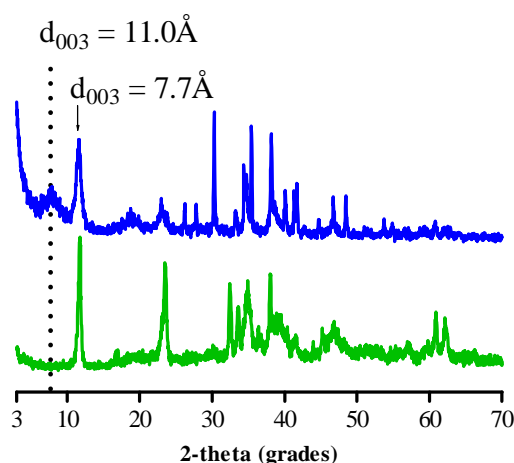


Figure 3 XRD patterns of a) IPL₂₆₀ and b) IPL_C after five consecutive runs. Basal peaks of (003) and (006) plane of HT with immobilized PLL. Additional peaks correspond to sodium carbonate phase (JCPDS: 19-1130)

After the final run, used catalysts were also characterised by HRTEM. These results show differences between the fresh and reused IPL₂₆₀ and IPL_C catalysts (Figure 4). The interlayer space of HT_{rus} in the IPL₂₆₀ material is better preserved after five consecutive runs (Figure 4b). Nevertheless, the HRTEM image of reused IPL_C catalyst also reveals that the lattice fringe at 11.1 Å observed in the fresh catalyst disappeared after the fifth consecutive run. Interestingly, the (003) plane of the HT structure was centered at 7.6 Å (Figure 4d).

These results are in agreement with the XRD analysis of the reused IPL₂₆₀ and IPL_C catalysts (Figure 3), which indicates that IPL_C material, containing PLL_C without any C-terminal groups, is no longer intercalated between the HT layers.

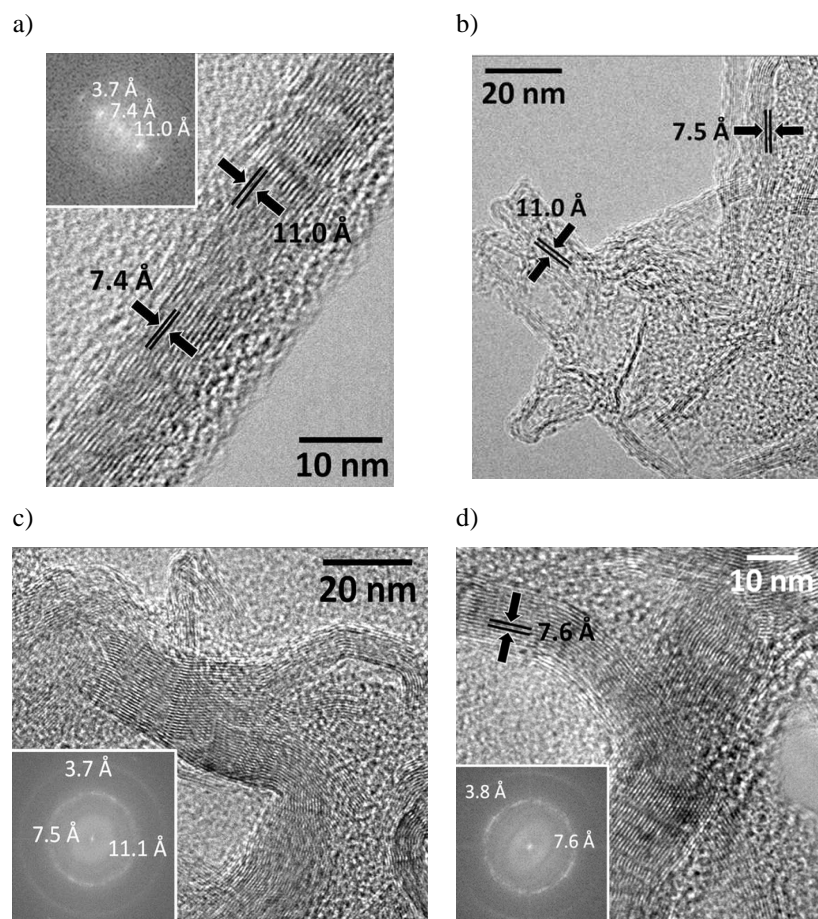


Figure 4 HRTEM images of (b) IPL₂₆₀ and (d) IPL_C after five consecutive runs. Fresh (a) PLL₂₆₀ and (c) PLL_C are shown as a reference.

In order to understand the lower activity during the first run with the IPL₂₆₀ catalyst, simultaneous TG/DTA analyses of pure HT_{rus}, fresh IPL₂₆₀, IPL₂₆₀ after first run and IPL₂₆₀ after the second consecutive run were performed. Table 5 shows the total weight loss from the TGA analysis for all these compounds. In concordance with the results shown in Chapter 2, section 2.2.4, HT_{rus} exhibited total weight loss of 42.9%, while after immobilisation of PLL₂₆₀ the total weight loss increased to 52.1%. Differences in these values (9.25%) correspond to the initial content of PLL₂₆₀ in the fresh IPL₂₆₀.

After the first run and several washes with ethylacetate and toluene, the content of PLL decreases to 1.57%, while after the second consecutive run, there are no significant leaching losses of the PLL. This fact could explain the different activity observed during the

2.2 Results and results

first run of the epoxidation of chalcone using IPL2₆₀ as the catalyst due to the necessity of a pre-activation in the first run as also observed by Geller *et al.* [17].

Table 5 Total weight loss of IPL2₆₀ nanohybrid material used as catalyst

Material	Total weight loss (% w/w) ^a
HT _{rus}	42.9
PLL2 ₆₀	100.0
IPL2 ₆₀	52.1
IPL2 ₆₀ after 1 st run	50.6
IPL2 ₆₀ after 2 nd run	49.6

^aResults obtained by TGA analysis

3. PLL/HT Nanohybrid Materials as Catalyst in Claisen-Schmidt-Juliá-Colonna one-pot Reaction

3.1 Experimental

3.1.1 Synthesis of materials

Calcined hydrotalcite (HT_{cc}) was obtained by calcination of as-synthesised HTs containing nitrate anions (HT_{asym}) at 450°C overnight. Rehydrated Hydrotalcite under ultrasound treatment (HT_{rus}) was obtained in accordance with the protocol exposed in Chapter 2, section 2.1.1. PLL2₆₀ was synthesised by ROP using triethylamine as initiator at 60°C in accordance with the protocol presented in Chapter 4, section 2.1.1 and 2.1.2. Immobilising of PLL2₆₀ in HT_{rus} (IPL2₆₀) was performed by anion-exchange as described in Chapter 4, section 3.1.2.

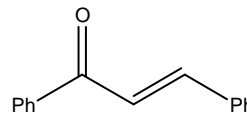
3.1.2 Claisen-Schmidt reaction

Typical Claisen-Schmidt reaction was performed in a tube of 10 mL where benzaldehyde (40.5 µL, 0.39 mmol), acetophenone (44.4 µL, 0.37 mmol), water (315 µL) and the indicated catalyst were added. The mixture was stirred at indicated temperature for 3 hours. The mixture was diluted in 1 mL of ethylacetate for the work-up. The catalyst (solid phase) was washed several times with toluene. The organic fraction was dried with

MgSO₄ and, separated by filtration. Then, the solvent in the organic phase was evaporated. Products were identified by ¹H NMR.

1,3-Diphenyl-2-propen-1-one (5)

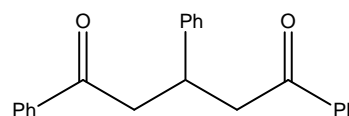
¹H NMR (400 MHz, CDCl₃) δ = 7.96-7.17 (m, 11H), 7.74 (d, 1H) ppm.



Secondary products were also identified by ¹H NMR as follows:

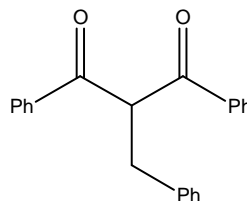
1,3,5-Triphenyl-1,5-pentadione (6)

¹H NMR (400 MHz, CDCl₃): δ = 7.95 (d, 4H), 7.55 (t, 2H), 7.29-7.25 (m, 4H), 7.20-7.16 (m, 1H), 4.09-4.04 (m, 1H), 3.50 (dd, 2H), 3.36 (dd, 2H) ppm.



2-Benzyl-1,3-diphenylpropane-1,3-dione (7)

¹H NMR (400 MHz, CDCl₃): δ = 7.88-7.90 (m, 4H), 7.51-7.55 (m, 4H), 7.38-7.42 (m, 4H), 7.22-7.26 (m, 5H), 5.51 (t, 1H), 3.45 (d, 2H) ppm.



3.1.3 Claisen-Schmidt-Julia-Colonna one-pot reaction

In a tube of 10 mL, benzaldehyde (40.5 μL, 0.39 mmol), acetophenone (44.4 μL, 0.37 mmol) MQ-water (315 μL) and the indicated catalyst were added. The mixture was stirred at 80°C for 3 hours. After that time, the reaction mixture was cooled down to room temperature and TBAB (7.3 mg, 0.024 mmol), NaOH 5M (636 μL, 10 equiv.) and the indicated solvent (1 mL) were added. The mixture was finally stirred for 10 minutes and H₂O_{2(aq)} (334 μL, 11.9 equiv.) was added. The mixture was stirred at room temperature for 1.5 hour more. To work-up the mixture it was diluted in 1 mL of ethylacetate. The catalyst (solid phase) was washed several times with toluene. The organic fraction was dried with MgSO₄ and separated by filtration. Then, the solvent in the organic phase was evaporated. The crude organic fraction was purified by silica-gel column chromatography with a 10:1 hexanes:EtOAc mixture as the eluent to give the

3.1 Experimental

different products. The *trans*-(2R,3S)-(1) was identified by ^1H NMR (400 MHz, CDCl_3): $\delta = 4.01$ (s, 1H), 4.23 (s, 1H), 7.32-7.45 (m, 7H), 7.54 (d, 1H), 7.94 (d, 2H) ppm. The ee was determined by ^1H NMR using Europium tris[3-(heptafluoropropylhydroxymethylene)-(+)-camphorate] ($\text{Eu}(\text{hfc})_3$) as the chiral shift reagent.

3.2 Results and discussion

3.2.1 Claisen-Schmidt reaction

The results obtained for the synthesis of (5) using different materials based on hydrotalcite-like compounds as catalysts are present in Table 6.

These results showed that HT_{asym} and HT_{cc} were practically inactive catalyst under neat conditions after 3 hours of reaction or using dry toluene as the solvent (Table 6, entries 1 and 2). Nevertheless a slight increase in activity was observed by adding water to the reaction media (Table 6, entry 3). When the organic solvent was changed by water, the conversion increased to 54.3% in agreement with Tichit *et al.* who exposed that increases of the activity are due to rehydroxylation and formation of active hydroxyl groups in the calcined hydrotalcite [15]. Moreover, increasing of the reaction temperature also increased the conversion up to 82.1% (Table 6, entry 5).

From the point of view of the solvent, difference in the conversions with HT_{cc} using toluene and water are explained by the acidity of the solvent. Toluene which has a pK_a of 41, is attracted by strong basic centers presented in the HTs, this strong centers are the OH's located on the edges of the HTs. while water with a pK_a of 15.7 was attracted by the basic sites with medium strength. In other words, using toluene the active sites from the HTs are poisoned during the reaction. These facts conclude that the catalytic Claisen-Schmidt reaction is carried out through the stronger basic centers of the HTs susceptible of solvent poisoning. And low acidic solvents or neat conditions improved the activity of the HT_{cc} as the catalyst. The HT_{rus} as the catalyst also showed high activity and selectivity towards the desired product (5) in under neat and water conditions but it was necessary to increase its concentration 15 wt% to 100 wt% respect to acetophenone (Table 6, entries 7 and 8).

Table 6 Claisen-Schmidt reaction

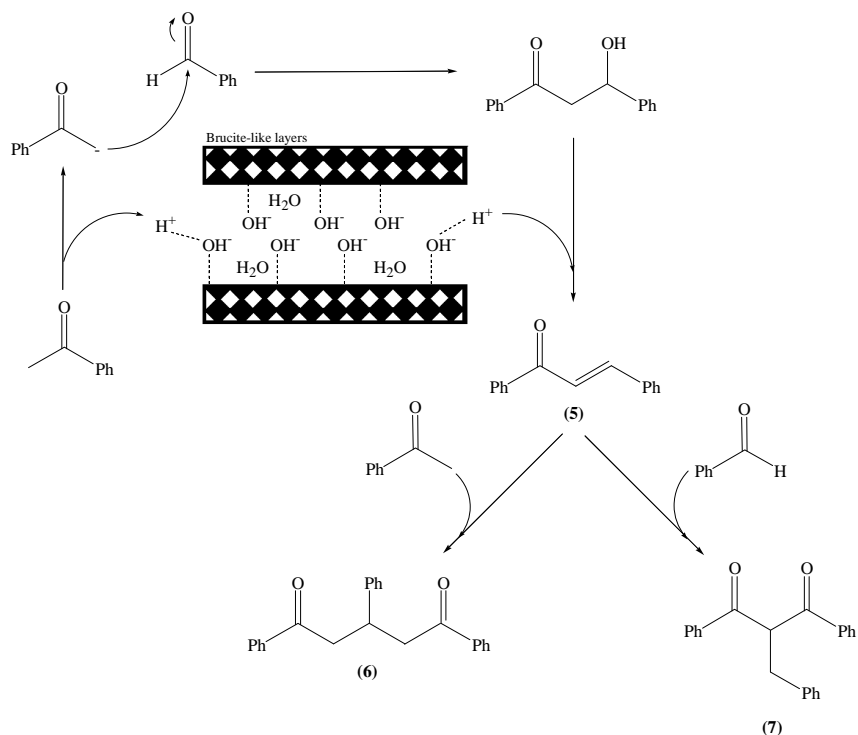
Entry ^a	Catalyst ^b	Temperature (°C)	Solvent ^c	%C ^d	%S ₍₅₎ ^{d,e}	%S ₍₆₎ ^{d,e}	%S ₍₇₎ ^{d,e}
1	HT _{asym}	60	-	-	-	-	-
2	HT _{cc}	60	T	-	-	-	-
3	HT _{cc}	60	T + W ^f	5.5	99.9	-	-
4	HT _{cc}	60	W	54.3	99.9	-	-
5	HT _{cc}	80	W	82.1	97.6	2.3	-
6	-	80	W	-	-	-	-
7	HT _{rus}	80	-	26.7	99.9	-	-
8	HT _{rus} ^g	80	-	81.4	88.0	12.0	-
9	HT _{rus} ^h	80	-	85.8	85.1	14.9	-
10	HT _{rus} ^h	80	W	85.1	90.1	-	9.9
11	IPL2 ₆₀ ^h	80	W	87.1	88.2	-	11.8
12	PLL2 ₆₀	80	W	-	-	-	-

^aReaction conditions: 0.39 mmol of benzaldehyde, 0.37 mmol acetophenone and indicated catalyst (15 wt% respect to acetophenone) were mixed and stirred for 3 hours at indicated temperature. ^bHT= hydrotalcite; HT_{asym}= As-synthesised HT; HT_{cc}= calcined HT; HT_{rus}= rehydrated HTs under ultrasound treatment; PLL2₆₀= Poly-L-Leucine synthesised by ROP at 60°C; IPL2₆₀= immobilised PLL2₆₀ in HT_{rus} by anion-exchange method. ^cT= toluene and W = water. ^dDetermined by ¹H NMR. ^eS_(x) indicates selectivity toward x compound, where x = 5, 6 and 7. (5). ^fUsing 35wt% of water respect to acetophenone. ^g100 wt% of catalyst was used. ^h200 wt% of catalyst was used.

About the selectivity, in most cases, the major product was chalcone (5) with the formation of the condensation side-products 1,3,5-Triphenyl-1,5-pentadione (6) and 2-Benzyl-1,3-diphenylpropane-1,3-dione (7). In agreement with de Jong *et al.*, detection of chalcone as the major product is due to the extraction of a proton from the α -carbon atom of the acetophenone by a strong base site on the HTs to form a reactive enolate [36]. This enolate attacks to the carbonyl group of the benzaldehyde to produce an intermediate alkoxide which form the aldol product by deprotonation of water from the HT interlayer space (Scheme 3). Moreover, detection of (6) and (7) suggests that condensation reaction between reagents with the formed chalcone also occurs [15].

3.2 PLL/HT materials as catalyst in Claisen-Schmidt-Juliá-Colonna epoxidation reactions

3.2 Results and discussion – Claisen Schmidt reaction

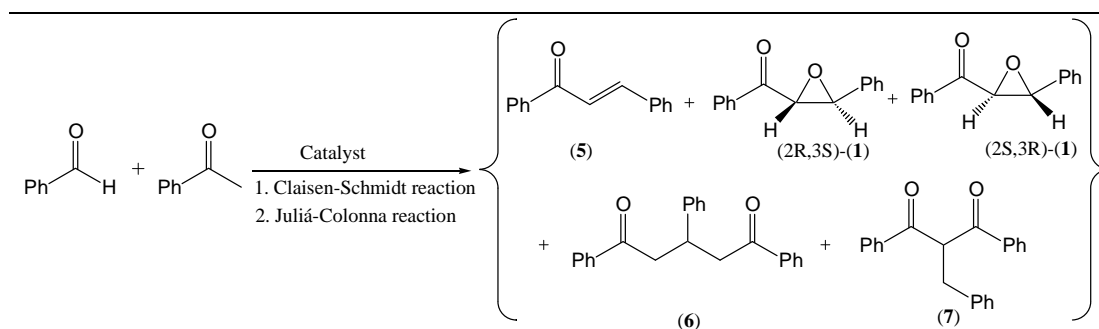


Scheme 3 Proposed catalytic mechanism of Claisen-Schmidt reaction using benzaldehyde, acetophenone and HT as catalyst

PLL₂₆₀ in the reaction conditions did not present any activity for the Claisen-Schmidt reaction (Table 6, entry 12). Nevertheless, IPL₂₆₀ showed slightly better activity as the catalyst in Claisen-Schmidt reaction with HT_{rus}. Therefore, the nanohybrid catalyst kept the appropriate active basic sites even after immobilisation of PLL₂₆₀ (Table 6, entry 13). The bionanohybrid catalyst, as it has been explained in Chapter 4, could have totally or partially occupied the interlayered hydroxyl groups and/or OH⁻ anions located on the edges of the HTs. In addition, the large chains of the PLLs make the access to OH⁻ anions of these materials quite difficult. So, at this point, seems that also the basic sites on the surface of the support could be involved in the catalytic process.

3.2.2 Claisen-Schmidt-Juliá-Colonna one-pot reaction

In accordance with the results previously shown and using the reaction conditions established in Section 2, Claisen-Schmidt-Juliá-Colonna one-pot reaction was also investigated. Preliminary results are summarised in Table 7 where the conversion given were calculated from acetophenone.

Table 7 Claisen-Schmidt-Juliá-Colonna one-pot reaction – Reusability of the catalyst

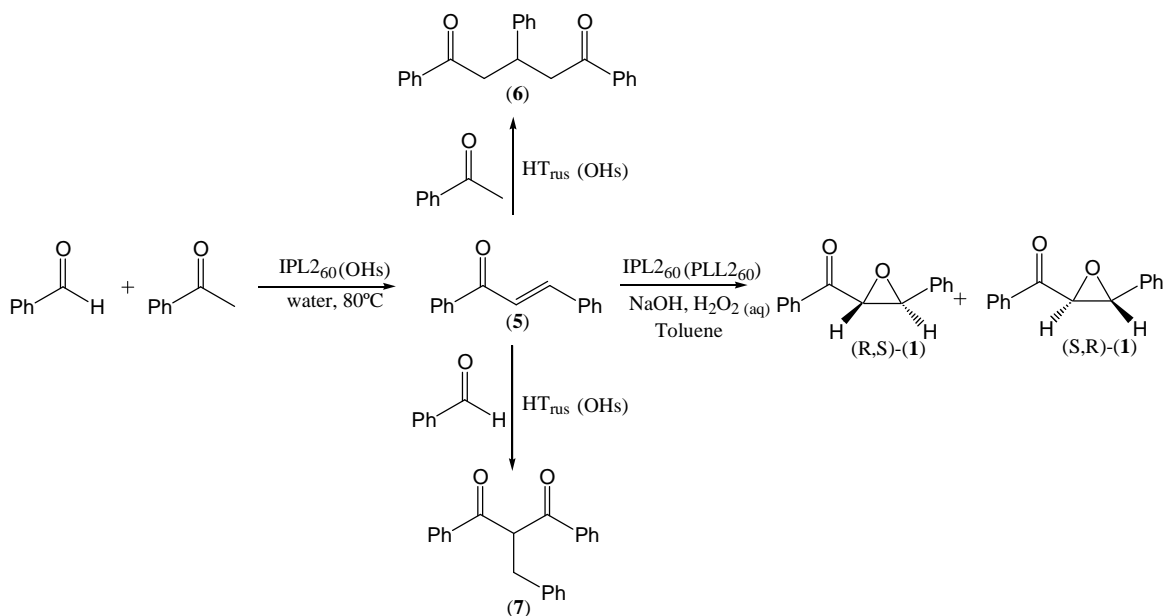
Entry ^a	Run	%C ^b	%S ₍₅₎ ^b	%S _{Epoxy(1)} ^b	%ee ^c	%S ₍₆₎ ^b	%S ₍₇₎ ^b
1	1	93.9	16.2	62.1	83.0	12.9	8.8
	2	81.4	43.1	40.1	56.5	16.8	-
	3	92.1	52.0	27.4	45.0	20.6	-
	4	90.4	61.4	23.1	41.9	15.5	-
2	1 ^d	80.4	87.0	-	-	-	13.0
	2 ^d	96.9	84.0	-	-	-	16.0
	3 ^d	90.5	79.4	-	-	7.9	11.9
	4	100	29.0	51.9	75.7	8.1	11.0
3	1 ^e	99.9	-	99.9	79.9	-	-
	2	98.7 ^f	52.4	47.6	74.3	-	-
	3	93.4 ^{f,g}	57.6	42.4	69.0	-	-
	4	69.2 ^{f,g}	73.7	26.3	53.6	-	-

^aReaction conditions of reusability catalytic test with four consecutive runs: 0.39 mmol of benzaldehyde, 0.37 mmol acetophenone and indicated catalyst (25 wt% of PLL2₆₀ respect to benzaldehyde) were mixed and stirred for 3 hours 80°C, after that time, the reaction was cooled to r.t. and H₂O₂ 334 μL (30 wt.%, 11.9 equiv.), NaOH 5 M 636 μL (10 equiv.) and TBAB 7.3 mg (0.024 mmol) were added. The reaction was stirred for 1.5 hour more. ^bDetermined by ¹H NMR. ^cDetermined using Eu(hfc)₃ by ¹H NMR. ^dClaisen-Schmidt reaction without addition of reagents to Juliá-Colonna epoxidation. ^eUsing 150%wt of PLL2₆₀ respect to benzaldehyde.

In the study of the Juliá-Colonna epoxidation (Chapter 4), it was shown that HT_{rus} under water/toluene conditions was not active in the Juliá-Colonna reaction.

The use of IPL2₆₀ as the unique catalyst in the one-pot reaction gave a conversion up to 93.9% with 62.1% of final selectivity to (1) with an enantioselectivity of 83%. (Table 6, entry 1 first run). Nevertheless, one-pot reaction afforded (6) and (7) as a side-product in low percentage due to condensation between acetophenone and (5) and benzaldehyde and (5), respectively (Scheme 4).

3.2 Results and discussion – Claisen Schmidt-Juliá-Colonna one-pot reaction



Scheme 4 Claisen-Schmidt-Juliá-Colonna one-pot reaction using IPL2₆₀ nano hybrid material as catalyst. The suggested active sites, in accordance with literature [33-36], are presented in brackets: OHs = OH⁻ located on the edges of the HT_{rus}. PLL2₆₀ = Immobilised PLL and M = HT surface.

In order to investigate the stability of IPL2₆₀ in Claisen-Schmidt-Juliá-Colonna one-pot reaction, the recovery and reusability of the catalyst was studied carrying out a standard reusability test. Nevertheless, the results showed that under the new reaction conditions the selectivity towards (**1**) were decreasing after the first run down to 23.1% (Table 7, entry 1). To understand this unexpected behaviour of the catalyst, a new experiment was designed (Table 7, entry 2) where after three consecutive runs performing only the Claisen-Schmidt reaction, the fourth consecutive run was a Claisen-Schmidt-Juliá-Colonna one-pot reaction. The results showed a significantly higher final selectivity towards (**1**) (51.9%) than the one observed in the fourth consecutive run of the standard reusability test (23.1%) but a slightly lower final selectivity towards (**1**) than in the first run of the standard reusability test (62.1%) (Table 7, entry 1). These results suggest loss of activity in the Juliá-Colonna epoxidation reaction probably because the immobilised catalyst is modified during the reaction. It also could explain the decreases of the enantioselectivity from 83.0% e.e. in the first run to 41.9% e.e. (Table 7, entry 1). In order to investigate this hypothesis, a new experiment was performed (Table 7, entry 3). The amount of bionano hybrid catalyst IPL2₆₀ was increased. In these new reaction conditions, the stability and reusability of the catalyst were probed during four consecutive runs in the Claisen-Schmidt-Juliá-Colonna one-pot reaction. The results showed

total conversion and selectivity towards (**1**) in the first run. However, after 4 consecutive runs the selectivity decreased down to 26.3% as well as the enantioselectivity.

In order to find an explanation for the observed results, characterisation of the IPL2₆₀ nanohybrid material was evaluated by MALDI-TOF MS after the fourth consecutive run of the last experiment (Table 7, entry 3). The results are shown in Figure 5.

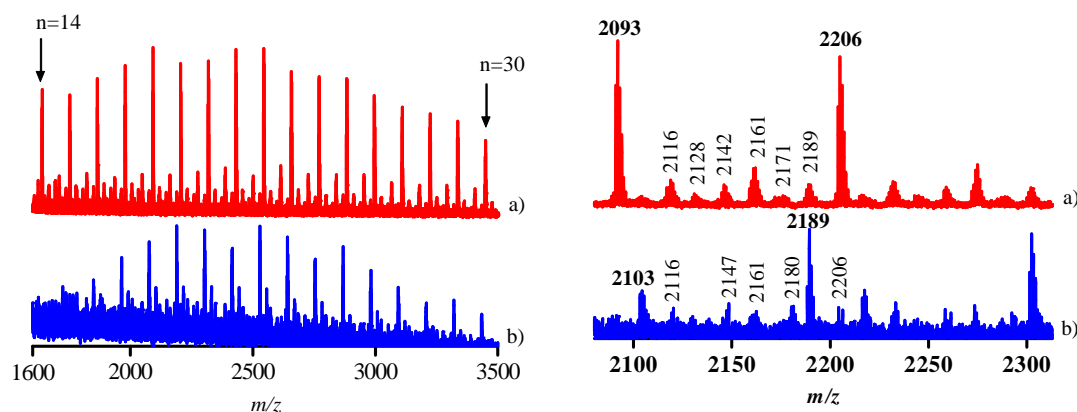


Figure 5 (left) MALDI TOF spectra of IPL2₆₀ a) before and b) after 4 consecutive reactions. (right) MALDI TOF spectra in the m/z range: 2085-2310.

As explained in Chapter 4, section 2.2.1, fresh PLL2₆₀ is composed mainly by PLL chains containing living groups which are interacting with the HT_{rus} after an anionic exchange reaction. Figure 5a (Right) shows the most intense peak at 2093 Da which is due to a PLL chain of 18 monomers doped with potassium, nevertheless this peak practically disappeared after the fourth reaction (Figure 5b, right), other peaks are related with PLL containing living and NCA endgroups (see Annex 3, Table 4). After the fourth consecutive run the spectrum shown in Figure 5b (Right) is formed by a series of 7 main peaks where the most intense is centered at 2189 Da. This peak is due to cyclic-PLL containing 19 monomers doped with potassium. The peaks at 2116 and 2206 Da due to PLL containing living groups are still presented in the material.

In contrast with the results obtained for the Juliá-Colonna reaction, where the catalyst showed high stability after 4 consecutive runs (section 2.2.3), in Claisen-Schmidt-Julia-Colonna one-pot reaction the immobilised PLL is cyclised during the catalytic process. As explained in Chapter 4, the temperature during the first run and also the basicity of the support could be the responsible for the changes in the immobilised PLLs structure. As a

result, both the final selectivity towards product (**1**) and the enantioselectivity decreased. In addition the absence of living groups for the reused catalyst indicates that cyclic PLL chains are also able to catalyse the one-pot reaction but with less activity and enantioselectivity for the lack of an α -helical conformation [13,37].

Finally, although MALDI-TOF is not a quantitative technique, decreases of the peaks intensity after four consecutive runs suggests that cyclisation of PLL chains also decrease the strength of the H-bond interactions. This could indicate leaching of the PLL from the HT_{rus}.

From the point of view of the material, these results are interesting because novel bio-nano hybrid materials based on PLL immobilised in HTs were reported by our group for the first time, and the understanding of their chemical properties is nowadays under investigation.

As it was expressed at the beginning of this chapter, this section is just the preliminary study of IPL materials in Claisen-Schmidt-Juliá-Colonna one-pot reactions which needs to be further investigated. In this context, this topic is currently in progress in our group and the complete study will be performed by Ms. Dana Georgiana Crivoi.

4. Conclusions

The challenge in achieving a well-defined catalytic process is to develop recyclable catalysts that guarantee the expected activity and selectivity for a reasonable number of consecutive runs. We have managed to fulfill this goal in the asymmetric epoxidation of *trans*-chalcone by preparing nano hybrid materials based on synthesised PLL and HT_{rus}. PLL₂₆₀ material synthesised by ROP at 60°C and using triethylamine as initiator resulted in a highly active PLL containing living groups with chain-lengths similar to those of PLL_C. Moreover, immobilisation of PLL₂₆₀ in HT_{rus} by anionic-exchange method in just 30 minutes afforded a nano hybrid material which exhibited high activity and selectivity comparable to those of PLL₂₆₀ and no catalyst pre-activation was necessary. The nano hybrid can be separated from the reaction mixtures by simple centrifugation. In this way, the catalyst can be recovered and reused keeping the same activity and enantioselectivity for at least five consecutive runs. In contrast, the nano hybrid based on the commercial PLL, IPL_C, presented a significant leaching

of PLL and a notable loss of activity and selectivity upon reuse. The reusability and reproducibility of the catalytic system in this process makes it viable and practical in economical and technical terms. These nanohybrid materials, being of economic and environmental interest, should therefore receive considerable attention in future scale-up applications and be used as bioactive catalysts in other asymmetric reactions.

Immobilisation of synthesised PLL in rehydrated HT affords an important family of nanohybrid materials which can act as bifunctional catalysts in interesting reactions to pharmaceutical and fine chemistry. This preliminary study shows the optimised conditions to Claisen-Schmidt reaction using HT_{cc}, HT_{rus} and IPL2₆₀. In this context, it was evaluated that some strong basic centers from the HT_{rus} remained accessible after immobilisation of PLL permitting to catalyse C-C bond-forming reactions. Interestingly, the strong basic centres remained active after four consecutive reactions. Moreover, using IPL2₆₀ nanohybrid material as catalyst allowed both good conversion and selectivity towards *trans*-chalcone.

Taking advantage of their excellent properties as reusable catalyst in Juliá-Colonna epoxidation reaction, IPL2₆₀ was used as catalyst in Claisen-Schmidt-Juliá-Colonna one-pot reaction where presented total conversion and selectivity conserving the good enantioselectivity of the pure PLL material. Nevertheless, decrease of the selectivity after first consecutive reaction indicated that the presence of NaOH at higher temperature during the Claisen-Schmidt reaction induces the cyclisation of the PLL forming a new less active catalyst which is not able to induce enantioselectivity in the formed *trans*-epoxy-chalcone.

These results presented an important advance in the understanding of the nature of PLL materials and also in the physical and chemical properties of nanohybrid materials which are able to catalyse several kinds of important reactions in pharmaceutical and fine chemistry with good activity, selectivity and enantioselectivity. Nevertheless, this topic needs to be more studied in order to understand the reach of these novel nanohybrid materials.

Finally, the total catalytic application of PLL/HT materials in the asymmetric Juliá-Colonna epoxidation reaction was published in the article:

“Asymmetric epoxidation of chalcone catalysed by reusable poly-L-leucine immobilised on hydrotalcite” Ronald-Alexander Miranda, Jordi Llorca, Francisco Medina, Jesús E. Sueiras, Anna M. Segarra. *J. Catal.* **2011**, 282, 65.

References

- [1] R. A. Jonson, K.B. Sharpless. In *Catalytic Asymmetric Synthesis*; Ojima, I. Ed. VCH:New York, **1993**
- [2] B.M. Adger, J.V. Barkey, S. Bergeron, M.W. Cappi, B.E. Flowerdew, M.P. Jackson, R. McCague, T.C. Nugent, S.M. Roberts, *J. Chem. Soc. Perkin Trans. 1* **1997**, 3501
- [3] R. Li, G.L. Kenyon, F.E. Cohen, X. Chen, B. Gong, J.N. Dominguez, E. Davidson, G. Kurzban, R.E. Miller, E.O. Nuzum, P.J. Rosenthal and J.H. McKerrow. *J. Med. Chem.* **1995**, *38*, 5031
- [4] A.T. Dinkova-Kostova C. Abeygunawardana and P. Talalay. *J. Med. Chem.* **1998**, *41*, 5287
- [5] R.J. Anto, K. Sukumaran, G. Kuttan, M.N.A. Rao, V. Subbaraju, R. Kuttan. *Cancer Lett.* **1995**, *97*, 33
- [6] M.W. Cappi, W.-P. Chen, R.W. Flood, Y.-W. Liao, S.M. Roberts, J. Skidmore, J.A. Smith and N.M. Williamson. *Chem. Commun.* **1998**, *10*, 1159
- [7] B.M. Adger, J.V. Barkley, S. Bergeron, M.W. Cappi, B.E. Flowerdew, M.P. Jackson, R. McCague, T.C. Nugent and S.M. Roberts. *J. Chem. Soc. Perkin Trans. 1* **1997**, 3501
- [8] L. Carde, D.H. Davies and S.M. Roberts. *J. Chem. Soc. Perkin Trans. 1* **2000**, 2455
- [9] P. Ray and S.M. Roberts. *Chem. Commun. J. Chem. Soc. Perkin Trans. 1* **2001**, 149
- [10] W.-P. Chen and S.M. Roberts. *J. Chem. Soc. Perkin Trans. 1* **1999**, 103
- [11] J.B.H. Warneck and R.A. Wisdom. *Eur. Pat. EP 0687305BI*, **1997**
- [12] S. Juliá and S. Colonna. *J. Chem. Soc. Perkin Trans. 1* **1982**, 1317
- [13] G. Carrea, S. Colonna, D.R. Kelly, A. Lazcano, G. Ottolina and S. M. Roberts. *Trends in Biotech.* **2005**, *23*, 507
- [14] P.A. Bentley, S. Bergeron, M.W. Cappi, D.E. Hibbs, M.B. Hursthouse, T.C. Nugent, R. Pulido, S.M. Roberts and L.E. Wu. *Chem. Commun.* **1997**, *8*, 739
- [15] T. Geller and S.M. Roberts. *J. Chem. Soc. Perkin Trans. 1* **1997**, 1397
- [16] M. Adger, J.V. Barkley, S. Bergeron, M.W. Cappi, B.E. Flowerdew, M.P. Jackson, R. McCague, T.C. Nugent and S.M. Roberts. *J. Chem. Soc. Perkin Trans. 1* **1997**, 3501
- [17] T. Geller, A. Garlach, C.M. Krüger and H.-C. Militzer. *J. Mol. Catal. A* **2006**, *251*, 71
- [18] D. Kelly and S.M. Roberts. *Biopolymers*. **2006**, *84*, 74
- [19] J.R. Dimmock, N.M. Kandepu, M. Hetherington, J.W. Quail, U. Pugazhenthii, A.M. Sudom, M. Chamankhah, P. Rose, E. Pass, T.M. Allen, S. Halleran, J. Szydowski, B. Mutus, M. Tannous, E.K. Manavathu, T.G. Myers, E. De Clercq and J. Balzarini. *J. Med. Chem.* **1998**, *41*, 1014
- [20] J. F. Ballesteros, M. J. Sanz, A. Ubeda, M.A. Miranda, S. Iborra, T. M. Paya and M. J. Alcaraz. *J. Med. Chem.* **1995**, *38*, 2794
- [21] A.T. Dinkova-Kostova C. Abeygunawardana and P. Talalay. *J. Med. Chem.* **1998**, *41*, 5287
- [22] T. Akihisa, H. Tokuda, M. Ukiya, M. Iizuka, S. Schneider, K. Ogasawara, T. Mukainaka, K. Iwatsuki, T. Suzuki, H. Nishino. *Cancer Lett.* **2003**, *201*, 133

- [23] N.C. Veitch and R.J. Grayer. *Nat. Prod. Rep.* **2008**, *25*, 555
- [24] D.N. Dhar, *Chemistry of Chalcones and Related Compounds*, Wiley, New York, 1982.
- [25] D. Tichit and B. Coq. *Cattech.* **2003**, *7*, 206
- [26] B. M. Choudary, M.L. Kantam, C.V. Reddy, K.K. Rao and F. Figueras. *J. Mol Catal A.* **1999**, *146*, 279
- [27] A. Guida, M.H. Lhouty, D. Tichit, F. Figueras and P. Geneste. *Appl. Catal. A.* **1997**, *164*, 251
- [28] J. C. A. A. Roelofs, D. J. Lensveld, A. J. van Dillen and K. P. de Jong. *J. Catal.* **2001**, *203*, 184
- [29] S. Abelló, F. Medina, D. Tichit, J. Pérez-Ramírez, J.C. Groen, J.E. Sueiras, P. Salagre and Y. Cesteros. *Chem. Eur. J.* **2005**, *11*, 728
- [30] R. J. Chimentão, S. Abelló, F. Medina, J. E. Sueiras, Y. Cesteros and P. Salagre. *J. Catal.* **2007**, *252*, 249.
- [31] A. Berkessel, N. Gasch, K. Glaubitz and Christoph Koch. *Org. Lett.* **2001**, *3*, 3839
- [32] G. Carrea, S. Colonna, A.D. Meek, G. Ottolina and S.M. Roberts. *Chem. Commun.* **2004**, *12*, 1412
- [33] J. Lopez, J. Sanchez Valente, J.-M. Clacens and F. Figueras. *J. Catal.* **2002**, *208*, 30
- [34] A. Kumar and Akanksha. *J. Mol. Catal. A.* **2007**, *274*, 212
- [35] S. Shimizu, S. Shirakawa, T. Suzuki and Y. Sasaki. *Tetrahedron.* **2001**, *57*, 6169
- [36] M. Sugiura, N. Sato, Y. Sonoda, S. Kotani and M. Nakajima. *Chem. Asian. J.* **2010**, *5*, 478
- [37] A. Berkessel, N. Gasch, K. Glaubitz and C. Koch. *Org. Lett.* **2001**, *3*, 3839

SUMMARY OF THIS THESIS

Bio-nano hybrid materials based on the combination of biomolecules and inorganic supports are interesting by their versatile applications in regenerative medicine, drug delivery, bio-engineering and catalysis. In that context, understanding of organic/inorganic interactions offers an important key to design new and more complex bio-systems with modified interactions.

In this thesis, nano hybrid materials based on L-Leucine (L-Leu), L-Proline (L-Pro) or synthesised Poly-L-Leucine (PLL) immobilised in hydrotalcite-like materials (HTs) were synthesised looking for a clarification of the nature of their organic/inorganic interactions and their possible applications as heterogenised organocatalysts.

HTs present properties which were approached in the immobilisation of biomolecules. In this aspect, increase of the basic character using ultrasound treatment during the rehydration of the calcined HTs afforded a material with stronger and more accessible basic centres than using other methodologies. Increasing of the basic character of the HT rehydrated under ultrasound treatment (HT_{rus}) even permitted the immobilisation of L-Pro which has a high pKa of 10.6. Another important property of HTs is their excellent swelling which permitted the immobilisation of amino acids (AAs) or PLL chains in their interlayer space. As the catalyst, HT_{rus} was active to C-C bond-forming reactions and did not present any loss of activity after four consecutive runs. In this context, presence of weak and strong basic centres permitted to design experiments where HT_{rus} can act as the catalyst or lose its activity through changes in the used solvent.

One important goal of this thesis was the total control over the immobilisation of biomolecules on the edges or in the interlayer space from the HT structure, but not on the surface. In all cases the immobilisation started with an anionic exchange reaction between the carboxylate group from the biomolecule and the more accessible OH^- anions from the HTs. Although the interaction does not occur directly with the metals in the brucite-like structure,

this ionic interaction afforded stable nanohybrid materials with dependence on the basic character of the HT due to their zwitterionic nature. Increase of the temperature during the synthesis of materials favoured the swelling of the HT layers permitting the immobilisation of biomolecules in the interlayer space. In this topic, the nature of the organic/inorganic interaction depended on the method of synthesis. Moreover, the characterisation data showed that L-Leu and L-Pro could be immobilised in a bilayered conformation increasing the immobilisation capacity of HT_{rus}.

This thesis also included a complete description about the synthesis of PLLs and the role of the kind of initiator, monomer/initiator ratio and temperature of synthesis. Our results demonstrated that under our reaction conditions the synthesis of PLLs mainly formed by living groups using triethylamine as the initiator was possible. Additionally, the role of water in the media was clarified and now it is clear that although traces of water could initiate the ring-opening polycondensation (ROP), excess of water afforded PLL materials containing complex cyclic chains, possible β -sheet configurations and cyclisation of the entire PLL chain. On the other hand, lower amounts of HT_{rus} could initiate the ROP and form PLL mainly containing living groups, nevertheless using an excess of HT_{rus} complex collateral reactions were observed.

We presented that the immobilisation of PLL in HT_{rus} by an anionic exchange protocol in just 30 minutes was enough to obtain good stabilised nanohybrid materials. The basic character of the HT_{rus} permitted the immobilisation of PLL through anionic interaction, but also the stabilisation of the α -helical conformation through H-bonding interactions with the HT layers. This kind of immobilisation did not affect the α -helical structure of the synthesised PLLs. Moreover, HT_{rus} also favoured the opening of NCA endgroups present in some PLL chains increasing the immobilisation degree.

In order to evaluate the chemical properties of the synthesised bio-nanohybrid materials, these materials were used in one of four reactions: asymmetric Julia-Colonna epoxidation reaction, asymmetric direct aldol reaction, Claisen-Schmidt reaction and Claisen-Schmidt-Julia-Colonna one-pot reaction. In all cases controlled immobilisation of biomolecules in HT_{rus} afforded materials with excellent synergistic behaviour. Materials based on L-Leu immobilised in HT_{rus} (LL/HT) presented an interesting catalytic behaviour because

separately L-Leu and HT_{rus} were not active in the asymmetric Juliá-Colonna epoxidation reaction. The results highlighted in this thesis showed that control on the location of immobilised L-Leu permitted to obtain materials with different catalytic properties. Immobilisation on the edges of the HT_{rus} increased the accessibility and also the total conversion. Immobilisation in the interlayer space decreased the accessibility but induced slightly enantioselectivity towards (S,R)-epoxy-chalcone.

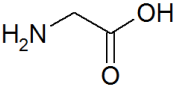
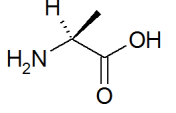
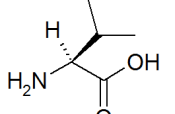
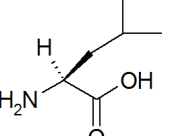
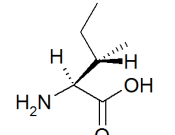
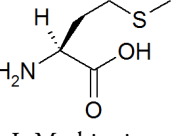
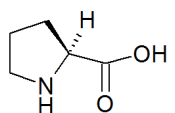
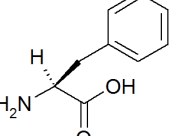
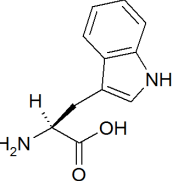
Similar behaviour was observed using L-Pro immobilised in HT_{rus} (LP/HT). In that case, the synergistic behaviour was observed because direct asymmetric aldol reaction requires both amino and carboxylic groups from the pure L-Pro. Immobilisation of L-Pro occurred through its carboxylate group; however, the activity towards aldol product was high due to the joint work between HT_{rus} and the immobilised L-Pro. In the same way as LL/HT materials, immobilization in the interlayer space decreased the accessibility reducing the total conversion but increased the enantioselectivity showing inversion of this parameter.

Finally, nanohybrid materials based on PLL immobilised in HT_{rus} (IPL) presented excellent stability toward asymmetric Juliá-Colonna epoxidation reaction of chalcone. Moreover, IPL nanohybrid materials were easily recovered and reused in four consecutive runs without significant leaching of the immobilised PLL. Nevertheless the thermally sensitive structure of the PLL made its use difficult in the Claisen-Schmidt reaction at 80°C by the modification of the active centres from the PLL by cyclisation of the chains which reduce the activity and enantioselectivity of the formed *trans*-epoxy-chalcone.

In general, immobilisation of biomolecules in HT_{rus}, under controlled conditions, permitted to obtain nanohybrid material with different organic/inorganic interaction. Moreover, these bio-nanohybrid materials showed catalytic activity in interesting pharmaceutical and fine chemical reactions. LL/HT, LP/HT and IPL are ecofriendly nanohybrid materials, easy to synthesise through clean and efficient methodologies, and no pre-activation was needed when they were used as catalysts. Moreover, the complete understanding of the immobilisation nature opens the opportunity to synthesise more complex materials using proteins, enzymes or chiral ligands which could be used as the catalyst in several enantioselective reactions.

GENERAL INFORMATION

Table 1.1 Classification and properties of most common AA in the protein structures

Aminoacid structure	pI	pKa ₁ (α -COOH)	pKa ₂ (α -NH ₃)	Aminoacid structure	pI	pKa ₁ (α -COOH)	pKa ₂ (α -NH ₃)
AA with nonpolar side chains							
	6.06	2.35	9.78		6.01	2.35	9.87
Glycine (Gly)				L-Alanine (Ala)			
	6.00	2.39	9.74		6.01	2.33	9.74
L-Valine (Val)				L-Leucine (Leu)			
	6.05	2.32	9.76		5.74	2.13	9.28
L-Isoleucine (Ile)				L-Methionine (Met)			
	6.30	1.95	10.64		5.49	2.20	9.31
L-Proline (Pro)				L-Phenylalanine (Phe)			
	5.89	2.46	9.41				
L-tryptophan (Trp)							
AA with polar but nonionised side chains							

	5.41	2.14	8.72		5.65	2.17	9.13
L-Asparagine (Asn)				L-Glutamine (Gln)			
	5.68	2.19	9.21		5.60	2.09	9.10
L-Serine (Ser)				L-Threonine (Thr)			
AA with acidic side chains							
	2.85	1.99	9.90		3.15	2.10	9.47
L-Aspartic acid (Asp)				L-Glutamic acid (Glu)			
	5.64	2.20	9.21		5.05	1.92	10.70
L-Tyrosine (Tyr)				L-cysteine (Cys)			
AA with basic side chains							
	9.60	2.16	9.06		10.76	1.82	8.99
L-Lysine (Lys)				L-Arginine (Arg)			
	7.60	1.80	9.33				
L-Histidine (His)							

CHARACTERISATION TECHNIQUES

Molecular formulae were calculated since elemental analyses (EA) and inductively coupled plasma analyses (ICP) results. EA were performed on an elemental analyser EA-1108 C.E. instrument from Thermo Fisher Scientific with a microbalance Mettler Toledo MX5. The analyses were carried out using atropine as patron and Vanadium as the additive to facilitate combustion. ICP analyses were performed in an ICP-OES Spectro Arcos FHS16 Instrument.

Powder X-ray diffraction (XRD) patterns of the samples were performed on a Bruker-AXS D8-Discover diffractometer with 2θ angle ranging from 1° to 70° . Samples were dispersed onto low background Si (510) sampler holder. The data were collected with an angular step of 0.03° at 5s per step and sample rotation. CuK_α radiation ($\lambda = 1.54056 \text{ \AA}$) was obtained from a copper X-ray tube operating at 40 kV and 40 mA. The crystalline phases were identified using JCPDS files. The interlayered spaces were analysed with the reflection bands of the (003) and (006) and calculated using the Bragg law. High-resolution transmission electron microscopy (HRTEM) was performed at Institut de Tècniques Energètica from Universitat Politècnica de Catalunya (Spain) for Prof. Dr. Jordi Llorca who used a JEOL 2010F instrument equipped with a field emission source and working at an acceleration voltage of 200 kV. The point-to-point resolution of the microscope was 0.19 nm, and the resolution between lines was 0.14 nm.

Fourier transform infrared spectra (FT-IR) were recorded with Nicolet Nexus Fourier Transform instrument provided with a DTGS KBr detector. Each analysis was performed using 100 scans in the range $4000\text{--}400 \text{ cm}^{-1}$ with resolution of 4 cm^{-1} . For the analysis of skeletal vibrations KBr pressed disks were used. To spectra analysis OMNIC software provided by ThermoElectron Corporation was used. Raman spectra were obtained using a Renishaw Raman in via reflex instrument. The polarized radiation ($\lambda=785 \text{ nm}$) of a Renishaw diode laser of 500 mW was used. A Laica DM2500 optical microscope was used to determine the analysed part of the sample. Ramascope was calibrated using a silicon wafer. Focus (maximum opening 100%) and power (50%) were carefully optimized in order to not alter the sample during the measurement. The spectral resolution was $2\text{--}3 \text{ cm}^{-1}$; with an exposure time of 10 s and 5 accumulations for each run.

^{13}C and ^{27}Al Magic Angle Spinning-Nuclear Magnetic Resonance (MAS-NMR) spectra were obtained on a Varian Mercury VXR-400S spectrometer operating at 104.2 MHz with a pulse width of 1 ms. A total of 4000 scans were collected with a sweep width of 100 kHz and an acquisition time of 0.2s. An acquisition delay of 1s between successive accumulations was selected to avoid saturation effects. ^{13}C MAS NMR spectra were recollected using tetramethylsilane (TMS) as reference.

MALDI-TOF analysis were performed using a Voyager-DE STR MALDI mass spectrometer (Applied Biosystems) equipped with nitrogen laser (emission wavelength 337 nm, pulse duration 3ns, 20 Hz repetition rate). MALDI targets were prepared using a solution of 10 mg/mL of α -ciano-4-hydroxycinnamic acid (CHCA) in acetonitrile-0.1% TFA (1:1, v/v) as matrix solution. 10 μL of material solution (1.5 mg/mL of a mixture TFA/chloroform 1:1, v/v) was mixed with 10 μL of matrix solution and 5 μL of potassium trifluoroacetate in THF solution (1mg/mL). 0.5 μL of the resulting mixture was applied to each spot of the sample plate. Samples were dried at room temperature. Spectra were recorded in positive ion mode using 20kV acceleration voltage, delayed extraction (200 ns), reflector mode, grid voltage set to 66%, 0.002% guide wire voltage and an extraction delay of 200 ns. Survey spectra of the materials were obtained by accumulating data of 100 laser shots. External calibration was carried out using the protonated molecules of Leucine-enkephalin, substance P, neurotensin and ACTH (fragment 18-39).

ElectroSpray Ionization Mass Spectrometry (ESI-MS) spectra in the direct infusion mode were recorded on a hybrid quadrupole/time-of-flight Qstar Pulsar mass spectrometer fitted with an IonSpray source. Samples were diluted in 70% formic acid to a final concentration of 10 μM . The instrument was calibrated using a 3mM solution of cesium iodide in a 2-propanol/ H_2O mixture (1:1, v/v).

Thermal evolution

Thermogravimetric analyses and Differential Thermal Analyses (TG/DTA) were measured on TGA7 instrument from Perkin Elmer. The analyses were carried out using a sample amount of 10 mg under N_2 atmosphere. The heating rate was $10^\circ\text{C}\cdot\text{min}^{-1}$ within the range 30-900 $^\circ\text{C}$.

In situ IR experiments were achieved by using a conventional gas manipulation apparatus connected to the cell under static conditions and by transmission method. Self supporting disk of KBr pressed disk was heated outgassing up to 450 $^\circ\text{C}$ directly in the IR cell. The FTIR spectra were recorded at the specified temperatures with previous cooling of the disk at room temperature under vacuum (10 $^{-4}$ mbar).

CHARACTERISATION RESULTS

1. Characterisation results from Chapter 2

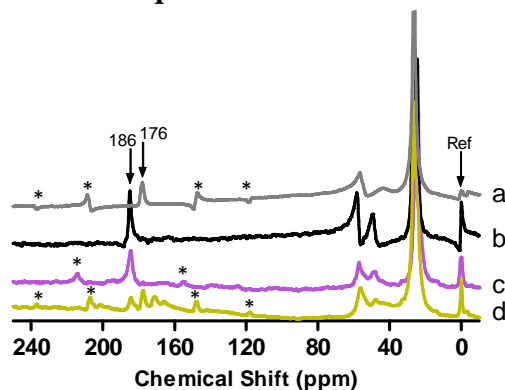


Figure 1 ^{13}C -MAS NMR of a) L-Leu, b) LL/HT_{rus}-A2_{1.09}, c) LL/HT_{rus}-R1_{0.95} and d) LL/HT_r-R2_{0.92}. Ref=TMS.

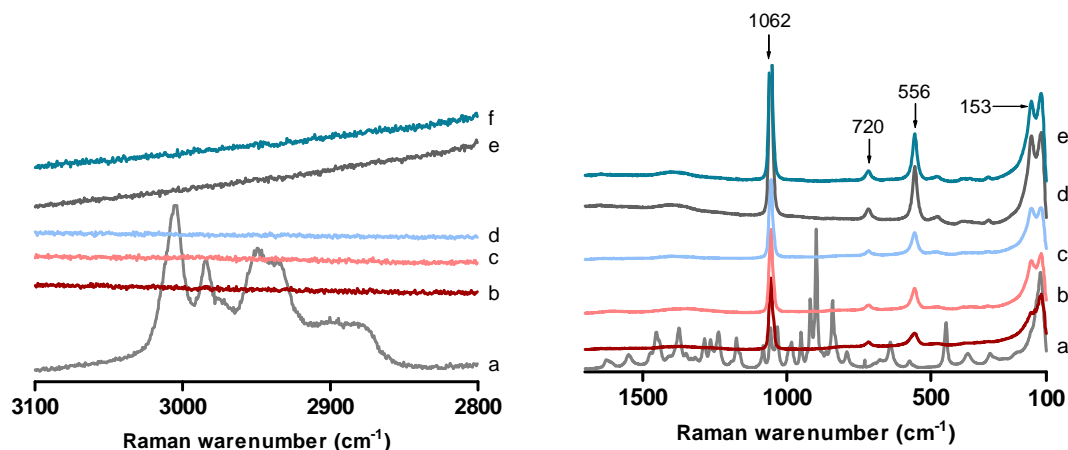


Figure 2 Raman spectra of a) L-Pro, b) HT_{rus}, c) LP/HT_{rus}-R1_{0.95} and d) LP/HT_r-R2_{0.92}. Left: increase scale in the frequency region 3100-2800 cm^{-1} . Right: Raman spectra in the frequency region 1700-100 cm^{-1} .

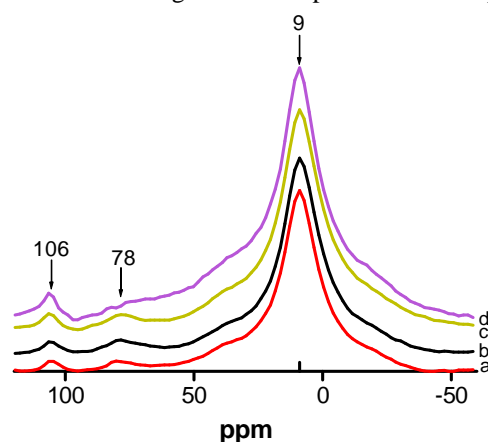


Figure 3 ^{27}Al MAS NMR spectra of a) HT_{rus}, b) LP/HT_{rus}-A2_{0.57}, c) LP/HT_{rus}-R1_{0.60} and LP/HT_r-R2_{0.70}

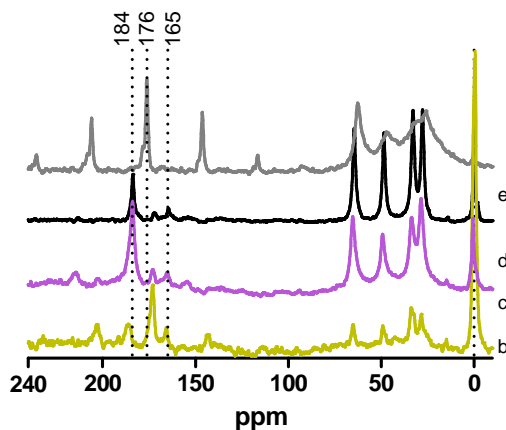


Figure 4 ^{13}C MAS NMR of a) L-Pro, b) LP/HT_{rus}-A2_{0.57}, c) LP/HT_{rus}-R1_{0.60} and LP/HT_r-R2_{0.70}

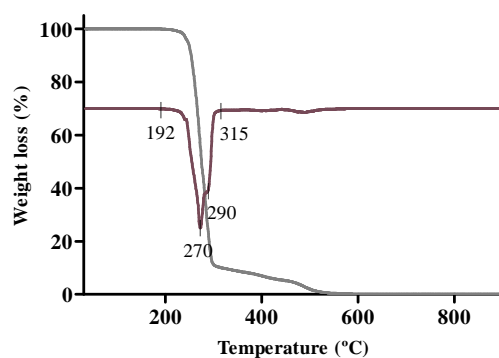


Figure 5 TG/DTA thermal experiment of L-Pro

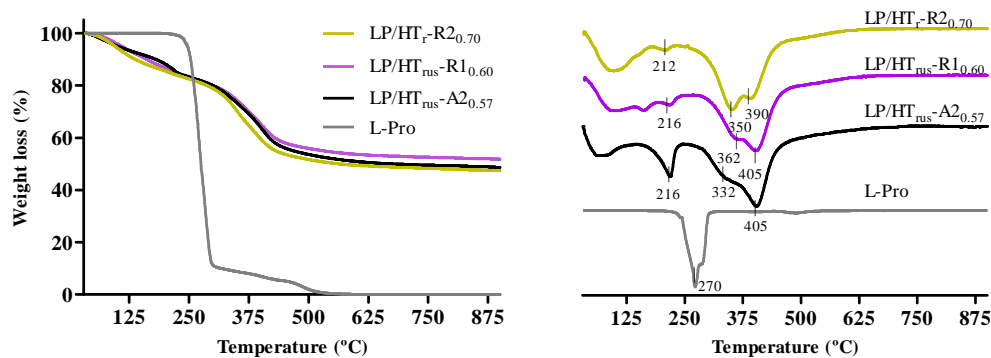


Figure 6 TG (left) and DTA (right) thermal experiment of LP/HT_{rus}-A2_{0.57}, LP/HT_{rus}-R1_{0.60} and LP/HT_r-R2_{0.70}

Characterisation results from Chapter 2

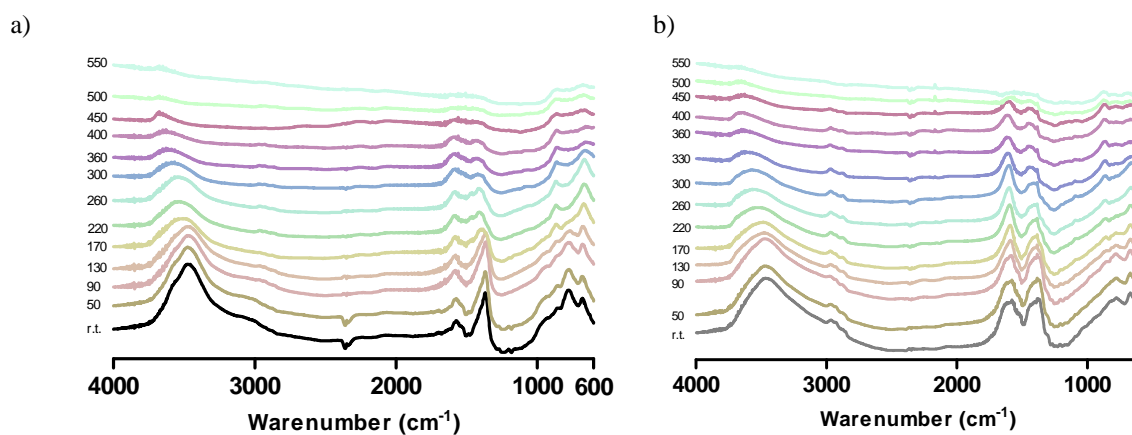


Figure 7 FTIR at increasing temperature of a) LP/HT_{rus}-A2_{0.57}, and b) LP/HT_r-R2_{0.70}

2. Characterisation results from Chapter 4

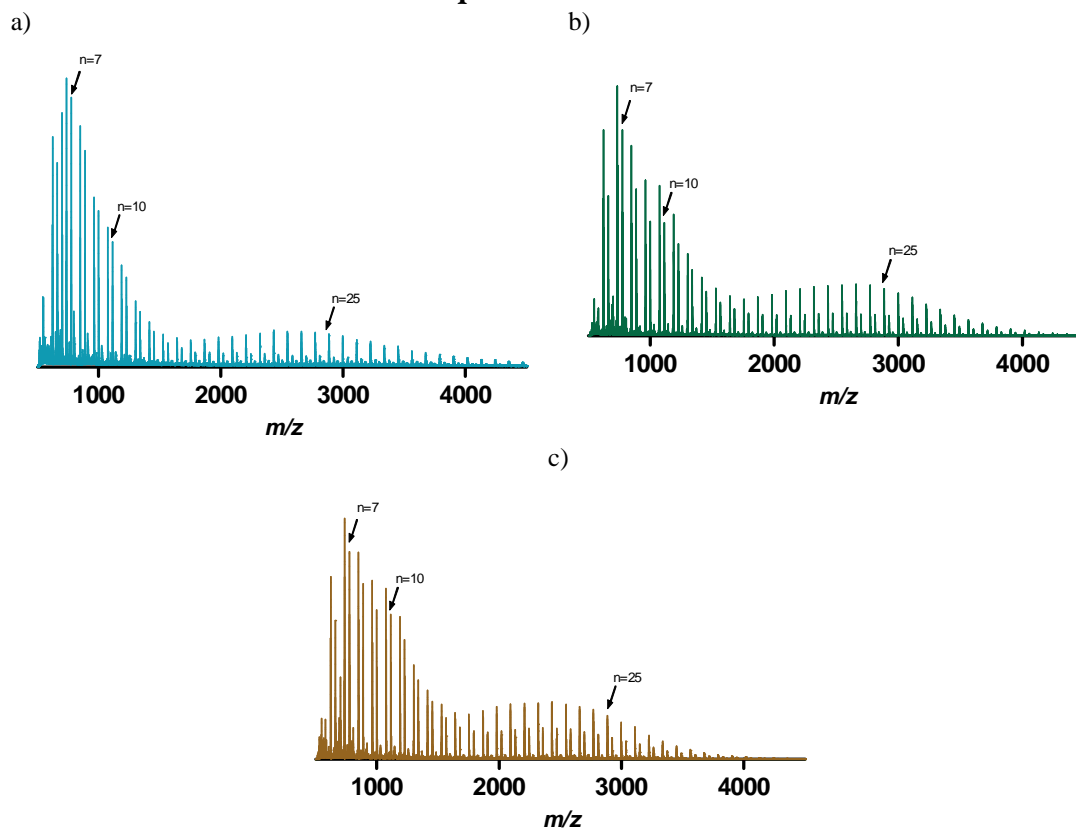


Figure 8 MALDI TOF spectra of a) PLL1_{3d}, b) PLL2_{3d} and c) PLL3_{3d}

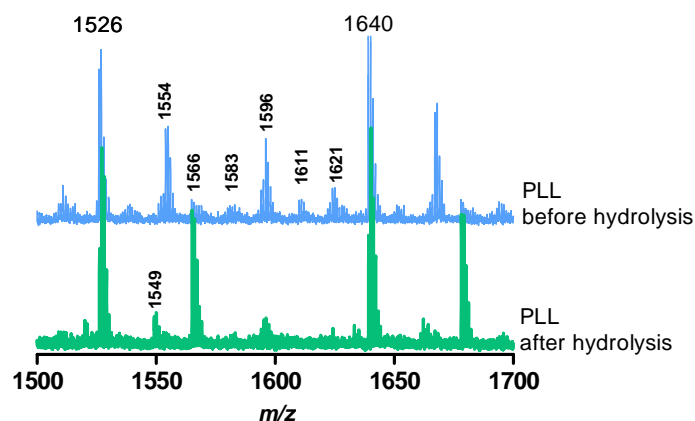


Figure 9 Hydrolysis effect in the synthesis of PLL

Table 1 Correspondences of the peak showed in Figure 9

Peak (Da)	Correspondence	Kind of endgroup
1526	$13^*L\text{-Leu} + H/OH + K^+$	Living
1549	$13^*L\text{-Leu} + H/OH + K^+ - H_2O$	Cyclic chain
1554	$12^*L\text{-Leu} + H/NCA + K^+$	NCA
1566	$13^*L\text{-Leu} + H/OH + 2K^+ - H^+$	Living
1583	$13^*L\text{-Leu} + H/OH + H^+ - H_2O$	Cyclic chain
1596	$12^*L\text{-Leu} + H/NCA + K^+ + 46\text{ Da}$	NCA
1611	$12^*L\text{-Leu} + H/NCA + H^+ - H_2O$	Cyclic chain
1621	$14^*L\text{-Leu} + H/OH + H^+ - H_2O$	Cyclic chain

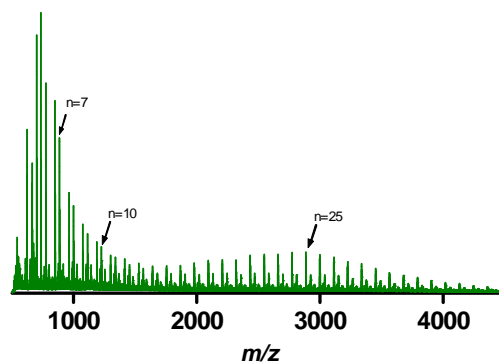


Figure 10 MALDI TOF spectrum of PLL₁₆₀

Table 2 Relationship between areas of amide I and II bands at increasing temperature

PLL3 T (°C)	Amide I (cm ⁻¹)	Amide II (cm ⁻¹)	Amide I/ AmideII	IPL3 T (°C)	Amide I (cm ⁻¹)	Amide II (cm ⁻¹)	Amide I/ AmideII
60	1,45	0,82	1,76	60	0,28	0,14	1,97
90	1,47	0,82	1,78	90	0,28	0,14	2,01
130	1,51	0,83	1,81	130	0,28	0,14	1,98
170	1,56	0,87	1,81	170	0,28	0,15	1,94
220	1,600	0,87	1,83	220	0,29	0,15	1,93
260	1,60	0,84	1,90	260	0,29	0,15	1,88
300	1,62	0,84	1,90	300	0,29	0,15	1,88
330	1,61	0,86	1,88	330	0,29	0,15	1,89
360	1,46	0,84	1,26	360	0,28	0,15	1,89
400	0,58	0,75	1,93				

Characterisation results from Chapter 4

PLL2 ₆₀ T (°C)	Amide I (cm ⁻¹)	Amide II (cm ⁻¹)	Amide I/ AmideII	IPL2 ₆₀ T (°C)	Amide I (cm ⁻¹)	Amide II (cm ⁻¹)	Amide I/ AmideII
60	0,60	0,35	1,72	60	0,16	0,08	2,06
90	0,60	0,35	1,73	90	0,16	0,08	2,08
130	0,61	0,36	1,73	130	0,16	0,08	2,04
170	0,63	0,36	1,73	170	0,16	0,08	2,03
220	0,65	0,37	1,74	220	0,16	0,08	1,99
260	0,67	0,38	1,78	260	0,16	0,09	1,80
300	0,68	0,38	1,79	300	0,16	0,09	1,78
330	0,68	0,37	1,83	330	0,16	0,09	1,74
360	0,66	0,36	1,86	360	0,13	0,07	1,75
400	0,37	0,19	1,94				

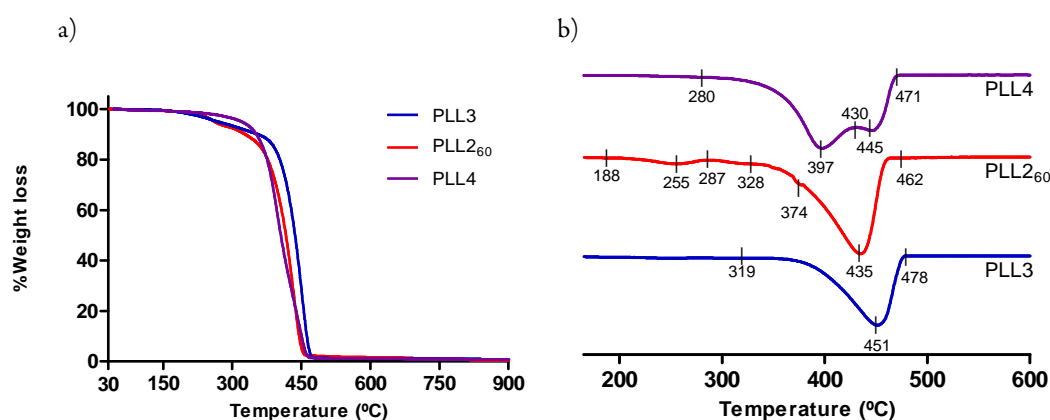


Figure 11 a) TG and b) DTA experiments of PLL3, PLL₂₆₀ and PLL4.

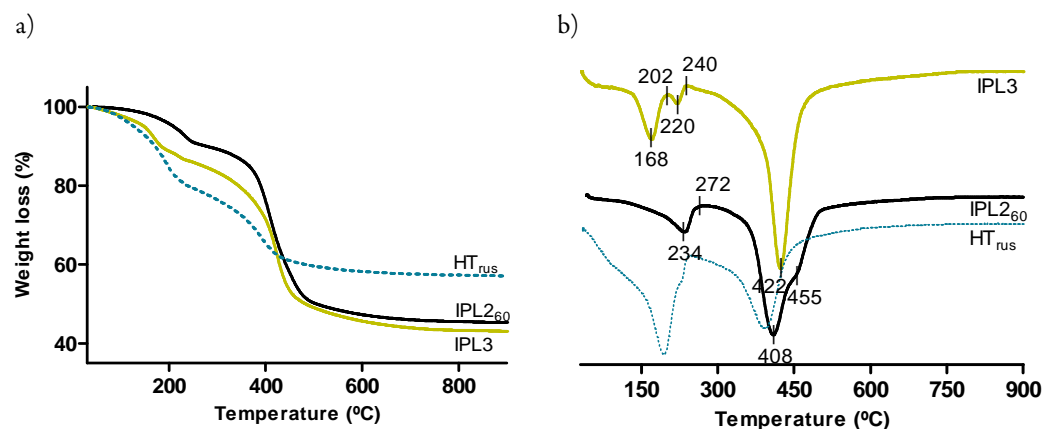


Figure 12 a) TG and b) DT analyses of IPL3 and IPL₂₆₀. HT_{rus} is showed as a reference.

3. Characterisation results from Chapter 5

In order to understand the influence of the solvent in the immobilisation of PLL materials in HT_{rus}, and also in the catalytic activity of the obtained materials, modifications in

the protocol of immobilisation were performed and they are shown in Table 3 and Figures 13-16.

Table 3 Synthetic conditions of nanohybrid materials based on PLLs

Entry ^a	Material ^b	Method	PLL	Immobilisation solvent	Immobilisation ratio ^c
1	IPL2 _{60-1W}	1	PLL ₂₆₀	Water	0.196
2	IPL2 _{60-1T}	1	PLL ₂₆₀	THF	0.082
3	IPL2 _{60-2W}	2	PLL ₂₆₀	Water	0.085
4	IPL2 _{60-2T}	2	PLL ₂₆₀	THF	0.130
5	IPL2 _{60-3W} ^d	3	PLL ₂₆₀	Water	0.225 ^e
6	IPL2 _{60-3T}	3	PLL ₂₆₀	THF	0.180
7	IPL _{C-1W}	1	PLL _C	Water	0.071
8	IPL _{C-2W}	2	PLL _C	Water	0.037
9	IPL _{C-3W}	3	PLL _C	Water	0.076

^aMethod 1: Magnetic stirring for 2 days at 80°C. Method 2: Magnetic stirring for 1 hour at room temperature. Method 3: Ultrasound treatment for 30 minutes. ^bIPLW_{x-yz}: W = numeration in accordance with M/I ratio (2 = M/I of 5 and C = commercial); x = temperature of synthesis; y = method of immobilization and z = W (water) or T (THF). ^cImmobil. ratio = mg PLL/mg HT_r. Calculated by thermogravimetric (TG/DT) analysis. ^dIPL2_{60-3W} correspond to IPL₂₆₀ material exposed in Chapter 4 and 5. ^eImmobilization ratio of 0.225 mg PLL/mg HT_{rus} corresponds to a molecular formula of [Mg_{2.39}Al_{1.00}(OH)_{6.79}](Leu*)_{1.68}(CO₃²⁻)_{5.20}(NO₂⁻)_{0.10}·0.70H₂O calculated by AE and ICP.

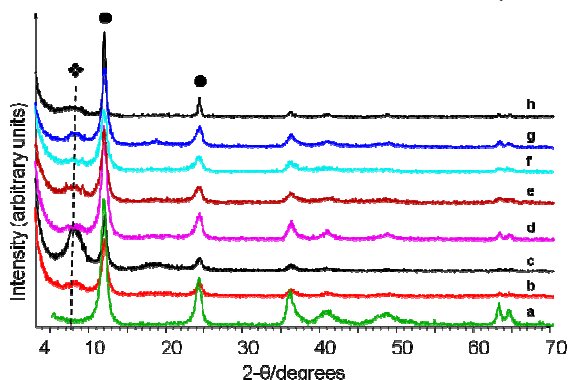


Figure 13 XRD patterns of nanohybrid PLL/HT_r materials: (a) HT_r, (b) IPL_{C-3W}, (c) IPL2_{60-3W}, (d) IPL2_{60-3T}, (e) IPL2_{60-2W}, (f) IPL2_{60-2T}, (g) IPL2_{60-1W} and (g) IPL2_{60-1T}. ❖ Basal peaks of (003) plane with PLL immobilized ● Basal peaks of (003) and (006) planes from the starting HT_r material.

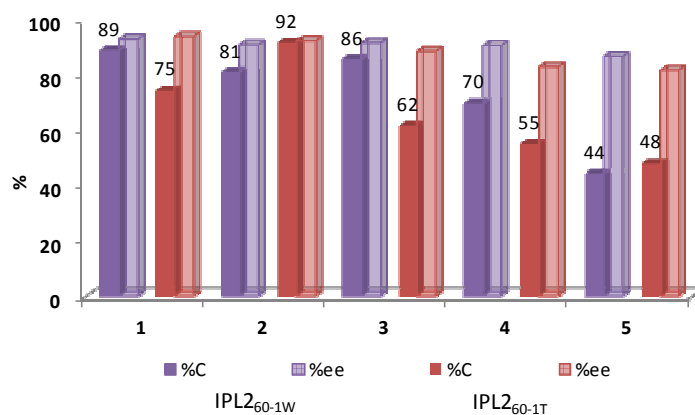


Figure 14 Reusability of IPL2_{60-1W} and IPL2_{60-1T}. Reaction conditions: 10 equiv. NaOH 2M, 11.9 equiv. H₂O₂ (30 wt.%) for 1 hour at r.t.. Total diastereoselectivity towards trans-1,2-epoxy-1,3-diphenylpropane-1-ona

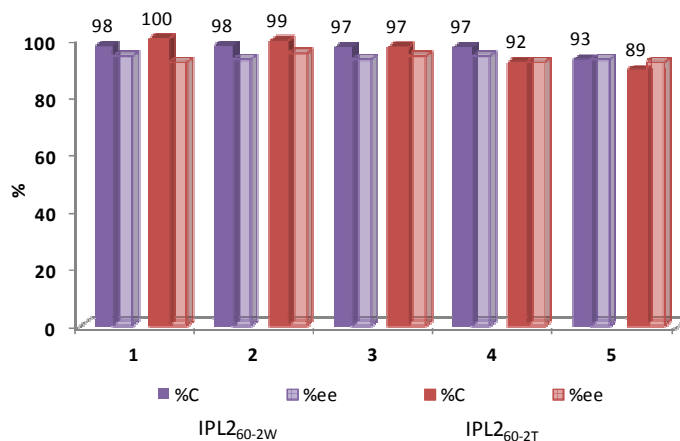


Figure 15 Reusability of IPL2_{60-2W} and IPL2_{60-2T}. Reaction conditions: 10 equiv. NaOH 2M, 11.9 equiv. H₂O₂ (30 wt.%) during 1 h at r.t.. Total diastereoselectivity towards trans-1,2-epoxy-1,3-diphenylpropane-1-ona

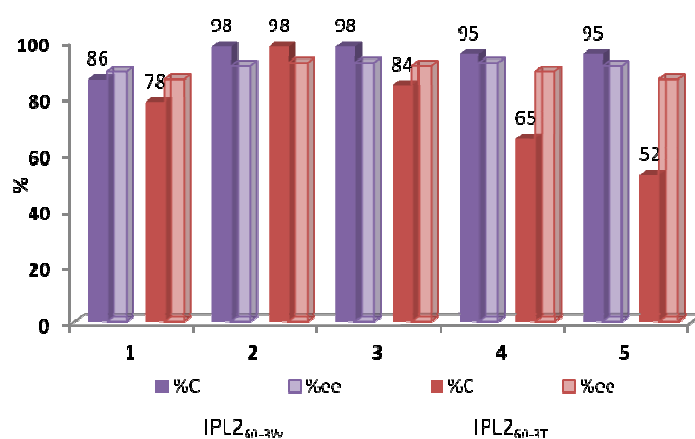


Figure 16 Reusability of IPL2_{60-3W} and IPL2_{60-3T}. Reaction conditions: 10 equiv. NaOH 2M, 11.9 equiv. H₂O₂ (30 wt.%) for 1 h at r.t.. Total diastereoselectivity towards trans-1,2-epoxy-1,3-diphenylpropane-1-ona

Table 4 Correspondences of the peak to IPL2₆₀ before and after reaction

IPL2 ₆₀	MALDI-T of Mass (Da)	Assignment	Kind of endgroup
Before Reaction	2093	18*Leu + H/OH + K ⁺	Living
	2116	18*Leu + H/OH + Na ⁺ + K ⁺ - H ⁺	Living
	2128	18*Leu + H/OH + 2K ⁺ - H ⁺	Living
	2142	17*Leu + H/NCA + 2K ⁺ - H ⁺ - H ₂ O	Cyclic chain
	2161	17*Leu + H/NCA + K ⁺ + 46Da	NCA
	2171	19*Leu + H/OH + H ⁺	Living
	2189	19*Leu + H/OH + K ⁺ - H ₂ O	Cyclic chain
After Reaction	2103	17*Leu + H/NCA + K ⁺ - H ₂ O	Cyclic chain
	2116	18*Leu + H/OH + Na ⁺ + K ⁺ - H ⁺	Living
	2147	19*Leu + H/OH + H ⁺ - H ₂ O	Cyclic chain
	2161	17*Leu + H/NCA + K ⁺ + 46Da	NCA
	2178	18*Leu + H/NCA + H ⁺ - H ₂ O	Cyclic chain
	2189	19*Leu + H/OH + K ⁺ - H ₂ O	Cyclic chain
	2206	19*Leu + H/OH + K ⁺	Living

PUBLICATIONS

1. Article I

Ronald-Alexander Miranda, Jordi Llorca, Elisabetta Finocchio, Giangido Ramis, Francisco Medina, Jesús Sueiras and Anna M. Segarra. "Novel nanohybrid materials based on L-Leucine on hydrotalcite clays: Asymmetric epoxidation reaction of chalcona", *Catal. Today*, **2011**, *172 (1)*, 48

2. Article II

Ronald-Alexander Miranda, Jordi Llorca, Francisco Medina, Jesús E. Sueiras and Anna M. Segarra. "Asymmetric epoxidation of chalcone catalysed by reusable poly-L-Leucine immobilized on hydrotalcite". *J. Catal.* **2011**, *282 (1)*, 65

3. Articles under revision

- "*L-Leucine Immobilised in Hydrotalcite-like Materials. Understanding of the Immobilization Nature*" Ronald-Alexander Miranda, Elisabetta Finocchio, Francisco Medina, Gianguido Ramis, Jesús E. Sueiras, Jordi Llorca and Anna M. Segarra. Proposal Journal: *J Chem. Mater.*
- "*Nanohybrid Materials Based on L-Proline and Hydrotalcites as Catalysts for Direct Asymmetric Aldol Reaction*" Ronald-Alexander Miranda, Elisabetta Finocchio, Francisco Medina, Gianguido Ramis, Jesús E. Sueiras and Anna M. Segarra. Proposal Journal: *Langmuir.*

- “*Synthesis and Characterization of Poly-L-Leucine Initialized and Immobilised by Rehydrated Hydrotalcite. Understanding of the Stability and Interaction Nature*”. Ronald-Alexander Miranda, Elisabetta Finocchio, Francisco Medina, Gianguido Ramis, Jesús E. Sueiras, Jordi Llorca and Anna M. Segarra. Proposal Journal: J Chem. Mater.